

Synthesis and Characterization of Functionalized, Fully π -Conjugated Cyclo[n]thiophenes

Dissertation

zur Erlangung des akademischen Grades

Dr. rer. nat.

der Fakultät für Naturwissenschaften

Universität Ulm

vorgelegt von

Melanie Bader

Ulm, 2014

Amtierender Dekan: Prof. Dr. Joachim Ankerhold

Erstgutachter: Prof. Dr. Peter Bächerle

Zweitgutachter: Prof. Dr. Sven Rau

Tag der Promotionsprüfung: 22. Juli 2014

Fakultät für Naturwissenschaften, Universität Ulm, 2014

ACKNOWLEDGEMENT – DANKSAGUNG

An erster Stelle möchte ich mich bei meinem Doktorvater Prof. Dr. Peter Bächer für die Aufnahme in seinen Arbeitskreis und die Vergabe eines synthetisch anspruchsvollen und interessanten Themengebiets bedanken. Zudem bedanke ich mich für seine fachliche Unterstützung in den letzten vier Jahren und der Finanzierung von Konferenzteilnahmen und Forschungsaufenthalten im Ausland, an denen ich mit großer Freude und Begeisterung teilnahm.

Ein weiterer Dank gilt Prof. Dr. Sven Rau für die freundliche Übernahme des Zweitgutachtens.

Danken möchte ich ebenfalls meinen Kollegen Dr. Elena Mena-Osteritz für die andauernde Diskussionsbereitschaft im Bereich der optischen Spektroskopie sowie Dr. Günther Götz für seine stete Unterstützung als Gruppenleiter und helfende Hand bei allen Fragen rund um die Elektrochemie.

Des Weiteren danke ich Dr. Markus Wunderlin und Eduard Brier für die Aufnahme sämtlicher Massenspektren, den Herren Dr. Udo Werz und Ulrich Ziegler für alle NMR-spektroskopischen Dienstleistungen, Margit Lang für die Durchführung der Elementaranalysen, Bernhard Müller für die Vermessung der Röntgenstruktur und Prof. Dr. Matthias Weil für deren Auswertung. Ferner danke ich Fabian Ehret für die Durchführung der ESR-Messungen. Zuletzt möchte ich mich bei meinen Kollegen Dr. Sylvia Schmid und Dr. Stefan Haid für die Aufnahme unzähliger NMR-Spektren bedanken.

Ein weiteres Dankeschön geht an meine Praktikantin Julia Neumann, die mich mit viel Engagement unterstützte und auch vor Ansätzen im großen Grammmaßstab nicht zurückschreckte.

Ein großer Dank geht an alle Mitarbeiter des Instituts für Organische Chemie II und Neue Materialien, mit denen ich alle Höhen und Tiefen des synthetischen Arbeitsalltags durchlief, die mir immer hilfreich zur Seite standen und zu einer gelungenen Arbeitsatmosphäre, zum Teil auch außerhalb des Labors, beitrugen. Ein ganz besonders herzlicher Dank geht an meine Laborkollegen Dr. Ilona Stengel, Semih Atasever und Manuel Meckle.

An alle Korrekturleser geht ebenfalls ein aufrichtiges Dankeschön.

Der größte und liebste Dank geht an meine Familie, besonders an meine Eltern, die mich all die Jahre finanziell und moralisch stark unterstützt haben.

*Forschung ist planbar,
Resultate nicht!*

CONTENTS

CONTENTS	I
Abbreviations	V
CHAPTER 1	
Introduction and Aim of the Work	1
CHAPTER 2	
From Cyclic Oligothiophenes to Fully α-Conjugated Cyclo[n]thiophenes	9
2.1 General synthetic strategies towards nanosized macrocycles	10
2.1.1 The kinetic controlled approach towards macrocycles	10
2.1.2 The thermodynamic controlled approach towards macrocycles	16
2.2 General macrocycles	18
2.2.1 Cyclic oligothiophenes with disrupted conjugation	18
2.2.2 Cyclic oligothiophenes with complete conjugation	23
2.2.2.1 α,β -Cross-linked cyclic oligothiophenes	23
2.2.2.2 α,α -Conjugated cyclic oligothiophenes	26
2.3 Fully α -conjugated cyclo[n]thiophenes using the 'metal-assisted template method'	33
2.4 Reaction mechanism of the formation of Pt ^{II} (COD)metallacycles	37
2.5 General remarks to reductive eliminations from transition metal complexes	38
2.6 Summary	39
2.7 References	40
CHAPTER 3	
Acceptor-Functionalized α-Conjugated Cyclo[n]thiophenes	45
3.1 Introduction	46
3.2 Design of acceptor-substituted oligothiienyl precursors	47

3.3	Synthesis of acceptor-substituted oligothieryl macrocycles	50
3.3.1	Synthesis of the acceptor-substituted oligothieryl precursors	50
3.3.1.1	Access to the DTB core unit	50
3.3.1.2	Synthesis of DTB-containing quaterthiophene 53	53
3.3.2.1	Access to the DCP core unit	55
3.3.2.2	Synthesis of DCP-containing quaterthiophene 61	56
3.3.3	Macrocyclization via the ‘metal-assisted template method’	57
3.3.3.1	DTB-containing macrocyclic Pt ^{II} oligothieryl complexes	57
3.3.3.2	Fully α -conjugated DTB-functionalized cyclo[<i>n</i>]thiophenes via thermally induced reductive elimination	62
3.3.3.3	DCP-containing macrocyclic Pt ^{II} oligothieryl complexes	66
3.3.3.4	Fully α -conjugated DCP-functionalized cyclo[<i>n</i>]thiophenes via oxidatively induced reductive elimination	68
3.4	Deprotection of cyclic ketals	71
3.4.1	Attempts towards deprotection of macrocycle C[12]DTB 67a	73
3.5	Approaches to by-pass carbonyl protections	74
3.6	Synthesis of linear DTB and DCP-containing oligothiophenes as model compounds	76
3.7	Optical properties of acceptor-functionalized cyclo[<i>n</i>]thiophenes	77
3.7.1	Optical properties of acceptor-functionalized linear oligothiophenes	83
3.8	Characterization of different redox states of acceptor-functionalized cyclo[<i>n</i>]thiophenes	84
3.8.1	Electrochemical properties of acceptor-functionalized C[12]DTB 67a	84
3.8.1.1	Electrochemical properties of transition metal complex Pt(COD)[12]DTB 64a	89
3.8.2	Characterization of different redox states of macrocycle C[12]DTB 67a via UV/vis/NIR absorption spectroscopy	90
3.9	Characterization of doubly oxidized species C[12]DTB ²⁽⁺⁾ via electron spin resonance	95
3.10	Single-crystal X-ray diffraction analysis of C[12]DTB 67a	97
3.11	Summary	99
3.12	Experimental section	100
3.13	Notes	120
3.14	References	135

CHAPTER 4

Donor-Functionalized α-Conjugated Cyclo[<i>n</i>]thiophenes	139
4.1 Design of a donor-substituted oligothieryl precursor	140
4.2 Synthesis of donor-substituted oligothieryl macrocycles	141
4.2.1 Synthesis of a donor-substituted oligothieryl precursor	141
4.2.1.1 General introduction of the synthesis of <i>N</i> -alkylated DTPs	141
4.2.1.2 Access to <i>N</i> -hexyl 4T-DTP 85	143
4.2.1.3 Attempts to halogenate 4T-DTP 85	145
4.2.1.4 Stannylation reaction of diiodinated 4T-DTP 87	146
4.2.1.5 Access to <i>N</i> -propyl 4T-DTP 93	146
4.2.2 Macrocyclization via the 'metal-assisted template method'	147
4.2.2.1 DTP-containing macrocyclic Pt ^{II} oligothieryl complexes	147
4.2.2.2 Fully α -conjugated DTP-functionalized cyclo[<i>n</i>]thiophenes via oxidatively induced reductive elimination	152
4.3 Synthesis of a linear DTP-containing oligothiophene as model compound	154
4.4 Optical properties of donor-functionalized C[12]DTP 96	155
4.5 Characterization of different redox states of donor-functionalized C[12]DTP 96	158
4.5.1 Electrochemical properties of donor-functionalized C[12]DTP 96	158
4.5.2 Characterization of different redox states of C[12]DTP 96 via UV/vis/NIR absorption spectroscopy	161
4.6 Characterization of doubly oxidized species C[12]DTP ²⁽⁺⁾ via electron spin resonance	165
4.7 Summary	166
4.8 Experimental section	167
4.9 References	177

CHAPTER 5

Peripherally Functionalized π-Conjugated Cyclo[<i>n</i>]thiophenes	179
5.1 Introduction	180
5.2 Synthesis of aldehyde-substituted oligothieryl macrocycles	181
5.2.1 Synthesis of aldehyde-substituted oligothieryl precursors	181
5.2.1.1 Synthesis of dendritic terthiophene TMS-3T 99	181
5.2.1.2 Synthesis of dendritic terthiophene CHO-3T 106	183

5.2.1.3	π -Conjugated peripherically functionalized cyclo[<i>n</i>]thiophenes via oxidatively induced reductive elimination	185
5.3	Optical properties of peripherically functionalized macrocycles	191
5.4	Electrochemical properties of peripherically functionalized macrocycles	193
5.5	Synthesis of a non-isomeric, peripherically functionalized macrocycle	194
5.5.1	Optical properties of non-isomeric peripherically functionalized macrocycle 123	198
5.6	Summary	199
5.7	Experimental section	200
5.8	References	210
	Summary	211
	Zusammenfassung	217
	Curriculum Vitae	224

Abbreviations

Alox	aluminium oxide
AM 1	Austin Model 1
BINAP	2,2'-bis(diphenylphosphino)-1,1'-binaphthyl
Bu	butyl
<i>n</i> -BuLi	<i>n</i> -butyl lithium
C	carbon
calcd.	calculated
CI	chemical ionization
C[<i>n</i>]T	cyclo[<i>n</i>]thiophene; <i>n</i> = number of thiophene units
COD	1,5-cyclooctadien
conc.	concentrated
CV	cyclic voltammetry
d	day or doublet concerning NMR spectra
DABCO	1,4-diazabicyclo[2.2.2]octan
dba	dibenzylideneacetone
DDQ	2,3-dichloro-5,6-dicyano-1,4-benzochinone
DCM	dichloromethane
DMF	<i>N,N'</i> -dimethylformamide
DMSO	dimethyl sulfoxide
dppf	1,1'-bis(diphenylphosphino) ferrocene
dppp	1,3-bis(diphenylphosphino) propane
E_{ox}	oxidation potential
EE	ethyl acetate
EI	electron ionisation
ESR	electron spin resonance
eq.	equivalent
EtOH	ethanol
Fc/Fc ⁺	ferrocene/ferrocenium couple
GC-MS	gas chromatography with coupled mass spectrometry
GPC	gel permeation chromatography
h	hour
HBF ₄	tetrafluoroboric acid
HCl	hydrochloric acid

Abbreviations

Hex	hexyl
HOMO	highest occupied molecular orbital
HOPG	highly oriented pyrolytic graphite
HPLC	high performance liquid chromatography
HRMS	high resolution mass spectrometry
I	current
I_t	tunneling current
LDA	lithium diisopropylamine
LUMO	lowest occupied molecular orbital
m	multiplet
m/z	isotopic mass
M	molar
mbar	millibar
MALDI-TOF	matrix assisted laser desorption ionization with coupled time of flight detector
MLCT	metal-to-ligand charge transfer
min	minute
Mp	melting point
MS	mass spectrometry
mV/s	millivolt per second
MW	molecular weight
NBS	<i>N</i> -bromosuccinimide
NIR	near infrared
NIS	<i>N</i> -iodosuccinimide
NMR	nuclear magnetic resonance
ppm	parts per million
Pt	platinum
rt	room temperature
s	singlet
sat.	saturated
SEC	size exclusion chromatography
SOMO	single occupied molecular orbital
STM	scanning tunneling microscope
t	triplet
TCB	tetrachlorobenzene
VI	

Th	thiophene
THF	tetrahydrofurane
TBAF	tetra- <i>n</i> -butylammonium fluoride
TBAPF ₆	tetra- <i>n</i> -butylammonium hexafluorophosphate
TDBPA ⁺ SbCl ₆ ⁻	tris(2,4-dibromophenyl)aminium hexachloroantimonat
TMEDA	<i>N,N,N',N'</i> -tetramethylethylenediamine
TMS	trimethyl silyl
TMSCl	chlorotrimethyl silane
TMSnCl	chlorotrimethyl stannane
UV	ultraviolet
V	voltage
V _{bias}	bias voltage
vis	visible
vol.	volumetric
vs.	versus
δ	chemical shift
ε	extinction coefficient
λ	wavelength

CHAPTER 1

Introduction and Aim of the Work

The study of shape-persistent, fully π -conjugated macrocycles with a well-defined structure on the nanometer scale is an important field of research in chemical, physical, and materials sciences. Such molecules are not only interesting from an experimental and theoretical perspective, but also due to possible application in nanotechnology. The most challenging task for organic chemists in generating nanoscale macrocyclic systems is the synthesis itself. The preparation of cyclic structures is a complex and demanding aspect, although several general synthetic approaches towards macrocyclizations exist. It is still most challenging to arrange linear conjugated organic molecules into a well-defined circular shape and overcome aspects of entropy, which often results in limited yields of the product materials. Rational molecular design, efficient synthetic strategies, and tedious purification procedures are key components for a successful and productive preparation of fully π -conjugated macrocycles. The structure-property relationships of these macrocyclic systems are also an interesting field of study due to their unusual photophysical and electrochemical characteristics. The circular structures provide infinite, ideal model compounds to their corresponding oligomeric or polymeric structures without perturbing end-effects and disrupting structure-property correlation. Additionally, the macrocycles can be selectively designed and functionalized with binding sites on both the inside and/or the outside of the cavity. These binding sites can serve to organize the molecules in ordered multidimensional assemblies in the solid state and can be used to build up nanosized channels with lateral packing also by interacting with external media like molecules or ions.^[1-13] One-, two-, or threedimensional structures are reported to arise from π - π - or convex/concave-interactions. The macrocycles possess a large, planar π -surface, which promotes effective π - π -stacking and intermolecular electronic delocalization through organized tubular materials with efficient charge transport properties, which makes them attractive candidates for the application in nanoelectronics. The formation of well-ordered self-assemblies can be observed on highly ordered pyrolytic graphite (HOPG) surfaces via STM measurements.^[14-18] The formed channels are not only interesting on an electronic purpose, but also for the application in recognition, binding of guest molecules or catalysis.^[19-28]

Oligo- and polythiophenes are among the most widely investigated and promising π -conjugated materials for organic electronics.^[29-30] Due to their outstanding optical behaviour, notable redox- and charge transport properties, stability in the conducting as well as semiconducting state, they have found application in nanoelectronic devices^[31] such as organic field effect transistors (OFETs) and organic solar cells.^[32] Feasible synthetic access, combined with elaborate purification processes, allow for the preparation of well-defined oligothiophene structures. Thorough characterization studies have been used to gain valuable information about structure-property relationships, which is important for future molecular design and engineering of advanced materials. Plenty of thiophene-based architectures with various shapes have been prepared and investigated.^[33-34]

It is now appealing to connect these two systems, macrocycle and thiophene, and concentrate on fully, π -conjugated macrocyclic oligothiophenes, which can be designated as cyclo[n]thiophenes, where ' n ' represents the number of thiophene units. With a cyclic structure, no undesired perturbing end-effects would influence the physical properties. A macrocyclic structure inherently combines an infinite chain of an idealized polymer with the structural features of a well-defined oligomer. Cyclo[n]thiophenes^[35-39] represent a distinct class of organic semiconductors, which reveal unique optical^[38-43] and electrochemical as well as self-assembling properties.^[18, 44-45] Self-assembly into 3D-nanostructures by π -expanded conjugated thiophene rings is promoted by S-S, S- π , or π - π interactions.^[46-47] The macrocycles are also interesting materials from a theoretically point of view.^[48-54]

The first approach of our institute was to prepare fully α -conjugated thiophene-based macrocycles from terminally ethynylated oligothiophenes in a modified Eglinton-Glaser coupling reaction under high-dilution conditions. A statistical macrocyclization resulted, albeit in low yields. The obtained cyclooligothienyldiacetylenes were transformed with sodium sulfide into the desired fully α -conjugated cycles (Chart 1.1, top).^[37] To improve yields, the strategy was advanced by the stoichiometric addition of a Pt^{II} complex, which promoted a template-assisted formation of the cyclic structures. Stable, coordinatively bound Pt^{II}(σ -acetylide-oligothiophene) complexes could be isolated. After oxidatively induced reductive elimination, which gives rise to C-C bond formation, the butadiyne-bridged macrocycles were transformed into fully π -conjugated systems by reaction with sodium sulfide (Chart 1.1, middle).^[35-36] Later, a more direct entry into C[n]Ts was elaborated at our institute by efficiently modifying the 'metal-assisted template method'^[39] (Chart 1.1, bottom).

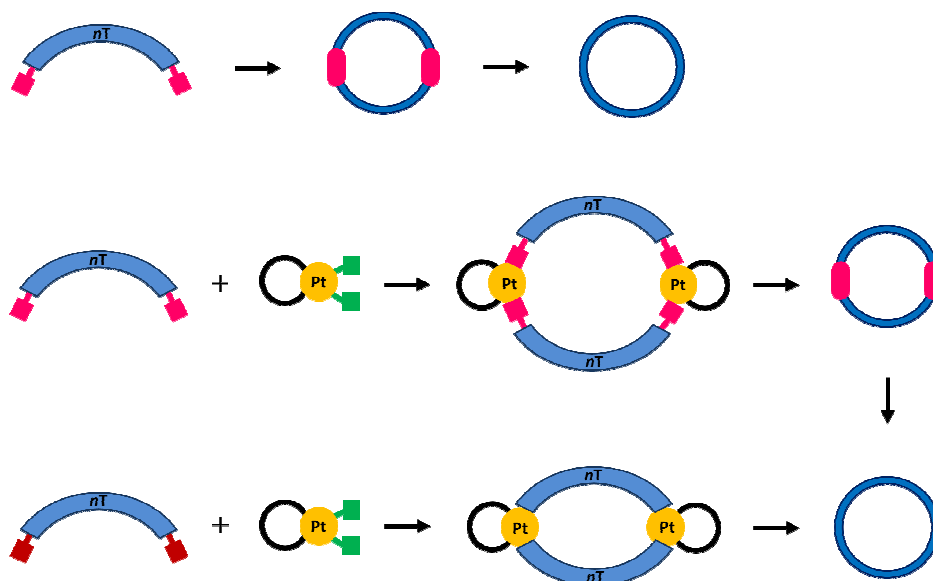


Chart 1.1: Schematic presentation of the development of the 'metal-assisted template approach' to generate macrocycles in a more efficient way. nT : oligothiophene; purple: ethynyl unit; red: tin group; green: chlorine.

In this synthetic strategy, various tin-substituted oligothiophene monomer units were coupled directly, without an ethynyl spacer, to the transition metal and stable Pt^{II}oligothienyl complexes were formed in good overall yields. Subsequent thermal induced reductive elimination led to fully π -conjugated cyclo[*n*]thiophenes by decreasing the number of reaction steps and increasing yields. Numerous C[*n*]Ts were successfully synthesized and fully characterized by means of proton NMR-spectroscopy, mass-spectrometry, absorption- and fluorescence-spectroscopy, as well as cyclic voltammetry. The ring-shaped structures were additionally confirmed by X-ray crystallographic analysis.^[38-39, 41]

The main focus of this thesis was synthetic methodologies accompanied with the modification of the electronic properties of cyclo[*n*]thiophenes. Thus, our established platinum-assisted template approach^[39] towards fully α -conjugated thiophene-based macrocycles was investigated for scope and limitation of functionalized building blocks since the modification of pure c[*n*]Ts was realized by using two molecular design concepts: 1) Introduction of functional groups within the cyclic backbone and 2) attachment of organic functionalities to the periphery of the cavity. This gives rise to fully π -conjugated macrocycles with structural enhancement and generates novel compounds with varied optical and electrochemical properties, as well as reactive centers to allow potential further chemical transformations. The modification processes are illustrated schematically in Chart 1.2.

The first concept focuses on the incorporation of electron withdrawing (acceptor) and electron donating (donor) groups into the cyclic backbone, which allows, compared to appropriate non-functionalized macrocycles, changes in the optoelectronic properties of the macrocycles due to the electronic influence of the substituents. Dithienobenzoquinone (DTB) and dithienocyclopentanone (DCP) were chosen as acceptor units, while dithienopyrrrole (DTP) was employed as a donor unit. The acceptor building blocks contain reactive ketone groups, which can potentially undergo subsequent organic transformations to give rise to various organic functionalities. These different moieties are supposed to tune the electronic properties of the materials as well. Alternatively, highly ordered networks can be prepared via intermolecular reactions between the macrocycles and supposed improved charge mobilities in the bulk promote the macrocycles to interesting candidates in the field of organic nanotechnology. Chapter 3 describes further synthetic and characteristic information about DTB- and DCP-macrocycles, while DTP-macrocycles are discussed in Chapter 4.

The second molecular design concept concentrates on the attachment of reactive organic functionalities to the outside of the cavity (Chart 1.2). These stable, shape-persistent macrocyclic oligomers possess the possibility to introduce various organic substituents through subsequent

chemical reactions or transformations and support the directing of the molecules into well-ordered assemblies with improved charge mobilities. Thus, a dendritic terthiophene with an aldehyde functionality (CHO-3T) was chosen as precursor. It provides additionally an extremely narrow inner angle, which should generate the formation of only one macrocycle size and facilitate the critical macrocyclization step. Further information about the synthesis and characterization of peripherally functionalized macrocycles are given in Chapter 5.

The concept behind the modification processes are the affordability of tailored, shape-persistent nanosized macrocycles with tunable characteristics. Starting from pure thiophene-based macrocycles, it is now feasible to direct the optoelectronic properties for possible applications in organic electronics and generate advanced, planar starting materials, which may self-assemble into well defined, highly ordered structures with improved charge mobilities.

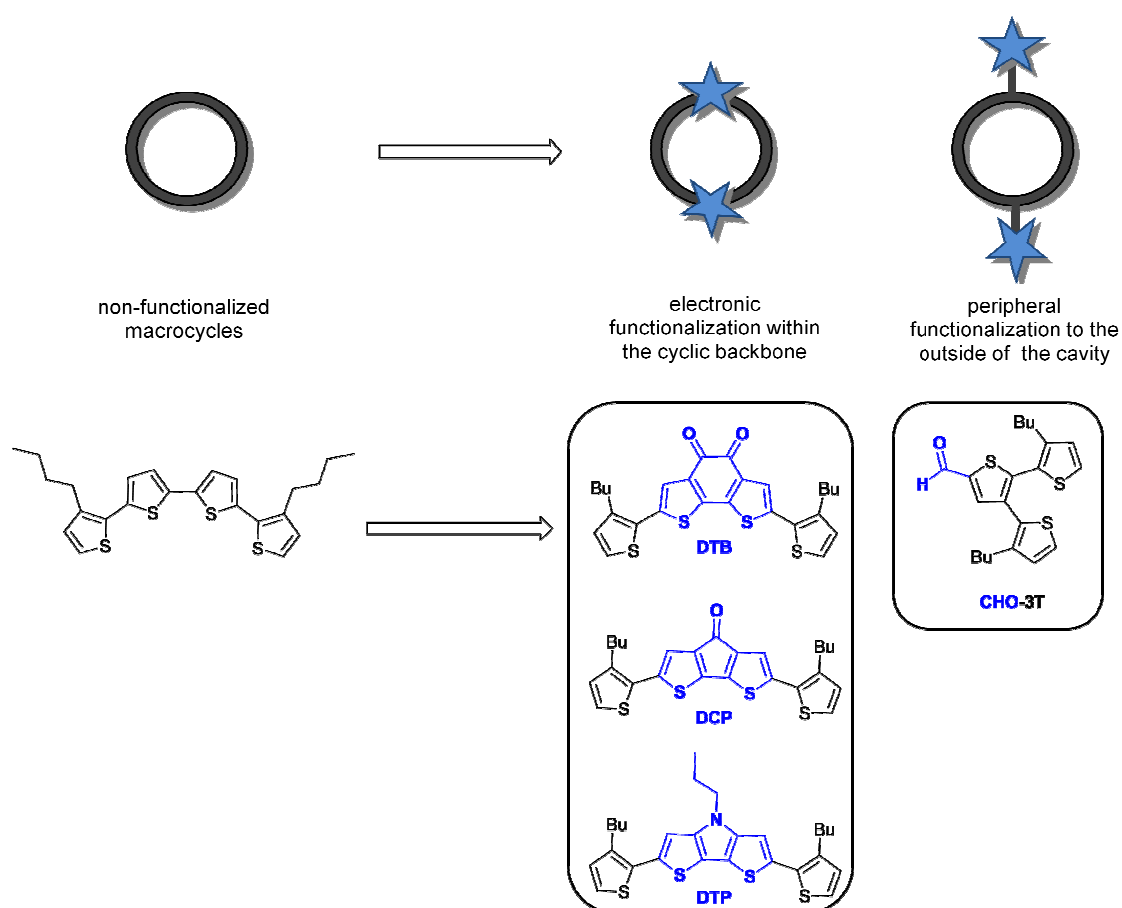


Chart 1.2: Modification of pure thiophene-based macrocycles within the cyclic backbone and at the periphery to generate tailored, shape-persistent nanorings with tunable characteristics.

References

- [1] H. Shimura, M. Yoshio, T. Kato, *Org. Biomol. Chem.* **2009**, *7*, 3205-3207.
- [2] C. Grave, A. D. Schlüter, *Eur. J. Org. Chem.* **2002**, 2002, 3075-3098.
- [3] O. Henze, D. Lentz, A. Schäfer, P. Franke, A. D. Schlüter, *Chem. Eur. J.* **2002**, *8*, 357-365.
- [4] D. Venkataraman, S. Lee, J. Zhang, J. S. Moore, *Nature* **1994**, *371*, 591-593.
- [5] *Modern Supramolecular Chemistry: Strategies for Macrocyclic Synthesis*, Eds.: Diederich, F.; Stang, P. J.; Tykwinski, R. R., Wiley-VCH, Weinheim **2008**.
- [6] S. Höger, *Angew. Chem.* **2005**, *117*, 3872-3875; *Angew. Chem. Int. Ed.* **2005**, *44*, 3806-3808.
- [7] M. Iyoda, *J. Synth. Org. Chem., Jpn.* **2012**, *70*, 1157-1163.
- [8] M. Iyoda, J. Yamakawa, M. J. Rahman, *Angew. Chem.* **2011**, *123*, 10708-10740; *Angew. Chem. Int. Ed.* **2011**, *50*, 10522-10553.
- [9] K. Kawase, *Synlett* **2007**, 2609-2626.
- [10] B. Schmaltz, A. Rouhanipour, H. J. Räder, W. Pisula, K. Müllen, *Angew. Chem.* **2009**, *121*, 734-738; *Angew. Chem. Int. Ed.* **2009**, *48*, 720-724.
- [11] W. Zhang, J. S. Moore, *Angew. Chem.* **2006**, *118*, 4524-4548; *Angew. Chem. Int. Ed.* **2006**, *45*, 4416-4439.
- [12] W. Zhang, J. S. Moore, *Adv. Synth. Catal.* **2007**, *349*, 93-120.
- [13] T. Kawase, H. Kurata, *Chem. Rev.* **2006**, *106*, 5250-5273.
- [14] S. Höger, *Pure Appl. Chem.* **2010**, *82*, 821-830.
- [15] S.-S. Jester, E. Sigmund, S. Höger, *J. Am. Chem. Soc.* **2011**, *133*, 11062-11065.
- [16] S.-H. Jung, W. Pisula, A. Rouhanipour, H. J. Räder, J. Jacob, K. Müllen, *Angew. Chem.* **2006**, *118*, 4801-4806; *Angew. Chem. Int. Ed.* **2006**, *45*, 4685-4690.
- [17] S. K. Maier, S.-S. Jester, U. Müller, W. M. Müller, S. Höger, *Chem. Commun.* **2011**, *47*, 11023-11025.
- [18] E. Mena-Osteritz, P. Bäuerle, *Adv. Mater.* **2006**, *18*, 447-451.
- [19] T. Kawase, K. Tanaka, N. Fujiwara, H. R. Darabi, M. Oda, *Angew. Chem.* **2003**, *115*, 1662-1666; *Angew. Chem. Int. Ed.* **2003**, *42*, 1624-1628.
- [20] L. Arnold, H. Norouzi-Arasi, M. Wagner, V. Enkelmann, K. Müllen, *Chem. Commun.* **2011**, *47*, 970-972.
- [21] Y. Hosokawa, T. Kawase, M. Oda, *Chem. Commun.* **2001**, 1948-1949.
- [22] S. Anderson, H. L. Anderson, A. Bashall, M. McPartlin, J. K. M. Sanders, *Angew. Chem.* **1995**, *107*, 1196-1200; *Angew. Chem. Int. Ed.* **1995**, *34*, 1096-1099.
- [23] L. Yu, J. S. Lindsey, *J. Org. Chem.* **2001**, *66*, 7402-7419.
- [24] L. G. Mackay, R. S. Wylie, J. K. M. Sanders, *J. Am. Chem. Soc.* **1994**, *116*, 3141-3142.
- [25] Y. Che, D. E. Gross, H. Huang, D. Yang, X. Yang, E. Discekici, Z. Xue, H. Zhao, J. S. Moore, L. Zang, *J. Am. Chem. Soc.* **2012**, *134*, 4978-4982.
- [26] M. Fritzsche, A. Bohle, D. Dudenko, U. Baumeister, D. Sebastiani, G. Richardt, H. W. Spiess, M. R. Hansen, S. Höger, *Angew. Chem.* **2011**, *123*, 3086-3089; *Angew. Chem. Int. Ed.* **2011**, *50*, 3030-3033.
- [27] T. Kawase, M. Oda, *Pure Appl. Chem.* **2006**, *78*, 831-839.
- [28] L. Zang, Y. Che, J. S. Moore, *Acc. Chem. Res.* **2008**, *41*, 1596-1608.
- [29] *Handbook of Oligo- and Polythiophenes*, Eds.: Fichou D., Wiley-VCH, Weinheim, Germany **1999**.

- [30] P. Bäuerle, in *Oligothiophenes in Electronic Materials: The Oligomer Approach*, Eds.: K. Müllen, G. Wegner, Wiley-VCH, Weinheim, Germany **1998**.
- [31] P. Bäuerle, in *Handbook of Thiophene-based Materials: Applications in Organic Electronics and Photonics*, Eds.: Perepichka, I. F., Perepichka, D. F., Jon Wiley & Sons Ltd. **2009**.
- [32] A. Mishra, P. Bäuerle, *Angew. Chem.* **2012**, *124*, 2060-2109; *Angew. Chem. Int. Ed.* **2012**, *51*, 2020-2067.
- [33] J. Roncali, *Chem. Rev.* **1997**, *97*, 173-206.
- [34] A. Mishra, C.-Q. Ma, P. Bäuerle, *Chem. Rev.* **2009**, *109*, 1141-1276.
- [35] G. Fuhrmann, *PhD Thesis, University of Ulm, Germany* **2006**.
- [36] G. Fuhrmann, T. Debaerdemaecker, P. Bäuerle, *Chem. Commun.* **2003**, *8*, 948-949.
- [37] J. Krömer, I. Rios-Carreras, G. Fuhrmann, C. Musch, M. Wunderlin, T. Debaerdemaecker, E. Mena-Osteritz, P. Bäuerle, *Angew. Chem.* **2000**, *112*, 3623-3628; *Angew. Chem. Int. Ed.* **2000**, *39*, 3481-3486.
- [38] F. Zhang, G. Götz, E. Mena-Osteritz, M. Weil, B. Sarkar, W. Kaim, P. Bäuerle, *Chem. Sci.* **2011**, *2*, 781-784.
- [39] F. Zhang, G. Götz, H. D. F. Winkler, Christoph A. Schalley, P. Bäuerle, *Angew. Chem.* **2009**, *121*, 6758-6762; *Angew. Chem. Int. Ed.* **2009**, *48*, 6632-6635.
- [40] M. Bednarz, P. Reineker, E. Mena-Osteritz, P. Bäuerle, *J. Lumin.* **2004**, *110*, 225-231.
- [41] E. Mena-Osteritz, F. Zhang, G. Götz, P. Reineker, P. Bäuerle, *Beilstein J. Nanotechnol.* **2011**, *2*, 720-726.
- [42] J. Casado, M. Z. Zgierski, G. Fuhrmann, P. Bäuerle, J. T. López Navarrete, *J. Chem. Phys.* **2006**, *125*, 44518-44527.
- [43] O. Varnavski, P. Bäuerle, T. Goodson III, *Opt. Lett.* **2007**, *32*, 3083-3085.
- [44] E. Mena-Osteritz, P. Bäuerle, *Adv. Mater.* **2001**, *13*, 243-246.
- [45] E. Mena-Osteritz, *Adv. Mater.* **2002**, *14*, 609-616.
- [46] K. Nakao, M. Nishimura, T. Tamachi, Y. Kuwatani, H. Miyasaka, T. Nishinaga, M. Iyoda, *J. Am. Chem. Soc.* **2006**, *128*, 16740-16747.
- [47] F. J. M. Hoeben, P. Jonkheijm, E. W. Meijer, A. P. H. J. Schenning, *Chem. Rev.* **2005**, *105*, 1491-1546.
- [48] P. Flores, P. Guadarrama, E. Ramos, S. Fomine, *J. Phys. Chem. A* **2008**, *112*, 3996-4003.
- [49] S. Fomine, *J. Nanopart Res.* **2012**, *14*, 979-991.
- [50] S. Fomine, P. Guadarrama, P. Flores, *J. Phys. Chem. A* **2007**, *111*, 3124-3131.
- [51] M. Garcia, P. Guadarrama, S. Fomine, *J. Phys. Chem. A* **2010**, *114*, 5406-5413.
- [52] S. Huang, A.-M. Ren, L.-Y. Zou, Y. Zhao, J.-F. Guo, J.-K. Feng, *J. Mol. Model.* **2012**, *18*, 393-404.
- [53] S. Thomas, Y. A. Pati, *J. Phys. Chem. A* **2010**, *114*, 5940-5946.
- [54] S. S. Zade, M. Bendikov, *J. Org. Chem.* **2006**, *71*, 2972-2981.

CHAPTER 2

From Cyclic Oligothiophenes to Fully α -Conjugated Cyclo[n]thiophenes

2.1 General synthetic strategies towards nanosized macrocycles

2.1.1 The kinetic controlled approach towards macrocycles

Organic chemists have made a lot of effort to establish efficient synthetic strategies towards nanosized macrocycles (1-2 nm in diameter), since synthesis and purification strategies turned out to be challenging and afford very limited availability of material. Carbon-carbon cross coupling reactions play a crucial role in the preparation of cyclic structures with a bonus to functional group tolerance. Four major types of strategies have been employed and are often used in macrocyclic chemistry. The methods are displayed schematically in Figure 2.1.: A) cyclooligomerization, B) intramolecular ring closure of α,ω -difunctionalized oligomers, C) intermolecular coupling between several oligomers and D) templated cyclization of several oligomeric fragments.^[1]

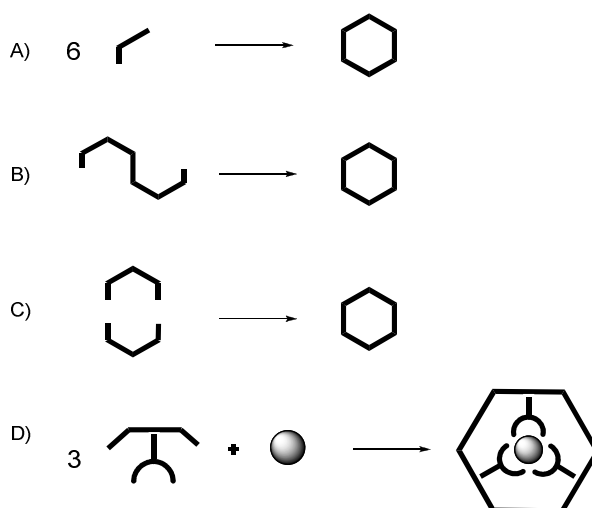
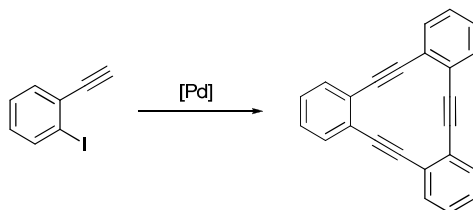


Figure 2.1: Four main kinetically controlled methods towards macrocyclization: A) cyclooligomerization, B) intramolecular ring closure, C) intermolecular coupling, D) templated cyclization.

Despite of a variety of metal-catalyzed cross-coupling reactions, the efficient preparation of macrocycles is hindered by the fact that all procedures are kinetically controlled. The irreversible nature of the reaction is especially problematic at the cyclooligomerization process, as undesired bond formation cannot be corrected and oligomers, which are composed of a higher number of monomer units than the target macrocycle, cannot be shortened. Depending on the monomer, cyclooligomerization can take place either in a homocoupling or cross-coupling reaction, respectively. If the monomer unit possesses two identical reactive centers, like acetylene groups, a homocoupling cyclooligomerization will occur. However, if the starting material is difunctionalized with a halogen atom and an acetylene group, cross-coupling cyclooligomerization will take place. Both reactions have been widely applied to arylene-ethynylene macrocycles using Sonogashira- or Glaser/Eglinton-conditions. An example by Pan and co-workers is outlined in Scheme 2.1, who utilized a palladium-

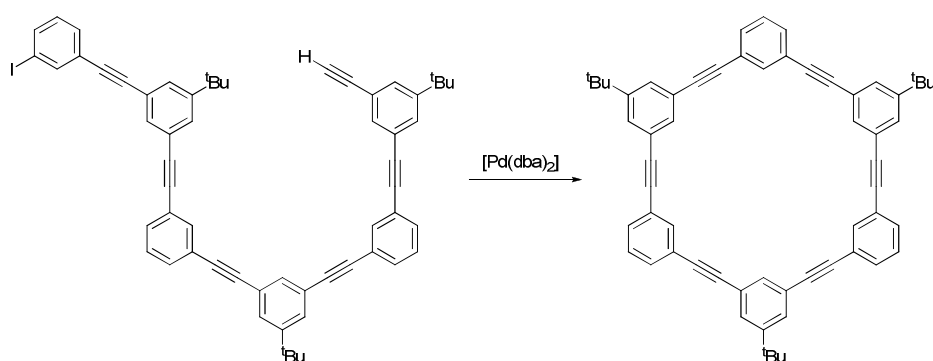
catalyzed Sonogashira cross-coupling reaction to obtain a trimeric macrocycle in a one-step reaction directly from the iodoarylacetylene monomer unit in 30% yield.^[2]



Scheme 2.1: Synthesis of a trimeric macrocycle via one-step cross-coupling cyclooligomerization according to Sonogashira-conditions.^[2]

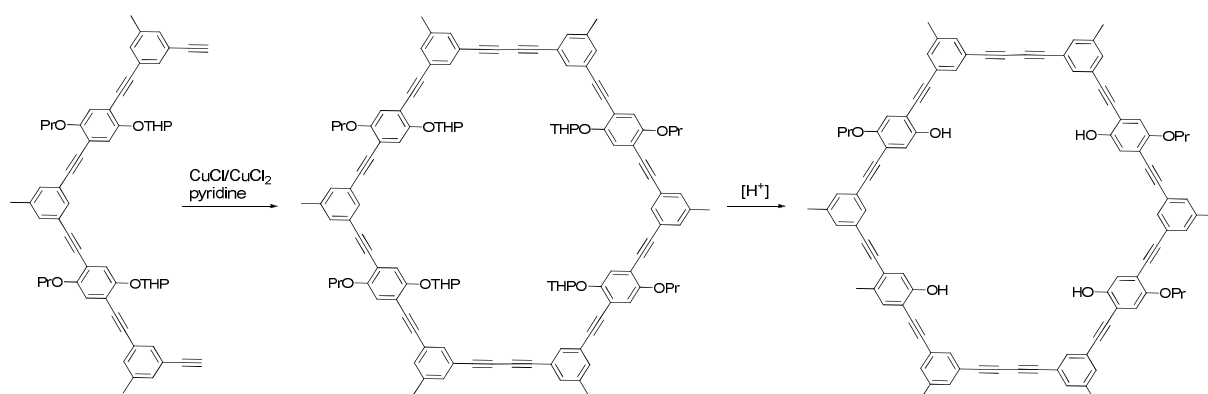
The easily accessible monomer units and the one-step synthesis are two advantages of the cyclooligomerization strategy. However, the crucial cyclization step is hard to regulate since it competes with the formation of linear oligomers. As a result, a random distribution of a variety of cyclic and linear oligomers of different chain length occurs. A low yield for the desired ring system results and purification is time-consuming and exertive. Thus, the cyclooligomerization approach can be regarded as unsuitable for large scale synthesis. The latter could be achieved using the intramolecular ring closure method, which supports the formation of a distinct ring size and facilitates the purification process by simultaneously gaining better yields.^[1]

For the strategy of intramolecular ring closure, a well-defined precursor with a specific chain length is required. This includes, in most cases, a large number of synthetic steps and intense purification to obtain the final α,ω -difunctionalized target sequence. The macrocyclization step is usually carried out under highly dilute or pseudo-highly dilute conditions, since they favour intramolecular ring closure over intermolecular C-C bond reactions in case of non-tensed macrocycles. Besides improved yields, compared to the cyclooligomerization process, a further advantage of this method is the possible oligomer-functionalization.^[1] The stepwise buildup of the oligomer precursors enables specific modification and design through controlled incorporation of defined units, which allows the tuning of different geometrical shapes or the attachment of reactive sides of the prospective macrocycles. An example for the intramolecular ring closure reaction is given in Scheme 2.2. The group of Moore presented the stepwise synthesis of an α,ω -difunctionalized oligomer chain containing six phenylacetylene moieties.^[3-4] They subsequently carried out a palladium-catalyzed ring closure reaction to obtain a hexameric macrocycle in 75% yield.^[3] The high conversion is probably due to the rigid phenylacetylene sequence that strongly favours one ring size and prevents the formation of other cyclic structures.



Scheme 2.2: Palladium-catalyzed intramolecular ring closure reaction from a hexameric precursor.^[3]

Another synthetic strategy towards macrocycles is the intermolecular ring closure. This method has been elaborated to avoid the time-consuming synthesis and intense purification of the oligomer-precursors employed for the intramolecular ring closure method, but tie in with the advantage of defined macrocyclic structures and good yields. It was found, that two oligomeric sequences with an appropriate chain length and functionalities can be subjected to an intermolecular coupling to afford macrocycles with a defined ring size.^[1] The yields of the macrocyclization step are often lower than these of the intramolecular ring closure strategy (15-45% vs. 60-80%), but the overall yield is clearly higher since fewer reaction steps are needed to prepare the desired oligomeric moiety. Nevertheless, even under high dilution conditions, the formation of linear oligomers or polymers is not completely suppressed.^[1] An example of this method is published by the group of Höger and illustrated in Scheme 2.3.^[5] The cyclization was performed via an intermolecularly modified Glaser/Eglinton coupling of bisacetylene precursors, whereby the macrocycle could be isolated in 45% yield. After elimination of the protecting groups, this was the first example of an amphiphilic shape-persistent structure which could induce a more hydrophilic or hydrophobic interior through free rotation of the chain links.

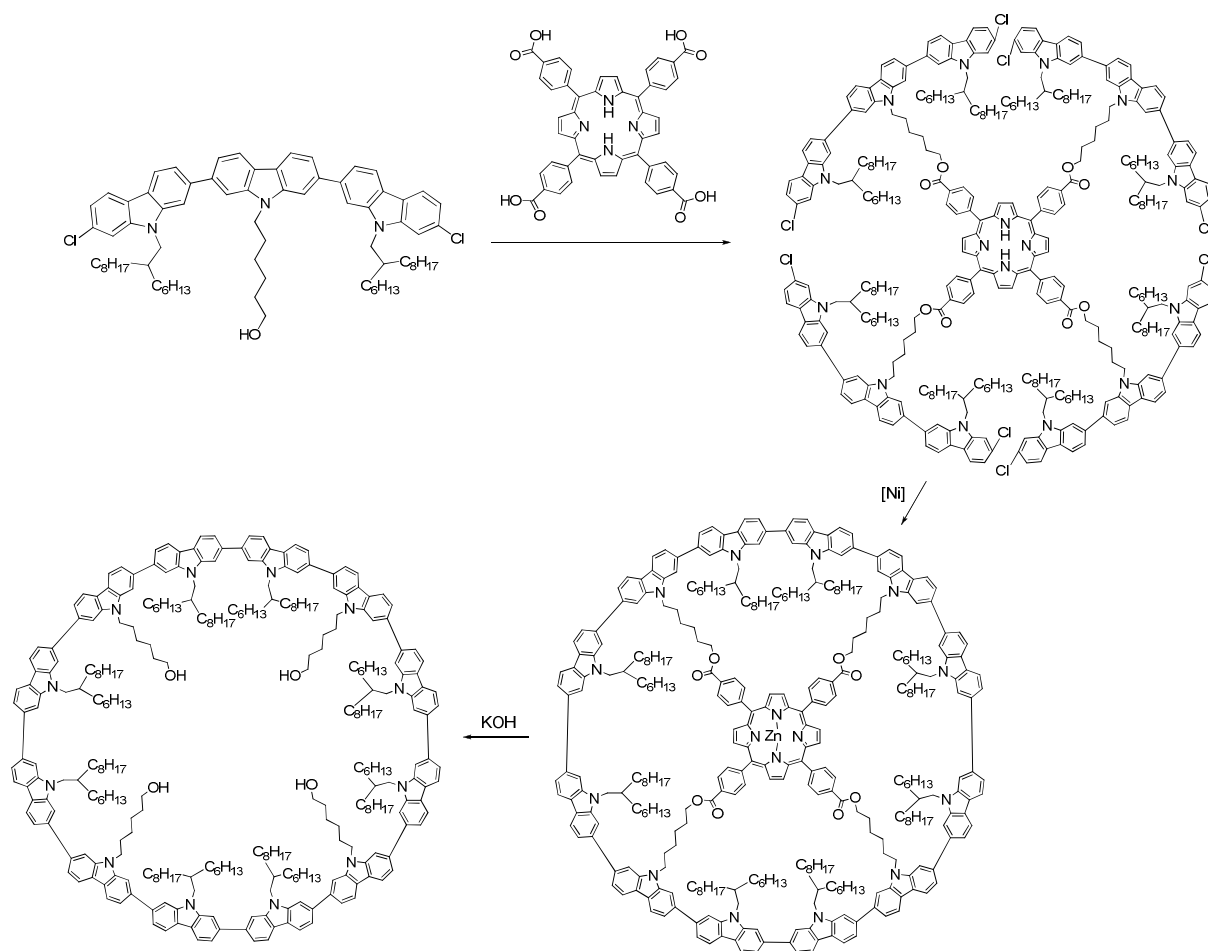


Scheme 2.3: Intermolecular coupling of an oligomeric bisacetylene precursor under Glaser/Eglinton conditions.^[5]

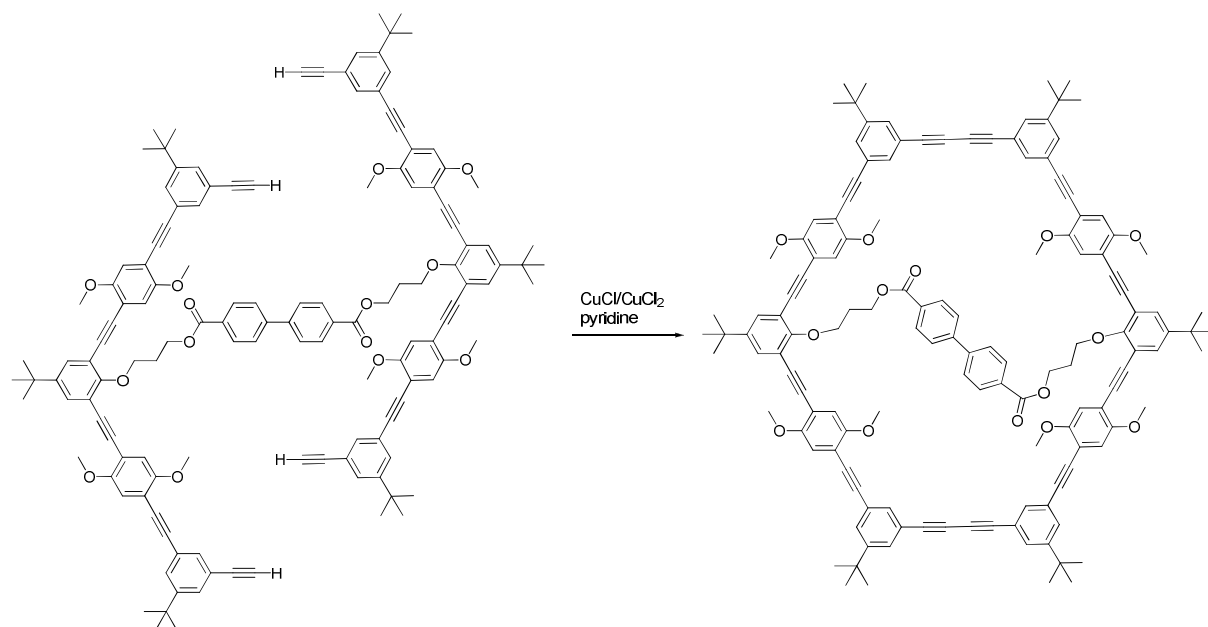
To attempt a more facile preparation of the monomer units, smaller oligomers were utilized for the intermolecular coupling between three or more building blocks which lowered the yield in favour of

linear oligomerization.^[1] Therefore, a template method has been established to provide a more efficient intermolecular coupling between readily accessible small precursors while maintaining a high cyclization yield. The reason for the kinetically controlled high selectivity of the reaction is the defined arrangement of the monomer moieties around an appropriate template with a specific size and reaction functionality. After the precursors assemble through covalent binding around the template moiety, intermolecular cyclization occurs, whereby the circular backbone is formed. The size of the rings can be controlled by template design and the template is afterwards chemically eliminated from the cavity rendering the macrocycles in moderate to high yields.^[1] The drawback of this method is the limitation of possible substrates, since they require specific binding groups to covalently bind to the template. Furthermore, extra reaction steps are required for the attachment and elimination of the template.^[1] An example of a template-assisted macrocyclization is published by Müllen and co-workers and shown in Scheme 2.4.^[6] A porphyrin acted as a template for the carbazole-based precursors and generated the templated macrocycle in 75% yield. The final macrocyclization step was performed via nickel-mediated Yamamoto coupling reaction in high dilution to prevent intermolecular coupling. The product was obtained in only 9% yield, presumably due to the high number of simultaneous C-C-bond forming reactions. The template was afterwards eliminated by hydrolysis with KOH to generate the conjugated ring.

Höger et al. utilized ester linkages covalently bond to a template to cyclize bisacetylenes using Glaser coupling methods.^[7-8] The cyclization step included only two homocoupling reactions at the same time (compared to the fourfold reaction in Scheme 2.4) and resulted in remarkable 92% yield (Scheme 2.5). Subsequently performed base-catalyzed hydrolysis gave the symmetric macrocycle.



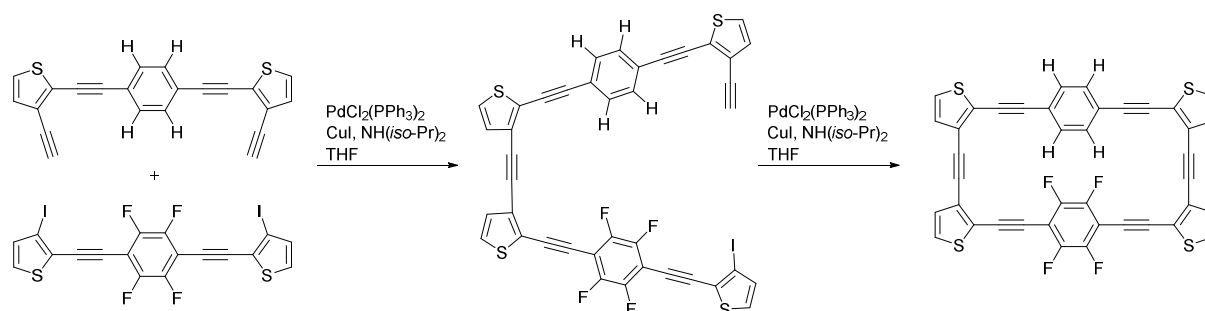
Scheme 2.4: Templated cyclization strategy of a carbazole-derived precursor with a porphyrin acting as a template.^[6]



Scheme 2.5: Synthesis of a phenylacetylene-derived macrocycle by a template-assisted strategy.^[7-8]

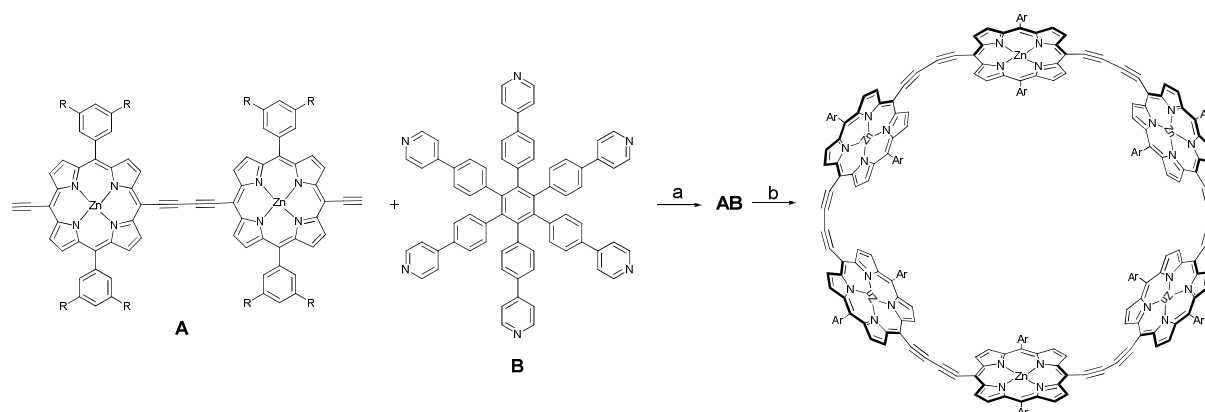
Marsella et al. used electrostatic interactions to template thiophene-based acetylenic cyclophanes (Scheme 2.6).^[9] They reported an example of a solution-state cyclization influenced by $\text{Ar}_\text{H}-\text{Ar}_\text{F}$

interactions. The formation of the cyclophane proceeded via a stepwise Sonogashira coupling reaction, which firstly generated a linear intermediate. Its conformation played the crucial role. The favoured interaction between the proton- and fluoro-aryl units led to an approach of both subunits and promoted the formation of the cyclic structure over a polymer. The linear intermediate served both as template and substrate. The reaction was carried out under high dilution and yielded the ring in 30% yield.



Scheme 2.6: Templat-assisted method via electrostatic interactions between Ar_H - Ar_F moieties.^[9]

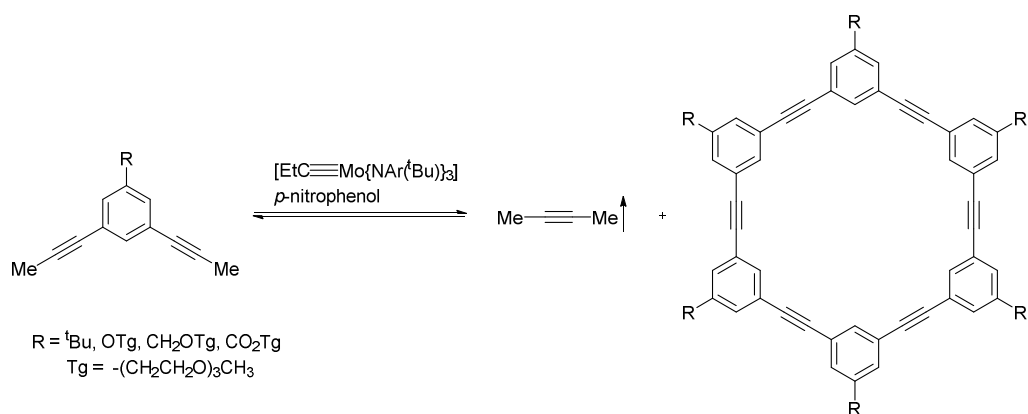
The research group of Anderson also employed the template-directed cyclization method and showed impressive studies on large π -conjugated porphyrin nanorings (Scheme 2.7).^[10-12] A porphyrin dimer **A** reacted with a hexapyridyl template **B** in a trimerization with subsequent oxidative homocoupling under Pd/Cu catalysis with iodine and oxygen. A highly stable cyclic hexamer complex **AB** was formed in 44% yield. The template was released by using the tertiary amine DABCO to obtain a porphyrin[6] macrocycle.



Scheme 2.7: Template-directed synthesis of a π -conjugated porphyrin[6] nanoring. a) $[\text{PdCl}_2(\text{PPh}_3)_2]$, CuI, I_2 , $\text{NH}(\text{iso-Pr})_2$, air. b) DABCO. R = *tert*-butyl.^[11]

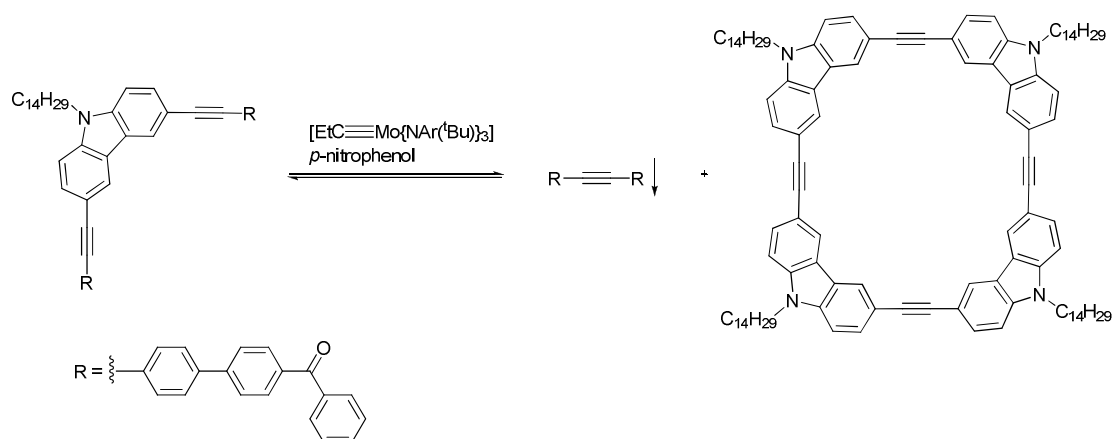
2.1.2 The thermodynamic controlled approach towards macrocycles

The major disadvantage of the synthetic strategies introduced above is that they involve kinetically controlled reactions with irreversible bond formation having no possibility to correct undesired C-C bond formation. This gives rise to low yields for the formation of the desired macrocycles. To favour macrocyclization, thermodynamically controlled reactions are considered to be more effective. The product distribution follows the relative stability of the products and is based on equilibrium processes. Such processes are not possible for most covalent bond forming reactions since the conditions required to initialize the back reactions by breaking undesired bonds and forming the thermodynamically most stable products are too harsh. However, there are some functional groups that can undergo equilibration or back reactions such as esters, acetals, hydrazones, imines or olefines (metathesis).^[1] Thermodynamically controlled metathesis reactions, such as imine, alkene, or alkyne metathesis, can be classified into the category of dynamic covalent chemistry. This methodology has been successfully applied to the preparation of shape-persistent macrocycles due to its reversible nature. Alkyne metathesis reactions are conventionally classified as vacuum- or precipitation-driven metathesis. For the first method, molybdenum or tungsten complexes have been used as catalyst to provide arylene ethynylene macrocycles.^[1] The catalysts should possess broad substrate compatibility and promote cyclooligomerization efficiently at low temperatures, and not require highly dilute conditions. Over the course of the reaction volatile by-products, such as acetylene, are constantly removed by vacuum which favourably shifts the monomer-oligomer equilibrium. In general, alkyl-substituted alkynes are more reactive than aryl-substituted alkynes, and electron-rich aryl-alkynes react faster than electron-poor aryl-alkynes.^[1] This is problematic in the reaction of an electron-deficient aryl-alkyne monomer unit, where an alkyl-alkyne is produced as the byproduct. If the byproduct cannot be efficiently removed from the reaction, a 'pseudopoisoning' effect will occur where competing metathesis reactions will take place with the more reactive alkyl-functionalized byproduct instead of the desired monomer.^[1,13] Phenylene-ethynylene-derived macrocycles published by Moore et al. reached yields in the range of 61-79%.^[13] However, large scale production failed and resulted in low yields presumably due to the 'pseudopoisoning' effect of the byproduct on the metathesis catalyst (Scheme 2.8).



Scheme 2.8: Conventional vacuum-driven alkyne metathesis reaction to produce arylene-ethynylene macrocycles.^[13]

To circumvent the 'pseudopoisoning' effect, a precipitation-driven alkyne metathesis was employed, in which the byproduct has low solubility in the reaction solvent and therefore precipitates from the reaction mixture. Further reaction with the catalyst is avoided and the byproduct can easily be removed from the mixture by filtration. With this method, large scale production of cyclic structures is possible since the undesired interference of the byproduct is overcome due to its non-reactivity. Metathesis reactions are advantageous due to the good accessibility of the precursor oligomers and high yields. However, growing structures have to remain soluble and should still be able to take part in the reversible reaction. As well, the synthesis of strained systems is clearly not favoured.^[1,14] Moore and co-workers synthesized a carbazole-based cyclo-tetrameric structure via a precipitation-driven metathesis, which is outlined in Scheme 2.9. The square-planar macrocycle was the only product formed and could be isolated in 84% yield.^[15]



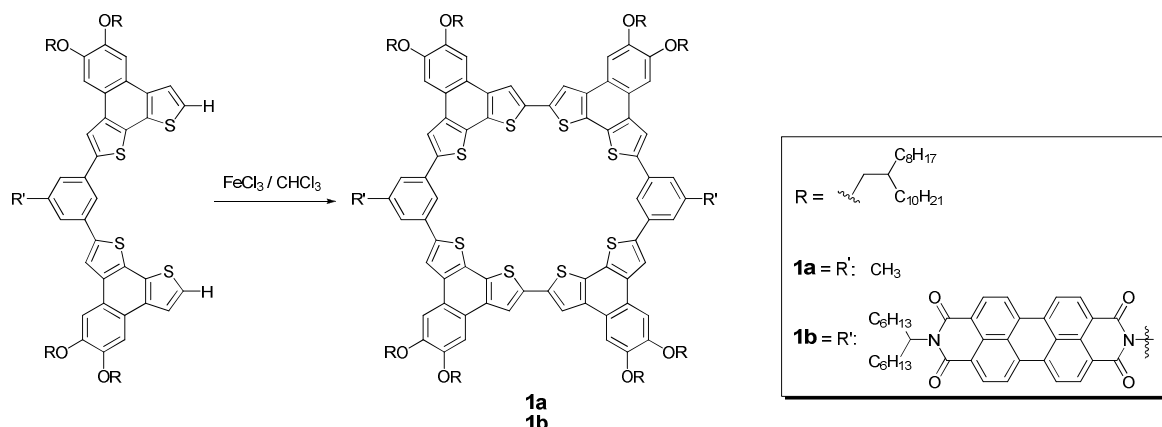
Scheme 2.9: Formation of a tetrameric macrocycle via precipitation-driven alkyne metathesis.^[15]

2.2 General macrocycles

Macrocycles have attracted increasing interest over the last few decades and a variety of different subgroups of macrocycles have emerged. Chemists have concentrated on fully conjugated *para*-phenylene or partially conjugated phenylene-macrocycles^[16-26], *ortho*-, *meta*-, *para*-phenylene-acetylene- and diacetylene-macrocycles^[27-44], carbazole^[6,45-51] and fluorene-containing rings^[52], pyrrole^[53-58] and pyridine-derived macrocycles^[59-63], naphthylene macrocycles^[28, 64] as well as Schiff base cycles^[65-67] and perethynylated dehydroannulenes.^[68-69] Since our institute focuses on thiophene-based advanced materials, an overview on mainly thiophene-containing macrocycles will be presented in the following sections.

2.2.1 Cyclic oligothiophenes with disrupted conjugation

Höger and co-workers studied macrocycles which contain thiophene moieties and revealed an incomplete conjugation due to incorporated benzene moieties which are linked via *meta*-positions.^[70-72] They have recently published shape-persistent electron-rich thiophene macrocycles with peripherically attached electron-poor perylenebisimide (PBI) units as well as methyl moieties.^[71] The key synthetic step included an intermolecular coupling of thiophene precursors using a FeCl₃-mediated oxidative coupling under high dilution conditions (Scheme 2.10). The macrocycles **1a** and **1b** were obtained in 27% and 23% yield, respectively, after purification by recycling-GPC. The fused subunits reduce rotational degrees of freedom of the thiophene units and are supporting the crucial cyclization step. UV/vis spectra clearly revealed the disrupted conjugation in the macrocycles since there are several separated maxima, which correspond to the perylenebisimide units as well as to the thiophene moieties. Macrocycle **1b** does not fluoresce, which can be ascribed to an electron transfer from the cyclic backbone to the PBI unit within the acceptor/donor ring. The ring was also investigated for its aggregation behaviour on a graphite surface using STM analysis, since the PBI blocks were not only introduced because of their electronic influence but also due to their strong attractive forces between the large π -expanded regions to gain supramolecular structure formation. In fact, assemblies into 1D chains are found on HOPG which are caused by intermolecular stacking of PBI units. As the alkoxy side chains adsorb entirely on the surface without any interdigitation, interactions between adjacent chains are diminished and prevent a 2D crystalline packing. The latter is only generated in small parts on the surface, where the alkoxy side chains do not completely cover the surface (Figure 2.2).^[71]



Scheme 2.10: Formation of methyl- and PBI-functionalized dithienonaphthalene macrocycles **1a** and **1b**.^[71]

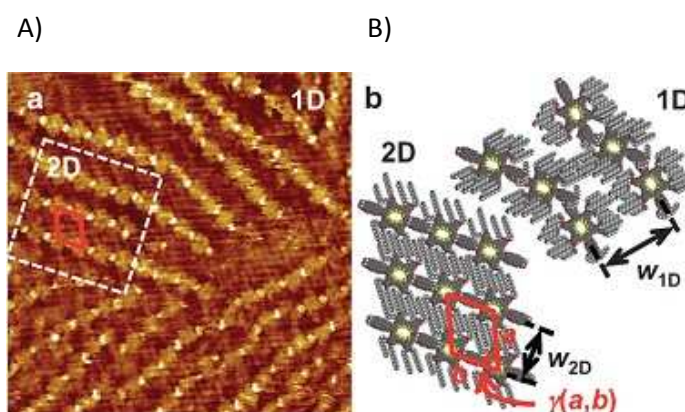
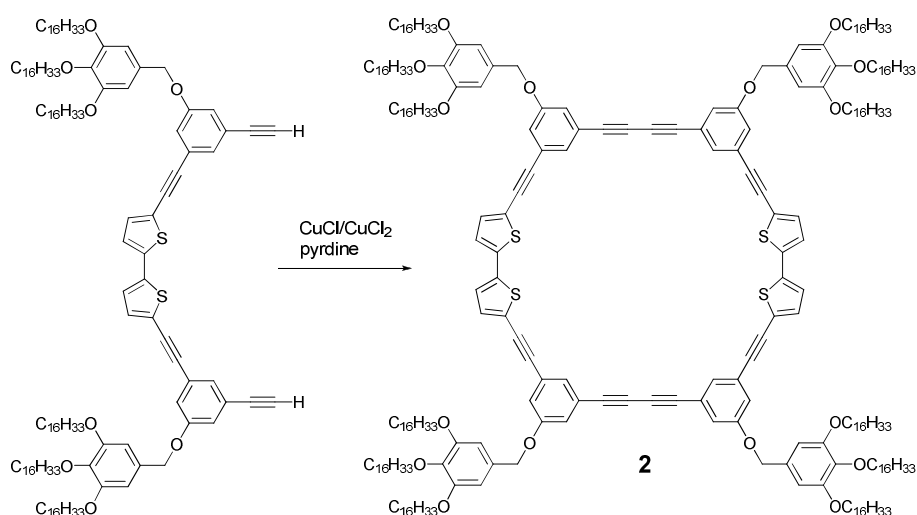


Figure 2.2: A) STM image of **1b** at the TCB/HOPG interface ($V_s = -0.7$ V, $I_t = 30$ pA). 1D arranged chains of **1b** through intermolecular stacking of PBI-units (bright spots) and 2D arrangements can be observed. B) Molecular models reflecting the 1D and 2D assemblies on the surface.^[71] Reproduced by permission of The Royal Society of Chemistry.

Höger et al. described other 2D structural arrangements of thiophene-based shape-persistent macrocycles on HOPG (Scheme 2.11, Figure 2.3).^[72] Macrocycle **2** was prepared via a Glaser-Eglinton coupling reaction under pseudo high-dilution conditions from a bisacetylene-terminated bithiophene derivative and obtained in 3% yield after gel permeation chromatography. The molecules self-assemble into a 2D structural monolayer on HOPG and have a perfect regular ordering over expanded large areas. Fullerenes were then co-adsorbed and STM measurements displayed superstructures with a 1:2 stoichiometry (**2**: C_{60}) due to the presence of two bithiophene moieties within one macrocycle. The C_{60} molecules are not trapped inside the cavity, but rather located at the periphery of the macrocycles, merely interacting with the bithiophene units. A donor-acceptor interaction between the electron rich thiophene and fullerene is most likely responsible for this kind of superstructure.^[72] A proposed structural model of the 1:2 adsorbate is depicted in Figure 2.3.



Scheme 2.11: Synthesis of macrocycle **2** via a Glaser-Eglinton coupling reaction.

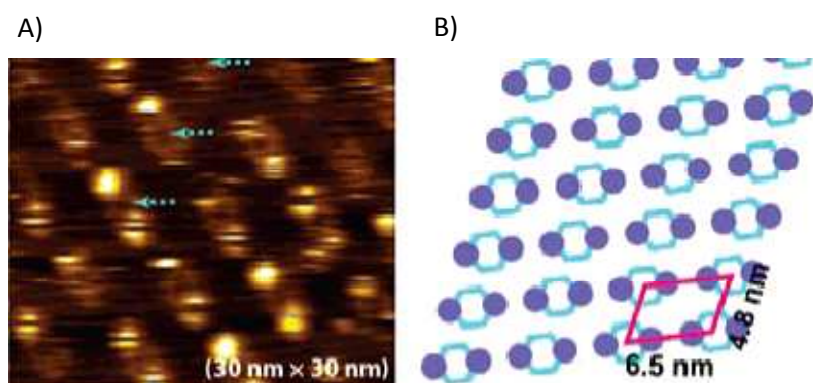


Figure 2.3: A) High-resolution STM image of the ordered adsorbates of C_{60} on **2** on HOPG ($V_{\text{bias}} = 1.0$, $I_t = 0.3$ nA). B) Proposed structural model of the absorption of fullerene molecules on top of the ordered macrocycle arrays. Blue structures represent **2** while the purple circles are C_{60} molecules.^[72] Reprinted with permission from *J. Am. Chem. Soc.* **2006**, 128, 4218. Copyright 2006 American Chemical Society.

Recently, Pan and Höger described the simultaneous deposition of a thiophene-based macrocycle and a cyclic metal-containing compound on a HOPG surface.^[70] Macrocycle **3** has been synthesized according to Glaser-Eglinton conditions starting from terminated acetylene precursors. The intermolecular, oxidatively induced dimerization was performed under pseudo high-dilution conditions and **3** was isolated in 20% yield after chromatography on recycling-GPC. STM images and structural models are presented in Figure 2.4. It was discovered that the macrocycles are arranged in a well-defined structural ordered monolayer on HOPG and act as a template for the deposition of the adlayer of metallacycle **4**. For each macrocycle, only one metallacycle was found and 1:1 substructures were formed. The exact array of the thiophene macrocycles was transformed to the layer of guest metallacycles. Interactions between the electron-rich thiophene moieties and electron-poor metallacycles are supposed to be the driving force for this behaviour.^[70]

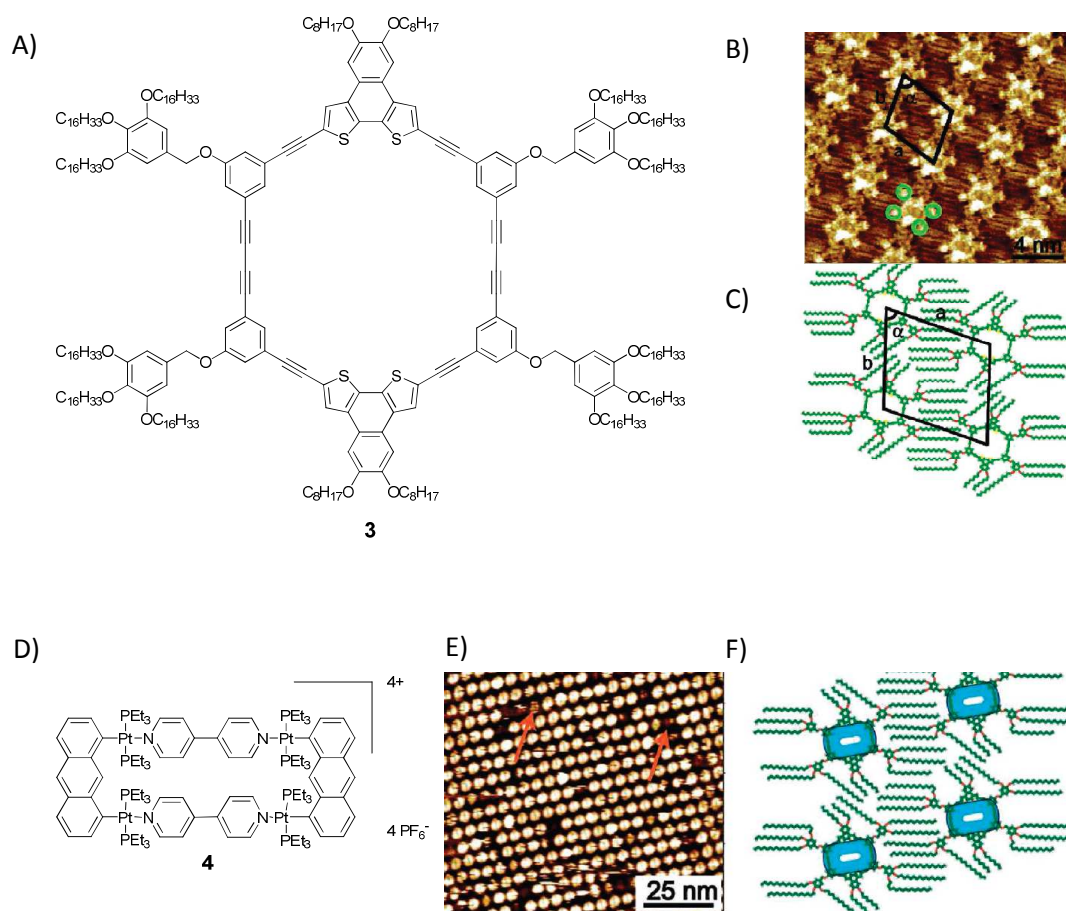
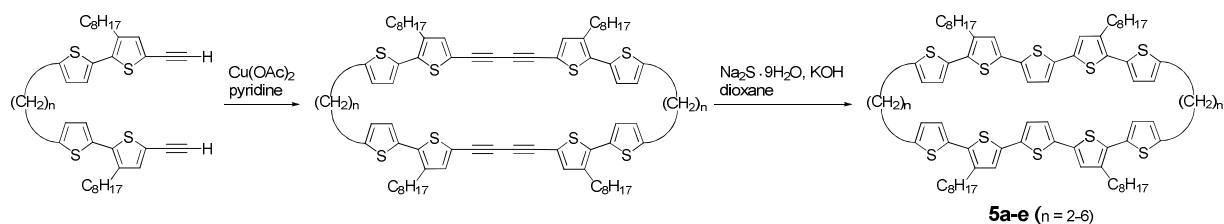


Figure 2.4: A) Structure of macrocycle **3**. B) High-resolution STM image of ordered monolayers of **3** on a HOPG surface at a concentration of $c = 0.5 \times 10^{-5}$ M ($V_{\text{bias}} = 408$ mV, $I_t = 694$ pA). C) Proposed structural model of the aggregation of **3**. An oblique unit cell is indicated in black. D) Structure of metallacycle **4**. E) STM image of ordered arrays of compounds **3** and **4** on HOPG ($V_{\text{bias}} = 1.17$ V, $I_t = 201$ pA). The red arrows indicate the underlying macrocycles. F) Proposed structural model of metallacycles **4** directly adsorbed on top of templated macrocycles **3**. The green structures represent **3** and the blue rectangles metallacycle **4**.^[70] Reprinted with permission from *J. Am. Chem. Soc.* **2010**, *132*, 1328. Copyright 2010 American Chemical Society.

Aso and Otsubo et al. worked on $[n.n]$ quinquethiophenophanes **5a-e**, which were considered as model compounds for charge carriers in conductive polythiophenes (Scheme 2.12).^[73-74] The macrocycles have been synthesized using an intermolecular double Eglinton-coupling reaction of twofold terminated alkyne precursors under high dilution conditions. Consecutive transformation of the incipient butadiyne units into thiophene moieties was performed by treatment with disodium sulfide. Yields of the macrocycles were in the range of 17-52%. Purification was accomplished using column chromatography followed by GPC. The two oligothiophene blocks within the cyclophane ring are arranged in a double-decker structure in a known typical anti- or syn-stacking fashion. This can be proven by ¹H NMR spectroscopy, where the β -protons are shifted up-field due to the diamagnetic ring current of the opposite oligophene. The cyclophanes were stepwise chemically oxidized using FeCl₃ in dichloromethane and investigated by means of UV/vis/NIR-absorption spectroscopy. The recorded spectra revealed that an one-electron-oxidation step results in a charge-delocalized radical cation (polaron) while double oxidation gave rise to a π -dimer formed from two radical cationic

species (polaron pair) instead of a bipolaron configuration. The π -dimerization was also confirmed by ESR analysis, whereby no positive ESR signal appeared due to the interaction of both radical cations.^[73-74]



Scheme 2.12: Synthesis of $[n.n]$ quinquethiophenophanes **5a-e** via an intermolecular Eglinton reaction.^[73-74]

Some years later, the same group published a rectangular oligothiophene-based macrocycle **6** containing benzothiophene units in the corners by using the same method as presented above. Macrocycle **6** is soluble in most common organic solvents due to a high number of *n*-decyl side chains which makes it accessible for solution-processed semiconducting devices. In fact, when **6** was used as a p-type semiconductor in organic field effect transistors (OFETs) a hole mobility of $7.3 \times 10^{-3} \text{ cm}^2 \text{ V}^{-1} \text{ s}^{-1}$ was measured (Chart 2.1).^[75]

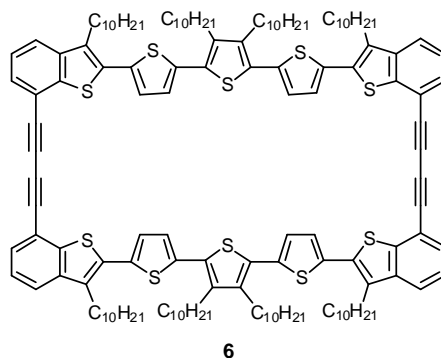


Chart 2.1: Structure of rectangular benzothiophene macrocycle **6**.^[75]

Very recently, cyclic structure **7** composed of dithienothiophene units and sulfur atoms has been presented by the group of Mazaki and was synthesized via a palladium-catalyzed coupling reaction.^[76] The fused moieties are connected to each other via sulfur atoms (Chart 2.2). Further characteristics and investigations are currently under preparation.

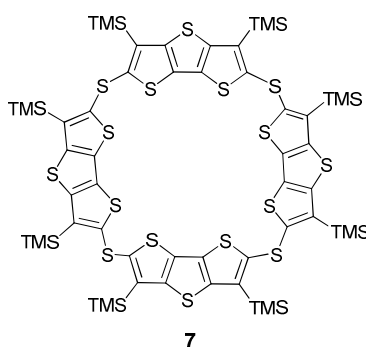


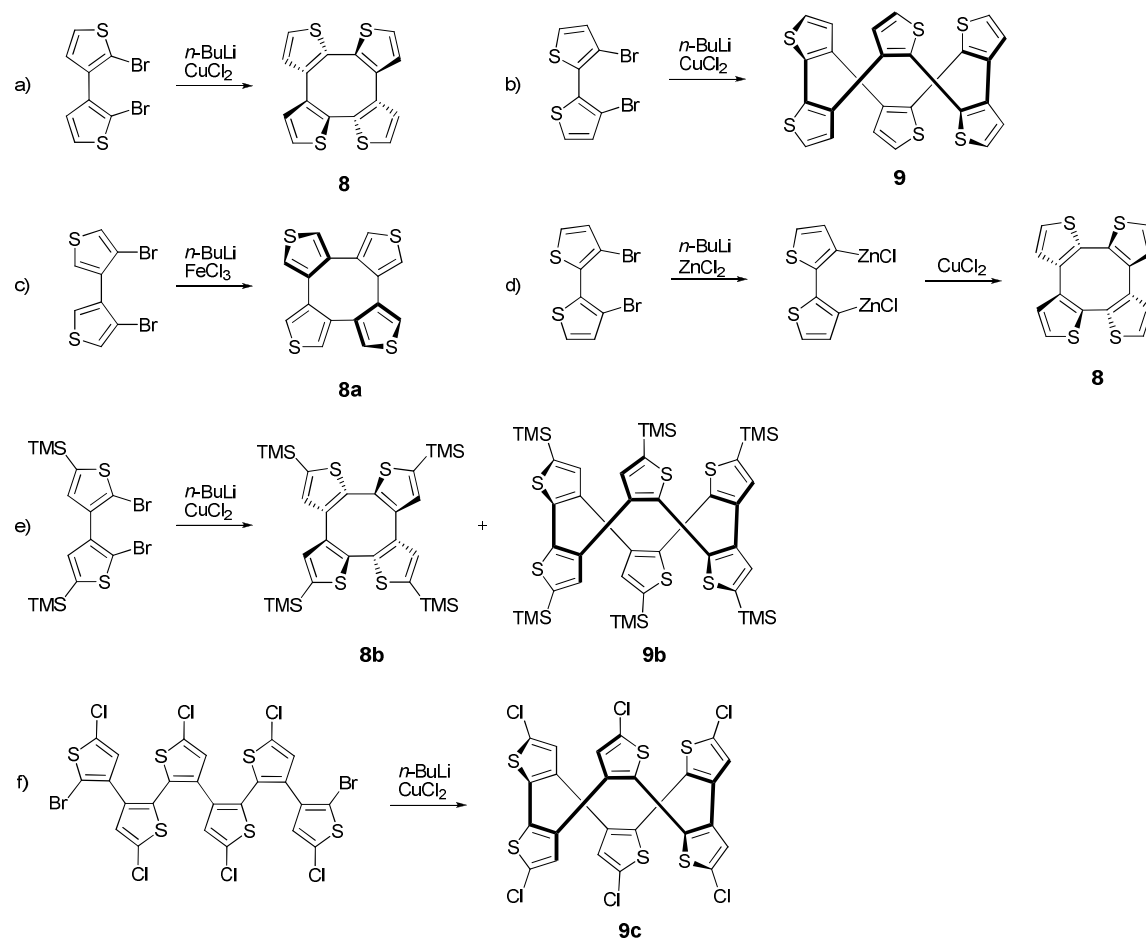
Chart 2.2: Structure of dithienothiophene composed macrocycle **7**.^[76]

2.2.2 Cyclic oligothiophenes with complete conjugation

2.2.2.1 α,β -Cross-linked cyclic oligothiophenes

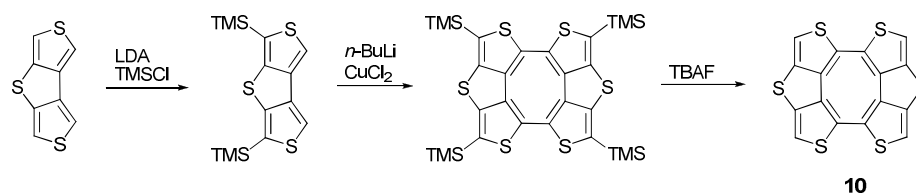
To date, only few examples of nanoscale π -expanded fully conjugated thiophene-containing macrocycles have been reported so far.^[27,77-86] Some examples are listed and discussed with respect to synthesis, photophysical, and aggregation properties in the following section.

An early synthesis of cycles comprising only thiophene moieties along the backbone was accomplished by Kauffmann and co-workers in the late 1970s.^[87-88] They subjected 2,2'-dibromo-3,3'-bithiophene to a metal-halogen exchange reaction with subsequent copper-catalyzed oxidative homocoupling and obtained α,β -cross-conjugated macrocycle **8** in 23% yield. The corresponding trimeric cycle was prepared from 3,3'-dibromo-2,2'-bithiophene under the same reaction conditions, affording **9** in 4% yield. The macrocycles were non-planar, which was confirmed by X-ray crystallographic analysis for molecule **8a** (Scheme 2.13). The cycles did not exhibit a strong absorption due to β,β' -linkages of the thiophene units, which gave weak conjugation and poor overlapping of the π -orbitals.^[87-88] Iyoda et al. later improved the synthesis of macrocycle **8** using a copper-mediated coupling reaction of organozinc species and gained 40% yield (Scheme 2.13, d).^[89] Seven years later, Wang et al. reported the synthesis of trimethylsilyl (TMS)-substituted cross-conjugated macrocycles **8b** and **9b** in 41% and 36% yield, respectively (Scheme 2.13, e).^[90] The advantage of this strategy was the introduction of TMS protecting groups at the α -positions in the 2,2'-dibromo-3,3'-bithiophene monomer unit which prevented undesired side reactions occurring at the acidic α -positions during halogen-lithium exchange. The TMS groups are easily cleaved off under acidic conditions to generate target cycles **8** and **9**. Marsella et al. synthesized α,β -linked cyclic sexithiophene **9c** with chlorine atoms attached at the peripheral thienyl positions (Scheme 2.13, f).^[91] These provide reactive groups for further functionalization such as covalent extensions via cross-coupling chemistry, as well as influences the solid-state structure via Cl...Cl interactions that induce a zigzag-type arrangement which was determined by X-ray crystallographic analysis. The synthetic procedure included the buildup of a sexithiophene precursor followed by a copper-catalyzed oxidative coupling as the final step. Cross-conjugated compound **9c** was obtained in 20% yield.



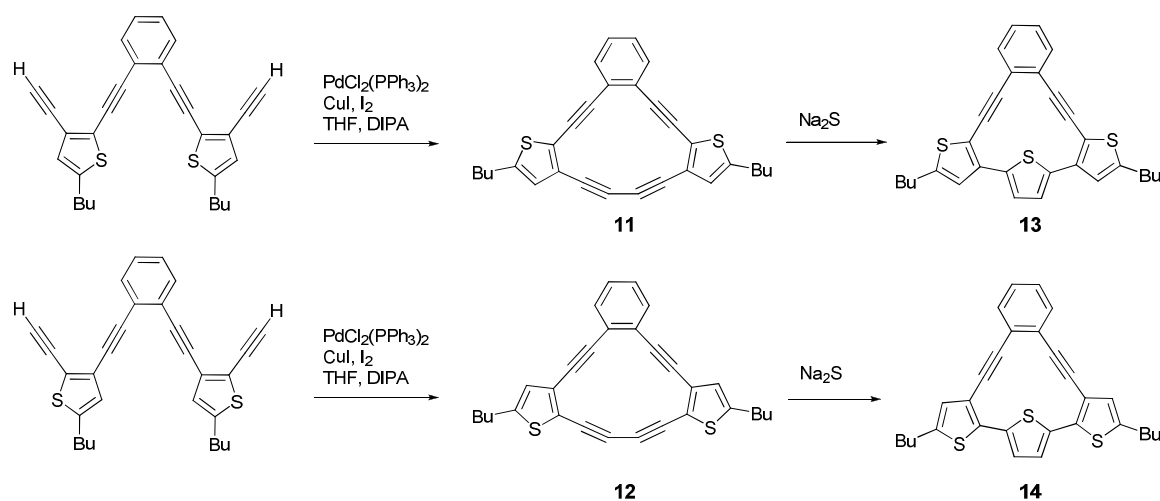
Scheme 2.13: Copper-, ferrocene- and zinc-mediated oxidative couplings to generate α,β -cross linked conjugated macrocycles.

Iyoda et al. modified the α,β -cross-conjugated cycle **8** by synthesizing a cyclic tetrathiophene **10** bearing a planar cyclooctatetraene core unit (Scheme 2.14). The planarity can be adjusted by the different bond lengths of utilized bridging atoms in the fused units. The synthesis is started from a α -TMS-protected dithienothiophene unit, which prevents undesired side reactions in the crucial macrocyclization step. Herein, lithiation of the remaining free α -positions of the annulated dithienothiophene is performed followed by an intermolecular copper-mediated dimerization to gain the α -TMS-protected ring in 45% yield. The TMS groups are then quantitatively cleaved off with TBAF, revealing symmetrical macrocycle **10**.^[92]



Scheme 2.14: Synthesis of the planar thiophene-derived macrocycle **10**, bearing a cyclooctatetraene core unit.^[92]

Haley et al. described expanded cyclic α,β -cross conjugated oligothiophenes by concentrating on dehydrothieno[14]annulenes and their conversion into terthiophene derived cycles.^[83,93] These macrocycles were mainly investigated for their cyclic conjugation. Synthesis included Sonogashira cross-coupling reactions to generate various acetylene-terminated units, which were subjected to an intramolecular acetylenic homocoupling cyclization (Scheme 2.15). Moderate yields, which averaged around 50%, were achieved for diynes **11** and **12**.^[83] Subsequent transformation of the butadiyne linkages to terthiophene moieties was accomplished with disodium sulfide to form cycles **13** and **14**. The end-capped butyl groups should improve solubility and stability and prevent the macrocycles from undergoing undesired oxidation processes. In comparison to the dehydrothieno-annulenes **11** and **12**, the macrocycles with inserted terthiophene units (**13** and **14**) showed absorptions at lower energies due to a higher π -electron density caused by the additional sulfur atom and better electron delocalization. The bridging 1,2-diethynylphenyl unit diminishes the rotational freedom of the terthiophene subunit and increases π -orbital overlap as well. Both factors raise the HOMO energy and lower the LUMO energy level, thereby decreasing the HOMO-LUMO gap. Haley et al. also examined the influence of the orientation of the thiophene moieties in **11** and **12** in absorption spectroscopy and discovered a blue-shift of the maximum with an 'up'-configuration of the thiophene units adjacent to the butadiyne linkage.^[83,93] The exact cause of the effect has not yet been ascertained, although Haley gives some assumptions: One possible correlation is the decreased dipole moment in the 'up'-configuration, which enlarges the energy gap and results in a hypsochromic shift. Another consideration is the repulsion between a sulfur lone pair of an 'up' thiophene and the alkyne π -orbital of the bowed monoyne moiety, leading as well to the mentioned blue-shift. A reverse view would be a decreased interaction between the sulfur lone pair of a 'down' thiophene and the alkyne π -orbital of the dyine linkage, which causes a bathochromic shift.



Scheme 2.15: Synthesis of dehydro[14]annulenes **11** and **12** and their terthiophene-containing analogues **13** and **14**, presented by Haley et al.^[83,93]

2.2.2.2 α,α -Conjugated cyclic oligothiophenes

A great deal of effort has been made to synthesize fully α -conjugated aromatic macrocycles. First studies on this topic focused on [18]annulene **15**, published by Sondheimer^[94] which has been regarded as a fundamental structure in aromatic chemistry, since it follows Hückel's rule of a planar, monocyclic, and conjugated system with $[4n+2]$ π -electrons. The porphyrin system **16** can be formally regarded as a heteroatom-bridged structural variant of [18]annulene (Chart 2.3). These systems have been widely examined.^[53, 57-58] However, sulfur bridged derivatives like **17**, that contain α -connected thiophene units, have had considerably less attention.

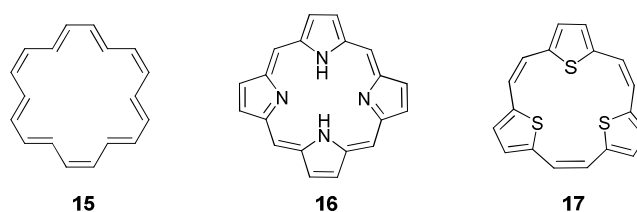
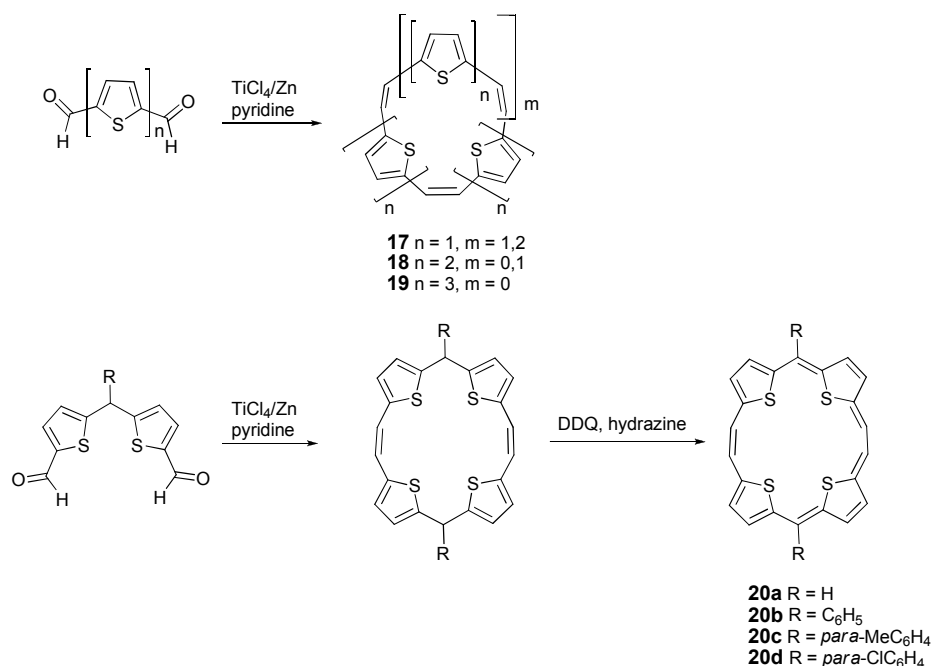


Chart 2.3: [18]annulene **15** and corresponding nitrogen **16** and sulfur **17** analogues.

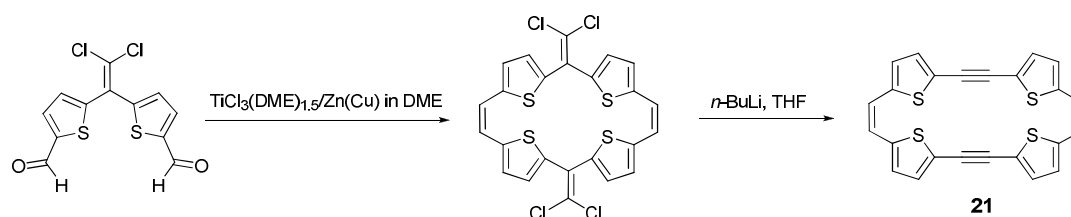
Cava et al.^[78] synthesized several neutral and oxidized thiophene-derived annulenes with thiophene units α -connected via ethylene bridges. The thiophene subunits consisted of either a mono-, bi-, or terthiophene moiety. The compounds were synthesized by an intermolecular cyclooligomerization using McMurry cross-coupling reactions as the key step starting from diformylated oligothiophenes (Scheme 2.16, top line). Yields were in the range of 4.7% for **17** ($m = 2$) to 64% for **19**. Macrocycle **17** ($m = 1$) showed no significant aromatic ring current in the proton NMR spectrum mainly due to its non-planarity, although it is a $[4n+2]$ π -system. The first neutral thiophene-derived annulene, which exhibits an aromatic ring current is the [22]annulene **20a**, which was obtained from a methylene-bridged bithiophene precursor (Scheme 2.16). After cyclization using McMurry reactions, the dihydro macrocycle was dehydrogenized and reduced by treatment with DDQ and hydrazine. The thiophene protons are strongly deshielded when examined by proton NMR spectroscopy and the corresponding signals are located far downfield in the recorded spectrum (10.86 and 10.84 ppm). Designated hexathiahomoporphycene **19**, a [28] annulene, complies with the $[4n]$ π -rule, but does not exhibit antiaromatic behaviour. The signals detected in the proton NMR spectrum revealed expected chemical shifts of the benzoid ring current of the single thiophene moieties itself (6.94 - 6.26 ppm). Partial conjugation can be observed in the absorption spectroscopy since several strong maxima appeared. Macrocycle **19** was then subjected to oxidation by means of sulfuric acid in order to generate an aromatic 26 π -electron dication. This planar species exhibited a strong peripheral aromatic ring current effect in the ^1H NMR spectrum and the greatly deshielded protons are strongly shifted downfield (12.10 - 11.28 ppm).^[78]



Scheme 2.16: Synthesis of several thiophene-derived annulenes by Cava et al.^[78] and Singh et al.^[95]

In 2010, Singh and co-workers^[95] advanced the work of Cava by preparing neutral aromatic *meso*-substituted tetrathia[22]annulene derivatives **20b-d** (Scheme 2.16). The macrocycles were as well synthesized by a McMurry-coupling reaction with subsequent dehydrogenation of the bridging methylene groups. The aromaticity of the 22 π -electron systems was confirmed by proton NMR spectroscopy, which indicated a peripheral aromatic ring current. The substituents at the bridging positions alter the stacking pattern in the solid state and improve electric transport properties to make them promising active materials for organic field effect transistors.^[95]

In contrast to the non-planar macrocycles of Cava, Oda and co-workers worked with planar annulenes consisting of thienyl, acetylene, and ethynylene subunits (Scheme 2.17). Macrocycle **21** was prepared by a McMurry-cyclooligomerization reaction from a dialdehyde precursor. The chlorinated intermediate was treated with *n*-BuLi (2.2 eq.) and a Fritsch-Buttenberg-Wiechell rearrangement yielded **21** in 30%.^[80] Characterization by X-ray crystallography revealed a nearly planar structure in the solid state. However, the 24 π -electron system does not show any peripheral anitaromatic ring current assuming almost no conjugation within the ring due to a non-planar conformation in solution. Since no changes occur in the ^1H NMR spectra at -90°C , it is likely that the conformation does not change in the frozen state. Another explanation for the absence of the ring current is the strong aromatic resonance energy of the thiophene units, which gives them the tendency to remain an isolated 6 π -electron system.^[80]



Scheme 2.17: Synthesis of macrocycle **21** by Oda et al.^[80]

Anand and his research group studied neutral, stable aromatic and antiaromatic cyclic oligothiophenes. Inspired by antiaromatic isophlorin **22** (Chart 2.4), they synthesized 20 π -electron isophlorin derivative **23**, which consists of furan and thiophene units (Scheme 2.18). The synthetic strategy is a modified Rothemund-type synthesis, wherein diols are condensed with furanes or oligothiophenes under Lewis-acidic conditions with consecutive oxidation using FeCl_3 to obtain fully conjugated systems. Macrocycle **23** was isolated in 6% yield and represents a stable isophlorin derivative due to the strong electron withdrawing effect of the pentafluorophenyl groups on the *meso* carbons of the macrocycle. The cycle obeys Hückel's $[4n]$ π -electron rule and showed a paratropic ring current in the proton NMR spectrum confirming its antiaromaticity.^[96]

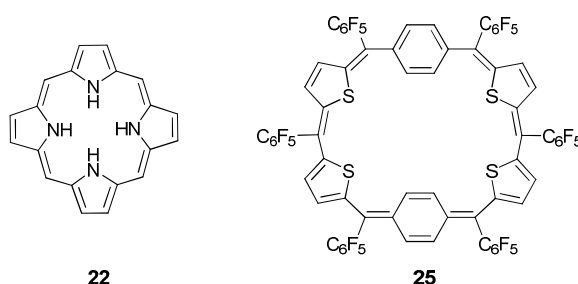
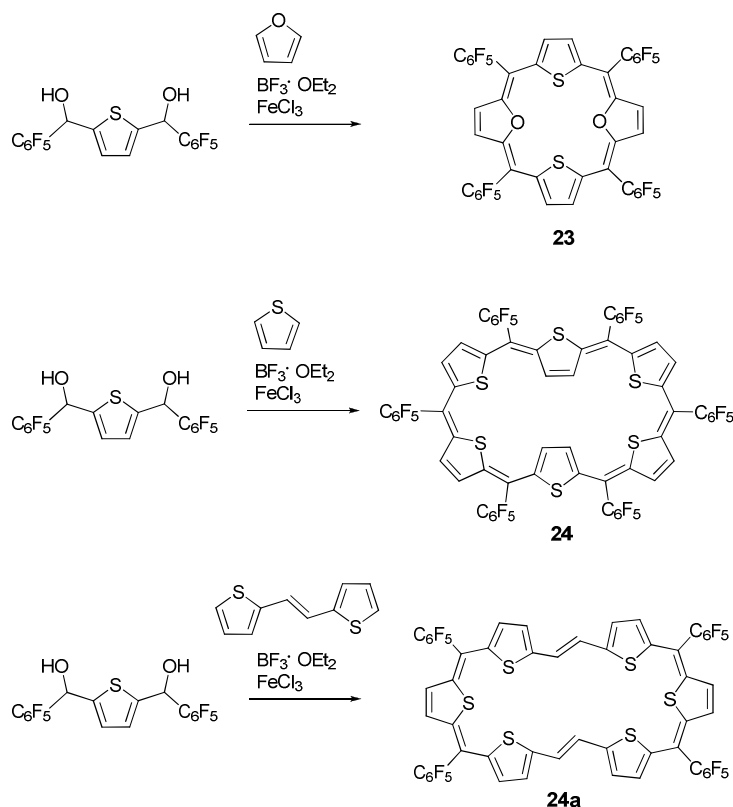


Chart 2.4: Isophlorin **22** and cyclic oligothiophene **25**, published by Anand et al.^[84]

One year later, Anand et al. published the expanded thiaisophlorin system **24** by inserting additional heterocyclic rings and increasing the length of the π -conjugated network (Scheme 2.18). The 30 π -electron macrocycle is an aromatic system with a diatropic ring current confirming the annulenoid structure with delocalized π -electrons along the cyclic backbone. The synthesis also follows the modified Rothemund-type method and is carried out under high dilution conditions, in which **24** was isolated in 11% yield.^[97] Recently, Anand et al. substituted two methine carbon bridges of **24** by two ethylene moieties to convert the $[4n+2]$ π -electron system into the $[4n]$ π -electron system **24a**. The expanded π -electron delocalization with annulenoid character is well demonstrated by a large red-shift of the absorption maximum around 500 nm. These relatively small macrocycles possess a more red-shifted absorption maximum than larger cyclo[*n*]thiophenes presented in this thesis with values around 450 nm. Macrocycle **24a** did not show any change in the absorption maximum upon treatment with oxidizing reagents like 2,3-dichloro-5,6-dicyano-1,4-benzochinone (DDQ), thus confirming the stability of the 32 π -electron system. The broad and weakly intense absorption band

in the range of 600 - 900 nm can result from unequal participation of the heteroatoms in the delocalized π -electron system.^[86] The C_6F_5 -substituted systems were found to assemble into well-defined supramolecular structures in the solid state through strong intermolecular C-H \cdots F and π - π -interactions and may present good materials for organic electronics.^[97]

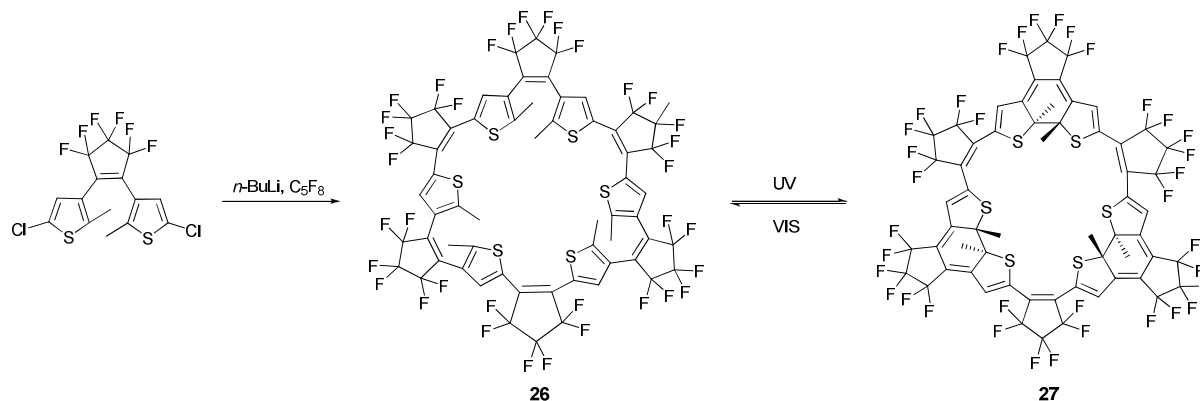


Scheme 2.18: Synthesis of expanded isophlorins reported by Anand et al.^[86, 96-97]

The same group published benzene-incorporated macrocycle **25**, which contains one quinoid and one Kekulé form for benzene within an α -conjugated thiophene-based macrocyclic system (Chart 2.4). The aromatic ring exhibited a diatropic ring current effect, whereby the phenylene protons appeared as a singlet since the exchange between the two forms – Kekulé and quinoid – is too fast and no differentiation between shielding and deshielding effect takes place on the NMR time scale.^[84]

Liu and co-workers^[98] studied the photochromic properties of perfluorinated thiophene-based macrocycles (Scheme 2.19) since photochromic materials are interesting due to their potential application in optoelectronic devices such as displays. Macrocycle **26** was prepared from dichlorinated bithienylperfluorocyclopentene, which was dehalogenated with *n*-BuLi and then reacted with perfluorocyclopentene to give **26** in 2.6% yield after column chromatography. The incorporated dithienylethene moiety is a thermally stable, resistant and photoactive system. Its photochromic effect is based on the reversible process of ring-closure and ring-opening upon

irradiation. This phenomenon has now been transferred to ring-opened macrocyclic compound **26**, which was subjected to irradiation with UV light and was converted into the fully π -conjugated closed-ring isomer **27**. The process was followed by absorption spectroscopy since the conjugated backbone of the closed form induced a red-shifted absorption band at 604 nm. Upon irradiation with visible light, the reverse reaction occurs and the mentioned absorption band diminished.



Scheme 2.19: Synthesis of photoactive ring **26** and photochromic effect: Induced ring-closure of macrocycle **26** by irradiation with UV light to obtain fully π -conjugated compound **27**.^[98]

In 2003, Mayor^[82] reported the fully conjugated giant macrocycle **28** consisting of ethynylene and butadiyne units connected via 2,5-thienyl and *para*-benzene subunits. The calculated inner diameter was 11.8 nm (Chart 2.5), which is enormous for these types of systems since they are typically around 1–4 nm.^[27] The preparation followed a stepwise synthesis of oxidative acetylene-coupling reactions to gain a final linear hexadecamer as the monomer unit. The intramolecular cyclization via an oxidative coupling reaction was performed under high dilution conditions and giant macrocycle **28** was isolated in 38% yield after purification via column chromatography. The absorption maximum is located at $\lambda = 461$ nm and reflects a conjugation along the cyclic backbone. Studies towards persistent ring currents in magnetic fields were planned.^[82]

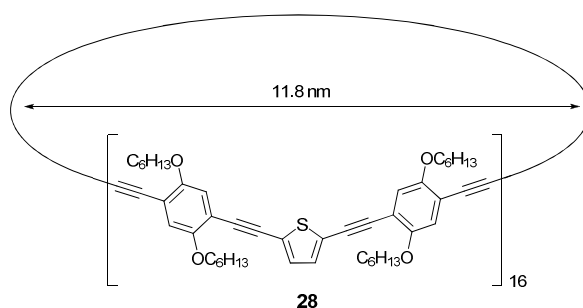


Chart 2.5: Structure of giant macrocycle **28** with an inner diameter of 11.8 nm.^[82]

Iyoda et al. studied π -conjugated nanosized macrocycles (more than 1 nm in diameter) and giant macrocycles with more than 2 nm in diameter. The macrocycles contained thienylene, ethynylene, and vinylene subunits and were prepared via a McMurry-coupling reaction starting from a five- or

six-membered diformylthienylacetylene unit using TiCl_4 -Zn-pyridine in tetrahydrofuran (Chart 2.6). The intermolecular cyclooligomerization took place under moderately dilute conditions to generate a mixture of the different cyclic oligomers **29a-e** and **30a-d** with up to 30 thiophene units and 6 nm inner cavities. The individual rings could be separated using gel permeation chromatography. Yields ranged between 39% for the smallest and 1.2% for the largest cycle. Intramolecular cyclization of the precursor units was not observed. Vinylene-free cyclo[n](2,5-thienylene-ethynylene)s **31a,b** were obtained from three different routes; a bromination-dehydrobromination procedure, intramolecular Sonogashira-coupling reaction from longer linear oligomers or a 'double elimination procedure' starting from the condensation of sulfone anions and aldehydes.^[79, 99-100]

The macrocycles were investigated by means of absorption and emission spectroscopy, whereby a red-shift for the absorption maxima with increasing number of thiophene units is observed reflecting almost full conjugation through the cyclic backbone. Even though the larger cycles are predicted to adopt a bended or twisted conformation in solution, the π - π overlap is still maintained. The emission maxima of the different macrocycles are located at nearly the same wavelength indicating the electron deactivation from the same excited energy state. Analysis by cyclic voltammetry exhibited two to three reversible redox waves with low first oxidation potentials. The number of transferred electrons per redox wave was investigated using rotating disc electrode and revealed a multiple-electron step. The oxidized states were as well induced by chemical oxidation with FeCl_3 and characterized by UV/vis/NIR absorption spectroscopy. The radical cation species were surveyed with electron spin resonance (ESR) and showed broad signals confirming the existence of radicals.^[99]

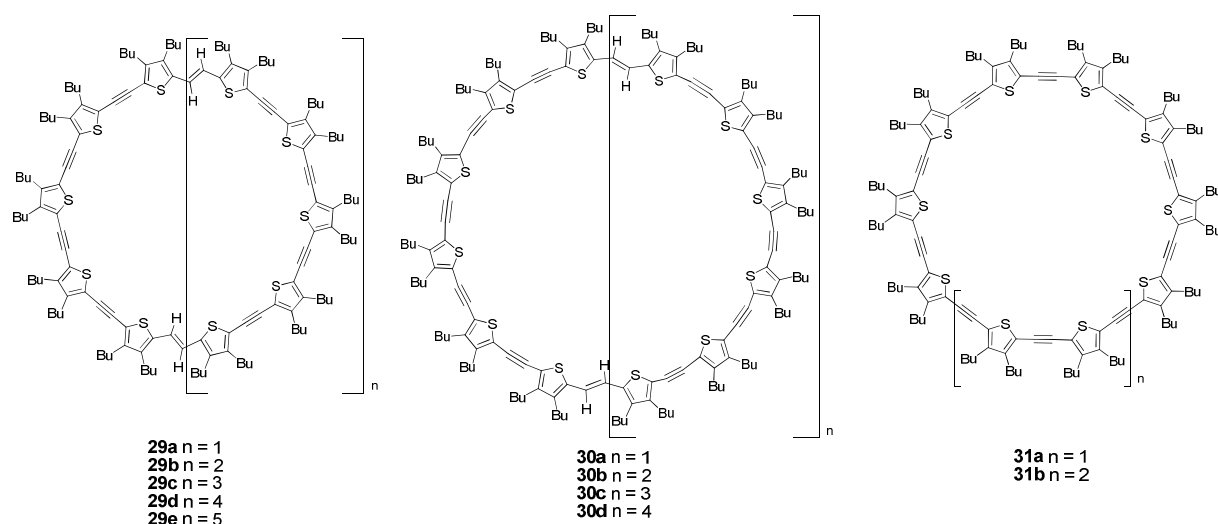


Chart 2.6: Structures of two series of vinylene-consisting macrocycles **29a-e** and **30a-d** and only acetylene included linkers **31a,b**.

The smallest cycles of the series **29a-e** and **30a-d** with a various number of unsaturated ethynylene bonds were investigated by X-ray crystallography. The crystal structures of **29a** and **30a** are shown in

Figure 2.5. A circularly shaped form with a *cisoid*-conformation, in which all sulfur atoms are directed into the insight of the cavity was observed for **29a**. The distance between the sulfur atoms ranged from 17.1 to 19.9 Å. The rings were partially stacked with a distance of 3.6 Å between molecules to form channels. In contrast to the nearly round-shaped structure **29a**, two molecules in **30a**, which are adjacent to the flexible double bonds, adopt a *transoid*-conformation and bend into the cavity to release ring strain.^[99-100]

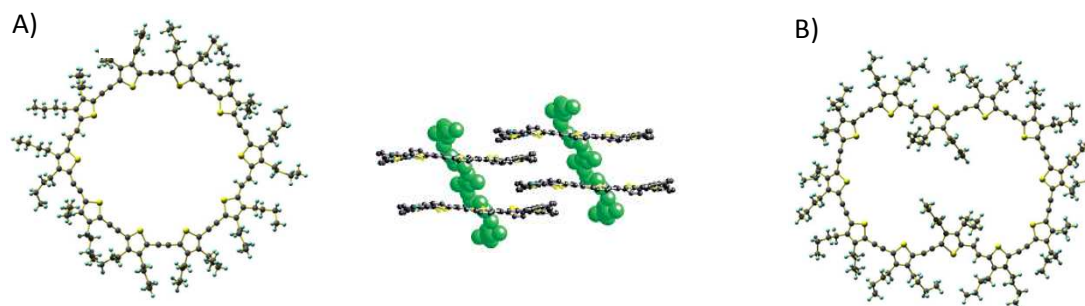


Figure 2.5: A) crystal structure of **29a**, B) crystal structure of **30a**.^[99-100] Reprinted with permission from *J. Am. Chem. Soc.* **2006**, 128, 16740; *J. Am. Chem. Soc.* **2008**, 130, 3252. Copyright 2006, 2008 American Chemical Society.

Although macrocycle **29a** formed single crystals from recrystallization, its larger analogues arranged into supramolecular structures, which are depicted in Figure 2.6. Macrocycles **29b** and **29c** with 15 and 20 thiophene units, respectively, arranged in nanofibers of 100-200 nm thickness, whereas **29d** and **29e**, with 25 and 30 moieties, formed chained nanoparticles of 300-800 nm size.^[101]

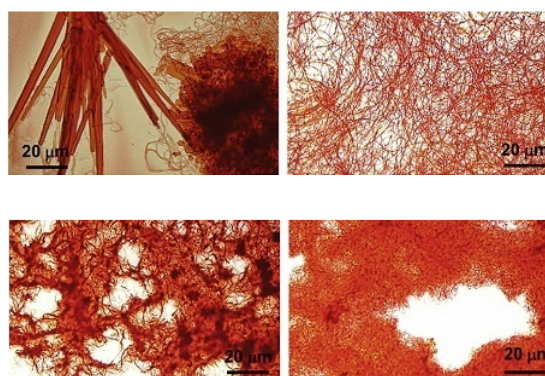
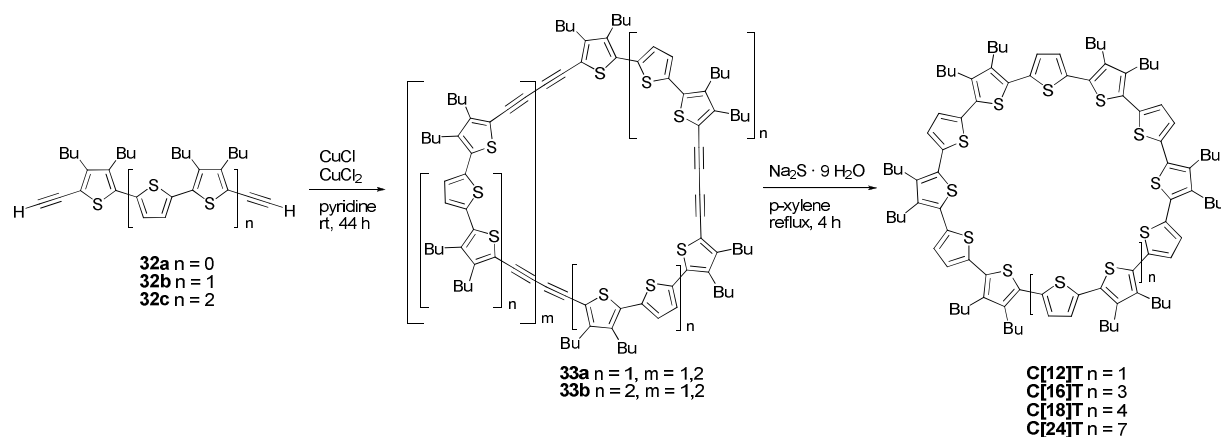


Figure 2.6: Microscopic images of nanofiber- and nanoparticle formation of higher macrocyclic analogues.^[101]

The next advanced step within the topic of cyclic π -conjugated oligothiophenes would be the synthesis of only thiophene-consisting, fully α -conjugated cyclo[n]thiophenes relating to well known α -oligo- and polythiophenes. The thiophene moieties should be α -connected via single bonds without any additional linkers such as phenyl-, ethylene-, or acetylene groups. The following chapter will give detailed insight into the development of the designated ‘metal-assisted template approach’, which was elaborated at our institute to generate cyclo[n]thiophenes with expanded π -conjugation.

2.3 Fully α -conjugated cyclo[*n*]thiophenes using the ‘metal-assisted template method’

A first attempt to synthesize fully α -conjugated cyclo[*n*]thiophenes was carried out in our institute in the late 1990s.^[102-103] The small building block 3,4-dibutyl-2,5-diethynylthiophene **32a** was subjected to various cyclooligomerization processes involving oxidative acetylene-coupling reactions under Glaser- (CuCl/ CuCl₂/ pyridine), Eglinton- (Cu(OAc)₂/ pyridine/ MeOH), or Hay-conditions (CuCl/ O₂/ TMEDA/ CHCl₃). An immediate reaction took place during all three reactions, producing a non-separable mixture of linear and cyclic products.^[102-103] In general, the efficiency of the macrocyclization step is influenced by the number of precursors involved. The lower the number of reacting monomer units, the higher the chance to minimize linear side products and shift the equilibrium towards ring production. Therefore, enlarged thiophene precursors were established and a first successful synthesis of fully α -conjugated thiophene macrocycles was managed by Krömer in 2000.^[81, 104-105] He prepared a series of different ring sizes based on terminally ethynylated ter- and quinquethiophene oligomers, **32b** and **32c**, respectively, under modified Eglinton-Glaser conditions (Scheme 2.20). Mixed cyclo(oligothiophene-diacetylenes) **33a,b** were obtained in 2-12% yield and subsequently converted with disodium sulfide into the desired fully π -conjugated cycles C[12]T, C[16]T, C[18]T, and C[24]T. Since this method was based on a statistical cyclooligomerization under high dilution conditions, product yields were very low. The inner diameter of the macrocycles were calculated on semiempirical level and revealed values up to 3 nm.^[81, 104-105]



Scheme 2.20: Synthesis of fully π -conjugated cyclo[*n*]thiophenes with 12, 16, 18, and 24 chain links.

No antiaromatic ring current was observed for the macrocycles in proton NMR spectra, although they obey Hückel's $[4n]$ π -electron rule. This indicates a more benzoid than annulenoid character of the rings. Besides the characterization via proton NMR spectroscopy and mass spectrometry, C[12]T was investigated with respect to its self-assembling properties on a HOPG surface and showed highly ordered 2D-crystalline monolayers. The images displayed in Figure 2.7 were recorded via STM measurements and revealed a perfect hexagonal ‘honeycomb’ pattern of the rings with an optimal

packing density and regular alignment over a large area at the solution/HOPG interface. Due to a certain distortion of each second thiophene moiety, the butyl side chains are not within the thiophene plane, but bent downwards to adopt a rather 'spiderlike' conformation. The butyl side chains allow intermolecular interactions between adjacent molecules. Van der Waals forces are typically the driving force for the self-organization of alkylated oligothiophenes and favour a close packing of the rings on the surface. On top of the uniformly C[12]T-covered surface, C₆₀-molecules adsorbed uniquely and ordered as a second monolayer to form 1:1 π -acceptor(A)- π -donor(D) complexes through host-guest interactions. The template layer of the macrocycles is not harmed by the deposition of the fullerene molecules. Even the D-A complexes remained stable during STM-measurements. The maximal π - π -integration between both molecules is located on top of the conjugated rim of the ring. Although a fullerene would fit into the interior of the macrocycle, the cavity is not occupied by the spherical molecule. Multiple complexation by more than one fullerene per macrocycle did not appear.^[106-107]

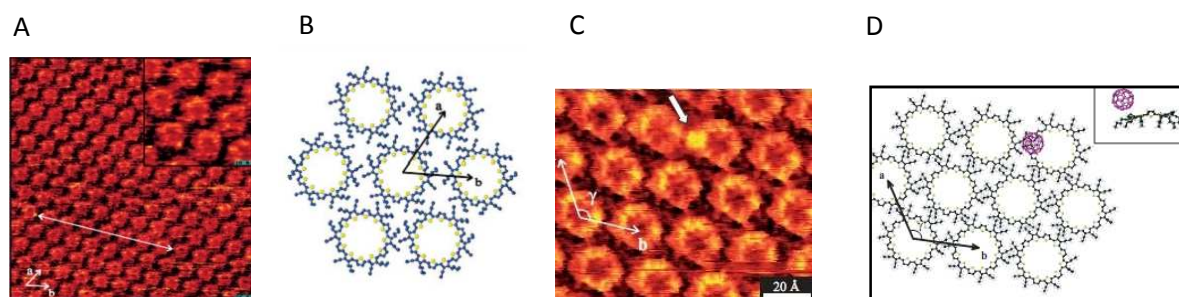
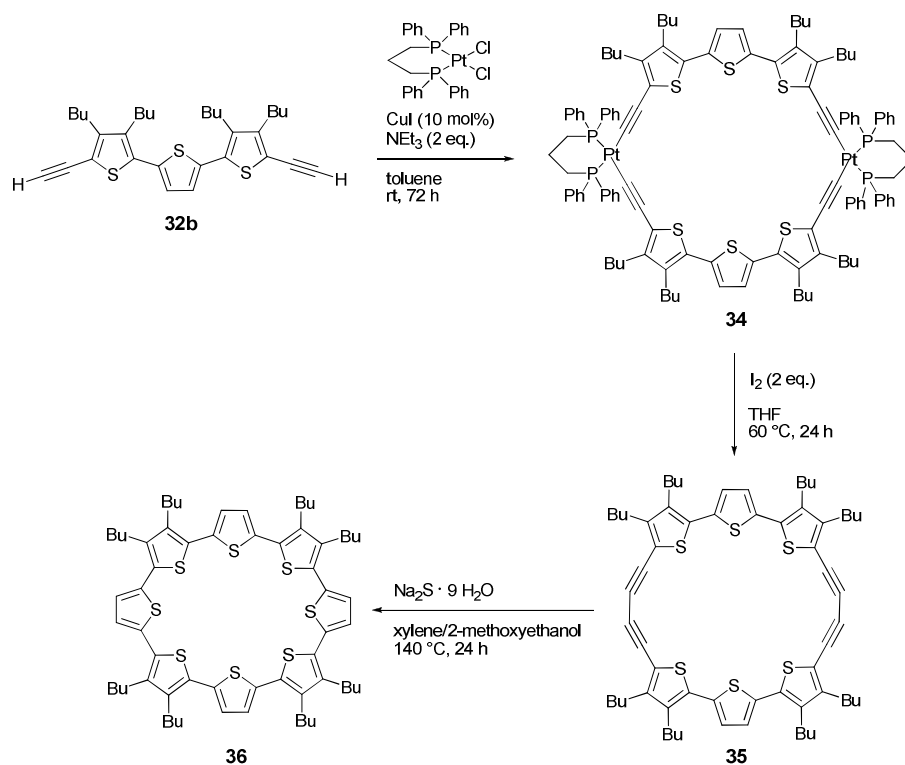


Figure 2.7: A) STM image of long range ordering of C[12]T on HOPG ($V_{\text{bias}} = -430$ mV, $I_t = 24$ pA), B) Calculated hexagonal 2D arrangement of the closest packing, C) STM image of a monolayer of C[12]T on HOPG with one C₆₀ adsorbed (white arrow) ($V_{\text{bias}} = -700$ mV, $I_t = 44$ pA), D) Calculated model of the hexagonal arrangement of C[12]T on HOPG with one C₆₀-C[12]T complex.^[106-107] Reprinted with permission from *Adv. Mater.* **2002**, *14*, 609; *Adv. Mater.* **2006**, *18*, 447. Copyright 2002, 2006 Wiley-VCH Verlag.

Three years later, Fuhrmann et al. published a more effective strategy for the synthesis of C[n]Ts by introducing transition metal centers as corner points within the cyclic backbone following the well-known templated cyclization methods.^[77] This process allowed a more controlled reaction with high conversion into defined cyclic Pt-intermediates and advanced the preliminary applied random and statistic cyclooligomerization. Platinum was chosen as transition metal since corresponding Pd-intermediates did not form stable and characterized aryl complexes. They readily undergo reductive elimination which is common for transition metal-catalyzed cross-coupling reactions. Fuhrmann firstly explored the formation of defined linear oligothiophenes via *cis*-Pt-(dppp)(σ -acetylide-oligothiophene) complexes. Successive reductive elimination gave bridged butadiyne compounds,^[108] which could be further transformed with Na₂S into the desired conjugated oligothiophenes.^[109] Based on these studies, the method was then extended to the efficient synthesis of macrocycles (Scheme

2.21).^[77] The utilized *cis*-transition metal complex $\text{PtCl}_2(\text{dppp})$ does not serve as a real template, but conducts the monomer units into a cyclic framework, because of its pseudo square planar geometry with two reactive halides at an angle of nearly 90° . Due to this attractive angle, platinum can be directly introduced as corner pieces into the cyclic backbone and supports the formation of shape-persistent metallacycles while suppressing linear oligomerization. Since platinum plays a key role in the macrocyclization step, the reaction is designated as 'metal-assisted template method'.



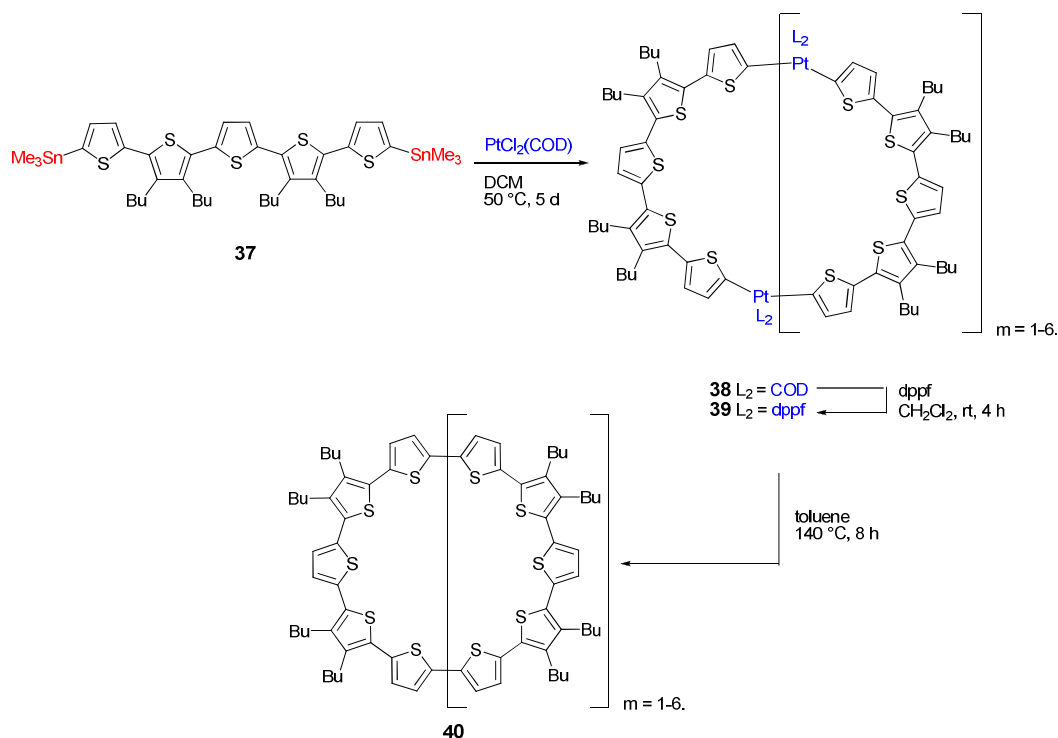
Scheme 2.21: *cis*-Pt-assisted macrocyclization towards fully π -conjugated C[8]T **36**.^[77]

Diethynylated terthiophene **32b** was reacted under basic conditions with $\text{PtCl}_2(\text{dppp})$ and formed metallacycle **34**, which underwent reductive elimination by the addition of iodine.^[77, 108] Mechanistic studies for the reductive elimination with iodine have been published^[110–112] and an oxidative addition of I_2 to Pt^{II} aryl complexes is known to form octahedral Pt^{IV} complexes with iodine attached via dative bonds to the transition metal. A *cis-trans* isomerization gives the most stable isomer. The elimination results in a rather uncontrolled process in which aryl-halide formation competes with the more common C-C bond formation.^[110–112] In her thesis, Fuhrmann suggested a mechanism for the oxidatively induced reductive elimination from cyclic $\text{Pt}^{\text{II}}(\sigma\text{-acetylide-oligothiophene})$ complexes based on her research. When treating one defined $\text{Pt}^{\text{II}}(\text{dppp})(\sigma\text{-acetylide-oligothiophene})$ complex with iodine, she observed the formation of a series of platinum-free diacetylene-macrocycles along with various side products and decomposition, confirming the uncontrollable nature of the reaction. The only exception was found for diplatinum metallacycle **34**, which formed only one defined butadiyne-bridged cycle **35**. Consecutive sulfur transformation via Na_2S by heating to high

temperatures gave C[8]T **36**. The purification of the macrocycle was performed by preparative high performance liquid chromatography (HPLC). The isolated ring was characterized by ^1H and ^{13}C NMR spectroscopy as well as mass spectrometry. A more detailed characterization was possible by single crystal X-ray crystallography. Further cyclic analogues have been built from butylated diethynylated quinque- and septithiophene units.

These results were the basis for the development of a more direct synthetic method towards cyclo[n]thiophenes. Zhang established a general one-pot coupling method to attach thiophene-precursors directly to the transition metal without an ethynyl spacer.^[85] With this strategy the number of reaction and purification steps as well as losses of product could be reduced. Reductive elimination was induced thermally in order to avoid competing side reactions and to succeed in a clean, concerted 1,1-elimination to generate defined macrocycles. The elaborated pathway is outlined in Scheme 2.22. Distannylated linear quinquethiophene **37** was treated with an equimolar amount of $\text{PtCl}_2(\text{COD})$ under high dilution conditions to form a mixture of multinuclear cyclic $\text{Pt}^{\text{II}}(\text{COD})(\text{oligothienyl})$ complexes **38** in an overall yield of 80%. Studies by proton NMR spectroscopy revealed characteristic signals of cycloocta-1,5-diene. The *cis*-transition metal complex $\text{PtCl}_2(\text{COD})$ supports the ring formation process for the same reasons as in the case of Fuhrmanns' strategy described above: A pseudo square planar geometry with two reactive halides in an angle of nearly 90° ,^[113] that the Pt^{II} corners act both as a template and as an angular building block to favour macrocyclization over linear oligomerization. The formed cyclic $\text{Pt}^{\text{II}}(\text{COD})\text{oligothienyl}$ complexes **38** were stable and could be isolated and purified. To overcome the stability towards carbon-carbon bond formation during reductive elimination, COD was displaced by the phosphine ligand 1,1'-bis(diphenylphosphino)ferrocene (dppf). Phosphines are usually used in transition metal complexes as neutral ancillary ligands, which do not take part in the elimination process. The elimination is favoured by electron poor and sterically demanding ligands or, in the case of bidentate ligands, by a large bite angle.^[114-116] Eaborn has described the ligand exchange of COD with target phosphine ligands by adding phosphine, for instance PPh_3 , PEt_2Ph , or dppe, and stirring the mixture at room temperature for a few hours.^[117] Zhang^[85] adopted this protocol to the mixture of multinuclear $\text{Pt}^{\text{II}}(\text{COD})\text{oligothienyl}$ macrocycles **38** and converted the complexes into $\text{Pt}^{\text{II}}(\text{dppf})\text{metallacycles}$ **39**. Thermal activation of reductive elimination at elevated temperatures of up to 140°C followed. After size exclusion chromatography of the crude material and mixture of macrocycles **40**, Zhang was able to obtain a complete series of pure macrocycles in various ring sizes spanning from C10T to C35T in an overall yield of 57%. The structures were fully characterized and investigated by means of optical and electrochemical measurements as well as X-ray crystallography analysis. For the first time, a series of thiophene-containing macrocycles with an odd number of repeating units was available. Zhang also prepared macrocycles from alkylated quater- and septithiophene monomer units in

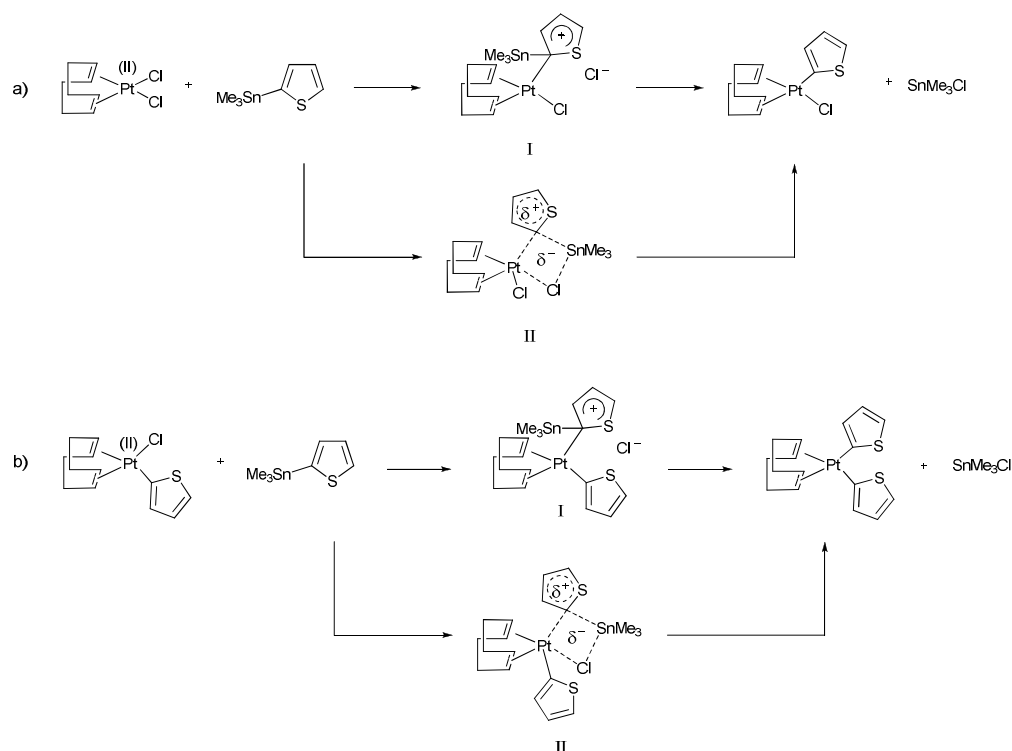
addition to macrocycles containing chiral side chains. The unique optical and electrochemical properties will be discussed later in this thesis.



Scheme 2.22: Established one pot synthesis for the ‘metal-assisted template method’ to produce a series of $\text{C}[n]\text{Ts}$ **40**.^[85]

2.4 Reaction mechanism of the formation of $\text{Pt}^{\text{II}}(\text{COD})$ metallacycles

A reaction mechanism of the effective and easily accessible ‘metal-assisted template method’ between a Me_3Sn -substituted aryl and transition metal complex $\text{PtCl}_2(\text{COD})$ was first presented by Eaborn et al.^[117] They investigated the efficient formation of an aryl-transition metal bond from aryl-tin compounds and platinum. One or both chloride ligands of $\text{PtCl}_2(\text{COD})$ could be selectively replaced by aryl groups when reacted with aryltrimethylstannyl reagents. A broad spectrum of benzene derivatives as well as heteroaryls such as thiophene or furan could be bound to the metal. Eaborn disclosed the fact that while SnMe_3R ($\text{R} = \text{aryl}$) reacted with bis(phosphine)complexes $[\text{PtCl}_2(\text{PR}_3)_2]$ very slowly or not at all, aryl groups can be efficiently attached to platinum when a COD ligand was used.^[118] The arylation procedure with a tin reagent is also more attractive compared to a Grignard or an organolithium reagent, since both are less selective and often form biaryl complexes even when used in stoichiometric proportions to gain a monoaryl complex. Work-up usually involves a hydrolysis step, which may cause complications as well.^[119] Eaborn et al. proposed two reaction mechanism for the arylation that can be regarded as an electrophilic aromatic substitution and is pictured in Scheme 2.23.^[117]



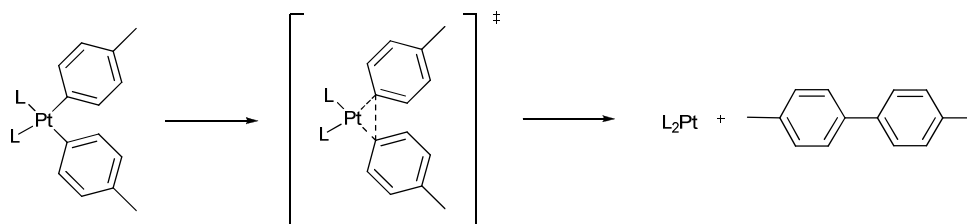
Scheme 2.23: a) Proposed reaction mechanism of the monoarylation of $\text{PtCl}_2(\text{COD})$ with a tin-substituted thiophene either through a Wheland intermediate (I) or through a four-center process (II). b) Corresponding reaction mechanism of the biarylation.

The mono thienyl-Pt-complex can either be formed through a Wheland intermediate (I), as such transition states are usually generated during an electrophilic aromatic substitution, or through a concerted four-center process (II), in which a substantial degree of positive charge is located on the aromatic ring. The biarylation to a bis(thienyl)-Pt-complex proceeds via the same transitions states as proposed for the monoarylated Pt-complex. The second Pt-Cl bond is normally replaced more slowly than the first, since the electron withdrawing effect of only one remaining chlorine atom does not make the platinum center as electrophilic and reactive for a second reaction as it is the case for starting material $\text{PtCl}_2(\text{COD})$. Steric effects are probably also not negligible.

2.5 General remarks to reductive eliminations from transition metal complexes

Carbon-carbon bond formation by reductive elimination from transition metal organyl complexes plays an important role in organometallic synthesis and catalysis. During reductive elimination, described as the product-releasing step, the formal oxidation state and the coordination number of the metal are reduced by two. Although the mechanistic process of a 1,1-reductive elimination from Pd^{II} and Pt^{II} complexes is not fully understood, some characteristics are proven theoretical and experimental. In their theses, Fuhrmann^[108] and Haid^[120] summarized several different research

studies in the context of reductive elimination from transition metal complexes in detail, particularly those of group 10 of the periodic table of elements. There are some important facts worth noting. The elements of group 10 in the oxidation state of II prefer four coordinated square-planar d^8 -complexes with 16 valence electrons, which is based on orbital correlation diagrams. The ease of reductive elimination is dependent on the metal, but also on its oxidation state and coordination environment. Within group 10, the stability of the transition metal complexes decreases in the order $Pt > Pd > Ni$. In the case of nickel, the activation energy barrier for C-C bond formation is none, whereby the elimination from Pd- and Pt-complexes are less facile and more energy is necessary.^[121] In addition, 16-electron complexes are usually more stable in comparison to 18-electron complexes, which undergo reductive elimination easily.^[122] A number of kinetical studies have shown that bond formation follows first order kinetics and succeeds intramolecularly between two molecules. Also some crossover experiments were carried out, where the intramolecular character of the reductive elimination was evidenced.^[121, 123-124] As an example, a mixture of the complexes $(dppm)Pt^{II}(p\text{-tolyl})_2$ and $(dppm)Pt^{II}Ph_2$ gave only products which are expected by a concerted unimolecular first-order elimination.^[123] Braterman et al. concluded a concerted 1,1-elimination with a cyclic transition state, as no regioisomers were formed during reductive elimination (Scheme 2.24).



Scheme 2.24: Assumed cyclic transition state during the concerted 1,1-elimination by Braterman et al.

The auxiliary ligands, mainly phosphines, do not take part in the reductive elimination, but play a crucial role. Bulky, sterically demanding and electron poor ligands favour the process, as well as bidentate ligands with a large bite angle.^[114-116]

2.6 Summary

This chapter gave an overview about the state of the art of thiophene-based macrocycles and started with the description of the different synthetic strategies towards cyclic ring systems. The cyclic oligothiophenes are summarized in different categories such as macrocycles with disrupted conjugation, macrocycles with complete conjugation and fully α -conjugated cyclo[n]thiophenes. The latter cyclic systems were firstly synthesized and characterized in our institute and present the base for this thesis.

2.7 References

- [1] W. Zhang, J. S. Moore, *Angew. Chem.* **2006**, *118*, 4524-4548; *Angew. Chem. Int. Ed.* **2006**, *45*, 4416-4439.
- [2] Y. Li, J. Zhang, W. Wang, Q. Miao, X. She, X. Pan, *J. Org. Chem.* **2005**, *70*, 3285-3287.
- [3] J. S. Moore, J. Zhang, *Angew. Chem.* **1992**, *104*, 873-874; *Angew. Chem. Int. Ed.* **1992**, *31*, 922-924.
- [4] J. Zhang, D. J. Pesak, J. L. Ludwick, J. S. Moore, *J. Am. Chem. Soc.* **1994**, *116*, 4227-4239.
- [5] S. Höger, V. Enkelmann, *Angew. Chem.* **1995**, *107*, 2917-2919.
- [6] S.-H. Jung, W. Pisula, A. Rouhanipour, H. J. Räder, J. Jacob, K. Müllen, *Angew. Chem.* **2006**, *118*, 4801-4806; *Angew. Chem. Int. Ed.* **2006**, *45*, 4685-4690.
- [7] S. Höger, A.-D. Meckenstock, H. Pellen, *J. Org. Chem.* **1997**, *62*, 4556-4557.
- [8] S. Höger, A.-D. Meckenstock, *Chem. Eur. J.* **1999**, *5*, 1686-1691.
- [9] M. J. Marsella, Z.-Q. Wang, R. J. Reid, K. Yoon, *Org. Lett.* **2001**, *3*, 885-887.
- [10] D. V. Kondratuk, L. M. A. Perdigao, M. C. O'Sullivan, S. Svatek, G. Smith, J. N. O'Shea, P. H. Beton, H. L. Anderson, *Angew. Chem.* **2012**, *124*, 6800-6803; *Angew. Chem. Int. Ed.* **2012**, *51*, 6696-6699.
- [11] M. Hoffmann, J. Kärnbratt, M.-H. Chang, L. M. Herz, B. Albinsson, H. L. Anderson, *Angew. Chem.* **2008**, *120*, 5071-5074; *Angew. Chem. Int. Ed.* **2008**, *47*, 4993-4996.
- [12] M. C. O'Sullivan, J. K. Sprafke, D. V. Kondratuk, C. Rinfray, T. D. W. Claridge, A. Saywell, M. O. Blunt, J. N. O'Shea, P. H. Beton, M. Malfois, H. L. Anderson, *Nature* **2011**, *469*, 72-75.
- [13] W. Zhang, S. Kraft, J. S. Moore, *J. Am. Chem. Soc.* **2004**, *126*, 329-335.
- [14] W. Zhang, J. S. Moore, *J. Am. Chem. Soc.* **2005**, *127*, 11863-11870.
- [15] W. Zhang, J. S. Moore, *J. Am. Chem. Soc.* **2004**, *126*, 12796-12796.
- [16] E. S. Hirst, R. Jasti, *J. Org. Chem.* **2012**, *77*, 10473-10478.
- [17] A. V. Zabula, A. S. Filatov, J. Xia, R. Jasti, M. A. Petrukhina, *Angew. Chem.* **2013**, *125*, 5137-5140; *Angew. Chem. Int. Ed.* **2013**, *52*, 5033-5036.
- [18] W. Pisula, M. Kastler, C. Yang, V. Enkelmann, K. Müllen, *Chem. Asian J.* **2007**, *2*, 51-56.
- [19] V. Hensel, A. D. Schlüter, *Chem. Eur. J.* **1999**, *5*, 421-429.
- [20] T. Iwamoto, Y. Watanabe, T. Sadahiro, T. Haino, S. Yamago, *Angew. Chem.* **2011**, *123*, 8492-8494; *Angew. Chem. Int. Ed.* **2011**, *50*, 8342-8344.
- [21] R. Jasti, J. Bhattacharjee, J. B. Neaton, C. R. Bertozzi, *J. Am. Chem. Soc.* **2008**, *130*, 17646-17647.
- [22] E. Kayahara, Y. Sakamoto, T. Suzuki, S. Yamago, *Org. Lett.* **2012**, *14*, 3284-3287.
- [23] H. Omachi, S. Matsuura, Y. Segawa, K. Itami, *Angew. Chem.* **2010**, *122*, 10400-10403; *Angew. Chem. Int. Ed.* **2010**, *49*, 10202-10205.
- [24] H. Omachi, Y. Segawa, K. Itami, *Acc. Chem. Res.* **2012**, *45*, 1378-1389.
- [25] Y. Segawa, S. Miyamoto, H. Omachi, S. Matsuura, P. Šenel, T. Sasamori, N. Tokitoh, K. Itami, *Angew. Chem.* **2011**, *123*, 3302-3306; *Angew. Chem. Int. Ed.* **2011**, *50*, 3244-3248.
- [26] S. Yamago, Y. Watanabe, T. Iwamoto, *Angew. Chem.* **2010**, *122*, 769-771; *Angew. Chem. Int. Ed.* **2010**, *49*, 757-759.
- [27] M. Iyoda, J. Yamakawa, M. J. Rahman, *Angew. Chem.* **2011**, *123*, 10708-10740; *Angew. Chem. Int. Ed.* **2011**, *50*, 10522-10553.
- [28] K. Kawase, *Synlett* **2007**, 2609-2626.

- [29] T. Kawase, K. Tanaka, N. Fujiwara, H. R. Darabi, M. Oda, *Angew. Chem.* **2003**, *115*, 1662-1666; *Angew. Chem. Int. Ed.* **2003**, *42*, 1624-1628.
- [30] J. A. Marsden, M. M. Haley, *J. Org. Chem.* **2005**, *70*, 10213-10226.
- [31] H. Shimura, M. Yoshio, T. Kato, *Org. Biomol. Chem.* **2009**, *7*, 3205-3207.
- [32] L. Shu, M. Müri, R. Krupke, M. Mayor, *Org. Biomol. Chem.* **2009**, *7*, 1081-1092.
- [33] A. Blaszczyk, M. Chadim, C. von Hänisch, M. Mayor, *Eur. J. Org. Chem.* **2006**, 3809-3825.
- [34] C. Grave, A. D. Schlüter, *Eur. J. Org. Chem.* **2002**, 2002, 3075-3098.
- [35] R. Friederich, M. Nieger, F. Vögtle, *Chem. Ber.* **1995**, *126*, 1723-1732.
- [36] M. M. Haley, *Macrocyclic Oligo(phenylacetylenes) and Oligo(phenyldiacetylenes) in Topics in Current Chemistry*, vo.201, Eds.:de Meijere A., Springer, Berlin, Heidelberg **1999**.
- [37] S. Höger, *Angew. Chem.* **2005**, *117*, 3872-3875; *Angew. Chem. Int. Ed.* **2005**, *44*, 3806-3808.
- [38] S. Höger, K. Bonrad, A. Mourran, U. Beginn, M. Möller, *J. Am. Chem. Soc.* **2001**, *123*, 5651-5659.
- [39] Y. Hosokawa, T. Kawase, M. Oda, *Chem. Commun.* **2001**, 1948-1949.
- [40] S.-S. Jester, N. Shabelina, S. M. Le Blanc, S. Höger, *Angew. Chem.* **2010**, *49*, 6101-6105; *Angew. Chem.* **2010**, *122*, 6237-6241.
- [41] H. A. Staab, K. Neunhoeffer, *Synthesis* **1974**, 424.
- [42] Y. Tobe, A. Nagano, K. Kawabata, M. Sonoda, K. Naemura, *Org. Lett.* **2000**, *2*, 3265-3268.
- [43] D. Venkataraman, S. Lee, J. Zhang, J. S. Moore, *Nature* **1994**, *371*, 591-593.
- [44] Z. Wei, J. S. Moore, *Angew. Chem.* **2006**, *118*, 4524-4548; *Angew. Chem. Int. Ed.* **2006**, *45*, 4416 – 4439.
- [45] C. Maeda, T. Yoneda, N. Aratani, M.-C. Yoon, J. M. Lim, D. Kim, N. Yoshioka, A. Osuka, *Angew. Chem.* **2011**, *123*, 5809-5812; *Angew. Chem. Int. Ed.* **2011**, *50*, 5691-5694.
- [46] L. Arnold, H. Norouzi-Arasi, M. Wagner, V. Enkelmann, K. Müllen, *Chem. Commun.* **2011**, *47*, 970-972.
- [47] K. Balakrishnan, A. Datar, W. Zhang, X. Yang, T. Naddo, J. Huang, J. Zuo, M. Yen, J. S. Moore, L. Zang, *J. Am. Chem. Soc.* **2006**, *128*, 6576-6577.
- [48] A. D. Finke, D. E. Gross, A. Han, J. S. Moore, *J. Am. Chem. Soc.* **2011**, *133*, 14063-14070.
- [49] S. Maruyama, H. Hokari, T. Wada, H. Sasabe, *Synthesis* **2001**, *12*, 1794-1799.
- [50] B. Schmaltz, A. Rouhanipour, H. J. Räder, W. Pisula, K. Müllen, *Angew. Chem.* **2009**, *121*, 734-738; *Angew. Chem. Int. Ed.* **2009**, *48*, 720-724.
- [51] Y. Song, C.-a. Di, Z. Wei, T. Zhao, W. Xu, Y. Liu, D. Zhang, D. Zhu, *Chem. Eur. J.* **2008**, *14*, 4731-4740.
- [52] S. C. Simon, B. Schmaltz, A. Rouhanipour, H. J. Räder, K. Müllen, *Adv. Mater.* **2009**, *21*, 83-85.
- [53] J. L. Sessler, S. L. Weghorn, *Expanded, Contracted&Isomeric Porphyrins*, Pergamon, New York **1997**.
- [54] P. J. Chmielewski, *Angew. Chem.* **2010**, *122*, 1399-1401; *Angew. Chem. Int. Ed.* **2010**, *49*, 1359-1361.
- [55] H. Mori, N. Aratani, A. Osuka, *Eur. J. Org. Chem.* **2012**, 2012, 1913-1919.
- [56] S. Saito, A. Osuka, *Angew. Chem.* **2011**, *123*, 4432-4464; *Angew. Chem. Int. Ed.* **2011**, *50*, 4342-4373.
- [57] J. K. M. Sanders, *The Porphyrin Handbook*, vol 3, Eds.: Kadish K. M., Smith K. M., Guillard R., Academic Press, San Diego CA **2000**.
- [58] J. L. Sessler, D. Seidel, *Angew. Chem.* **2003**, *115*, 5292-5333; *Angew. Chem. Int. Ed.* **2003**, *42*, 5134-5175.
- [59] H. Abe, H. Kurokawa, Y. Chida, M. Inouye, *J. Org. Chem.* **2010**, *76*, 309-311.

- [60] C. Grave, D. Lentz, A. Schafer, P. Samori, J. P. Rabe, P. Franke, A. D. Schlüter, *J. Am. Chem. Soc.* **2003**, *125*, 6907-6918.
- [61] O. Henze, D. Lentz, A. Schäfer, P. Franke, A. D. Schlüter, *Chem. Eur. J.* **2002**, *8*, 357-365.
- [62] K. Miki, M. Fujita, Y. Inoue, Y. Senda, T. Kowada, K. Ohe, *J. Org. Chem.* **2010**, *75*, 3537-3540.
- [63] M. Venturi, F. Marchioni, V. Balzani, D. M. Opris, O. Henze, A. D. Schlüter, *Eur. J. Org. Chem.* **2003**, 4227-4233.
- [64] W. Nakanishi, T. Yoshioka, H. Taka, J. Y. Xue, H. Kita, H. Isobe, *Angew. Chem.* **2011**, *123*, 5435-5438; *Angew. Chem. Int. Ed.* **2011**, *50*, 5323-5326.
- [65] J. L. Sessler, E. Tomat, V. M. Lynch, *J. Am. Chem. Soc.* **2006**, *128*, 4184-4185.
- [66] A. J. Gallant, M. J. MacLachlan, *Angew. Chem.* **2003**, *115*, 5465-5468; *Angew. Chem. Int. Ed.* **2003**, *42*, 5307-5310.
- [67] S. Guieu, A. K. Crane, M. J. MacLachlan, *Chem. Commun.* **2011**, *47*, 1169-1171.
- [68] F. Diederich, M. Kivala, *Adv. Mater.* **2010**, *22*, 803-812.
- [69] F. Diederich, *Chem. Commun.* **2001**, 219-227.
- [70] T. Chen, G.-B. Pan, H. Wettach, M. Fritzsche, S. Höger, L.-J. Wan, H.-B. Yang, B. H. Northrop, P. J. Stang, *J. Am. Chem. Soc.* **2010**, *132*, 1328-1333.
- [71] S. K. Maier, S.-S. Jester, U. Müller, W. M. Müller, S. Höger, *Chem. Commun.* **2011**, *47*, 11023-11025.
- [72] G.-B. Pan, X.-H. Cheng, S. Höger, W. Freyland, *J. Am. Chem. Soc.* **2006**, *128*, 4218-4219.
- [73] T. Kaikawa, T. Kazuo, Y. Aso, T. Otsubo, *Org. Lett.* **2000**, *2*, 4197-4199.
- [74] T. Sakai, T. Satou, T. Kaikawa, K. Takimiya, T. Otsubo, Y. Aso, *J. Am. Chem. Soc.* **2005**, *127*, 8082-8089.
- [75] Y. Ie, T. Hirose, Y. Aso, *J. Mater. Chem.* **2009**, *19*, 8169-8175.
- [76] R. Inoue, M. Hasegawa, Y. Mazaki, *15th International Symposium on Novel Aromatic Compounds, 2013 Taipei, Posternumber-163*.
- [77] G. Fuhrmann, T. Debaerdemaeker, P. Bäuerle, *Chem. Commun.* **2003**, *8*, 948-949.
- [78] Z. Hu, J. L. Atwood, M. P. Cava, *J. Org. Chem.* **1994**, *59*, 8071-8075.
- [79] M. Iyoda, *J. Synth. Org. Chem., Jpn.* **2012**, *70*, 1157-1163.
- [80] K. Kawase, H. R. Darabi, R. Uchimiya, M. Oda, *Chem. Lett.* **1995**, 499-450.
- [81] J. Krömer, I. Rios-Carreras, G. Fuhrmann, C. Musch, M. Wunderlin, T. Debaerdemaeker, E. Mena-Osteritz, P. Bäuerle, *Angew. Chem.* **2000**, *112*, 3623-3628; *Angew. Chem. Int. Ed.* **2000**, *39*, 3481-3486.
- [82] M. Mayor, C. Didschies, *Angew. Chem.* **2003**, *115*, 3284-3287; *Angew. Chem. Int. Ed.* **2003**, *42*, 3176-3179.
- [83] M. J. O'Connor, M. M. Haley, *Org. Lett.* **2008**, *10*, 3973-3976.
- [84] J. S. Reddy, V. G. Anand, *Chem. Commun.* **2008**, *11*, 1326-1328.
- [85] F. Zhang, G. Götz, H. D. F. Winkler, Christoph A. Schalley, P. Bäuerle, *Angew. Chem.* **2009**, *121*, 6758-6762; *Angew. Chem. Int. Ed.* **2009**, *48*, 6632-6635.
- [86] T. Y. Gopalakrishna, J. S. Reddy, V. G. Anand, *Angew. Chem.* **2013**, *125*, 1807-1811; *Angew. Chem. Int. Ed.* **2013**, *52*, 1763-1767.
- [87] T. Kauffmann, B. Greving, R. Kriegesmann, A. Mitschker, A. Woltermann, *Chem. Ber.* **1978**, *111*, 1330-1336.
- [88] T. Kauffmann, H. P. Mackowiak, *Chem. Ber.* **1985**, *118*, 2343-2352.
- [89] S. M. H. Kabir, M. Miura, S. Sasaki, G. Harada, Y. Kuwatani, M. Yoshida, M. Iyoda, *Heterocycles* **2000**, *52*, 761-774.
- [90] Y. Wang, Z. Wang, D. Zhao, Z. Wang, Y. Cheng, H. Wang, *Synlett* **2007**, *15*, 2390-2394.

- [91] M. J. Marsella, K. Yoon, F. S. Tham, *Org. Lett.* **2001**, 3, 2129-2131.
- [92] T. Ohmae, T. Nishinaga, M. Wu, M. Iyoda, *J. Am. Chem. Soc.* **2010**, 132, 1066-1074.
- [93] M. J. O'Connor, R. B. Yelle, L. N. Zakharov, M. M. Haley, *J. Org. Chem.* **2008**, 73, 4424-4432.
- [94] F. Sondheimer, R. Wolovsky, R. Amiel, *J. Am. Chem. Soc.* **1962**, 84, 274-284.
- [95] K. Singh, A. Sharma, J. Zhang, W. Xu, D. Zhu, *Chem. Commun.* **2011**, 47, 905-907.
- [96] J. S. Reddy, V. G. Anand, *J. Am. Chem. Soc.* **2008**, 130, 3718-3719.
- [97] J. S. Reddy, V. G. Anand, *J. Am. Chem. Soc.* **2009**, 131, 15433-15439.
- [98] J. Yin, X. Cao, G.-A. Yu, S. H. Liu, *Tetrahedron Lett.* **2008**, 49, 1582-1585.
- [99] K. Nakao, M. Nishimura, T. Tamachi, Y. Kuwatani, H. Miyasaka, T. Nishinaga, M. Iyoda, *J. Am. Chem. Soc.* **2006**, 128, 16740-16747.
- [100] M. Williams-Harry, A. Bhaskar, G. Ramakrishna, T. Goodson, M. Imamura, A. Mawatari, K. Nakao, H. Enozawa, T. Nishinaga, M. Iyoda, *J. Am. Chem. Soc.* **2008**, 130, 3252-3253.
- [101] M. Iyoda, *Pure Appl. Chem.* **2010**, 82, 831-841.
- [102] C. Musch, *Diploma Thesis*, University of Würzburg, Germany **1995**.
- [103] G. Fuhrmann, *Diploma Thesis*, University of Ulm, Germany **1999**.
- [104] I. R. Carreras, *Diploma Thesis*, University of Ulm, Germany **1999**.
- [105] J. Krömer, *PhD Thesis*, University of Ulm, Germany **2000**.
- [106] E. Mena-Osteritz, *Adv. Mater.* **2002**, 14, 609-616.
- [107] E. Mena-Osteritz, P. Bäuerle, *Adv. Mater.* **2006**, 18, 447-451.
- [108] G. Fuhrmann, *PhD Thesis*, University of Ulm, Germany **2006**.
- [109] J. Krömer, P. Bäuerle, *Tetrahedron* **2001**, 57, 3785-3794.
- [110] A. Yahav, I. Goldberg, A. Vigalok, *Organometallics* **2005**, 24, 5654-5659.
- [111] A. Yahav-Levi, I. Goldberg, A. Vigalok, *J. Am. Chem. Soc.* **2006**, 128, 8710-8711.
- [112] A. Vigalok, *Chem. Eur. J.* **2008**, 14, 5102-5108.
- [113] J. L. Butikofer, E. W. Kalberer, W. C. Schuster, D. M. Roddick, *Acta Crystallogr., Sect. C: Cryst. Struct. Commun.* **2004**, C60.
- [114] J. M. Brown, P. J. Guiry, *Inorg. Chim. Acta* **1994**, 220, 249-259.
- [115] D. A. Culkin, J. F. Hartwig, *Organometallics* **2004**, 23, 3398-3416.
- [116] P. W. N. M. van Leuween, P. C. J. Kamer, J. N. H. Reek, P. Dierkes, *Chem. Rev.* **2000**, 100, 2741-2770.
- [117] C. Eaborn, K. Odell, A. Pidcock, *J. C. S. Dalton Transc.* **1978**, 357-368.
- [118] C. Eaborn, K. Odell, A. Pidcock, *J. Organomet. Chem.* **1975**, 96, C38-C40.
- [119] J. Chatt, B. L. Shaw, *J. Chem. Soc.* **1959**, 705-716.
- [120] S. Haid, *Diploma Thesis*, University of Ulm, Germany **2008**.
- [121] K. Tatsumi, R. Hoffmann, A. Yamamoto, J. K. Stille, *Bull. Chem. Soc. Jpn.* **1981**, 54, 1854-1867.
- [122] P. S. Braterman, R. J. Cross, *Chem. Soc. Rev.* **1973**, 2, 271-294.
- [123] P. S. Braterman, R. J. Cross, G. B. Young, *J. Chem. Soc., Dalton Trans.* **1976**, 1306-1310.
- [124] H. A. Brune, J. Ertl, D. Grafl, G. Schmidtberg, *Chem. Ber.* **1982**, 115, 1141-1153.

CHAPTER 3

Acceptor-Functionalized α -Conjugated Cyclo[n]thiophenes

3.1 Introduction

To advance the basic research of shape-persistent, fully α -conjugated cyclo[n]thiophenes, modified building blocks are aimed to be synthesized and subjected to macrocyclization reactions to generate enhanced C[n]Ts with local functionalities. Different molecular design concepts to tune pure C[n]Ts by inserting special substituted moieties are possible and presented in the following.

Concept 1 – electronic influence: Inserted acceptor- (**C-1/C-2**) or donor units (**C-3**) give rise to an electronic influence onto the ring systems (Chart 3.1). The substituents are incorporated directly into the conjugated cyclic backbone and expect to change the photophysical properties in comparison to non-functionalized C[n]Ts, which may be interesting for the application in organic electronics. The presented acceptor units provide additionally reactive centers to allow further chemical modifications into various organic functionalities, which initialize as well tuned physical properties.

Concept 2 – peripheral functionalization: Reactive groups are attached to the periphery of the rings and provide binding sites, which allow further chemical transformation and help to direct the cycles into highly ordered arrays (Chart 3.1, **C-4**). Through π - π -interactions between the cycles, channels with improved charge mobilities may be formed.

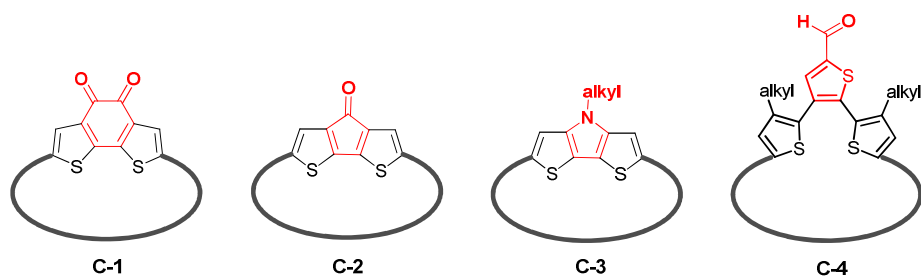


Chart 3.1 Schematic structures of acceptor- (**C-1/C-2**) and donor- (**C-3**) functionalized cycles as well as incorporated reactive centers to the periphery of the cyclic system (**C-4**).

Concept 3 – complexation at the outside: An inserted bithiazole unit (**C-5**) can be used to complex fourfold or fivefold coordinative metals, whereby the influence of the metal onto the optoelectronic properties of the cycles would be interesting to investigate. Additionally, perfect ordered monolayers of the corresponding macrocycles via metal-induced self-assembly can be expected (Chart 3.2).

Concept 4 – complexation at the inside : The usage of carbazole (**C-6**) or fluorene (**C-7**) building blocks gives access to complexation and catalytic reactions due to existing reaction centers inside the cavity (Chart 3.2).

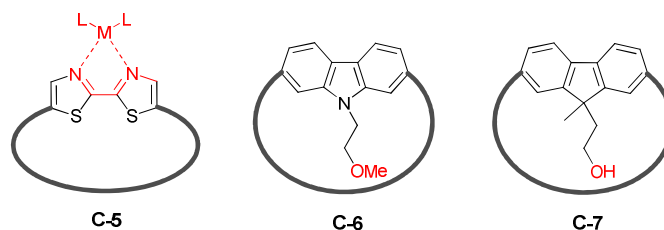


Chart 3.2: Schematic structures of bithiazole- (C-5), carbazole- (C-6) and fluorene- (C-7) containing macrocycles.

The focus of this thesis laid on the molecular design concepts 1 and 2; the electronic influence through the incorporation of electron-accepting (Chapter 3) and electron-donating (Chapter 4) units within the cyclic backbone as well as the peripheral functionalization through the attachment of organic functionalities at the outside of the rings (Chapter 5). Synthetic details, characterizations (proton NMR spectroscopy, mass spectrometry) and information about photophysical properties (UV/vis/NIR-absorption and fluorescence spectroscopy, cyclic voltammetry, X-ray crystallography), also in comparison to non-functionalized pure thiophene-based macrocycles, are given in the mentioned chapters.

3.2 Design of acceptor-substituted oligothieryl precursors

In order to design acceptor-functionalized α -conjugated cyclo[n]thiophenes, some aspects were taken into account for the preparation of suitable precursor units and are explained in this section. The modification process for the electron-withdrawing macrocycles is illustrated schematically in Chart 3.3. Two quaterthiophene-like molecules 4T-DTB and 4T-DCP were chosen as monomer building blocks, possessing a dithienobenzoquinone (DTB) and dithienocyclopentanone (DCP) core unit, respectively. Both fused heterocyclic units (DTB and DCP) are supposed to initiate a certain electronic influence onto the ring when incorporated into the conjugated backbone. Okada et al.^[1] already reported molecular orbital calculations for defined linear oligomers containing both mentioned heterocyclic substituents as inner moieties. The working group disclosed that electron-withdrawing groups at the bridged positions selectively stabilize the LUMO and electron-donating groups at the α -positions of the inner fused system destabilize the HOMO due to orbital symmetry. Thus, the reduced HOMO-LUMO band gap of the compounds causes an absorption towards higher wavelengths in UV/vis-absorption spectroscopy. Since decreasing of the electronic band gap has become a useful strategy for band gap engineering in π -conjugated copolymers and oligomers, these bridged systems and its derivatives are often incorporated into low band-gap polymers.^[2-3] Mono- and dicarbonyl-fused structures are also attractive systems in electron-transporting organic semiconductors with potentially air-stable OFET operation.^[4-5] By introducing these acceptor units

into the conjugated backbone of the macrocycles, the optoelectronic properties are expected to be influenced in contrast to non-functionalized cyclo[n]thiophenes and unique structure-property relationships can be explored.

The decision to work with the DTB and DCP core units did not only come from a certain electronic influence, but is also due to their inherent rigidity. The stiff and planar core units lead to a higher extend of conjugation within the macrocycle due to an improved π -orbital overlap and might lead to a closer π - π -stacking of the molecules which should improve charge transport properties in the bulk.

Due to synthetic reasons it was necessary to protect the mono and dicarbonyl groups. The literature known DTB and DCP building blocks were thus slightly modified by introducing acetalization with ethylene glycol groups. After deprotecting the prospective isolated cyclic structures, free carbonyl groups with a strong electron-accepting property would be regenerated. Additionally, the ketone group is known to undergo nucleophilic attacks, which offers the possibility of transformations into other organic functionalities leading to molecules with different characteristics and photophysical properties.^[2] Even linkages between two ketones using a McMurry reaction are imaginable to potentially assemble the rings into well-defined pattern and improve charge mobilities in the solid state.

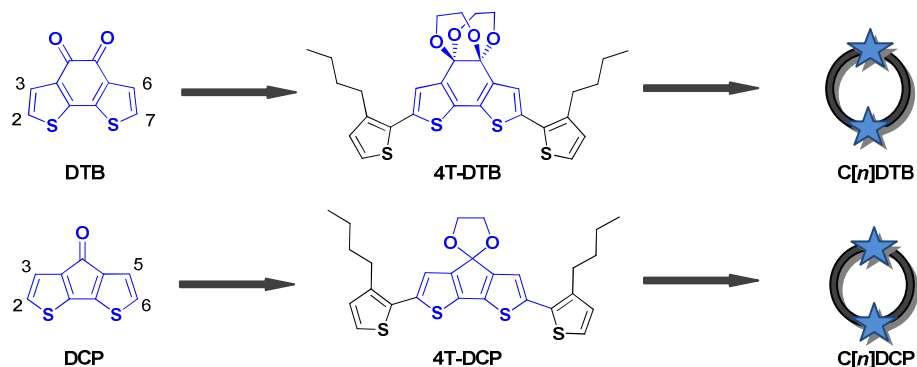


Chart 3.3: Structures of fused dicarbonyl (DTB) and monocarbonyl (DCP) moieties with corresponding quaterthiophene-like units 4T-DTB and 4T-DCP as well as prospective macrocyclic series C[n]DTB and C[n]DCP.

Elongation of the protected fused DTB and DCP core systems with one thiophene unit on each side generates quaterthiophenes 4T-DTB and 4T-DCP that are already bent in a hemicyclic shape when adopting a *syn*-conformation. The rounded profile should promote the cyclization reaction and is caused by the defined angulated structure of the fused moieties. It is meant to support the formation of only one preferred ring size by minimizing side products like linear oligomers. The introduced butyl side chains should provide sufficient solubility and increase the likelihood of the *syn*-conformation of the external thiophene units to maintain the mentioned hemicyclic shape. A possible *trans*-conformation of the terminal thiophene moieties is probably suppressed by sterical hindrance of the

butyl groups. The assumed all-*syn*-geometries of both precursors were optimized via semiempirical calculations using the Austin Model 1 (AM1) with defined Hartree Fock-conditions to get more information about the inner angle of the bent monomer units. The value of the inner angle was determined by drawing manually straight lines through the molecules parallel to the terminal CH-bonds as depicted in Chart 3.4. The calculation yielded an angle of about 75° for 4T-DTB and 93° for 4T-DCP. Since both building blocks possess an axial symmetry, highly symmetric macrocycles are expected.

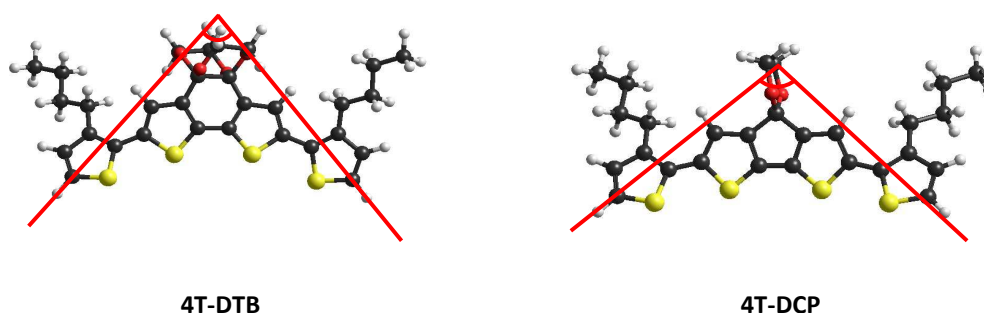
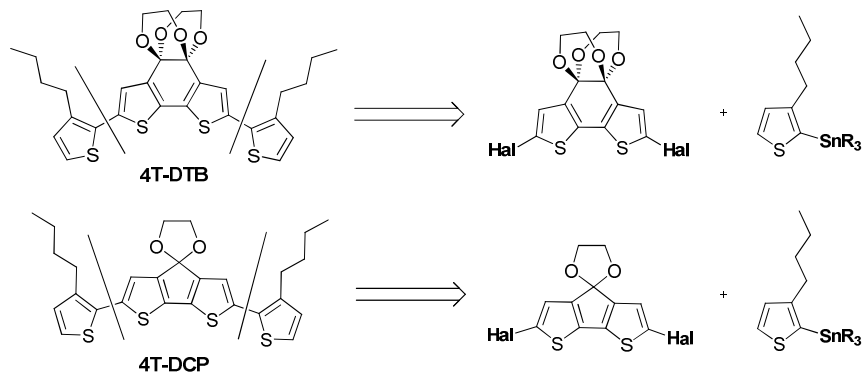


Chart 3.4: Calculated structures of 4T-DTB and 4T-DCP.

The buildup of the selected 4T-DTB and 4T-DCP-precursors has been realized by application of a Stille-type cross-coupling reaction^[6-8] to a dihalogenated and monostannylated segment, respectively (Scheme 3.1). Corresponding reactions as well as cyclization reactions are presented and discussed in the following sections.



Scheme 3.1: Retrosynthetic description of the presented 4T-DTB and 4T-DCP-precursors.

3.3 Synthesis of acceptor-substituted oligothiienyl macrocycles

3.3.1. Synthesis of the acceptor-substituted oligothiienyl precursors

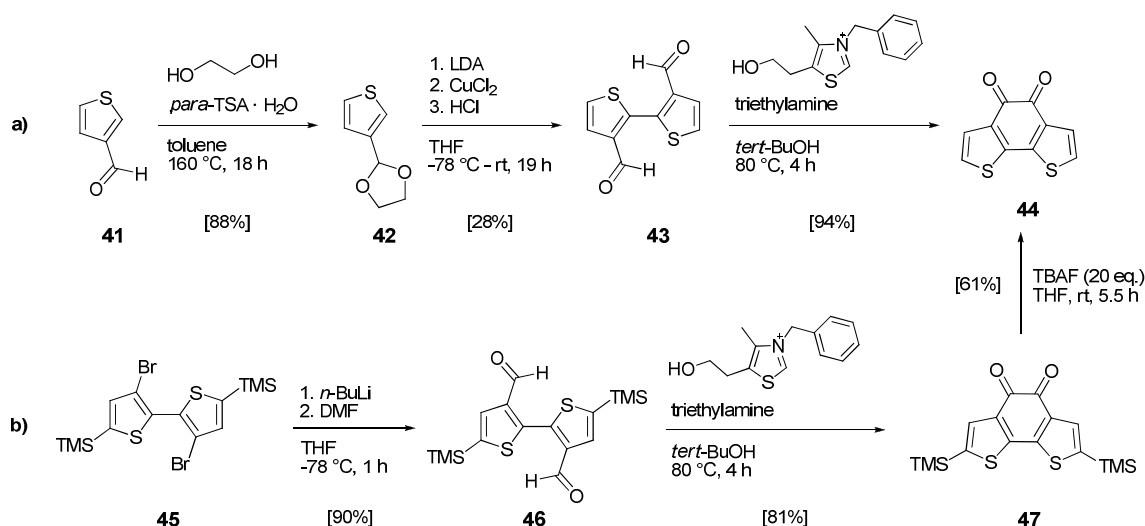
3.3.1.1. Access to the DTB core unit

The linkage between a dihalogenated acceptor core system and a tin-substituted external thiophene moiety by well-established Stille cross-coupling reaction requires the preliminary synthesis of both segments. The synthetic procedure for the dibrominated DTB moiety is depicted in Scheme 3.2a and started with the protection of the aldehyde group of commercially available 3-thiophene-carbaldehyde **41** with ethylene glycol and catalytic amounts of *para*-toluenesulfonic acid following a procedure by Rieger and Zotti.^[9-10] 2-(Thien-3-yl)-1,3-dioxolane **42** was obtained as a colorless liquid in 88% yield after purification via vacuum distillation.

The following step, formation of 2,2'-bithiophene, was performed via lithiation of the 2-position of **42** using LDA as organic base. Consecutive oxidative coupling was initiated by anhydrous CuCl₂. The reaction was quenched with 2 M hydrochloric acid and purification by column chromatography with dichloromethane afforded deprotected 2,2'-bithiophene-3,3'-dicarboxaldehyde **43** in 28% yield which is lower than the published yield of 53%.^[10] The analytical data of both compounds **42** and **43** are consistent with the literature.^[9-10]

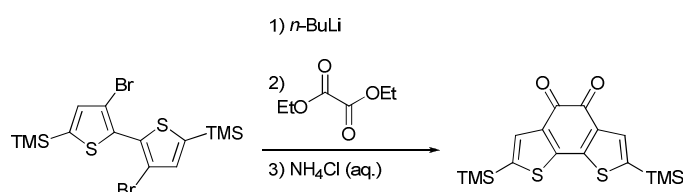
Subsequent intramolecular thiazolium salt-catalyzed benzoin condensation^[11] of **43** was performed at 80 °C in *tert*-BuOH within 4 h. The intermediate benzoin was oxidized in situ by oxygen to yield DTB core unit **44** as a pure deep red solid in 94% yield. The benzoin condensation of dialdehydes is commonly performed by utilizing different derivatives of thiazolium salts^[5, 10] or toxic inorganic sodium cyanide.^[12] Reactions applying the latter reactant resulted in low yields. The achieved analytical data for **44** are consistent with the listed literature.

Since the second reaction step, the formation of bithiophene derivative **43**, ended up in a moderate conversion, an alternative synthetic route to DTB core unit **44** with a higher overall yield was elaborated. The pathway is outlined in Scheme 3.2b and is based on an already published multi-step synthesis without attached TMS-groups by Marks et al.^[5] Starting material **45** was gained after a literature procedure published by Marder^[13] and will be discussed in Chapter 4. Substitution of both bromine atoms of bithiophene **45** was achieved via lithiation with *n*-butyl lithium, whereas the metal-halogen exchange was controlled via GC-MS-analysis and was completed after 15 min. DMF was added at -78 °C and the reaction was quenched at -40 °C with 2 M hydrochloric acid. After aqueous work-up and purification by column chromatography, literature unknown dialdehyde **46** was obtained as a yellow solid in 90% yield.



Scheme 3.2: Two different synthetic routes to DTB core unit **44**.

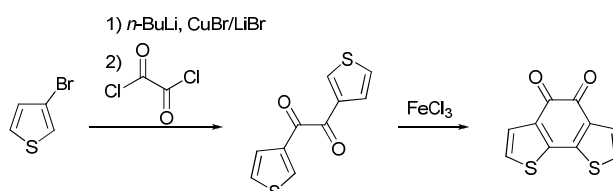
Subsequently, intramolecular benzoin condensation of dialdehyde **46** was performed in *tert*-BuOH at 80 °C within 4 h, followed by oxidation with air. Bis(trimethylsilyl)-substituted DTB-core unit **47** was afforded in 81% yield after purification by column chromatography. One year after this synthesis was performed, Marder et al. published the synthesis for the same molecule in a one-step reaction starting as well from halogenated bithiophene **45**.^[4] The α -dicarbonyl bridge was prepared using a double lithiation with *n*-butyl lithium followed by trapping the twofold charged intermediate with diethylxoxalate (Scheme 3.3). DTB **47** was isolated in 80% yield, which is slightly higher than the yield by our own procedure (overall yield of ~ 70%).



Scheme 3.3: One-pot reaction of the DTB moiety published by Marder et al.^[4]

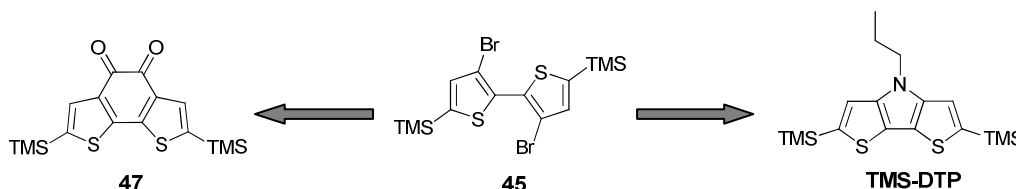
To remove both TMS protecting groups, DTB **47** was treated with 20 equivalents of tetra-*n*-butylammonium fluoride in THF at room temperature. After column chromatography, DTB **44** was obtained as a black solid in 61% yield. In a previous attempt to cleave off the protecting groups with cesium fluoride at room temperature, no conversion took place and starting material **47** was reisolated. In the meanwhile, other research teams succeeded in a more efficient elimination of TMS protecting groups from DTB systems. For instance Jen et al.^[14], who employed trifluoroacetic acid at refluxing conditions over several hours and gained target molecule **44** in 89% yield. Reynolds et al. utilized concentrated sulfuric acid and yielded nearly quantitative conversion of **44** in 95%.^[2] They mentioned synthetic problems during the elimination of the TMS groups via standard deprotection

methods such as fluorine sources or diluted acids since a high conversion of deprotection could not be accomplished. In their paper from 2012, Reynolds et al. also reported an effective synthetic route towards DTB-core unit **44** in a two-step reaction starting from inexpensive readily available 3-bromothiophene which was treated with *n*-butyl lithium and subsequently reacted with oxalyl chloride to form the diketone.^[2] This was subjected afterwards to oxidative ring closure using iron trichloride and DTB **44** was obtained in an overall yield of 82% (Scheme 3.4).^[2]



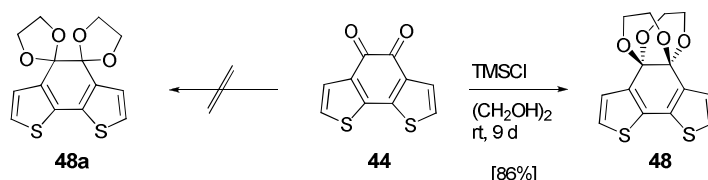
Scheme 3.4: Synthesis of DTB core unit presented by Reynolds.

The synthetic pathway shown in Scheme 3.2b starts from bis(trimethylsilyl)-substituted compound **45**. To obtain DTB derivative **47**, no TMS groups are actually necessary. However, silyl-substituted bithiophene **45** later on serves as starting material for another core unit, the *N*-alkylated dithienopyrrole **TMS-DTP**. As both fused center systems, **47** and **TMS-DTP**, can be achieved from the same silyl-functionalized basic bithiophene, **45** was selected to work with (Scheme 3.5). Details for the DTP-core unit are give in Chapter 4.



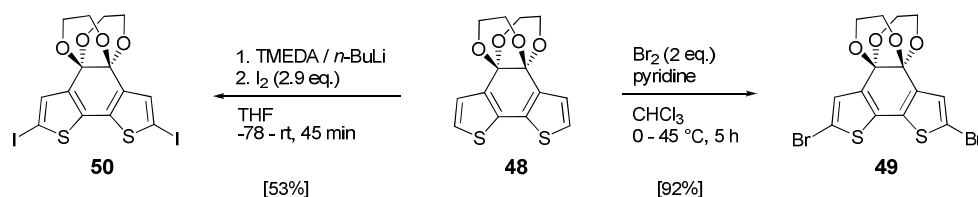
Scheme 3.5: Bithiophene-derivative **45** as staring material for both fused core units **47** and TMS-DTP.

Finally, protection of the carbonyl groups was achieved by the use of ethylene glycol and an excess of trimethylsilyl chloride at room temperature within 9 days.^[15-16] After crystallization from ethyl acetate, protected DTB **48** could be isolated pure in 86% yield (Scheme 3.6). The protection of the free ketone functionalities in DTB **48** is an important step to avoid a nucleophilic attack in a later carried out reaction with *n*-BuLi. The assembly of the protecting groups in **48** has already been determined by X-ray crystallography.^[10] Thus, a cyclic ketal via a six-membered ring as in DTB **48** is more stable than via a five-membered ring as in **48a**.



Scheme 3.6: Protection of ketone functionalities of DTB **44**.

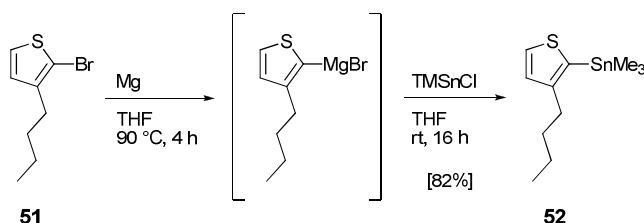
The final step to generate dihalogenated protected DTB core unit **49** included the introduction of bromine atoms at the free α -positions of **48**. DTB **49** was achieved by the use of elemental bromine under exclusion of light at 0 °C in chloroform in combination with pyridine. The addition of an organic base was necessary to capture formed hydrogen bromide and prevent the cleavage of the protecting groups. Molecule **49** was isolated pure as yellow needles in 92% yield after crystallization from ethyl acetate (Scheme 3.7). Iodination of DTB **48** was performed via lithiation of both free α -positions with *n*-butyl lithium and TMEDA in THF at -78 °C after a protocol of Okada et al.^[16] Subsequent treatment of the lithiated intermediate by elemental iodine resulted in DTB core unit **50** in a moderate yield of 53%.



Scheme 3.7: Synthesis of dibrominated and diiodinated DTB core systems **49** and **50**.

3.3.1.2 Synthesis of DTB-containing quaterthiophene **53**

Besides above described dihalogenated DTB-core unit **49**, a tin-substituted thiophene moiety **52** was synthesized in parallel (Scheme 3.8) to complete quaterthiophene **53** in a later Stille cross-coupling reaction.



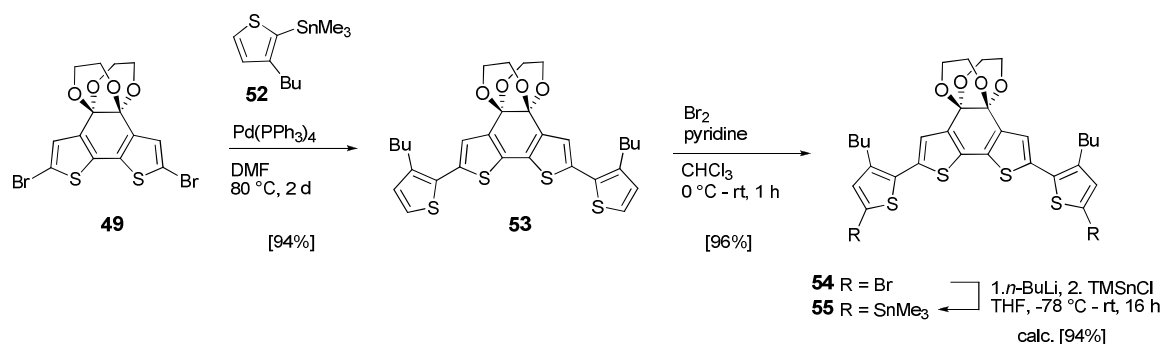
Scheme 3.8: Synthesis of tin-substituted 3-butyliophene **52**.

Target tin-compound **52** was synthesized using a Grignard reaction instead of the general utilized metal-halogen exchange with *n*-butyl lithium. Thus, the formation of regioisomers, in which the anion is located at the other α -position, should be avoided. 2-Bromo-3-butyliophene **51** was

converted via standard procedure with magnesium into the appropriate Grignard intermediate and treated subsequently with trimethyltin chloride. Complete conversion to the Grignard intermediate was controlled via GC-MS-analysis of a quenched reaction sample. After purification via distillation, thiophene **52** was afforded pure without any regioisomers as a colorless liquid in 82% yield.

To connect moieties **49** and **52**, C-C bond formation was performed under established Stille cross-coupling reaction conditions utilizing catalytic amounts of tetrakis(triphenylphosphine) palladium(0) at 80 °C. Conversion was completed after two days and quaterthiophene **53** was obtained as an orange oil in 94% yield after purification by column chromatography (Scheme 3.9).

Subsequent introduction of bromine atoms at the free α -positions was performed with elemental bromine and pyridine in chloroform at 0 °C and dihalogenated quaterthiophene **54** was gained as a yellow resin in 96% yield after column chromatography.



Scheme 3.9: Synthesis of distannylated macrocyclization precursor **55**.

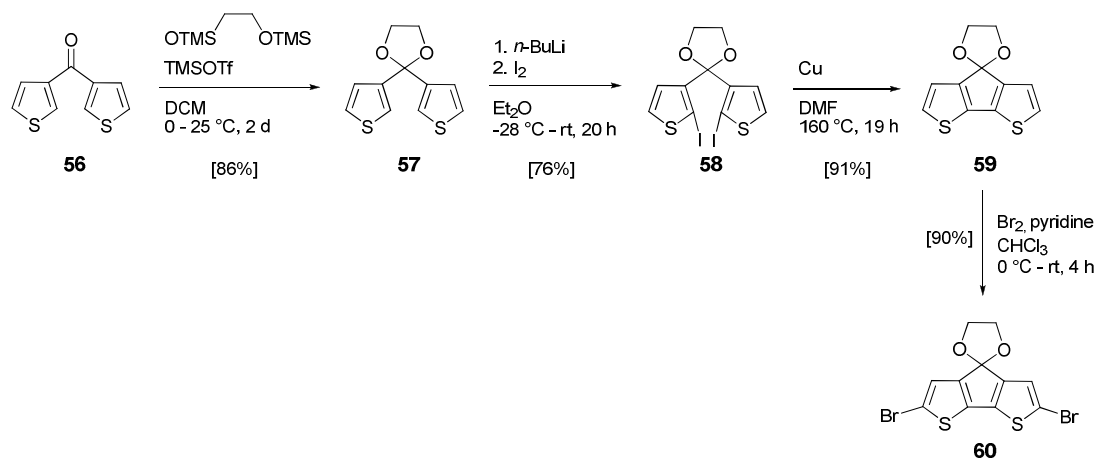
Eventually, a bromine-metal exchange with *n*-butyl lithium at -78 °C was performed in THF, followed by the treatment of trimethyltin chloride to gain distannylated target molecule **55**. The crude product was not further purified after aqueous work-up to avoid cleavage of the tin groups. The conversion was calculated via proton NMR spectroscopy and resulted in a yield of 94%. The monostannylated derivative occurred as a side product in 6% yield. Target molecule **55** was then applied as precursor in the Pt-assisted cyclization step (see Chapter 3.3.3.1).

3.3.2.1 Access to the DCP core unit

The DCP core unit was selected as second acceptor moiety in the concept of functionalized fully α -conjugated cyclo[*n*]thiophenes and the synthetic route towards its dihalogenated derivative **60** started from bis(thien-3-yl)methanone **56** and is outlined in Scheme 3.10.

DCP **57** was achieved by initial protection under aprotic conditions following a procedure by Breau et al.^[17] The acetalization step was performed under mild conditions using a combination of 1,2-bis(trimethylsilyloxy)ethane and trimethylsilyl trifluoromethane sulfonate at ambient temperature for 2 days. After purification via column chromatography, acetale **57** was isolated as colorless crystals in 86% yield. The reaction has already been described in literature in 66 and 72% yield when performed in benzene with ethylene glycol under reflux for 6 days.^[18]

Subsequently, iodine was introduced at the 2-positions of the thiophenes with *n*-butyl lithium and elemental iodine in diethyl ether at -28 °C to afford a brown solid of diiodide **58** in 76% yield. The synthesis followed a literature procedure published by Wynberg et al.^[19] and iodinated compound **58** was used without further purification for the next step, the copper-catalyzed Ullmann coupling reaction to fused system **59**. The latter derivative was prepared after a protocol by Su et al.^[20] and fused DCP-core unit **59** was achieved as a pink powder in 91% yield after column chromatography.



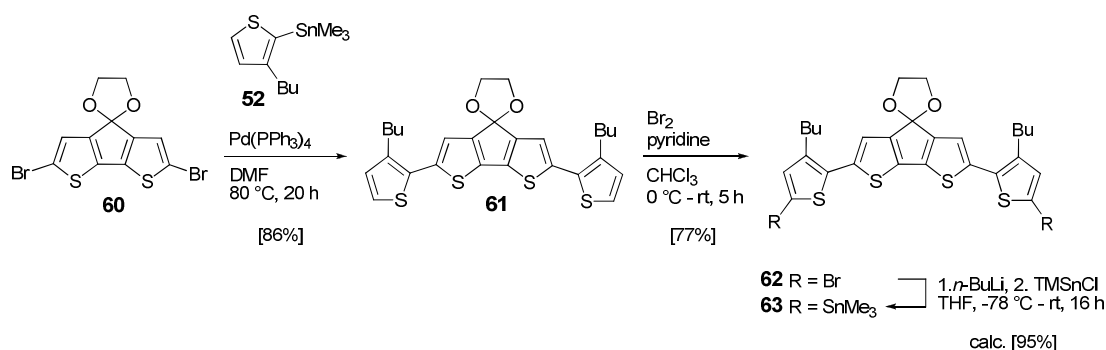
Scheme 3.10: Synthesis of dihalogenated fused DCP core unit **60**.

Finally, dibrominated DCP **60** was prepared from **59** by the use of elemental bromine with the addition of pyridine under exclusion of light at 0 °C. After purification via column chromatography **60** was afforded as a yellow solid in 90% yield.

3.3.2.2 Synthesis of DCP-containing quaterthiophene **61**

To synthesize oligomer **63** as desired precursor for the macrocyclization step, a Stille cross-coupling reaction of **60** and 3-butyl-2-(trimethyltin)thiophene **52** was performed under Pd(0) catalytic conditions (Scheme 3.11). After purification by column chromatography, quaterthiophene **61** was obtained as an orange oil in 86% yield.

Subsequently, introduction of bromine at the free α -positions of the external thiophene units was performed under general conditions utilizing elemental bromine with the addition of pyridine. The crude compound was purified by column chromatography and **62** was obtained in 77% yield as a yellow solid.



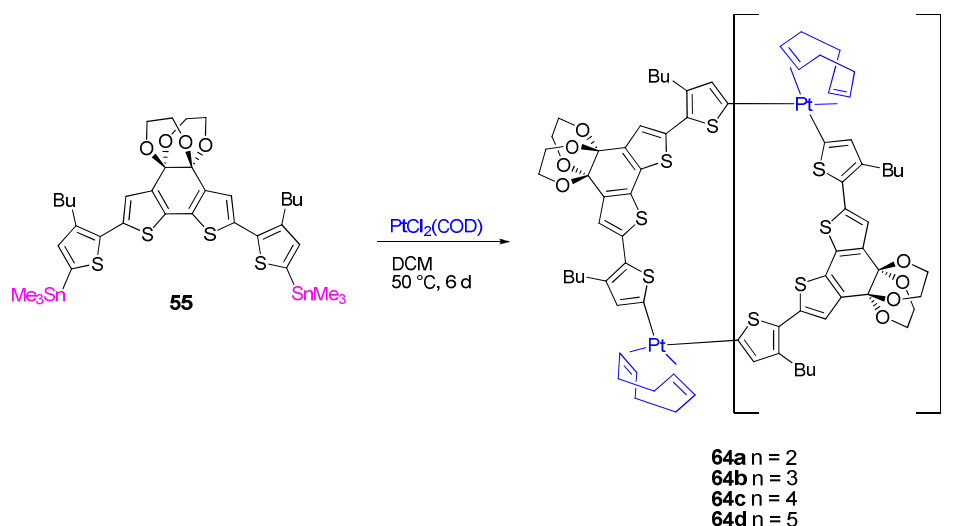
Scheme 3.11: Synthesis of distannylated macrocyclization precursor **63**.

Finally, a halogen-lithium exchange was generated with *n*-butyl lithium at -78 °C and the dilithiated intermediate was trapped with trimethyltin chloride. The yield of 95% for distannylated quaterthiophene **63** was calculated via proton NMR spectroscopy. As side products, the monostannylated derivative and dehalogenated starting material occurred. Like for the DTB-core unit described previously, quaterthiophene **63** was applied without further purification to the macrocyclization step.

3.3.3 Macrocyclization via the ‘metal-assisted template method’

3.3.3.1 DTB-containing macrocyclic Pt^{II}(COD)oligothienyl complexes **64a-d**

Distannylated DTB-quaterthiophene **55** was reacted with PtCl₂(COD) in dichloromethane under reflux for six days to obtain a mixture of multinuclear macrocyclic Pt^{II}(COD)oligothienyl complexes **64a-d** (Scheme 3.12).



Scheme 3.12: Synthesis of multinuclear macrocyclic Pt^{II}(COD)oligothienyl complexes **64a-d**.

The reaction was controlled via proton NMR spectroscopy after three and six days. Figure 3.1 shows the ¹H NMR spectra of distannylated precursor **55** (bottom) and a reaction sample after three days (top). The intensity of the singlet of the tin groups of starting material **55** at $\delta = 0.37$ ppm was compared to the intensity of the singlet of eliminated trimethyltin chloride at $\delta = 0.67$ ppm in the reaction sample, whereby the conversion of the reaction was calculated. After the mentioned reaction time of six days, no starting material could be detected and therefore the reaction was stopped.

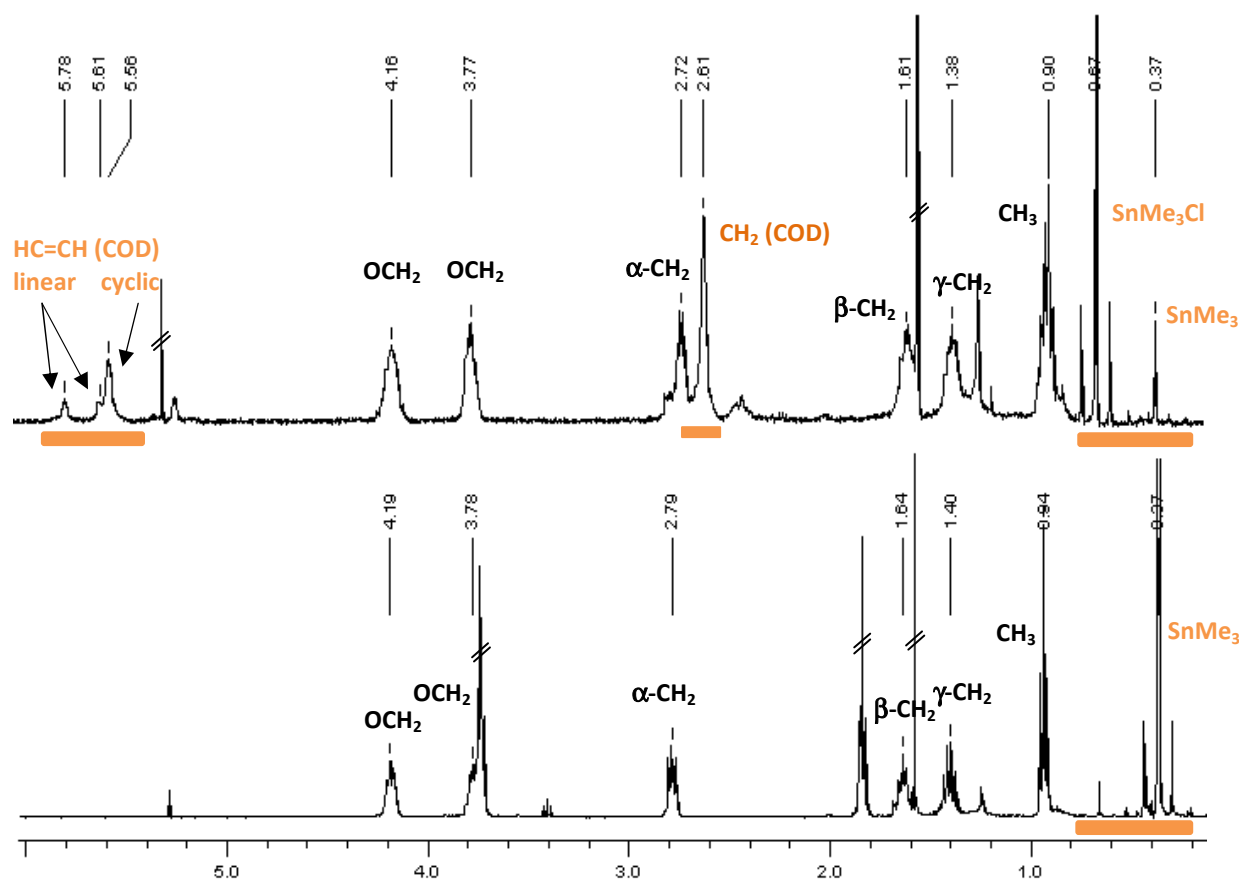


Figure 3.1: ^1H NMR spectra of a reaction sample after three days (top) and distannylated precursor **55** (bottom), measured in CDCl_3 (400 MHz). Impurities of THF and CH_2Cl_2 are present.

Two weak and broad signals at $\delta = 5.78$ and $\delta = 5.61$ ppm occurred in the spectrum, which correspond to the protons of the double bond (HC=CH) of the 1,5-cyclooctadien (COD) ligand in asymmetric linear intermediates with chlorinated end groups. A possible structure of such a linear intermediate **65** is proposed in Chart 3.5. A broad and strong signal at $\delta = 5.56$ ppm was observed at the same time and can be ascribed to the protons of the double bond (HC=CH) of COD in cyclic, symmetric structures (see also Figure 3.2). Thus, it was concluded that both cyclic and linear $\text{Pt}^{\text{II}}(\text{COD})$ oligothienyl complexes were formed whereby the amount of cyclic structures predominated according to ^1H NMR calculations. The signal at $\delta = 2.61$ belongs to the CH_2 -groups of the COD ligand. The signals of the butyl side chains of the reaction sample and precursor **55** were located at similar chemical shifts of around $\delta = 2.70$, 1.60 , 1.40 , and 0.90 ppm for the α -CH₂, β -CH₂, γ -CH₂, and CH₃-groups, respectively. The introduced ethylene glycol protecting groups (OCH₂) were at around $\delta = 4.00$ ppm. The aromatic regions of the spectra were omitted for clarity, since a huge number of singlet signals occurred in the spectrum of the reaction sample, which can be attributed to aromatic thiophene protons of the starting material, cyclic and linear intermediates.

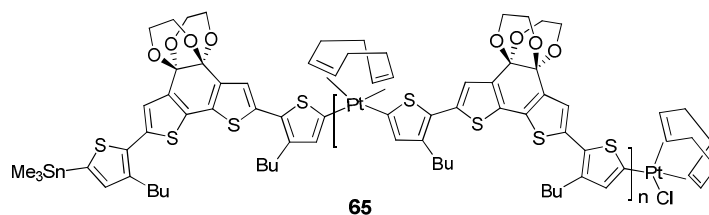


Chart 3.5: Proposed structure of an asymmetric linear intermediate during macrocyclization reaction.

The reaction product **64a-d** was filtered through a short plug of deactivated aluminium oxide to remove trimethyltin chloride from the reaction mixture.

To purify the mixture of cyclic $\text{Pt}^{\text{II}}(\text{COD})$ oligothienyl complexes, to separate linear side products, and to isolate the various metallacycles, raw material **64a-d** was extensively chromatographed via size exclusion chromatography (SEC) and four fractions were collected. The first three fractions contained only traces of material, whereas the last fraction comprised enough material to be investigated by proton NMR spectroscopy and mass spectrometry. The characterization revealed the cyclotrimeric macrocycle $\text{Pt}(\text{COD})[12]\text{DTB}$ **64a** (Chart 3.6) which could be isolated pure in 23% yield.

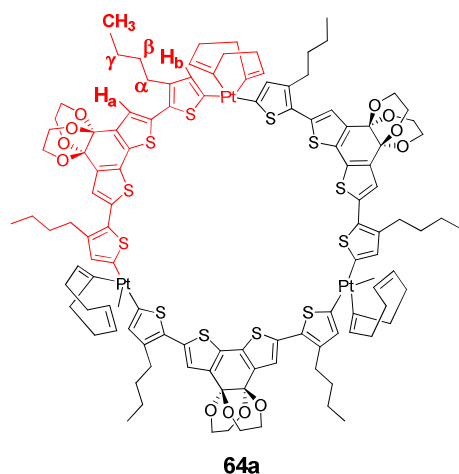


Chart 3.6: Structure of the cyclotrimeric platinum-containing macrocycle $\text{Pt}(\text{COD})[12]\text{DTB}$ **64a**.

In the ^1H NMR spectrum (Figure 3.2), characteristic signals of the aromatic thiophene protons of the cyclic backbone were found at $\delta = 7.05$ for H_a and 6.60 ppm for H_b . The multiplets of the COD ligand lie at $\delta = 5.55$ ppm ($\text{HC}=\text{CH}$) and 2.61 ppm (CH_2). Two signals which can be assigned to the ethylene glycol protecting groups (OCH_2) were observed at around $\delta = 4.00$ ppm. Corresponding triplet and multiplet signals of the attached butyl side chains were shifted up-field at $\delta = 2.72$, 1.60, 1.38, and 0.90 ppm for the $\alpha\text{-CH}_2$, $\beta\text{-CH}_2$, $\gamma\text{-CH}_2$, and CH_3 -groups, respectively.

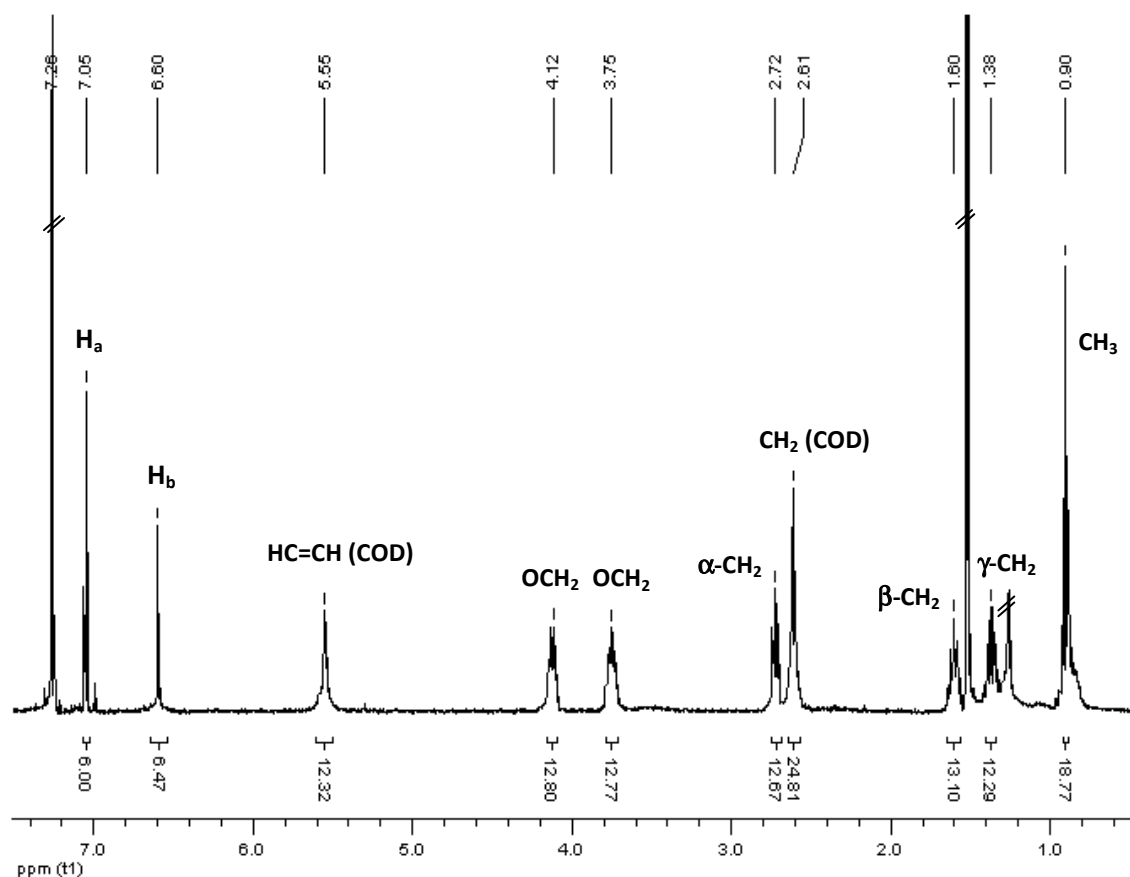
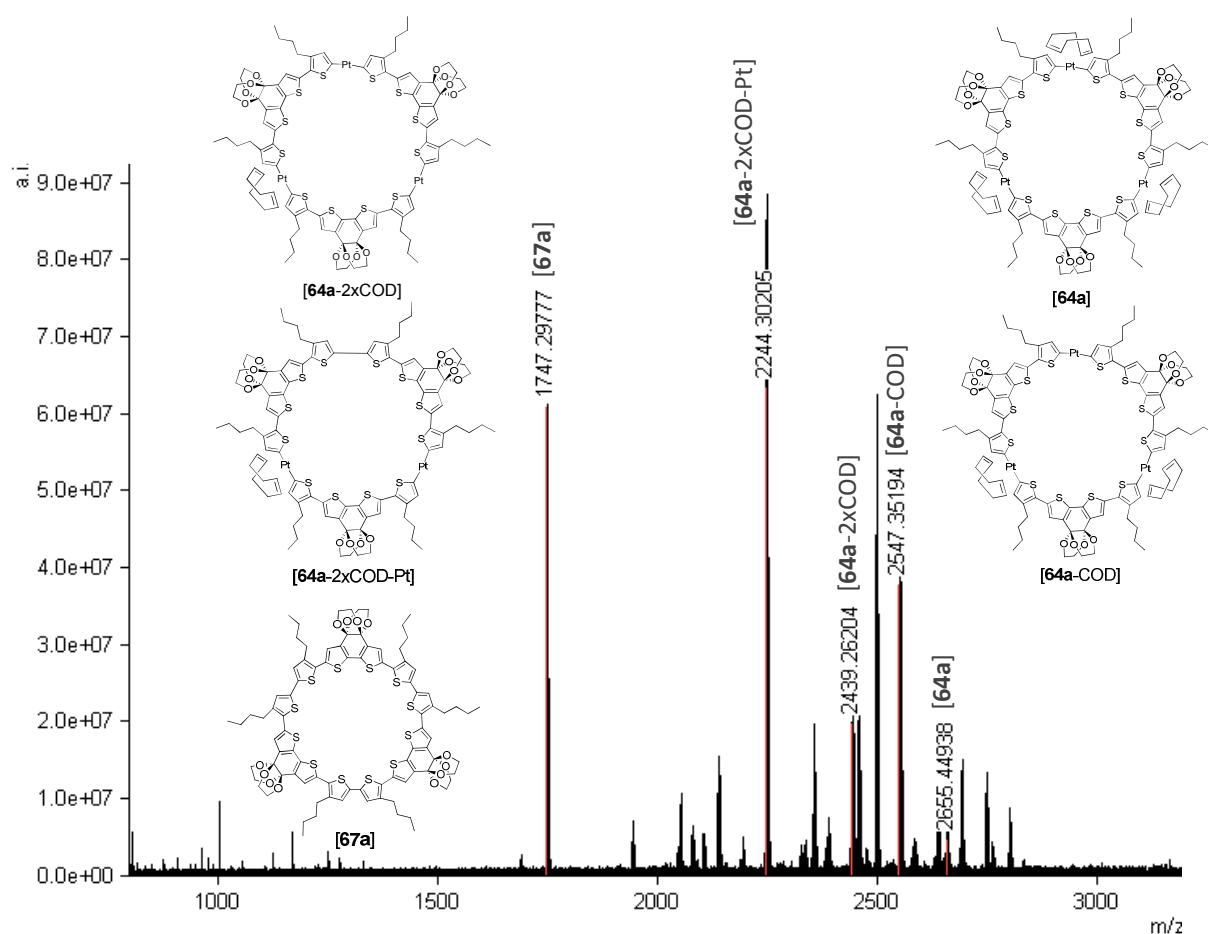


Figure 3.2: ^1H NMR spectrum of the highly symmetric metallacycle **64a**, measured in CDCl_3 (400 MHz). Impurities of *n*-hexane and water belong to the solvent.

The recorded spectrum of the mass analysis (MALDI-TOF) (Figure 3.3) exhibited for **64a** besides the calculated mass of $m/z = 2655.4$ also signals of fragments which evolved upon ionization and which followed a defined pattern. The data are summarized in Table 3.1 and a successive decomposition can be observed, since the measurement conditions were too harsh for the platinum-containing macrocycle. Firstly, one COD ligand was eliminated, then a second one combined with one platinum till the fully α -conjugated trimeric macrocycle **67a** was detected. Figure 3.3 shows the high resolution mass spectrum of **64a**.

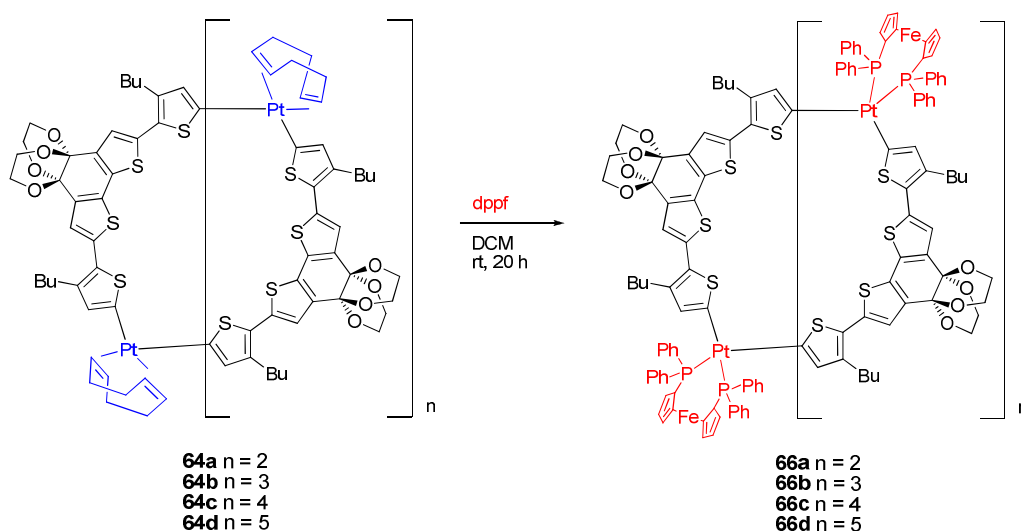
Table 3.1: Summarized data of the successive decomposition of **64a** during mass analysis.

metallacycle	<i>m/z</i>
[64a]	[M] ⁺ calcd. (C ₁₁₄ H ₁₂₆ O ₁₂ Pt ₃ S ₁₂): 2655.48410 / found [M] ⁺ : 2655.44938
[64a -COD]	[M] ⁺ calcd. (C ₁₀₆ H ₁₁₄ O ₁₂ Pt ₃ S ₁₂): 2547.39020 / found [M] ⁺ : 2547.35194
[64a -2xCOD]	[M] ⁺ calcd. (C ₉₈ H ₁₀₂ O ₁₂ Pt ₃ S ₁₂): 2439.29630 / found [M] ⁺ : 2439.26204
[64a -2xCOD-Pt]	[M] ⁺ calcd. (C ₉₈ H ₁₀₂ O ₁₂ Pt ₂ S ₁₂): 2244.33153 / found [M] ⁺ : 2244.30205
[67a]	[M] ⁺ calcd. (C ₉₀ H ₉₀ O ₁₂ S ₁₂): 1746.30808 / found [M+H] ⁺ : 1747.29777

**Figure 3.3:** MALDI-TOF mass spectrum of Pt(COD)[12]DTB **64a** and detected fragments.

Concerning the larger analogues **64b-d**, a characterization of these fractions proved to be difficult as too less amount of material was available for proton NMR spectroscopy and mass spectrometry did not reveal any significant results due to the instability of the platinum macrocycles during the measurement. Nevertheless, **64b-d** can be assigned to the larger macrocycles within the series of **64a-d**, since MALDI-TOF spectra of the platinum free, fully α -conjugated analogues in Chapter 3.3.3.2 showed the appropriate values for the higher analogues.

The next reaction step included a ligand exchange reaction of the mixture of multinuclear Pt^{II} metallacycles **64a-d** which was carried out in dichloromethane at ambient temperature overnight (Scheme 3.13). COD was completely replaced by 1,1'-bis(diphenylphosphino) ferrocene (dppf), which was followed by proton NMR spectroscopy of the crude material. Characteristic signals of the attached dppf ligands (multiplets around 7.40 ppm and 4.30 ppm) and cleaved off COD (singlets at 5.58 ppm and 2.38 ppm) were observed. The crude mixture of Pt^{II} (dppf)oligothienyl complexes **66a-d** was not further purified or investigated, but used directly into the next reaction step, the reductive elimination.

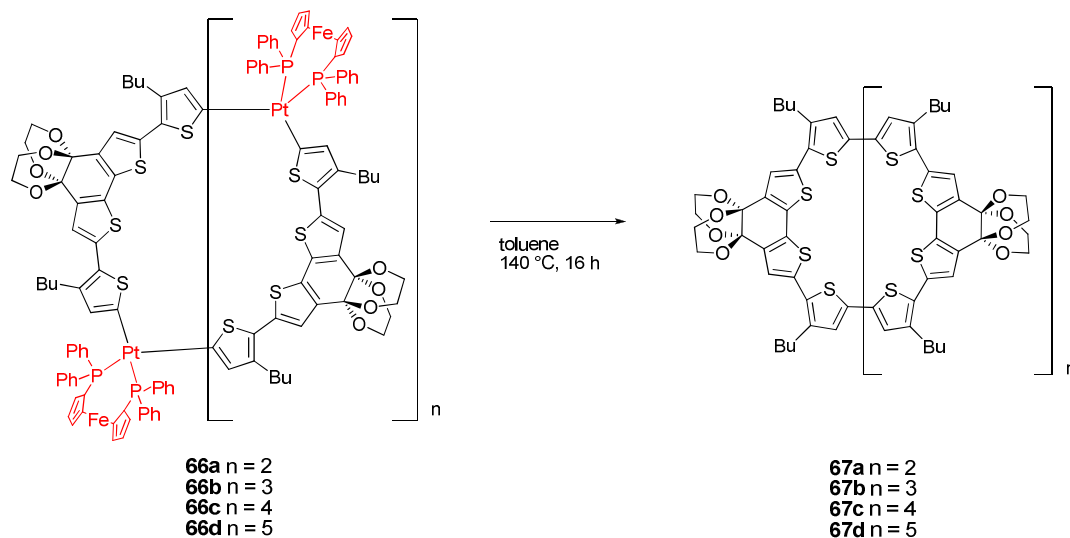


Scheme 3.13: Ligand exchange reaction with dppf towards DTB-based Pt^{II} (dppf)oligothienyl complexes **66a-d**.

3.3.3.2 Fully α -conjugated DTB-functionalized cyclo[n]thiophenes via thermally induced reductive elimination

The release of the platinum centers towards novel, fully α -conjugated acceptor-functionalized cyclo[n]thiophenes is outlined in Scheme 3.14. The thermally induced reductive elimination was carried out for the DTB-containing Pt^{II} (dppf) complexes **66a-d** in toluene at 140 °C within 16 h. The obtained crude mixture of **67a-d** was separated into the individual macrocycles via SEC. The collected fractions were characterized via mass analysis and four ring sizes with 12, 16, 20, and 24 thiophene units were detected. The mass values are: $m/z = 1746.4$ [M^+] for C[12]DTB (calcd.: $m/z = 1747.3$), $m/z = 2328.2$ [M^+] for C[16]DTB (calcd.: $m/z = 2328.4$), $m/z = 2912.7$ [M^+] for C[20]DTB (calcd.: $m/z = 2911.5$), and $m/z = 3492.3$ for C[24]DTB (calcd.: $m/z = 3492.6$). The cyclotrimeric species C[12]DTB was formed as the main product. The higher homologues occurred in considerable lower parts. The separated macrocycles were also characterized via proton NMR spectroscopy and showed next to

the cyclic signals also impurities of linear oligomers, which could be determined from appearing doublets of free, non-reacted α -protons of the external thiophene units.



Scheme 3.14: Thermally induced reductive elimination to DTB-containing macrocycles **67a-d**.

Further purification of the individual macrocycles was carried out by precipitation, whereat the different solubility of cyclic and linear species played the crucial role. The circularly shaped compounds form more facile aggregates compared to the flexible linear oligomers due to the relatively planar geometry of the rings and precipitate first. Thus, the impure compound was dissolved in dichloromethane and precipitated by adding *n*-hexane dropwise. Two acceptor-functionalized fully α -conjugated macrocycles, cyclotrimer C[12]DTB **67a** and cyclotetramer C[16]DTB **67b**, were obtained pure in an overall yield of 8% and 4%, respectively (Chart 3.7). The conversion was calculated from distannylated quaterthiophene **55**. Both isolated macrocycles were characterized by proton NMR spectroscopy (Figure 3.4) and mass spectrometry (Figure 3.5) and were as well investigated with respect to their optical and electronic properties. No pure products of the higher homologues **67c,d** could be obtained due to a low amount of material.

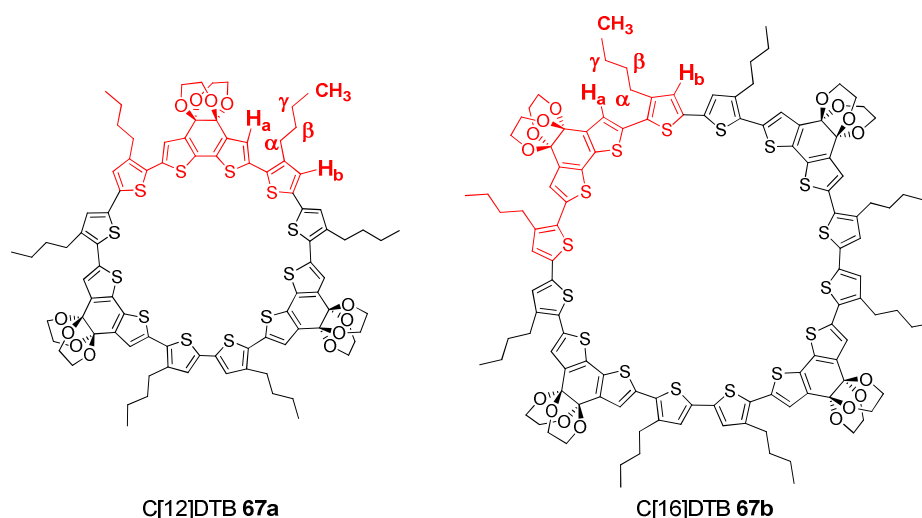


Chart 3.7: Structures of successfully isolated macrocycles C[12]DTB **67a** and C[16]DTB **67b**.

The ^1H NMR spectra of **67a** and **67b** revealed two typical downfield shifted singlets for the aromatic protons of the highly symmetric cyclic backbone (**67a**: $\delta = 7.17$ for H_a and 7.06 ppm for H_b , **67b**: $\delta = 7.18$ for H_a and 7.05 ppm for H_b). Triplet and multiplet signals of the attached butyl side chains ($\alpha\text{-CH}_2$, $\beta\text{-CH}_2$, $\gamma\text{-CH}_2$, CH_3) were shifted up-field towards the aliphatic region at $\delta = 2.78$, 1.70, 1.46, and 0.98 ppm, respectively. The signals of the ethylene glycol protecting groups (OCH_2) were located at around 4.00 ppm. The latter signals occurred for both macrocycles at the same chemical shifts, whereat it is noticeable, that the distance between the aromatic protons H_a and H_b increased slightly for the larger macrocycle C[16]DTB compared to C[12]DTB. No antiaromatic ring current could be detected, probably due to conformational flexibility in solution indicating a more benzoid than annulenoid character of the ring.

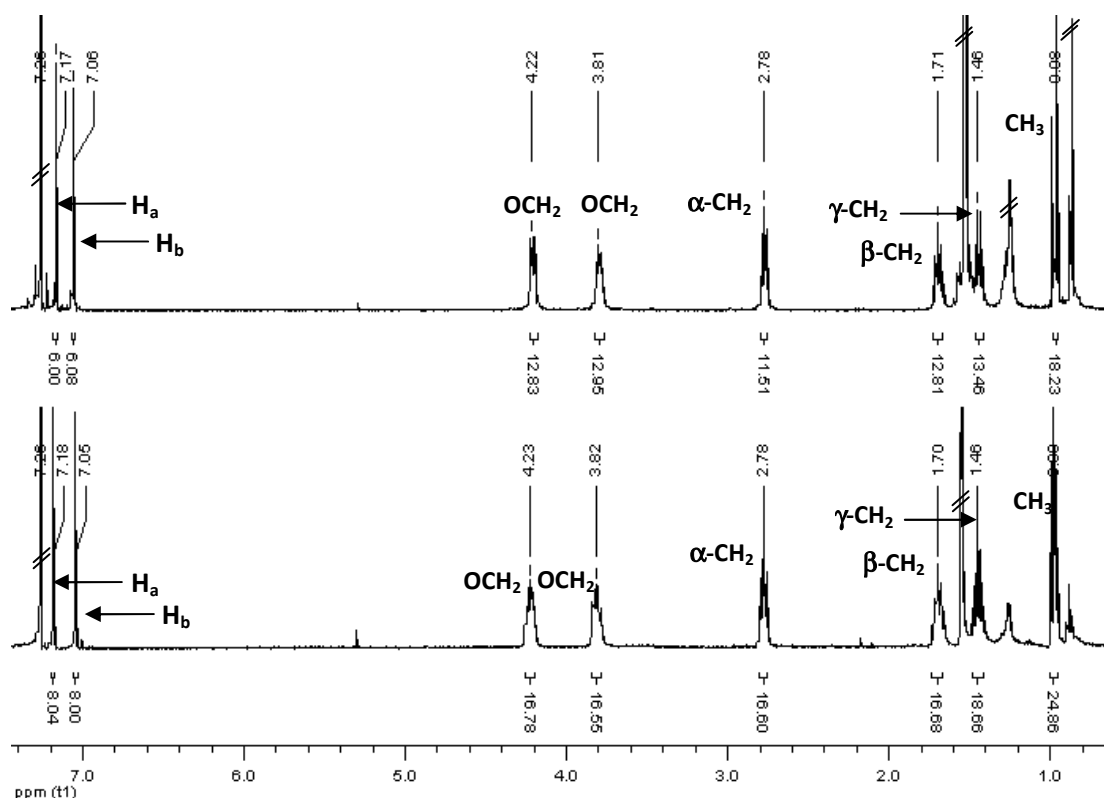


Figure 3.4: ^1H NMR spectra of the highly symmetric macrocycles **67a** (top) and **67b** (bottom), measured in CDCl_3 (400 MHz). Impurities of *n*-hexane and water are present.

The MALDI-TOF mass spectra of **67a** and **67b** showed characteristic single signals at $m/z = 1747.0$ [M^+] for **67a** and $m/z = 2328.5$ [M^+] for **67b** which well correspond to the theoretical calculated mass for both compounds (calcd.: $m/z = 1747.3$; $m/z = 2328.4$). The recorded high resolution MALDI-TOF mass spectra provided an accuracy of $\delta_{m/m} = 0.3$ and $\delta_{m/m} = 0.8$ ppm, respectively, whereby the experimental isotopic distribution was found to be in very good agreement with the calculated one.

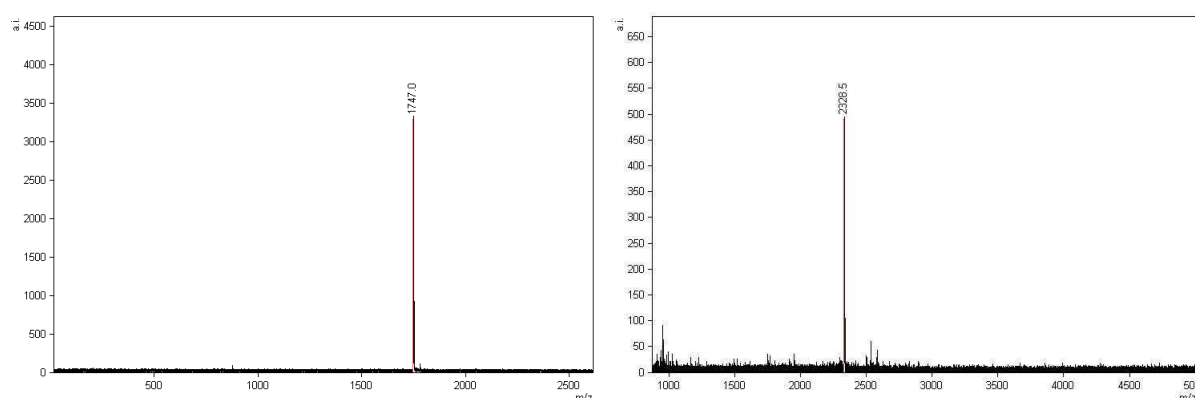


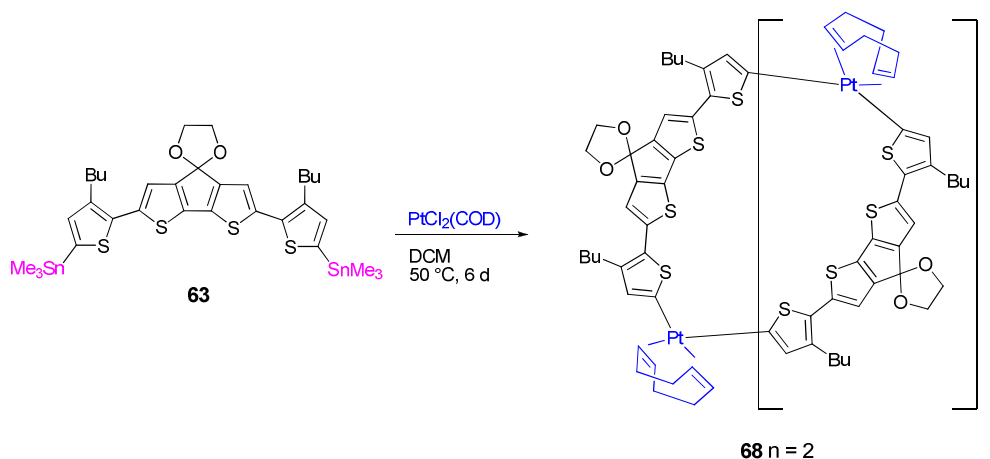
Figure 3.5: MALDI-TOF mass spectra of C[12]DTB **67a** (left) and C[16]DTB **67b** (right).

Furthermore, a single crystal of C[12]DTB **67a** was grown by diffusion of *n*-hexane into a solution of the trimeric cycle in chloroform at low temperatures. The obtained X-ray crystallographic structure analysis revealed a fully resolved cyclic backbone, proving the formation of a circularly shaped

material via the presented one-pot synthesis. Details on the structural analysis are given in Chapter 3.10.

3.3.3.3 DCP-containing macrocyclic Pt^{II}oligothienyl complexes

According to the DTB-containing system, DCP-based precursor **63** was as well reacted with PtCl₂(COD) in dichloromethane under reflux for six days (Scheme 3.15). The reaction was followed by proton NMR spectroscopy by comparing the intensity of the arising trimethyltin chloride at $\delta = 0.67$ ppm and the intensity of the tin groups of quaterthiophene **63** at $\delta = 0.37$ ppm. After a period of six days, the reaction was stopped and multinuclear macrocyclic Pt^{II}(COD)oligothienyl complex **68** was formed.



Scheme 3.15: Synthesis of multinuclear macrocyclic Pt^{II}(COD)oligothienyl complex **68**.

A comparison between the proton NMR spectrum of starting material **63** (bottom) and a reaction sample after six days (top) is shown in Figure 3.6. It is clearly visible that nearly no precursor **63** was left after the mentioned reaction time, since the singlet signal at $\delta = 0.37$ ppm is almost vanished. Instead, a huge singlet signal of arising SnMeCl₃ emerged at $\delta = 0.67$ ppm. At the same time, two broad signals belonging to the COD ligands in cyclic symmetric systems appeared at $\delta = 5.56$ (HC=CH) and 2.61 (CH₂) ppm. COD signals which can be assigned to linear asymmetric products and are usually located at around $\delta = 5.70$ and 5.60 ppm (see Chapter 3.3.3.1) did hardly appear. Therefore, the formation of a high amount of cyclic products with a low amount of linear byproducts was expected. This fact is also supported by the aromatic region of the spectrum of the reaction sample since, compared to its DTB-analogue, a manageable number of signals can be detected. No singlets of distannylated DCP-quaterthiophene **63** were left. Instead, two clear singlets at $\delta = 6.83$ and 6.66 ppm occurred which can be assigned to the aromatic thiophene protons of one macrocycle size. The remaining signals belong to different ring sizes and byproducts. The ethylene glycol protecting groups

(OCH₂) were located at around $\delta = 4.00$ ppm. The signals of the introduced butyl side chains showed similar chemical shifts for both the reaction sample and precursor **63** at around $\delta = 2.70$, 1.60, 1.40, and 0.90 ppm for the α -CH₂, β -CH₂, γ -CH₂, and CH₃-groups, respectively.

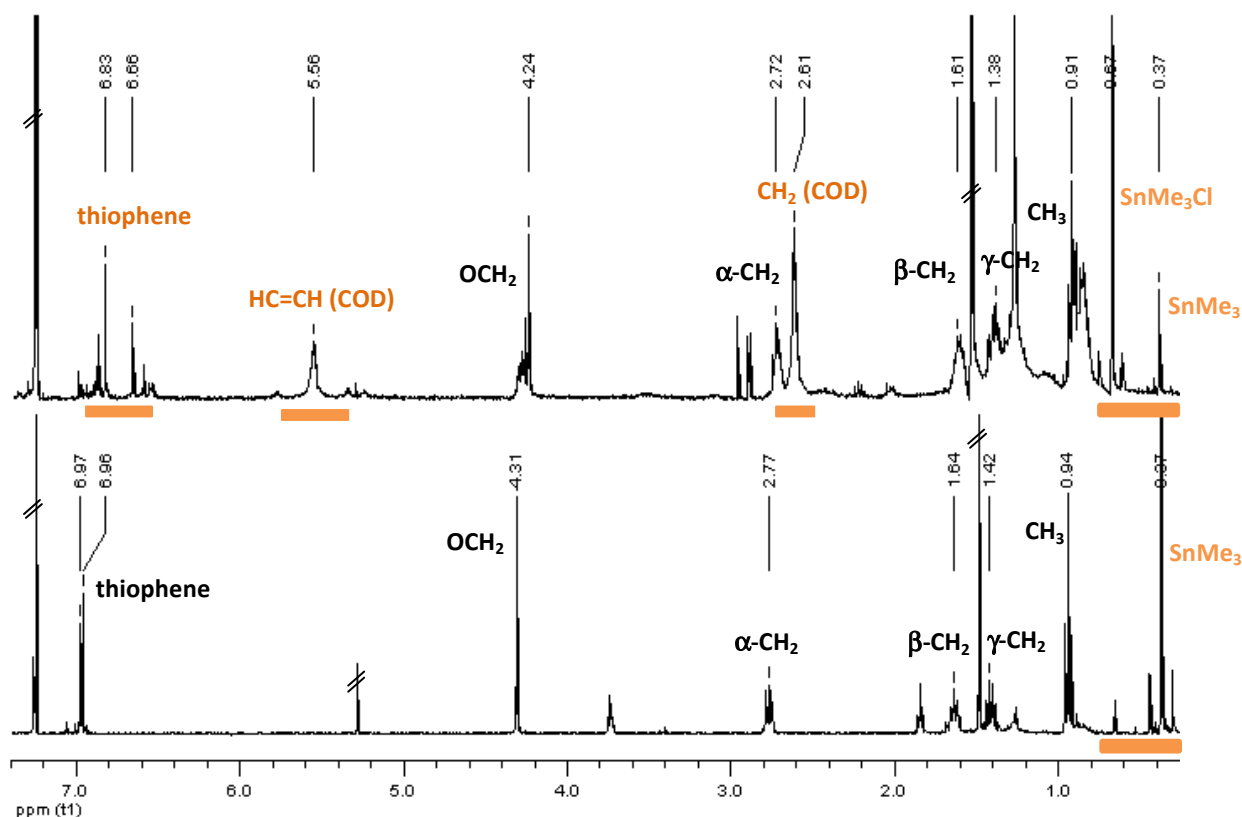
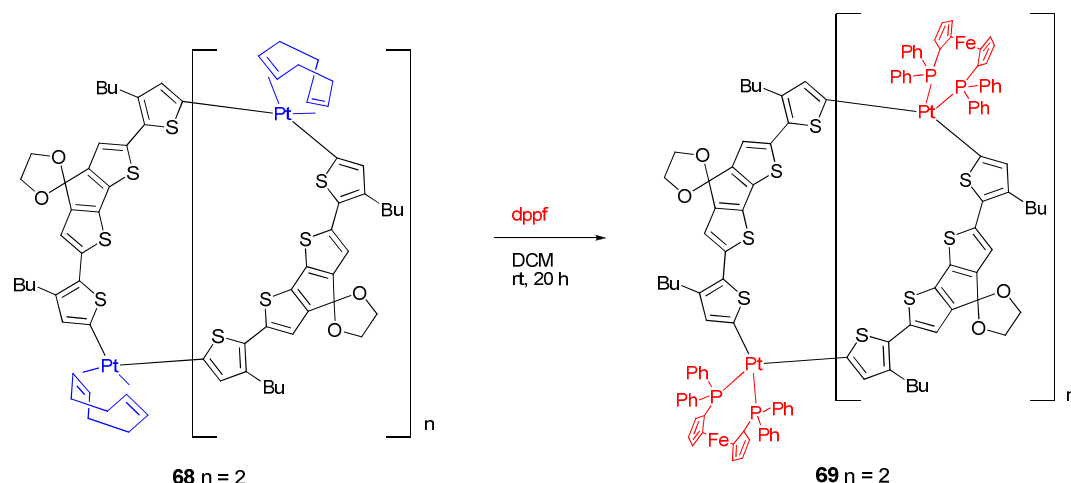


Figure 3.6: ¹H NMR spectra of a reaction sample after six days (top) and distannylated precursor **63** (bottom), measured in CDCl₃ (400 MHz).

The Pt^{II}(COD)oligothienyl complex **68** was filtered through a short plug of deactivated aluminium oxide to remove trimethyltin chloride from the reaction mixture and afterwards chromatographed via SEC to separate byproducts. However, the purification process could not deliver a pure ring, since the collected fraction was investigated via proton NMR spectroscopy and showed a considerable amount of impurities. It seemed that during purification little decomposition of the material evolved since the preliminary orange fraction-band exhibited a black tail. MALDI-TOF mass spectra did not show the calculated values either, which could mainly be due to the too harsh measurement conditions which decomposed the metallacycle. A purification of the macrocycle was no longer investigated and the crude product mixture **68** was used directly into the next reaction step, the ligand exchange reaction, which was carried out with dppf in DCM at room temperature overnight (Scheme 3.16).



Scheme 3.16: Ligand exchange reaction with dppf towards DCP-based $\text{Pt}^{\text{II}}(\text{dppf})$ oligothienyl complex **69**.

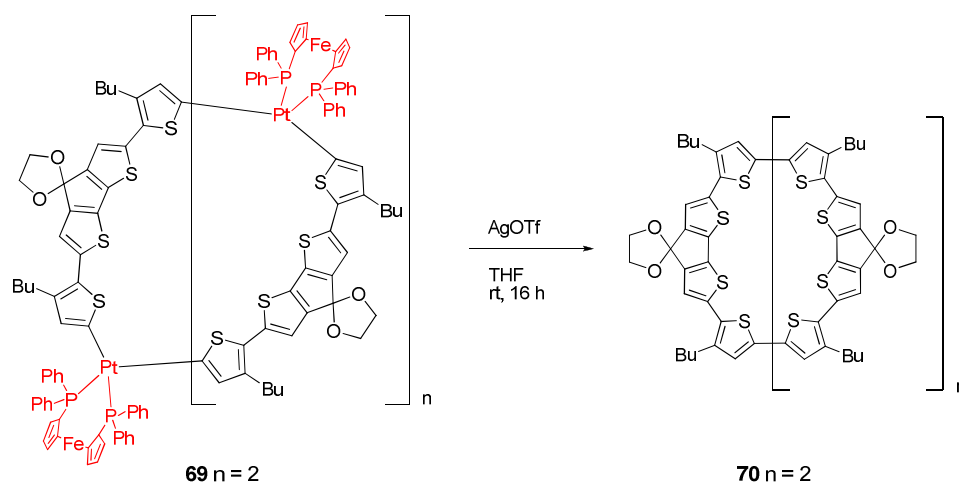
The reaction was followed by proton NMR spectroscopy of the crude material. Typical signals of the introduced dppf ligands (multiplets at around $\delta = 7.60$, 7.30 , and 4.30 ppm) as well as of eliminated COD (singlets at $\delta = 5.59$ and 2.37 ppm) indicated a successful conversion. Neither any purification processes nor investigations were performed with the crude $\text{Pt}^{\text{II}}(\text{dppf})$ oligothienyl complex **69**. The raw material was used directly into the next reaction step.

3.3.3.4 Fully α -conjugated DCP-functionalized cyclo[n]thiophenes via oxidatively induced reductive elimination

The initially thermally induced reductive elimination failed when the method was applied to the reaction mixture of DCP-metallacycle **69**. The release of the transition metal corners under simultaneous C-C bond formation obviously took place as some black solid precipitated, which might be assigned to elemental platinum. However, investigations via proton NMR and mass analysis showed no typical signals that could be ascribed to cyclic structures, but rather to polymeric material. The heat of the reaction (140°C) was obviously too harsh. A successful C-C bond formation seems difficult between the slightly bended oligothiophene moieties. The ring strain within the cyclic $\text{Pt}^{\text{II}}(\text{dppf})$ complex is probably too strong and no ring closure might occur due to thermally induced strong vibrations.

An alternative route to initialize a concerted 1,1-reductive elimination is the use of a chemical oxidant under mild reaction temperatures. Elemental iodine has already been used by Fuhrmann and dislocated an uncontrollable reaction by the simultaneous formation of several fully π -conjugated macrocycles starting the reaction from only one defined Pt-intermediate.^[21] Thus, the one-electron oxidant silver(I)triflate (AgOTf) was utilized as an effective oxidant, which has already been described

by Zhang, who promoted defined linear oligothiophenes from Pt^{II} oligothienyl complexes.^[22] The reaction for the macrocyclic compound is illustrated in Scheme 3.17.



Scheme 3.17: Oxidatively induced reductive elimination to DCP-containing macrocycle **70**.

The crude mixture of DCP- Pt^{II} (dppf)complex **69** was reacted with two equivalents of AgOTf per platinum atom at ambient temperature generating gentle reaction conditions. The reaction mixture of **70** was subsequently purified via size exclusion chromatography (Chart 3.8).

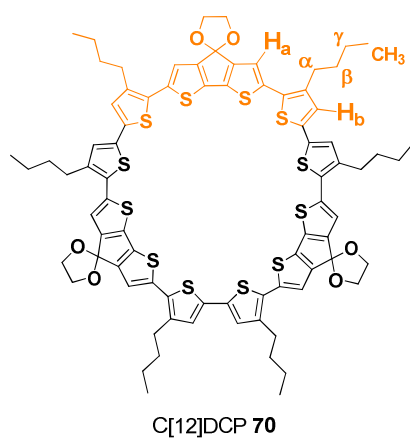


Chart 3.8: Structure of the successfully isolated trimeric macrocycle C[12]DCP **70**.

Noticeable with the purification of macrocycle **70** was the appearance of a black tail at the end of the fraction which might be a sign of decomposition. The tail was largely separated from the main band and the structure of fully α -conjugated C[12]DCP **70** was proven by mass spectrometric analysis (Figure 3.7). The single experimental detected value of $m/z = 1530.9$ is consistent with the theoretical expected one (calcd.: $m/z = 1530.2$).

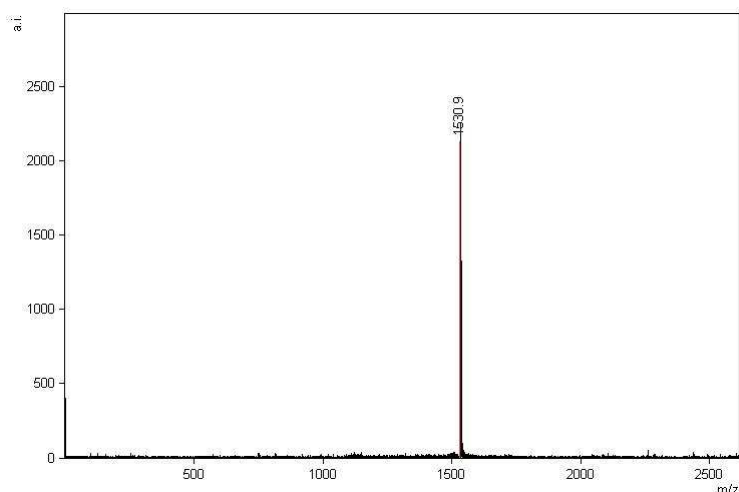


Figure 3.7: MALDI-TOF mass spectrum of C[12]DCP **70**.

The structure was also identified by proton NMR analysis due to two typical downfield shifted signals of the aromatic protons of the highly symmetric cyclic backbone ($\delta = 7.00$ ppm for H_a and 6.88 ppm for H_b) as well as characteristic signals of the ethylene glycol protecting groups (OCH_2) at $\delta = 4.34$ ppm (Figure 3.8). Triplet and multiplet signals of the butyl side chains were observed at $\delta = 2.73$, 1.67, 1.42, and 0.97 ppm for the α - CH_2 , β - CH_2 , γ - CH_2 , and CH_3 -groups, respectively. Also in this case, no paratropic ring current was observed. The macrocycle was obtained with a calculated purity of 96% and further purification processes were carried out. For instance, a second SEC column-run, various precipitation approaches and standard silica column chromatography. All attempts to enhance the purity grade failed. Instead, the more purification attempts were carried out, the more impure the material got. This could be seen in the aromatic region of the proton NMR spectrum, since the amount of unknown signals increased constantly. An instability of the dissolved macrocycle over a longer period of time is supposed.

C[12]DCP **70** was finally obtained in an overall yield of 11%. The conversion was calculated including all reaction steps starting from dibrominated quaterthiophene **62**.

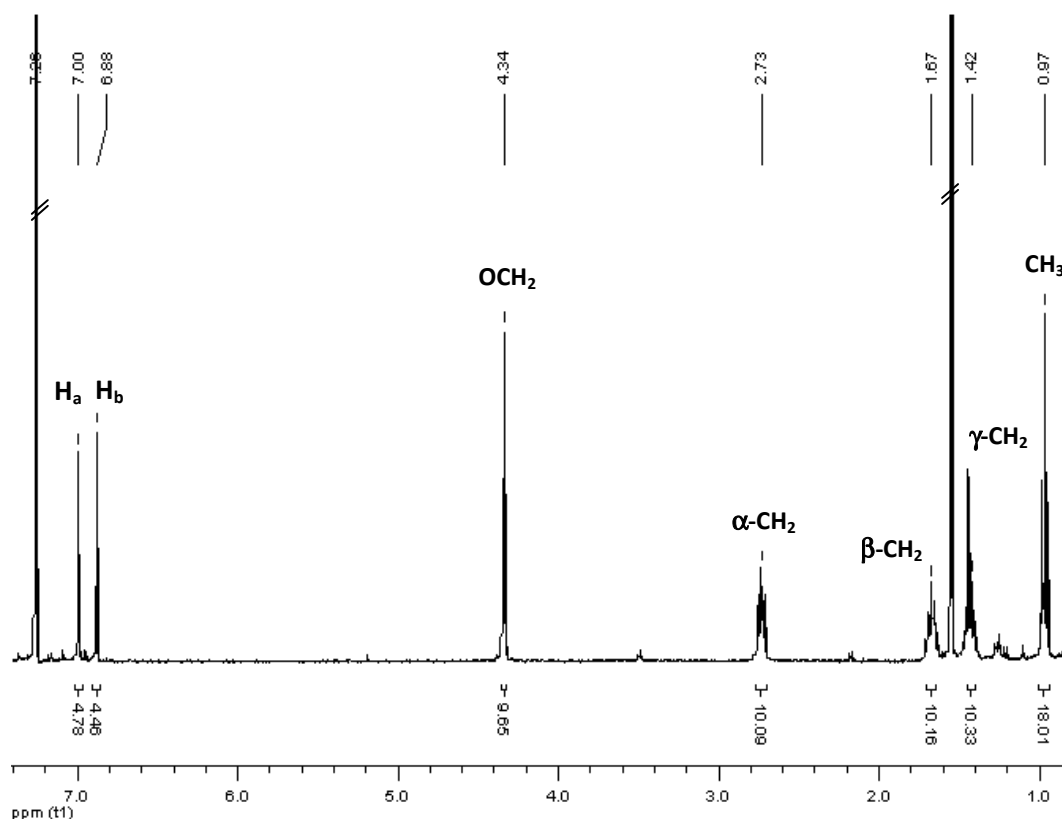
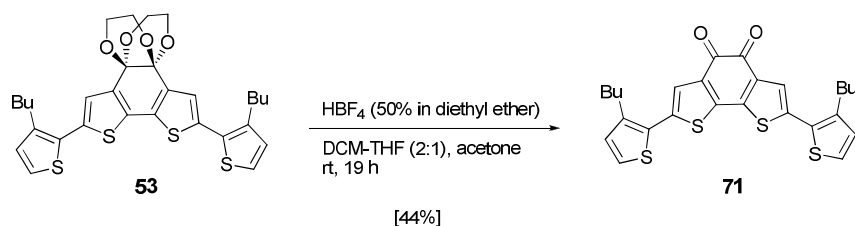


Figure 3.8: ^1H NMR spectrum of the highly symmetric macrocycle **70**, measured in CDCl_3 (400 MHz). Impurities of water belong to the solvent.

3.4. Deprotection of cyclic ketales

An important role after the isolation of the fully α -conjugated macrocycle C[12]DTB **67a** plays the deprotection of the cyclic ketals to regain free carbonyl groups, which supply a strong acceptor property and reactive centers for further chemical transformations into different organic functionalities. Several deprotection methods have been described in literature. Reiger described the decomposition of a protected DTB-quaterthiophene molecule when reacted with perchloric acid or *para*-toluenesulfonic acid. He succeeded in removing the protecting groups with the non-oxidizing tetrafluoroboric acid.^[10] Thus, quaterthiophene **53** was reacted with HBF_4 (50% in diethyl ether) at ambient temperature. Diethyl ether was added to increase the solubility of the inorganic acid in the organic solvent. Acetone should capture cleaved off ethylene glycol to shift the equilibrium towards the deprotected product. After purification via column chromatography, DTB-containing quaterthiophene **71** was obtained in 44% yield (Scheme 3.18).

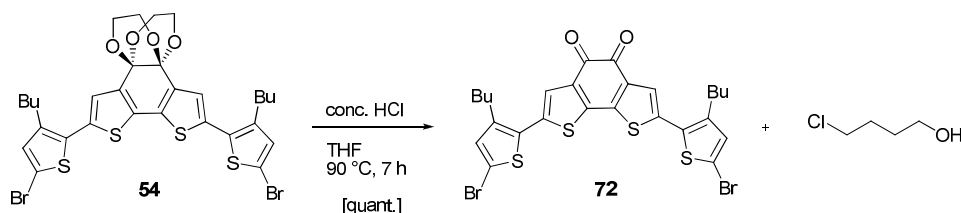


Scheme 3.18: Deprotection of the ethylene glycol protecting groups with HBF_4 to afford quaterthiophene **71**.

However, the conversion of the deprotection was too low to use these reaction conditions for the deprotection of the cyclic structures in which, in dependence of the ring size, six or even more acetals have to be deprotected at the same time. A nearly quantitative reaction was therefore needed. Admittedly, it has to be considered that the elimination of the ethylene glycol units in Scheme 3.18 was performed on a quaterthiophene with reactive α -positions at the external thiophene units which were activated for polymerization and oligomerization processes under these acidic conditions and led to a black precipitate.

The use of trifluoroacetic acid in THF at room temperature did not improve the above presented results. Instead, only starting material could be isolated without any formed product.

In literature or textbooks, the cleavage of acetals or ketals is often described by the use of concentrated hydrochloric acid. Dibrominated DTB-derivative **54** with bromine atoms at the external thiophene moieties was therefore treated with concentrated HCl in THF under reflux for 7 h (Scheme 3.19). The strong acidic conditions generated deprotected DTB **72** quantitatively. 1-Chloro-4-hydroxybutane was formed as a byproduct caused by the reaction of the solvent THF and concentrated HCl, but was removed without any problems under vacuum at slightly elevated temperatures.



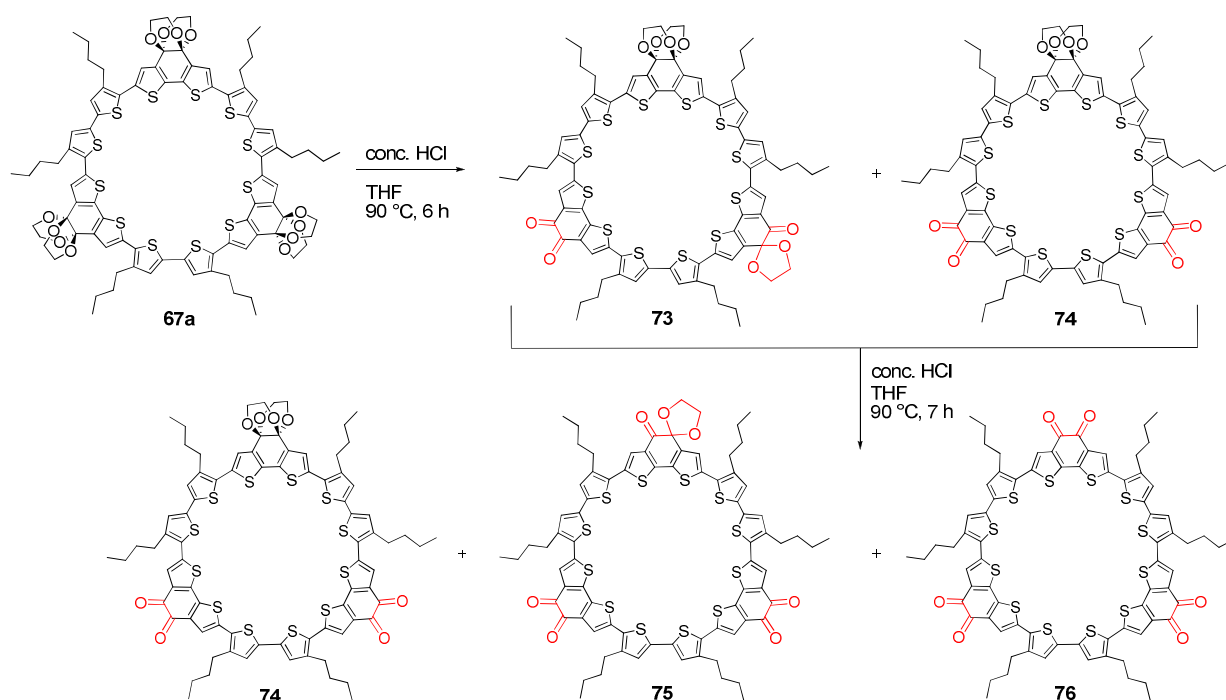
Scheme 3.19: Deprotection of the ethylene glycol protecting groups with concentrated HCl to afford DTB **72**.

The above described protocol for the deprotection of ketals by means of concentrated hydrochloric acid was then applied to macrocycle C[12]DTB **67a**.

3.4.1 Attempts towards deprotection of macrocycle C[12]DTB (**67a**)

Based on the promising results of the deprotection of the ethylene glycol units for 4T-DTB building block **54** with conc. HCl, reaction conditions were adopted and applied to macrocycle C[12]DTB **67a** to generate free carbonyl groups that provide a strong acceptor character and reactive sides to perform further chemistry (Scheme 3.20). Macrocycle **67a** was suspended in concentrated hydrochloric acid dissolved in THF and refluxed for 6 h. Partial deprotection of four ketals took place and the obtained macrocycles **73** and **74** were characterized via mass spectrometry. The experimental gained values of the mass analysis were $m/z = 1574.6$ for **74** (calcd. 1570.2) and $m/z = 1618.5$ for **73** (calcd. 1614.2). The detected masses of the crude products correspond to the respective fourfold protonated species due to remaining hydrochloric acid, since an aqueous work-up was not performed. The structures of the products were further proven by means of infrared (IR) spectroscopy. The IR spectra of the raw material clearly revealed strong bands, which are assigned to the carbonyl stretching mode of free ketone functionalities at $\nu = 1663\text{ cm}^{-1}$. Detected acetale stretching mode at $\nu = 1100\text{ cm}^{-1}$ diminished at the same time.

The low solubility of the partially deprotected macrocycles **73** and **74** hindered a successful conversion of the reaction, since they precipitated and could not react any longer with HCl. The experiment was repeated under more dilute conditions to largely dissolve the starting material and increase the reactivity towards HCl in general. During a reaction time of 7 h, a thick suspension was formed and a recorded mass spectrum exhibited the simultaneous existence of three macrocycles **74**, **75** and **76** with different numbers of free ketone functionalities. The fully deprotected target macrocycle **76** was formed. The detected signals showed the following values: $m/z = 1488.8$ for **76** (calcd. 1482.2), $m/z = 1532.9$ for **75** (calcd. 1526.2), and $m/z = 1576.0$ for **74** (calcd. 1570.2). The identified mass data revealed again higher values than the theoretically calculated isotopic mass due to remaining HCl. Separation of the compounds via SEC was not possible as the product mixture could not be dissolved.



Scheme 3.20: Deprotection of C[12]DTB **67a** with concentrated HCl and resulting partial deprotected macrocycles **73-76**.

The concentration of the reaction was varied in two following experiments, whereas the conversion of the deprotection reaction increased the more the concentration of the reaction was increased. In both cases again, an inseparable mixture of the above depicted cyclic structures **74**, **75**, and **76** was observed.

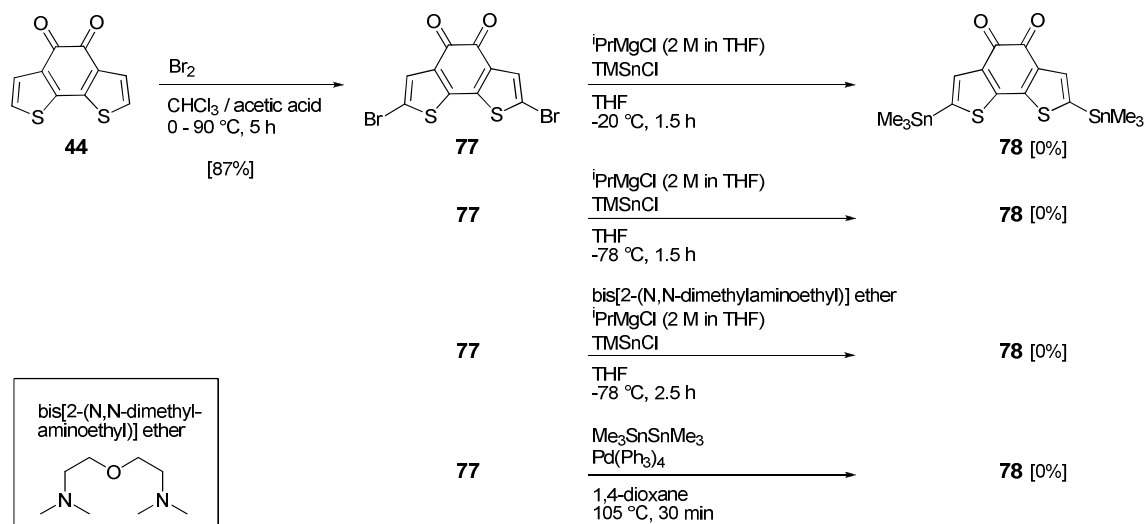
Another experiment was carried out with HBF_4 in a solvent mixture of dichloromethane and THF. A deprotection of the ketals hardly occurred.

The reason for the incomplete reaction is the low solubility of the partially deprotected species, since free carbonyl groups are in one plane with the DTB core unit and the whole molecule tends to adopt a planar and rigid configuration. This supports the assembly of the macrocycles in assumed stacked aggregates and facilitates precipitation. As soon as the cycles precipitate, no further reaction with HCl is guaranteed and the deprotection stops.

3.5 Approaches to by-pass carbonyl protections

Since a full deprotection of macrocycle **67a** failed due to solubility problems, some approaches have been undertaken to by-pass carbonyl protection reactions. Direct stannylation reactions to attach Me_3Sn -groups at the final cyclization-precursors were therefore investigated. The insertion of the tin groups is essential for the preparation of macrocycles, as pretemplated metallacycles only evolve due

to a reaction of the SnMe_3 -groups and the utilized Pt^{II} complex. The tin groups at the external thiophene units were formerly introduced using $n\text{-BuLi}$ as lithiation reagent. Thus, the free carbonyl groups of the DTB and DCP core units had to be protected in order to avoid a nucleophilic attack of $n\text{-BuLi}$ at the ketone functionalities. Four experiments have been carried out to investigate a direct insertion of the Me_3Sn -groups at the external free α -position, which are shown in Scheme 3.21.



Scheme 3.21: Four attempts to introduce tin groups via a direct stannylation process with free carbonyl groups present.

The reactions have been carried out on DTB core unit **44** which was treated with elemental bromine in a mixture of chloroform/acetic acid and refluxed for 5 h following a protocol by Höger et al.^[23] Dibrominated DTB **77** was obtained pure as a purple solid in 87% yield and the analytical data are consistent with the literature.^[23]

Using **77**, direct stannylation reaction was performed in THF with *iso*-propylmagnesium chloride (2 M in THF) at -20°C . A halogen-magnesium exchange^[24] to the corresponding Grignard-intermediate took place followed by trapping the metalated species with TMSnCl to capture reactive magnesium positions (Scheme 3.21, line 1). Soon after the reaction had started, a black oil occurred which indicated either decomposition or polymerization, which has been observed by proton NMR spectroscopy after work-up. By decreasing the reaction temperature to -78°C , like it is the case for a standard halogen-lithium exchange, no improvement was observed and the synthesis of **78** failed again since a black oil emerged (Scheme 3.21, line 2).

For both experiments it is likely that the formation of the organomagnesium intermediate is fast and trapped only slowly by trimethyltin chloride. The reactive metal-species is probably too instable and reacts therefore with adjacent molecules to polymers or attacks their free carbonyl functionalities. To deactivate the Grignard-species and thus prevent the organometallic intermediate to attack ketone groups, bis[2-(N,N -dimethylamino)ethyl] ether was added as an inhibitor in a third

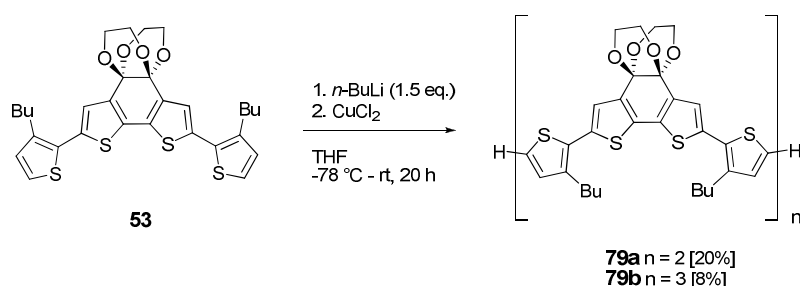
experiment (Scheme 3.21, line 3). A complex between the existing Grignard-reagent and the tridentate ether compound is expected to be formed, which is supposed to suppress side reactions as reported by Wang^[25]. Also in this case, only black oil and no product of **78** was formed.

In a fourth reaction, DTB **77** was reacted together with hexamethyldistannane and catalyst $\text{Pd}(\text{PPh}_3)_4$ in dry 1,4-dioxane and refluxed for 30 min (Scheme 3.21, line 4). During the reaction, a black oil was formed as previously described for the other experiments. The crude material was investigated by means of proton NMR spectroscopy and mass spectrometry, but no characteristic signals of **78** were observed.

3.6 Synthesis of linear DTB and DCP-containing oligothiophenes as model compounds

Linear DTB and DCP-containing oligomers were synthesized in order to investigate their optical and electronic properties and to compare them to the cyclic systems.

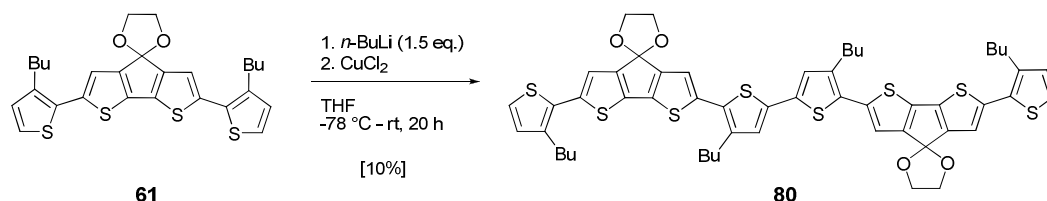
The synthesis of desired dodecamer **79b** was performed via reaction of **53** with *n*-butyl lithium (1.5 eq.) at -78°C followed by trapping the dilithiated species with copper(II) chloride to initiate oxidative C-C bond formation (Scheme 3.22). Dodecithiophene **79b** was gained as orange solid in only 8% yield after purification by column chromatography. Dimeric octithiophene L[8]DTB **79a** was isolated besides non-reacted starting material **53** in 20% yield. The presented pathway was chosen to generate linear oligomers in a fast and uncomplicated way without any additional synthetic steps by just starting from already available quaterthiophene **53**. In that process, yields played a less important role.



Scheme 3.22: Synthesis of linear oligothiophenes L[8]DTB **79a** and L[12]DTB **79b**.

Concerning the DCP core unit, the described oxidatively induced C-C bond formation with *n*-BuLi and CuCl_2 was also applied to quaterthiophene **61** and octithiophene L[8]DCP **80** was obtained in 10% yield after column chromatography (Scheme 3.23). The desired dodecithiophene L[12]DCP was also formed, but could not be isolated in pure form. Its structure was analyzed by proton NMR spectroscopy whereby undefined impurities in both the aromatic and aliphatic region were detected.

Further purification attempts using column chromatography did not succeed in a pure compound of L[12]DCP.



Scheme 3.23: Synthesis of linear octithiophene L[8]DCP **80**.

3.7 Optical properties of acceptor-functionalized cyclo[*n*]thiophenes

Shape-persistent cyclo[*n*]thiophenes initiate a unique behaviour in the photophysical analysis and exhibit fascinating optical properties in contrast to their linear analogues.^[26] Appealing structure property relationships were found for a series of macrocycles when compared to an appropriate linear oligomer.^[27] Cyclo[*n*]thiophenes represent ideal model compounds for corresponding oligomeric or polymeric structures without perturbing end-effects as generally, particularly for shorter oligomers, end-groups disrupt the structure-property correlation. In this respect, macrocycles provide an ‘infinite’ π -conjugated chain like an idealized polymer. The optical and electrochemical properties of the acceptor-functionalized ring systems and their linear analogues were investigated and results were compared to corresponding non-functionalized cyclothiophenes.

The photophysical characteristics were analyzed by absorption and fluorescence spectroscopy. Due to solubility problems of C[16]DTB **67b**, all spectra were recorded in chloroform as all compounds were molecularly dissolved. Figure 3.9 displays the absorption and emission spectra of acceptor-functionalized DTB-containing macrocycles C[12]DTB **67a** and C[16]DTB **67b** as well as corresponding linear analogues L[8]DTB **79a** and L[12]DTB **79b**. A summary of the absorption and emission maxima is given in Table 3.2.

Strong absorption maxima for the π - π^* transition of the cyclic compounds were observed at $\lambda = 453$ nm for **67a** and $\lambda = 457$ nm for **67b** with extinction coefficients of $\epsilon = 153.000$ and 140.000 $\text{Lmol}^{-1}\text{cm}^{-1}$, respectively. In accordance to a general conjugated series of linear oligomers, a red-shift in the main absorption band can be found for the bigger cycle since the conjugation length increases with increasing ring size. The red-shift is also present for both linear oligomers L[8]DTB **79a** ($\lambda = 457$ nm) and L[12]DTB **79b** ($\lambda = 474$ nm).

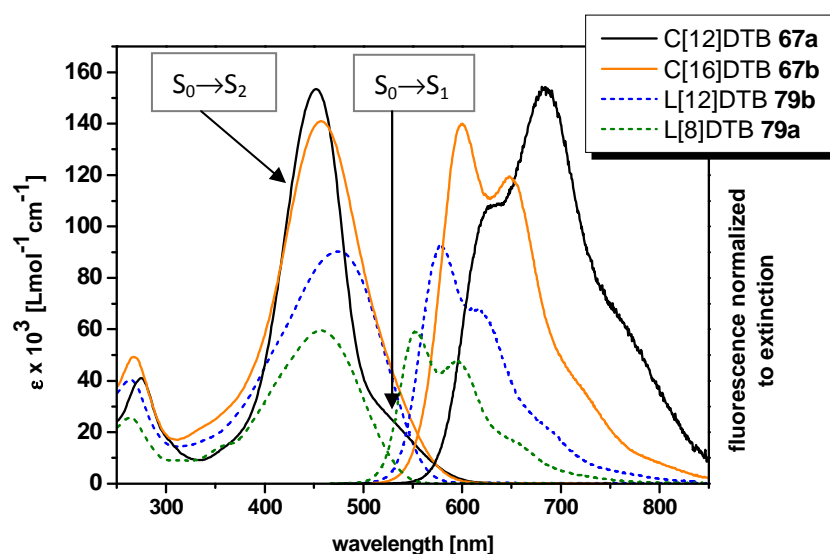


Figure 3.9: UV/vis absorption and emission spectra of macrocycles **67a** and **67b** as well as corresponding linear oligothiophenes **79a** and **79b**, measured in chloroform.

However, the absorption of C[12]DTB **67a** is not directly comparable with its linear analogue L[12]DTB **79b**, even though both possess the same number of thiophene units. The reason for that fact can be explained in their different geometry. As the selection rules for electronic transitions of cyclic compounds differ from those of linear homologues, different eigenfunctions and eigenvalues result for cyclic and linear systems concerning the same electronic transition.^[28] It is further disclosed by reason of the selection rules that in cyclic systems the energy of the first electronic transition $S_0 \rightarrow S_1$ is independent of the ring size and occurs constant at one defined energy, whereas the energy of the second transition $S_0 \rightarrow S_2$ is strongly ring size dependent and is progressively red-shifted with increasing number of thiophene units. A dipole moment perpendicular to the molecular ring plane (parallel to the z-axis) is required for the first excitation ($S_0 \rightarrow S_1$).^[26] Since all thiophene units along the conjugated backbone are arranged in the plane, no possible excitation can occur and this transition is theoretically forbidden. The calculated oscillator strength additionally results in a zero value. Nevertheless, the backbone of the macrocycle in the dissolved state is not completely flat, whereby some of the thiophene moieties slightly turn out of the plane and give access to a weak transition dipole moment. As a consequence, a very weak first transition band is observed for C[12]DTB **67a** as a shoulder bathochromically shifted to the main absorption band at $\lambda = 512$ nm. For the second electronic transition ($S_0 \rightarrow S_2$), the polarization of the dipole moment is oriented within the ring plane and parallel to the π -conjugated backbone (perpendicular to the z-axis). Since the required polarization is the case for the macrocycles, the second transition is theoretically permitted.^[26, 28-30] The present broad absorption bands for C[12]DTB **67a** ($\lambda = 453$ nm) and C[16]DTB **67b** ($\lambda = 457$ nm) can therefore be assigned to the $S_0 \rightarrow S_2$ transition. In the case of the UV/vis curve of C[16]DTB **67b**, the absorption band for the $S_0 \rightarrow S_1$ transition is overlapped by the stronger main absorption band.

Since the second excited state is degenerated, transition energies correspond approximately to energies for linear compounds with half the number of appropriate repeating units. Values for the extinction coefficients double and are thus very high compared to their linear analogues.^[26] With a closer look at the main maxima of C[16]DTB **67b** and L[8]DTB **79a**, both absorption bands occur in fact at the same energy. No vibronic splitting is observed in the UV/vis curves of the cyclic compounds indicating a delocalized π -system with conformational flexibility in the ground state.

Fine structures revealing up to three vibronic contributions were observed in the fluorescence spectra of the investigated systems. The macrocyclic conjugated backbone tends to planarize in the excited state and reduces the torsion angle between adjacent thiophene units by adopting a more quinoid electronic structure. The fluorescence spectrum of C[16]DTB **67b** is similar to the curves of both linear analogues with respect to its shape and it is very likely that the emission takes place from the first excited state $S_1 \rightarrow S_0$, whereby the transition $S_2 \rightarrow S_1$ proceeds free of radiation. Emission maxima are located at $\lambda = 600$ nm for C[16]DTB **67b** and at $\lambda = 578$ and 553 nm for L[12]DTB **79b** and L[8]DTB **79a**, respectively. However, differences concerning the shape of the emission band emerge for the strained macrocycle C[12]DTB **67a** and the wavelength of the maximum is red-shifted to $\lambda = 684$ nm. It can be assumed that, due to the high ring strain, the emission takes place from an energetically lower-lying level, for example a T_1 - or excimer state, which leads to the bathochromic shift. Fluorescence life-time measurements are suggested to be performed to determine the potential triplet state. To investigate the excimer state, fluorescence/excitation studies of concentrated solutions should be carried out.

Table 3.2: Summary of the optical data of cyclic oligothiophenes **67a**, **67b** and linear oligothiophenes **79a**, **79b**.

oligothiophene	$\lambda_{\text{abs,max}}$ [nm]	ϵ [Lmol ⁻¹ cm ⁻¹]	$\lambda_{\text{em,max}}$ [nm]
C[12]DTB 67a	453 ^{a)} /512 ^{b),c)}	153.000	684
C[16]DTB 67b	457 ^{a)}	140.000	600
L[12]DTB 79b	474 ^{b)}	93.000	578
L[8]DTB 79a	457 ^{b)}	59.000	553

^{a)} assigned to the $S_0 \rightarrow S_2$ transition.

^{b)} assigned to the $S_0 \rightarrow S_1$ transition.

^{c)} exact value calculated via Gaussian Fit (originPro 7.0).

The above presented results were compared to the photophysical properties of two series of non-functionalized cyclo[n]thiophenes derived from a butylated quinque- and terthiophene precursor, respectively (Figure 3.10, 3.11).^[26-28] Here, the $S_0 \rightarrow S_2$ absorption is progressively shifted to lower energies with increasing ring size and tends to reach a fixed value. The more thiophene units are

within the cyclic backbone, the broader gets the respective absorption band. Thus, the weak shoulder at lower energies reflecting the first electron transition $S_0 \rightarrow S_1$ (theoretically forbidden) can only be observed for the smallest cycles. In fluorescence spectroscopy, C10T showed a different behaviour compared to its larger homologues. Here, the emission maximum is strongly red-shifted due to its high ring strain, whereas the fluorescence curves of C15T-C35T resembled to the emission of linear oligomer L10T.^[26-28]

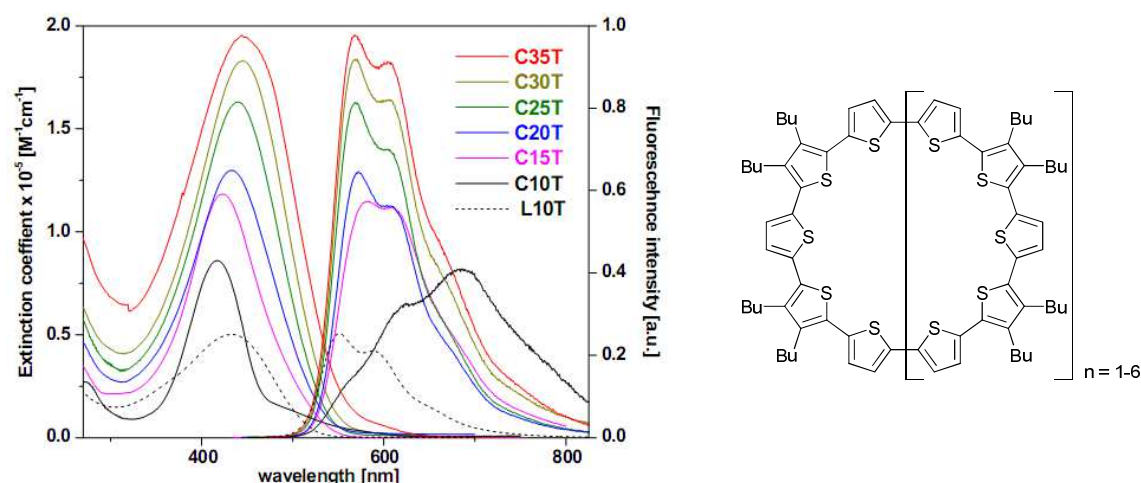


Figure 3.10: Absorption and fluorescence spectra of a series of quinquethiophene-derived macrocycles.^[27]

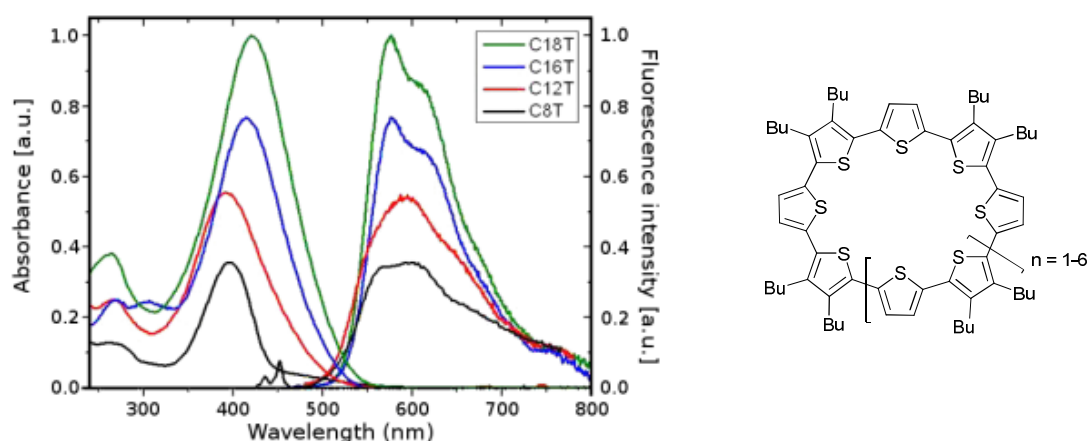


Figure 3.11: Absorption and fluorescence spectra of a series of terthiophene-derived macrocycles.^[26]

A comparable photophysical behaviour can be observed for both families of macrocycles (acceptor and non-functionalized) revealing the main absorption band to be a $S_0 \rightarrow S_2$, ring-size dependent transition and the emission behaviour to be similar to the one for linear oligomers, except for several strained small macrocycles. As another constant property counts the fact that the absorption of the macrocycles correlates to the absorption of linear oligomers with half the number of chain units. It is assumed that the introduced acceptor units does not influence the optical properties elementary, but rather maintains some kind of regularity.

A direct confronting of non-functionalized- and acceptor-substituted cyclic structures to investigate the electronic influence of the introduced acceptor units onto the optoelectronic behaviour seems interesting. The absorption and emission spectra of C[12]DTB **67a**, C[12]DCP **70**, and cyclothiophene C[12]T **81**^[31] are illustrated in Figure 3.12. C[12]T was chosen as model macrocycle due to the same number of repeating units and the same substitution pattern of alkyl side chains, avoiding an influence of the substitution pattern on the absorption.^[31]

The absorption maximum of C[12]T **81** for the π - π^* transition of the conjugated thiophene units is found at $\lambda = 427$ nm and blue-shifted compared to C[12]DTB **67a** ($\lambda = 453$ nm) and C[12]DCP **70** ($\lambda = 450$ nm). The bathochromic shift of the acceptor-functionalized macrocycles is due to the decreased optical band gap and was expected. All three macrocycles revealed next to the main absorption band a weak shoulder at lower energies around $\lambda = \sim 500$ nm for the symmetrical forbidden $S_0 \rightarrow S_1$ electron transition. The extinction coefficients differ from each other, but reach values over $\epsilon = 100.000 \text{ l mol}^{-1} \text{ cm}^{-1}$ with the lowest extinction ascribed to C[12]DCP **70**.

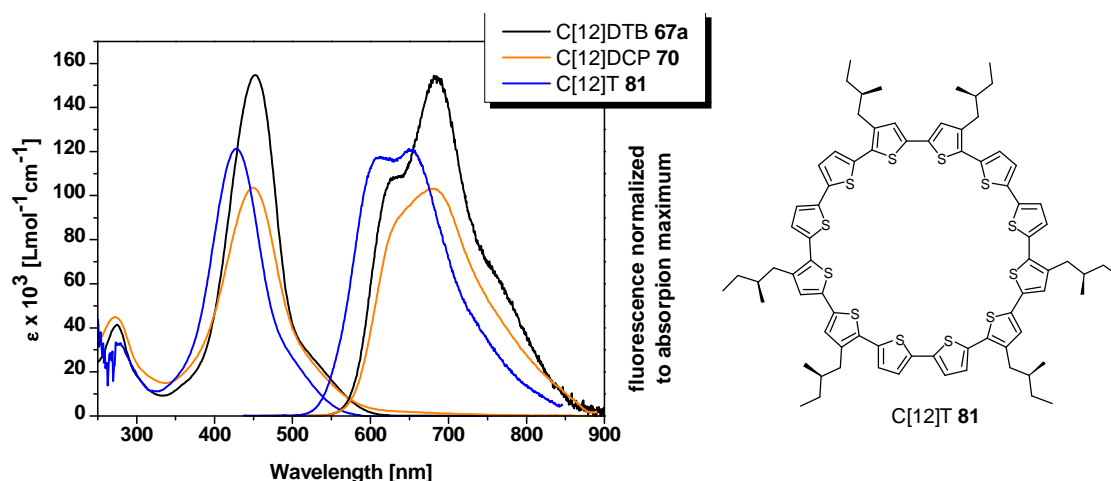


Figure 3.12: UV/vis absorption and emission spectra of macrocycles **67a**, **70a** and **81**, measured in chloroform.

The emission spectra of all cycles displayed vibronic splitting with up to three distributions due to the planar and more quinoid structure in the excited state. The shape of the curves for C[12]DTB **67a**, C[12]DCP **70** and C[12]T **81** exhibited similar characteristics with maxima at $\lambda = 684$, 678 , and 650 nm, respectively. It is likely that the emission for C[12]DCP and C[12]T takes place from an energetically low-lying level (T_1 - or excimer level), due to the strong ring strain, as it has been already described for C[12]DTB and non-functionalized C10T^[27]. The optoelectronic values are summarized in Table 3.3.

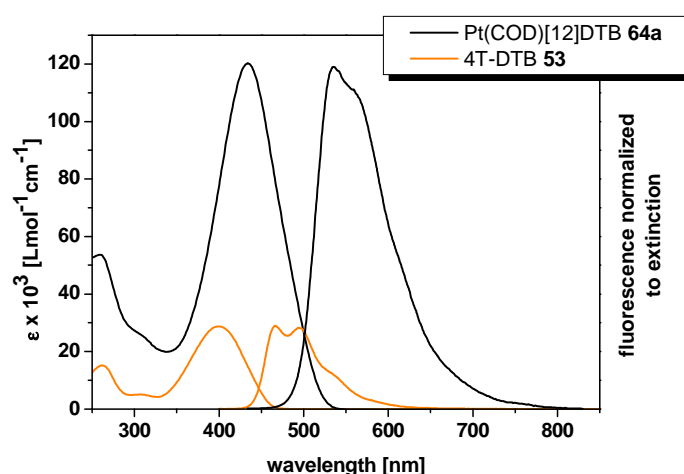
Table 3.3: Summary of the optical data of macrocycles **67a**, **70** and **81**.

macrocycle	$\lambda_{\text{abs,max}}$ [nm]	ϵ [Lmol ⁻¹ cm ⁻¹]	$\lambda_{\text{em,max}}$ [nm]
C[12]DTB 67a	453 ^{a)} /512 ^{b)}	153.000	684
C[12]DCP 70	450 ^{a)} /526 ^{b)}	103.000	678
C[12]T 81	427 ^{a)} /516 ^{b)}	121.000	650

^{a)} assigned to the $S_0 \rightarrow S_2$ transition.

^{b)} assigned to the $S_0 \rightarrow S_1$ transition, exact values calculated via Gaussian Fit (originPro 7.0).

Since the trimeric Pt^{II} metallacycle Pt(COD)[12]DTB **64a** was successfully isolated, the interplay of the conjugated thiophene moieties and the metal fragments was investigated by means of UV/vis and fluorescence spectroscopy. The absorption and emission spectra were recorded in chloroform and compared to the linear monomer 4T-DTB **53**. The obtained optical curves are depicted in Figure 3.13.


Figure 3.13: UV/vis absorption and emission spectra of metallacycle **64a** and quaterthiophene 4T-DTB **53**, measured in chloroform.

The absorption spectrum of the Pt^{II} complex showed one broad band with a maximum at $\lambda = 434$ nm, which is red-shifted by 34 nm and quadrupled in extinction coefficient compared to quaterthiophene 4T-DTB **53**. The broad absorption of the complex can mainly be derived from the π - π^* -transition of the single oligothieryl moieties and reflects the rotational freedom of the individual thiophene units in the ground state, since no vibronic splitting occurred. The shift towards higher wavelengths indicates an enhancement of the degree of π -conjugation through the platinum. An additional metal to ligand charge transfer (MLCT) from the Pt-centers to the thiophene units via $d\pi \rightarrow p\pi$ is very likely. However, this effect does not lead to a full conjugation. Similar observations have been reported in literature for oligothiophenes attached to platinum centers.^[21-22, 32-34] Both compounds showed vibronic fine structures in the emission bands with maxima at $\lambda = 535$ nm for **64a** and $\lambda = 466$ nm for

53 indicating a stiff and planar structure in the excited state. Values for the absorption and emission maxima as well as extinction coefficients are given in Table 3.4.

Table 3.4: Summary of the optical data of metallacycle **64a** and quaterthiophene-alike unit 4T-DTB **53**.

compound	$\lambda_{\text{abs,max}}$ [nm]	ϵ [Lmol ⁻¹ cm ⁻¹]	$\lambda_{\text{em,max}}$ [nm]
Pt(COD)[12]DTB 64a	434	119.000	535
4T-DTB 53	400	29.000	466

3.7.1 Optical properties of acceptor-functionalized linear oligothiophenes

The elimination of the ethylene glycol protecting groups to obtain a strong electron accepting property and to simultaneously generate reactive carbonyl groups for subsequent reactions was only successfully performed for linear DTB-quaterthiophenes **53** and **54** (see Chapter 3.4). Strong aggregation processes and precipitation led to synthetic problems for the deprotection of macrocycle C[12]DTB **67a**, which therefore failed.

However, the optoelectronic properties of deprotected DTB-oligomer **71** were investigated by UV/vis absorption spectroscopy to analyze the influence of the free carbonyl groups onto the chromophore. The spectrum was recorded in chloroform and opposed to the ethylene glycol bridged building block **53** (Figure 3.14). 4T-DTB **53** exhibited an absorption maximum for the π - π^* transition of the oligothiophene moiety at $\lambda = 400$ nm with an extinction coefficient of $\epsilon = 29.000$ Lmol⁻¹cm⁻¹. Quaterthiophene **71** with free carbonyl groups revealed one broad and strong blue-shifted absorption band at $\lambda = 340$ nm. Another band occurred at longer wavelength ($\lambda = 611$ nm) which can be ascribed to an intramolecular charge transfer from the donor to the acceptor moiety. Rieger already investigated the optical behaviour of a deprotected DTB-core unit in different solvents with respect to solvation effects. A bathochromic shift of the charge transfer band up to 30 nm was visible when measured in polar, chlorinated solvents like dichloromethane in contrast to cyclohexane or THF.^[10] Optical data for both quaterthiophene building blocks are shown in Table 3.5.

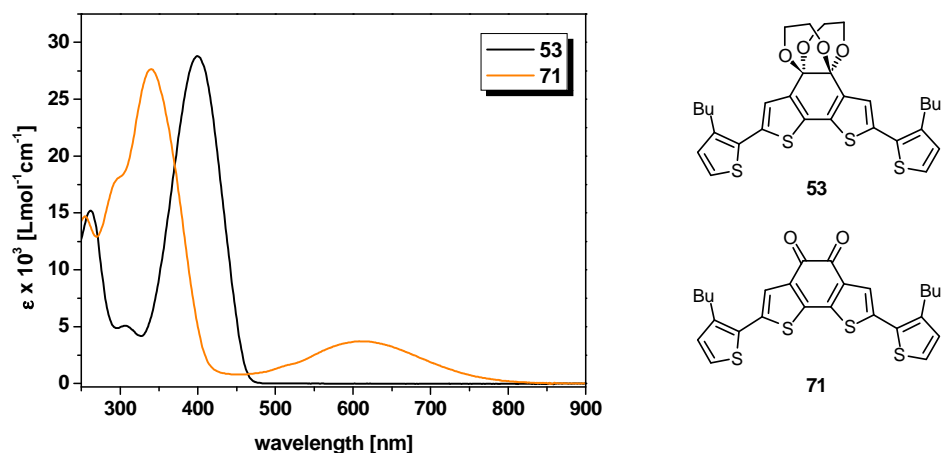


Figure 3.14: UV/vis absorption spectra of protected oligomer 4T-DTB **53** and deprotected quaterthiophene **71**, measured in chloroform.

Table 3.5: Summary of the optical data of protected 4T-DTB **53** and deprotected oligomer **71**.

oligothiophene	$\lambda_{\text{abs,max1}}$ [nm]	$\lambda_{\text{abs,max2}}$ [nm]	ϵ [Lmol ⁻¹ cm ⁻¹]
53	400	-	29.000
71	340	611	27.000

3.8 Characterization of different redox states of acceptor-functionalized cyclo[n]thiophenes

3.8.1 Electrochemical properties of acceptor-functionalized C[12]DTB (**67a**)

The redox properties of macrocycle C[12]DTB **67a** were studied by cyclic voltammetry and compared to those of non-functionalized macrocycle C[12]T **81**. The measurements were carried out in polar benzonitrile as solvent to prevent deposition of charged species on the electrode and to record voltammograms at higher temperatures. TBAPF₆ (0.1 M) was used as supporting electrolyte and ferrocene as internal standard. A Pt-electrode with a relatively large surface ($\phi = 3.4$ mm) served as working electrode to obtain even at low substrate concentrations of 0.1 mM reasonable results.

The cyclovoltammogram (CV) of cyclothiophene **67a** is displayed in Figure 3.15 (top, left) and shows several reversible oxidation steps. The electrochemical data are summarized in Table 3.6. The reversibility of the oxidation processes indicates the formation of stable charged species through the stepwise transfer of electrons. Due to the lack of free α -positions, the radicals are delocalized along the cyclic backbone and cannot undergo oligomerization. To determine the number of transferred electrons per oxidation step, ferrocene was used as standard and measured under consistent

conditions (295 K, 0.1 mM, benzonitrile). Since ferrocene shows an one-electron oxidation step in the first wave, its calculated integral was used as reference and compared to the redox waves of the deconvoluted voltammogram of **67a** (Figure 3.15, right). The amount of transferred electrons per oxidation wave could thus be determined in a relatively good approximation to $1e^- : 1.1e^- : 0.8e^-$ ($1^{st} : 2^{nd} : 3^{rd}$ redox wave), so to speak to $1e^- : 1e^- : 1e^-$. According to these calculations, macrocycle **67a** exhibited three reversible one-electron oxidation steps $E_{ox1}^0 - E_{ox3}^0$ (0.19 V, 0.59/0.66/0.77 V, 1.03 V), whereas the broad and well structured second wave consists of three closely sequenced oxidation processes $E_{2'}^0 - E_{2'''}^0$ (Figure 3.15, bottom). The first oxidation process E_1^0 at 0.19 V shows a slight shoulder, which is more pronounced when measured in DCM instead of benzonitrile (see Figure 3.18).

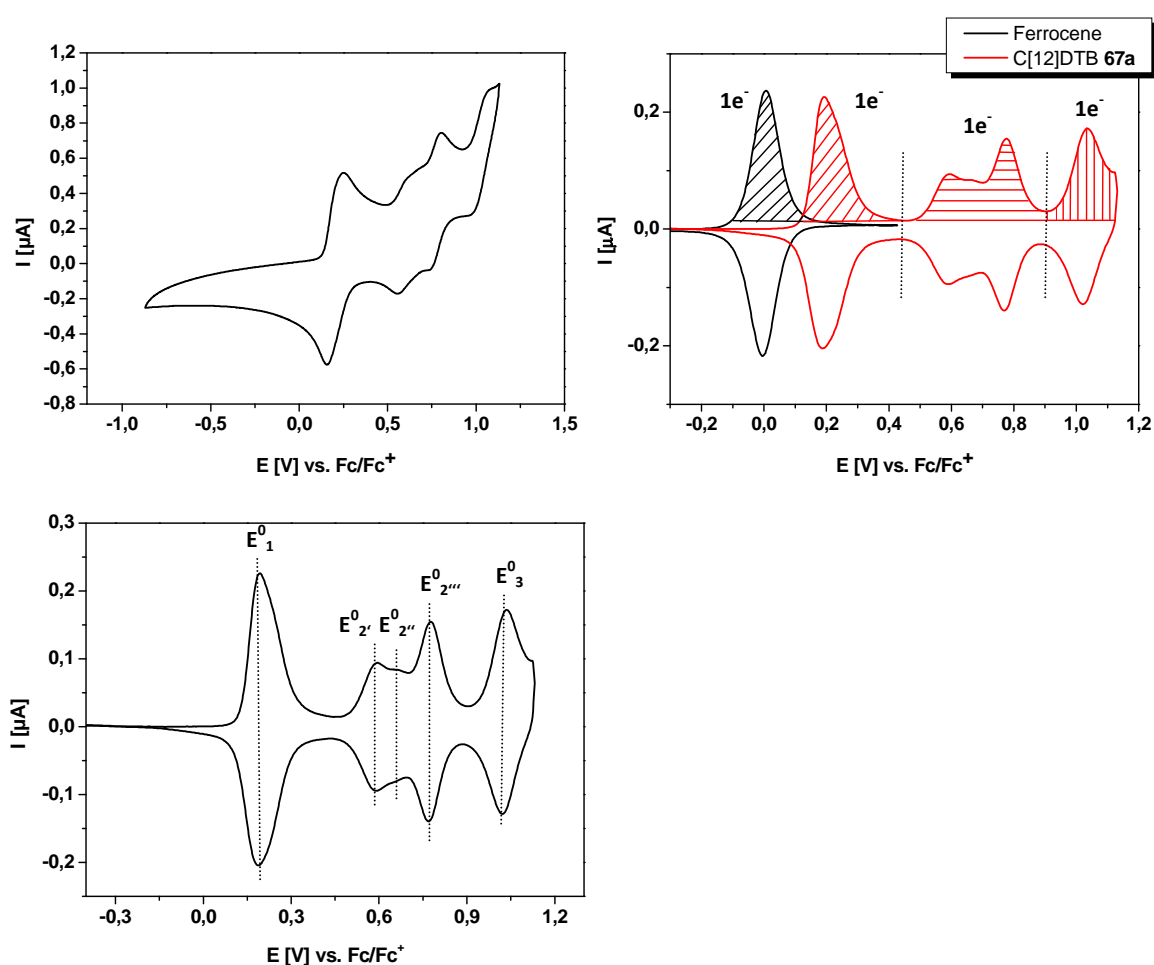


Figure 3.15: CV of C[12]DTB **67a** (top, left), comparison of the calculated integrals of ferrocene as standard and **67a** (top, right), and deconvoluted voltammogram of **67a** (bottom), measured at 295 K in benzonitrile/TBAPF₆ (0.1M) vs. Fc/Fc⁺, 20 mV/s, $c = 1.0 \times 10^{-4}$ M, respectively.

The splitting of the second wave and the shoulder in the first wave could be hints for the formation of dimeric species of differently charged macrocycles as a result of favorable π - π -interactions. This has already been observed for non-functionalized thiophene-based macrocycles during

electrochemical analysis and determined by temperature-dependent measurements (Figure 3.16)^[27] as well as for π -conjugated oligomers in the frame of charge transport in organic conductors.^[35]

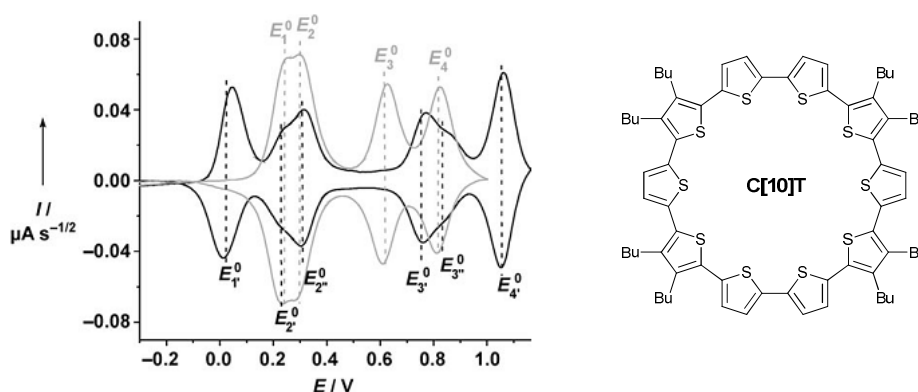


Figure 3.16: Deconvoluted CV of C[10]T (black line) and linear L[10]T (grey line), $c = 7.8 \times 10^{-4}$ M in TCE/TBAPF₆ (0.1M) vs. Fc/Fc⁺, 20 mV/s, 295 K. The splitting of the second redox wave ($E_{2'}^0$, $E_{2''}^0$) and third wave ($E_{3'}^0$, $E_{3''}^0$) denote the formation of dimeric aggregates, which were proven by temperature-dependent measurements. At higher temperatures clear one-electron transfer waves are visible indicating individual and non-aggregated macrocycles.^[27]

Thus, temperature-dependent measurements of **67a** were carried out. The heat was stepwise increased from ambient temperature to 60 °C, 70 °C, 80 °C, and 90 °C. The deconvoluted I/V-curves at room temperature and 90 °C are depicted in Figure 3.17. The measurements at elevated temperatures were only performed to a potential of 0.90 V to avoid deposition of organic material on the surface of the electrode. A temperature-dependence was confirmed since the oxidation waves at higher temperatures are considerably better structured. The two oxidation processes at potentials of 0.59 V and 0.66 V become one single wave, which is clearly separated from the third oxidation at 0.77 V. Like the first one-electron step at 0.19 V, it exhibits then a tendency towards a Gaussian curve. This is a hint of deaggregation of formerly formed assemblies at elevated temperatures to individual and non-aggregated cycles with clean oxidation processes.

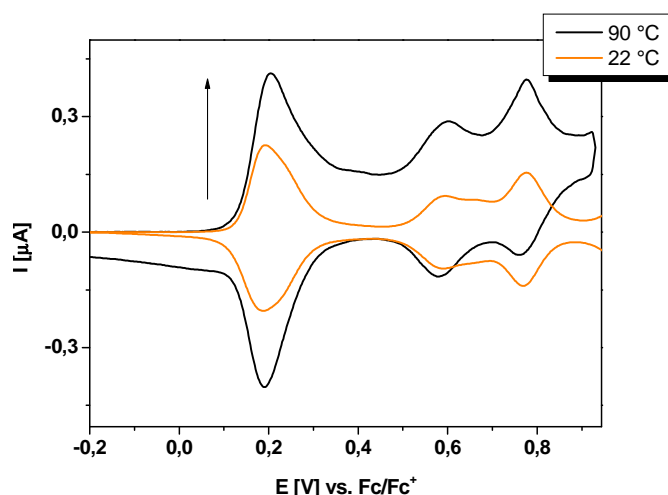
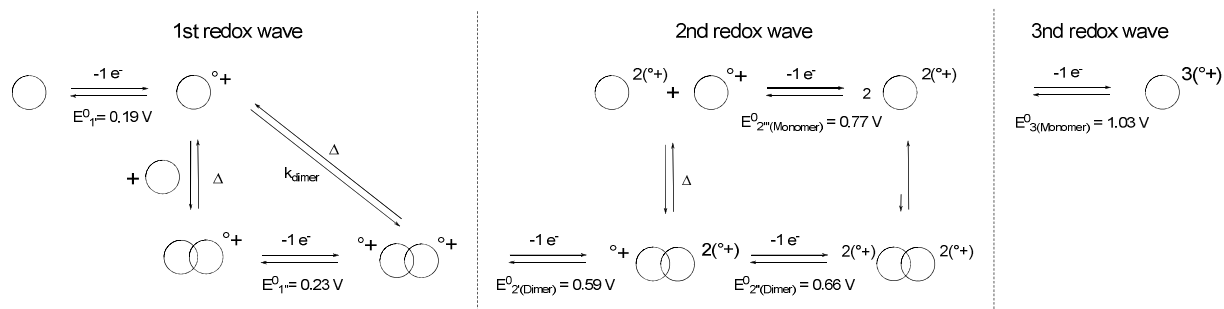


Figure 3.17: CVs of **67a** at 22 °C and 90 °C, measured in benzonitrile/TBAPF₆ (0.1M) vs. Fc/Fc⁺, 20 mV/s, *c* = 1.0x10⁻⁴ M. CVs at temperatures in between the maxima were omitted for clarity.

Due to the results of the temperature-dependent measurements of **67a** which confirm dimerization of charged macrocycles, assumptions of the oxidation processes on a molecular level, based upon the intermolecular aggregation through π - π interactions, are given in Scheme 3.24.

It is supposed that the singly charged C[12]DTB^{•+} can be formed through two different ways at the first electron transfer wave at $E_{1'}^0 = 0.19$ V. The radical cation can either be generated directly from neutral C[12]DTB or from oxidation of a dimeric structure arising from one neutral and one singly charged compound at $E_{1''}^0 = 0.23$ V.



Scheme 3.24: Schematic presentation of assumed oxidation processes of **67a** on a molecular level.

Presumably, three coexisting oxidation processes occur during the second one-electron oxidation step. It is likely that the oxidation at $E_{2'}^0 = 0.59$ V takes place from a dimer consisting of two monoradical cations, whereas a trication is formed which is equilibrated with the individual dicationic and monocationic species. The tricationic species could be further oxidized at $E_{2''}^0 = 0.66$ V to a tetracation, which undergoes consecutive disaggregation to monomeric twofold charged macrocycles. The third step at $E_{2''' }^0 = 0.77$ V would be a supposed clean one-electron transfer from a singly charged ring to a dication.

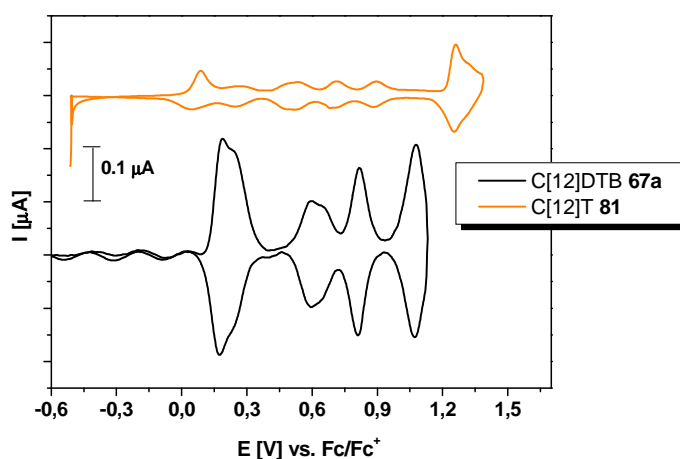
The third one-electron oxidation step at $E_3^0 = 1.03$ V provides the threefold charged compound.

Table 3.6: Summary of the oxidation potentials of the three one-electron oxidation steps of **67a**.

oligothiophene	E^0_{ox1} [V]	E^0_{ox2} [V]	E^0_{ox3} [V]
C[12]DTB 67a ^{a)}	0.19	0.59 / 0.66 / 0.77	1.03
C[12]DTB 67a ^{b)}	0.19 / 0.23	0.59 / 0.66 / 0.81	1.07

^{a)} Benzonitrile, ^{b)} DCM

To study further the electronic influence of the inserted DTB-acceptor units onto the physical properties of the macrocycle, C[12]DTB **67a** was compared to non-functionalized analogue C[12]T **81**. The CVs of both cycles were recorded in dichloromethane and their deconvolutions are shown in Figure 3.18. Three reversible one-electron transfer steps are visible for **67a**. This time, the splitting of the first redox wave at $E^0_{1'} = 0.19$ V and $E^0_{1''} = 0.23$ V is more visible compared to the measurement in benzonitrile (see Figure 3.15). The splitting of the second wave is as well more distinct with potentials at $E^0_{2'} = 0.59$ V, $E^0_{2''} = 0.66$ V, and $E^0_{2'''} = 0.81$ V. Six oxidation processes occur for **81** (0.09 V, 0.26 V, 0.53 V, 0.71 V, 0.90 V, 1.26 V). It is not clarified if the processes for **81** are one-electron or multiple-electron transfer steps, but dimerization of charged species for this kind of cycle is likely, too. The shift towards a higher first oxidation potential for **67a** can be attributed to the inserted acceptor functionalities. This electron-withdrawing effect influences the electrochemical oxidation and hampers electron delivery. A potential of 1.1 V was not crossed for **67a**, since the oxidation at such high voltages does not proceed fully reversible. The obtained potentials of the electrochemical investigation of **67a** in DCM are summarized in Table 3.6.


Figure 3.18: Deconvoluted voltammograms of **67a** and **81**, measured at 295 K in DCM/TBAPF₆ (0.1M) vs. Fc/Fc⁺, 20 mV/s.

3.8.1.1 Electrochemical properties of transition metal complex Pt(COD)[12]DTB (**64a**)

The CV of the isolated Pt-metallacycle **64a** was recorded in dichloromethane at ambient temperature versus the internal standard Fc/Fc⁺ and four irreversible redox waves were observed (Figure 3.19).

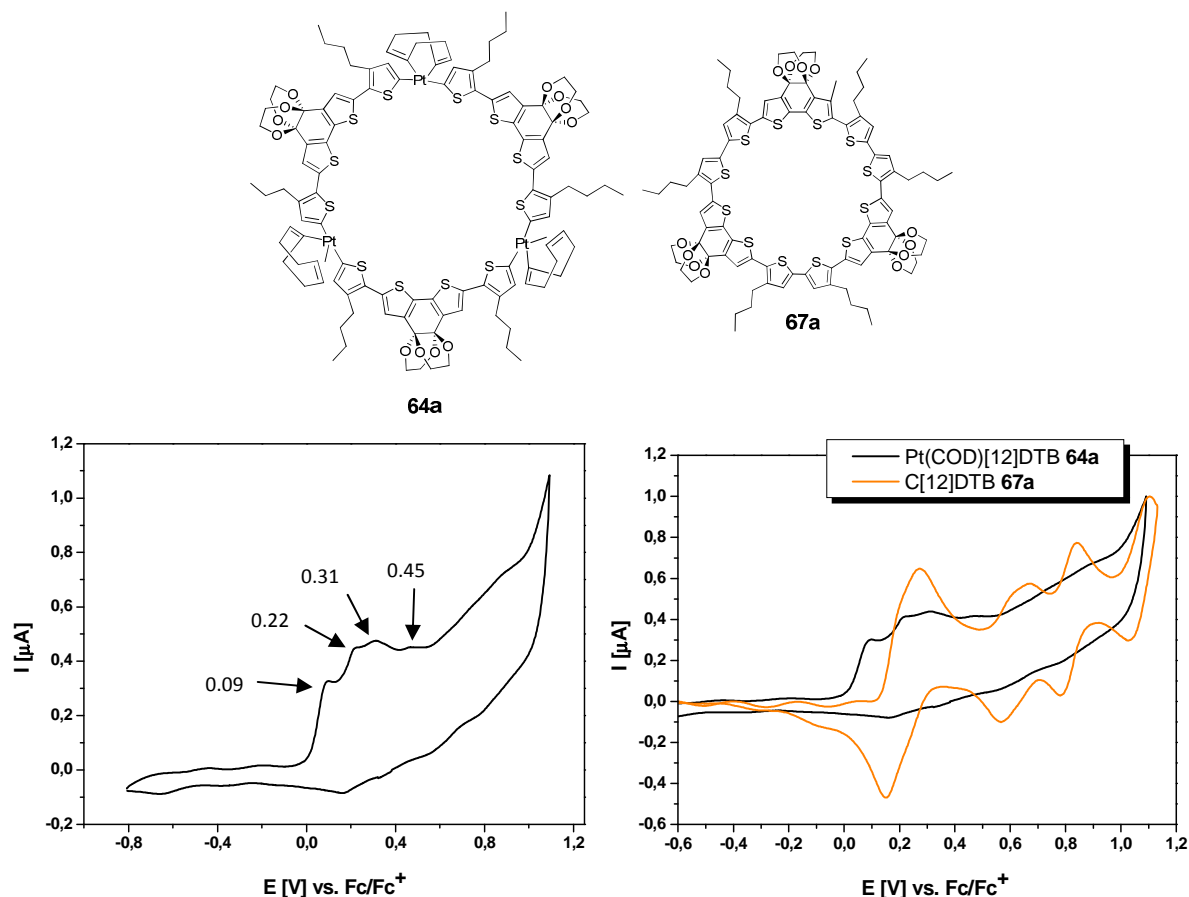


Figure 3.19: Top: Structures of metallacycle **64a** and fully conjugated macrocycle **67a**. Bottom: CV of metallacycle **64a** (left) and voltammograms of both Pt-cycle **64a** and fully conjugated macrocycle **67a** (right), measured at 295 K in DCM/TBAPF₆ (0.1M) vs. Fc/Fc⁺, 20 mV/s.

Independently, Zhang^[22] and Fuhrmann^[21] investigated the electrochemical properties of linear dppp(Pt)oligothienyl complexes as well as cyclic oligothieryl-diacetylene-Pt(dppp)complexes. Zhang assigned the first irreversible oxidation wave to the oxidation of the transition metal Pt^{II} to Pt^{IV}, whereas the following reversible redox waves belonged to the platinum-free linear secondary product, which was formed due to homo-coupling of the oligothieryl moieties. He drew conclusions by comparison of the voltammograms of the Pt-complex with a corresponding linear oligothiophene, which was synthesized in a standard batch reaction. Fuhrmann^[21] reported same perceptions. However, the redox waves of her electrochemical induced cyclic secondary product did not differ clearly from each other and could not be classified definitely as reversible. In consequence of changing the solvent to benzonitrile, she was able to characterize the electrochemical formed macrocycle with reversible oxidation steps. It is to mention that the characterization of the

voltammograms and the assignment of the oxidation steps gets more difficult the more platinum centers are involved within the investigated system. One platinum center was present in the linear complexes of Zhang and the number of enclosed transition metal centers increased to two for the cyclic diacetylene Pt^{II} complexes of Fuhrmann. Due to the complicated voltammogram illustrated in Figure 3.19 (left), a simultaneous coexistence of several species with different numbers of eliminated Pt-centers is assumed for macrocycle Pt(COD)[12]DTB **64a**. It is likely that the electrochemical induced elimination of three transition metals does not occur at the same time which results in overlapping redox waves of species with one or two platinum atoms left within the cyclic backbone. The voltammograms of **64a** and the fully conjugated macrocycle **67a**, which was recorded separately, were overlaid in Figure 3.19 (right). None of the emerging irreversible oxidations waves at E_2^0 - E_4^0 (0.22 V, 0.31 V, 0.45 V) fit to the reversible waves obtained for the cyclic oligothiophene, which supports the assumption of a multiplicity of different species.

3.8.2 Characterization of different redox states of macrocycle C[12]DTB (**67a**) via UV/vis/NIR absorption spectroscopy

Investigated macrocycle C[12]DTB **67a** showed three reversible redox waves during cyclic voltammetry. These stable oxidized states can also be characterized via absorption spectroscopy in the UV/vis and NIR region. The macrocycle was therefore partially oxidized by a chemical oxidant. This kind of analysis should give further information about the complex electronic states. Investigations of the optical properties of the charged species via spectroelectrochemistry were not carried out due to limited amount of the macrocycle.

Tris(2,4-dibromophenyl)aminium hexachloroantimonat (TDBPA⁺SbCl₆⁻) was utilized as chemical oxidant, which shows a first oxidation potential of $E_1^0 = 1.12$ V (measured in DCM vs. ferrocene). It can be categorized as a rather strong oxidant, with which a multiple electron oxidation up to a threefold charged C[12]DTB³⁺ should be possible according to the oxidation potentials obtained from the recorded cyclic voltammogram. All absorption spectra were recorded in dichloromethane, in which the oxidant is stable for several hours. It is noteworthy that the pure oxidant itself exhibits absorption bands in DCM at $\lambda = 370$ and 460 nm and one broad absorption band at higher wavelengths with a maximum around 800 nm. However, it is reduced and the increase of an absorption band below $\lambda = 300$ nm can be attributed to the formation of the neutral triarylamine, which shows no absorption in the NIR and visible region.

The samples were prepared from stock solutions of the macrocycle and the oxidant, whereby defined and increasing amounts of oxidant were added to a consistent concentration of the macrocycle.

The absorption spectra of the stepwise oxidized C[12]DTB **67a** are illustrated in the following figures and discussed. The cyclic voltammogram of **67a** in DCM exhibited for the first oxidation step two oxidation processes ($E_{1'}^0 = 0.19$ V and $E_{1''}^0 = 0.23$ V vs. Fc/Fc⁺). As discussed above, one electron is transferred in this step and the splitting of the redox wave leads to the assumption of the formation of dimeric species via π - π -interactions. The change in the absorption spectra through the successive addition of TDBPA⁺SbCl₆⁻ to 1.0 eq. is depicted in Figure 3.20.

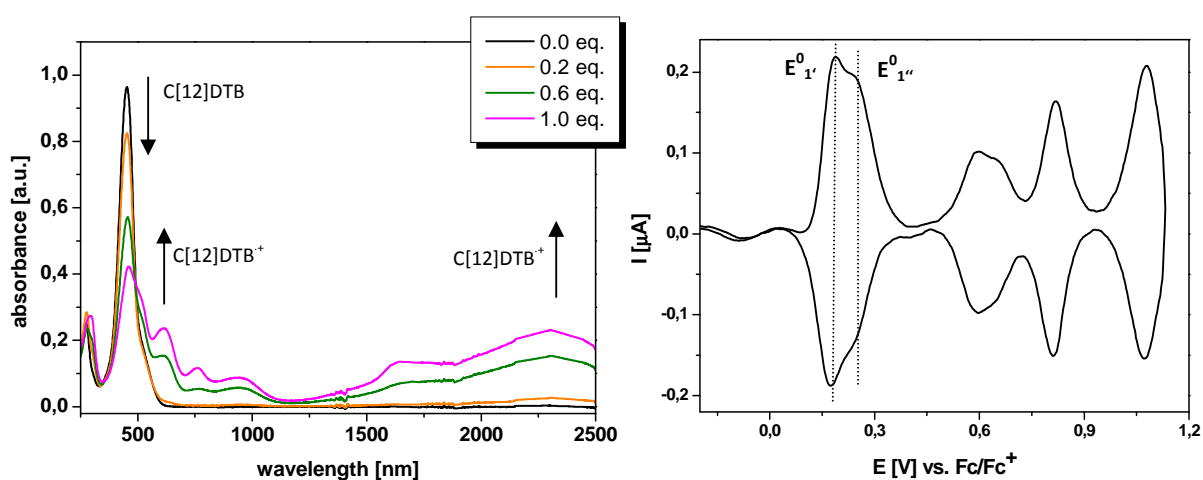
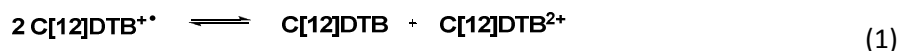


Figure 3.20: Absorption spectra of **67a** with successive addition of TDBPA⁺SbCl₆⁻ up to 1.0 eq. (left) and deconvoluted voltammogram of **67a** (right), both measured in DCM.

C[12]DTB in its neutral state exhibited one sharp absorption band at $\lambda = 453$ nm with an unresolved shoulder at $\lambda = 512$ nm which can be assigned to the $S_0 \rightarrow S_2$ and $S_0 \rightarrow S_1$ electron transition, respectively. Upon addition of 0.2, 0.6, and 1.0 eq. of TDBPA⁺SbCl₆⁻, the absorption band of the neutral state decreased with a simultaneous emergence of several new bands: One main sharp band at $\lambda = 617$ nm and another broad band in the near-infrared at $\lambda = 2304$ nm. These bands can be attributed to the singly charged radical cation C[12]DTB⁺. The band at lower wavelength can be assigned to an excitation from the singly occupied level to the LUMO, whereas the band at higher wavelength is ascribed to an excitation from the highest doubly occupied molecular orbital to the singly occupied level.^[36] The previously mentioned formation of aggregates between charged and uncharged species has to be considered as well. Dimers containing one neutral compound are likely since the corresponding absorption band for the neutral species diminished upon oxidation to 1.0 eq., but does not vanish completely, whereby still some unoxidized cycles are left. This result can be explained by a disproportionation equilibrium described in equation (1).^[36]



Thus, the additional signals inbetween the two absorption maxima can be derived from dimers which are illustrated in Scheme 3.25. The absorption band of the dicationic species described in equation (1) is probably overlapped by the dimeric ones.



Scheme 3.25: Proposed dimerization between charged and uncharged macrocycles.

Temperature-dependent measurements were additionally performed, whereby the oxidized sample (1.0 eq.) was cooled down to 0 °C. The cooling caused an increase of the intensity of the absorption bands at $\lambda = 761$ and 1641 nm with a simultaneous decrease of the absorption intensity at $\lambda = 617$ nm. Thus, the band at shorter wavelength ($\lambda = 617$ nm), which has already been assigned to the monomeric radical cation $\text{C[12]DTB}^{+\bullet}$, is now proven to be that species since less monomeric compound occurs at lower temperature. The other bands should belong to the reversible dimeric species between all singly charged or mixed neutral and singly charged cycles since aggregation is favoured at 0 °C. The aggregates were already characterized by previously presented cyclic voltammetry studies (also temperature-dependent). The spectra are depicted in Figure 3.21, whereby only dimers between radical cations are displayed schematically.

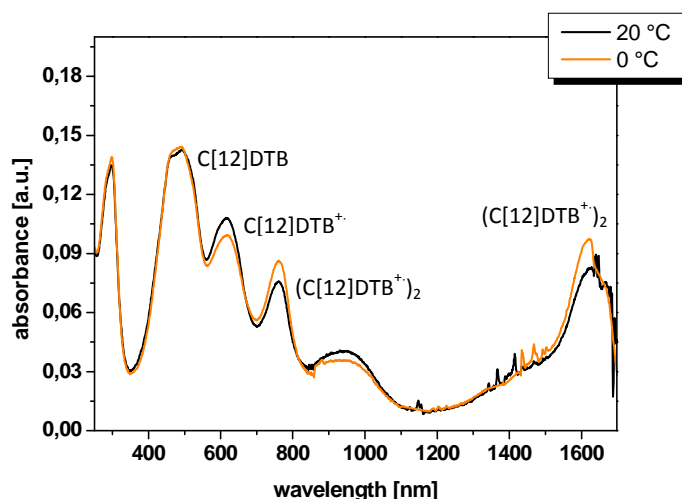


Figure 3.21: Temperature-dependent measurements of the oxidized macrocycle **67a** (1.0 eq.) at 20 °C and 0 °C, measured in DCM.

The characterization of different redox states via absorption spectroscopy in combination with temperature-dependent measurements for the radical cationic species of the thiophene-based

macrocycle C[10]T has already been published by Zhang.^[37] He also observed the formation of dimers, which deaggregated at higher temperatures. The temperature-dependence for C[12]DTB⁺ at the longest wavelength of $\lambda = 2304$ nm was not well resolved and will therefore not be further discussed in this context, but based on the results of Zhang, it is very likely that this band belongs to the monomeric radical cation.

Upon further oxidation with 1.5, 2.0, and 3.0 eqs. of TDBPA⁺SbCl₆⁻ to form the dicationic state, two very sharp intensive bands appeared at $\lambda = 755$ and 1625 nm (Figure 3.22). Next to the dicationic still some radical cation species is left, since the absorption band at $\lambda = 2304$ nm does not completely disappear, but yet is visibly to some amount. The observable shoulder to shorter wavelength next to the main absorption band at $\lambda = 1625$ nm could be a hint of the formation of charged aggregates, which would be consistent with the results obtained from the cyclic voltammetry at the second oxidation potential with values of $E_{2'}^0 - E_{2''}^0 = 0.59/0.66/0.81$ V. Vibrational splitting is also possible.^[38] However, no temperature-dependent measurements were carried out in the case of the dicationic species to prove reversible aggregation. The absence of distinct isosbestic points usually indicating a clean conversion of the neutral state C[12]DTB into the charged species C[12]DTB⁺ and C[12]DTB²⁺ can be deduced from the coexisting of different species like dimers and monomeric charged compounds. Treatment of the oxidized samples with an excess of hydrazine monohydrate allowed the recovery of the neutral state and indicates the reversibility of the oxidation processes.

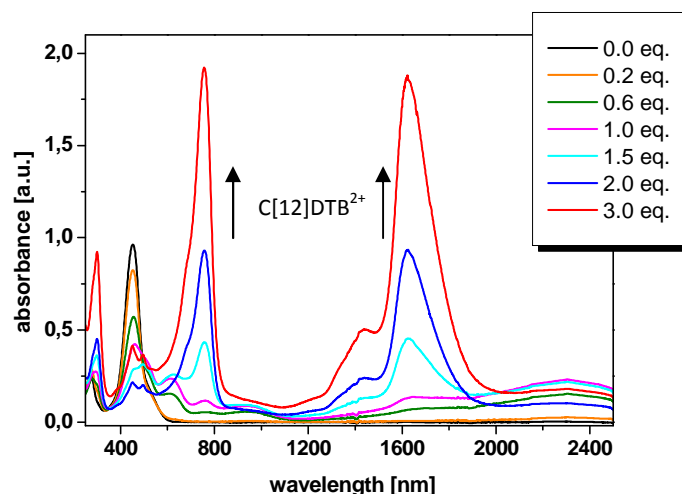


Figure 3.22: Absorption spectra of **67a** with the successive addition of TDBPA⁺SbCl₆⁻ up to 3.0 eqs., measured in DCM.

Further two new absorption bands at $\lambda = 791$ and 1198 nm occurred by increasing the amount of TDBPA⁺SbCl₆⁻ to 5.0 eqs. A clear decrease of intensity and overlapping of the two main absorption bands of the lower oxidized species is visible as well as the occurrence of a broad unresolved and structured band at higher energies at around $\lambda = 1056$ nm, which could be caused from a mixture of

different dimeric assemblies (Figure 3.23). However, at least 4.0 eqs. of oxidant were necessary to generate a threefold charged macrocycle $\text{C}[12]\text{DTB}^{3+}$. A stronger oxidant would have been probably more efficient to create defined conversions between the different oxidized states. The data of the absorption maxima of the different oxidized states are summarized in Table 3.7.

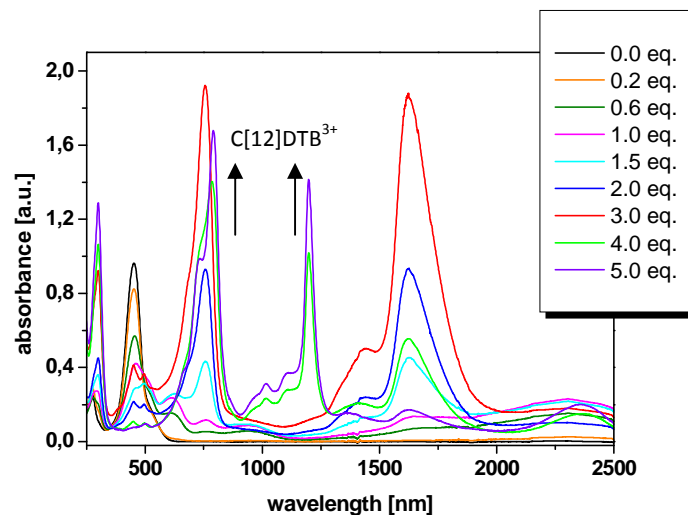


Figure 3.23: Absorption spectra of **67a** with the successive addition of $\text{TDBPA}^+\text{SbCl}_6^-$ up to 5.0 eqs., measured in DCM.

Table 3.7: Summary of the absorption maxima of **67a** at the respective oxidized states.

	$\text{C}[12]\text{DTB}$	$\text{C}[12]\text{DTB}^{+}$	$(\text{C}[12]\text{DTB}^{+})_2$	$\text{C}[12]\text{DTB}^{2+}$	$\text{C}[12]\text{DTB}^{3+}$
λ_{max} [nm]	452, 512	617, 2304	761, 1641	755, 1625 (1433)	791, 1198 (~1056)

In recent years, various experimental and theoretical studies have provided insight into the characteristics of the first and second stable oxidized state of oligothiophenes with a limited number of thiophene units.^[38-42] It is known that a single-electron oxidation forms a polaronic structure which corresponds to a radical cation associated with a geometric distortion along a certain length of the linear conjugated oligomer that is induced by the delocalized charge. Two different electronic structures have to be considered for the doubly oxidized species, a polaron pair-like configuration or a bipolaronic structure.^[36, 43-45] A polaron pair configuration consists of two individual polarons with a strong local geometric distortion. The two unpaired electrons can exist as singlet or triplet state with the spins in the same or opposite direction. The bipolaron system can be considered as a spinless dication with a pair of like charges and an associated strong local geometry deformation. It is favored for shorter oligomers, where two individual polarons cannot be stabilized without interacting with each other. Quantum mechanical calculations were already performed on a cyclo[12]thiophene with

respect to the electronic structure of a doubly oxidized state whereas charge localization was accompanied by a geometric distortion of the cycle. It was found that two separated polarons are more stable than a bipolaronic system.^[46] The possible electronic structures, referring to the doubly oxidized species of macrocycle C[12]DTB **67a**, are depicted in Figure 3.24.

From theoretical analysis, only one absorption band is expected for a closed-shell bipolaronic electronic structure in the UV/vis/NIR measurements. However, two electron transitions, ending up in two absorption bands, are assumed for a non-interacting polaronic pair structure.^[36, 47-48] The doubly oxidized macrocycle **67a** can therefore be denoted as C[12]DTB²⁽⁺⁾ for the polaronic pair case, since the UV/vis/NIR spectrum of the twofold charged species revealed two strong main absorption bands. Electron spin resonance (ESR) measurements might give further insight into the electronic structure of **67a**.

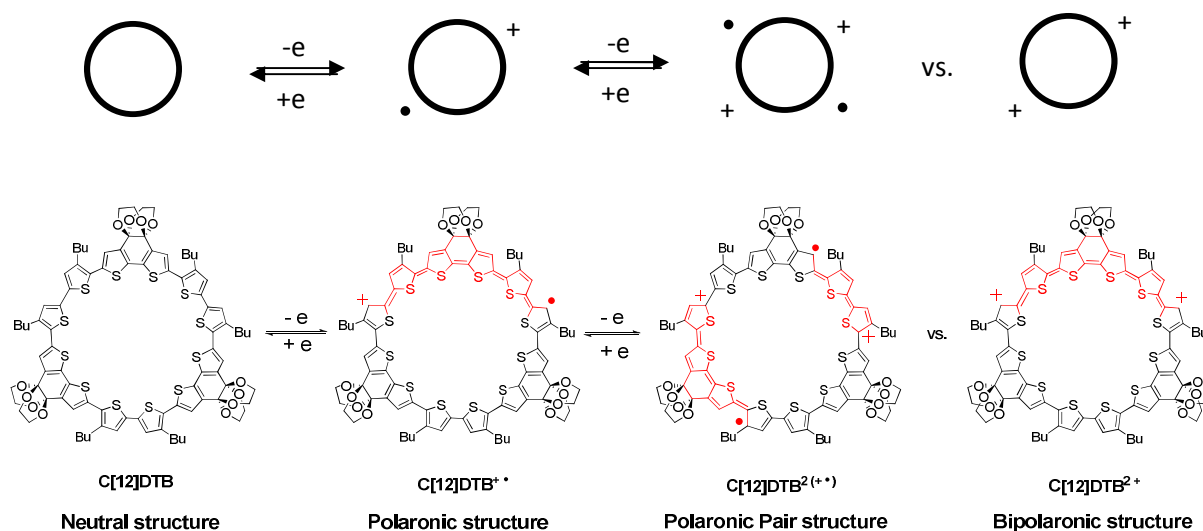


Figure 3.24: Possible electronic structures of macrocycle C[12]DTB **67a** in the neutral, singly and doubly oxidized state.

3.9 Characterization of doubly oxidized species C[12]DTB²⁽⁺⁾ via electron spin resonance

Electron spin resonance measurements of the first and second oxidized state of C[12]DTB **67a** were carried out at ambient temperature as well as in the frozen state at 120 K. The oxidized species were formed by addition of 1.0 and 2.5 eqs. of the chemical oxidant TDBPA⁺SbCl₆⁻ to a defined concentration of the macrocycle, respectively. The recorded spectra are depicted in Figure 3.25.

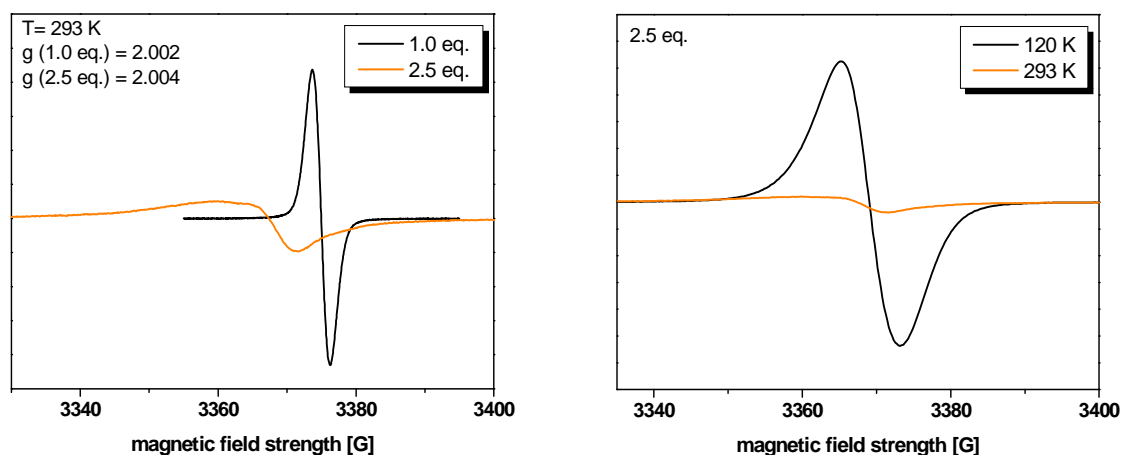


Figure 3.25: ESR-spectra of the singly and doubly oxidized species of **67a** at 293 K (left). ESR-spectra of the doubly oxidized species of **67a** at 120 and 293 K (right).

A well resolved and strong signal was obtained for the radical cation $\text{C}[12]\text{DTB}^{\cdot+}$ at room temperature, whereby the dicationic species exhibited a decrease of the ESR intensity (Figure 3.25, left). This can be attributed to a thermodynamically equilibrium of a singlet and triplet state of $\text{C}[12]\text{DTB}^{2(+)}$, whereas no strong signal can result.^[37] $\text{C}[12]\text{DTB}^{2(+)}$ was then subjected to temperature-dependent measurements by cooling the sample down to 120 K, whereby a much more intensive and symmetric signal resulted. Presumably, one of the spin states of the unpaired electrons, singlet or triplet, has to be favoured and resulted therefore in an enlarged signal (Figure 3.25, right). A small increase of the g factor is observed upon addition of oxidant, ranging from 2.002 (1.0 eq.) to 2.004 (2.5 eqs.). This could be attributed to an association of the spin-carrying π -system with the SbCl_6^- counter anions, which contain heavy elements with high spin-orbit coupling constants. This effect has also been observed for the ESR analysis of cyclo[10]thiophene by Zhang.^[37] The temperature-dependent measurements of the monoradical species $\text{C}[12]\text{DTB}^{\cdot+}$ showed the opposite effect as for the dicationic one and the signal diminished with decreasing temperature (Figure 3.26, left). This effect can result from the formation of aggregates as has already been described via cyclic voltammetry and UV/vis/NIR absorption spectroscopy. The shape of the ESR-signal of the dicationic species $\text{C}[12]\text{DTB}^{2(+)}$ at room temperature displayed a rather asymmetric curve (Figure 3.26, right). With an addition of 2.5 eqs. of oxidant, a light excess of $\text{TDBPA}^+\text{SbCl}_6^-$ is supposed to be left in the sample. The recorded signal for the dication could be slightly influenced by the oxidant, since it is itself of a radical cation, which exhibits also a signal during the ESR measurements.

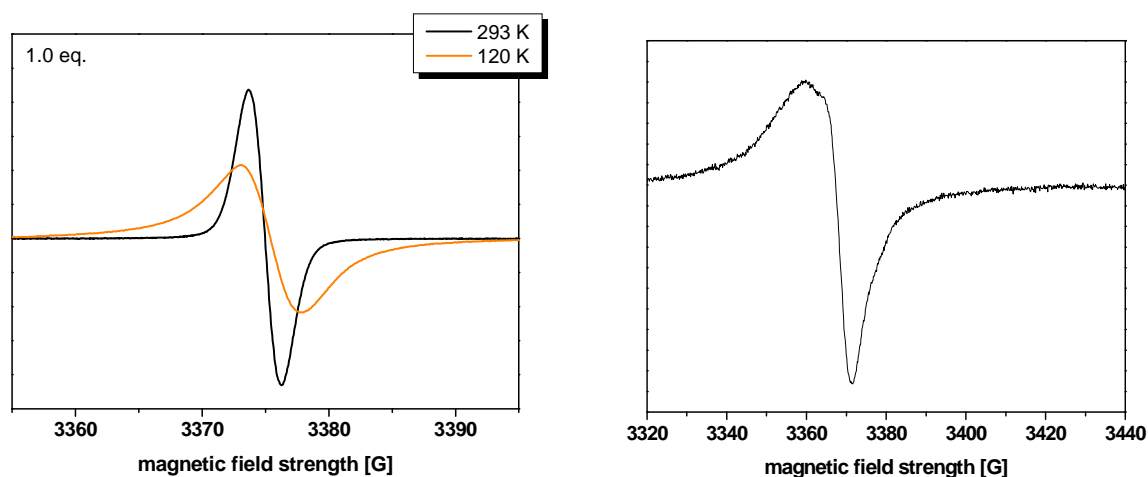


Figure 3.26: ESR-spectra of the singly oxidized species of **67a** at 293 and 120 K (left). ESR-spectrum of the doubly oxidized species of **67a** at 293 K (right).

Based on already published results for cyclo[10]thiophene by Zhang^[37] and a spectral evidence due to a positive electron spin resonance signal ($g = 2.004$) for the doubly oxidized species of macrocycle **67a**, a polaronic-pair configuration $C[12]DTB^{2(+)}$ is assumed, which is also in accordance with the obtained UV/vis/NIR absorption spectrum of the appropriate oxidized state.

3.10 Single-crystal X-ray diffraction analysis of C[12]DTB (**67a**)

Single-crystals of nanosized macrocycles are often difficult to grow and measure since solvent molecules are incorporated within the cavity during the growth process and their loss due to evaporation may cause destruction and collapsing of the crystals.^[49] Suitable single-crystals for X-ray diffraction measurements of **67a** were obtained by slow diffusion of *n*-hexane into a solution of the macrocycle in chloroform at low temperatures. The structural analysis provided a well resolved crystallographic structure of the acceptor-functionalized macrocycle. Detailed crystallographic data are given in the attachment.^[N1] The attached flexible side chains caused a degree of disorder and a weak distribution intensity, which resulted in a relatively high *R* value of 8.4%. In general, the *R* value describes the accuracy between the X-ray diffraction data and the model of the molecular structure. Macrocycle **67a** was found to crystallize in the triclinic space group P-1 with two molecules in the unit cell ($Z=2$). The top view of the structure proves the circular shape of the fully α -conjugated backbone with all thiophene units assembled in a *syn*-conformation meaning that all sulfur atoms are directed into the cavity of the centrosymmetric ring with an inner diameter of 12.2 – 12.9 Å (Figure 3.27). This conformation is in stark contrast to the prevailing *anti*-conformation of linear oligothiophenes.

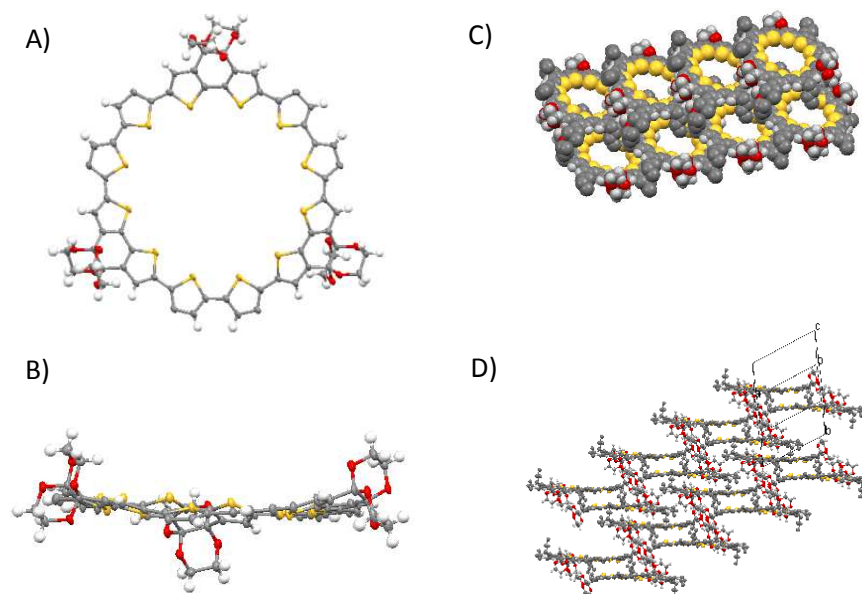


Figure 3.27: A) Top view of the molecular structure of C[12]DTB **67a** and B) side view. C) Top view of the packing diagram and D) side view.

The ethylene glycol protecting groups and most of the butyl groups were visible in the examined structure as well. The latter are arranged at the periphery of the cyclic structure and do not directly enter the cavity. Since only half of them exhibited a proper resolution due to their weak distribution intensity and allowed an exact determination of their alignment, the butyl groups were omitted for clarity in the mentioned figure. The inter-ring carbon-carbon bond lengths with values of 1.42 – 1.47 Å correlate with those of linear oligomers^[50] and theoretical calculations for *syn*-C20T.^[29] The carbon-sulfur bond lengths possess an average value of 1.72 Å. The molecular side view shows a weak twist of the thiophene rings out of the plane with the cyclic backbone lightly bent. The dihedral inter-ring angles between adjacent thiophene units reach up to 29.9°, which reflects some ring strain as a result of the almost complete planarity. The lowest torsion angle occurred between thiophene units integrated into the rigid fused DTB-core unit and showed a value of 1.27°. The arrangement of **67a** in the lattice can be described as stacks of macrocycles in which one cycle lays slightly displaced on top of each other. The butyl groups point into the cavity of the molecule on top or below. Due to a relative distance between rings in the same stack of ~ 7 Å, it is assumed that no significant π - π -interactions exist. Instead, neighboring stacks showed a slight overlap with each other with distances around 3.4 Å. These results were compared to those obtained for the non-functionalized macrocycle C[12]T^[31] **81**. This ring also crystallizes in the triclinic space group P-1, but with four molecules per unit cell. All thiophene molecules adopt a *syn*-conformation as well and reveal a round shape. The inner diameter of 12.4 – 12.7 Å is comparable to the value for **67a**. The torsion angles between adjacent molecules range from 4 to 39° and thus indicate a strained system. Regarding the molecule

from the side, it is bent in a stronger way than **67a**. The packing diagram is also similar to the acceptor-functionalized ring with the formation of stacks in which the molecules are not directly on top of each other but shifted. Two further single-crystals of thiophene-based macrocycles, namely C[10]T^[37] and C[14]T^[31] could be grown. The interesting perception for the larger cycle is the orientation of two of the thiophene moieties in an *anti*-conformation towards their neighbors. The rotation around the inter-ring C-C bond releases the ring strain in the molecule. The remaining thiophene units adopt a *syn*-conformation which creates the plane and circular shape. The *anti*-conformation for large cyclic oligothiophenes has already been determined theoretically, whereas smaller cyclooligothiophenes are more stable in an all-*syn*-conformation. Macrocycles larger than C[14]T bend significantly from their regular ring shape when oriented in an all-*syn*-conformation.^[29]

3.11 Summary

The successful synthesis of shape-persistent, acceptor-functionalized macrocycles via the elaborated 'metal-assisted template method' and the electronic influence of the incorporated electron-withdrawing DTB- and DCP-moieties onto the optical and electrochemical properties of the rings were described within this chapter. Required quaterthiophene oligomers 4T-DTB **53** and 4T-DCP **61** were prepared by common Stille cross-coupling reaction from a stannylated thiophene and a dibrominated fused acceptor-segment in good yields. Subsequent introduction of further tin groups at the external thiophene units was performed, followed by the crucial metal-assisted macrocyclization step by means of PtCl₂(COD). The special angle of the transition metal complex and the hemicyclic shape of the thiophene precursors supported the formation of cyclic metallaoligomers over linear byproducts. After relatively long reaction times up to 7 days, a mixture of pre-templated metallacycles was formed and Pt^{II}metallacycle Pt(COD)[12]DTB **64a** was isolated and characterized by proton NMR spectroscopy and mass spectrometry. Both pathways via either a thermally or an oxidatively induced reductive elimination under simultaneous C-C bond formation led to fully α -conjugated DTB- and DCP-macrocycles. After time-consuming and extensive purification processes by SEC and precipitation, C[12]DTB **67a**, C[16]DTB **67b**, and C[12]DCP **70** were successfully separated and isolated pure in 4-10% yield. Deprotection of the ketone groups in order to gain a stronger acceptor property and reactive centers for further organic chemistry failed due to a high aggregation and precipitation behaviour of partially deprotected cyclic species. Photophysical measurements were carried out for **67a**, **67b**, and **70** and results were opposed to non-functionalized macrocycle C[12]T **81**. Bathochromically shifted absorption spectra were recorded for both acceptor-substituted classes of macrocycles with a strong main absorption band for the S₀→S₂ transition and a shoulder

for the energetically lower and symmetry forbidden $S_0 \rightarrow S_1$ transition, which was merely observed for the smaller rings. During cyclic voltammetry, several reversible one-electron oxidation steps and a higher first oxidation potential due to the electron-withdrawing effect of the DTB unit were detected for **67a** and compared to C[12]T **81**. The aggregation tendency towards dimeric species between charged cycles via intermolecular π - π -interactions was additionally identified for **67a** (also through temperature-dependent measurements) and was in good agreement with formerly investigated pure thiophene-based macrocycles. Additional UV/vis/NIR spectroscopic measurements of different chemically oxidized states were carried out for **67a** to gain more information about the electronic structure of multiply charged species. During this kind of analysis, the formation of the mentioned dimers were determined by temperature-dependent measurements as well. The recorded spectra revealed the existence of a polaronic pair structure for the doubly oxidized macrocycle C[12]DTB²⁽⁺⁾ over a bipolaronic configuration. This assumption was also determined by electron spin resonance analysis. X-ray crystallographic analysis of **67a** allowed the evidence of a perfect cyclic and nearly completely planar shape with all thiophene units oriented in a *syn*-conformation. The electrochemical studies were only performed for **67a** as insufficient resolved spectra with indefinable signals were obtained for **67b** and **70**. The ‘metal-assisted template method’ was finally effectively applicable for functionalized oligothiophenes and offers the possibility to cyclize tailored, pre-functionalized oligomers.

3.12 Experimental section

General remarks about chemicals and synthesis

n-BuLi (1.6 and 2.5 M) was purchased from Acros, trimethyltin chloride from Aldrich, and 1,1'-bis(diphenylphosphino)ferrocene, tetrafluoroboric acid (50% in EtOH), and silver triflate from Alfa Aesar. Trimethylsilyl chloride, copper(II)chloride, diisopropylamine, triethylamine, tetrabutyl ammonium fluoride, ethylene glycol, bromine, magnesium, hydrochloric acid, 1,2-bis(trimethylsilyloxy)ethane, trimethylsilyl trifluoromethanesulfonate, iodine, copper powder, and other common reagents were purchased from Merck. Catalyst tetrakis(triphenylphosphine)palladium Pd(PPh₃)₄ was prepared according to an internal institute protocol,^[51] platinum complex PtCl₂(COD) was synthesized after a literature known protocol.^[52] Deuterated solvents for NMR spectroscopy were purchased from Aldrich (CDCl₃, DMSO-*d*₆) and Deutero (THF-*d*₈).

All solvents were purchased from Merck (VWR international) and dried for the use in reactions either according to standard protocol^[53] or were taken from the solvent purification system^[54] MB SPS-800

of MBraun. All solvents were distilled prior to the purification processes and used as received for work-up procedures. A 'Schlenk line'-apparatus was utilized for syntheses carried out under inert gas.

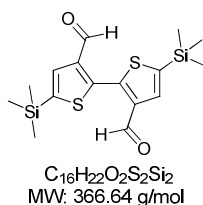
General remarks about analytical data and performed measurements

NMR spectra were recorded on a Bruker DRX400 spectrometer at 25 °C (Institute of Organic Chemistry I, University of Ulm). Chemical shift values (δ) are expressed in parts per million using residual solvent protons (CDCl_3 : ^1H δ = 7.26 ppm and ^{13}C δ = 77.36 ppm; THF-d_8 : ^1H δ = 3.57 ppm and ^{13}C δ = 67.20 ppm; DMSO-d_6 : ^1H δ = 2.50 ppm and ^{13}C δ = 39.43 ppm) as internal standard.^[55] The atom labels herein are chosen due to practical aspects for the assignment of NMR-signals and are not conform to IUPAC nomenclature. *Thin layer chromatography* was carried out on aluminium sheets pre-coated with silica gel (Merck TLC Silica gel 60 F₂₅₄) and aluminium oxide (Merck TLC Aluminium oxide 150 F₂₅₄, neutral), respectively. *Preparative column chromatography* was performed on glass columns packed with flash silica gel, particle size 0.04-0.064 nm, from Macherey-Nagel and basic aluminium oxide (alumina) "90", particle size 0.04-0.064 nm from Merck, respectively. The alumina was deactivated to "Brockmann" activity II-III and IV by adding 5% and 10% distilled water. Bio-Beads S-X1 (200-400 Mesh) from BIO-RAD were used as stationary phase for *size exclusion chromatography*. *GC mass spectra* were measured on a Varian 3800 gas chromatograph with a Varian Saturn 2000 mass detector. *CI-MS* were recorded on a Finnigan MAT SSQ-7000, *MALDI-TOF mass spectra* on a Bruker Daltonics Reflex III. *High resolution mass spectra* were measured with a Bruker solariX spectrometer with a MALDI or an ESI source. *Melting points* were determined using a Büchi B-545 apparatus and were not corrected. *Elemental analyses* were performed on an Elementar Vario EL (Institute of Analytical Chemistry, University of Ulm). Photophysical measurements were carried out in 1 and 0.1 cm cuvettes with Merck spectroscopic grade solvents (Uvasol grade DCM and chloroform). *UV/vis/NIR absorption spectra* were recorded at room temperature and cooled temperatures to 0 °C on a Perkin Elmer Lambda 19 spectrometer and *fluorescence spectra* at room temperature on a Perkin Elmer LS 55 spectrometer. The emission spectra were fully corrected for the photodetector response. *Cyclic voltammetry experiments* were performed with a computer-controlled Autolab PGSTAT30 in a three-electrode single-compartment cell with a platinum working electrode (ϕ = 3.4 mm), a platinum wire counter electrode and a Ag/AgCl reference electrode. All potentials were internally referenced to a ferrocene/ferrocenium (Fc/Fc^+) couple. Dried, freshly distilled and deaerated solvents (DCM and benzonitrile) were used. Tetrabutylammonium hexafluorophosphate was twice recrystallized from ethanol and dried under vacuum. *X-Ray diffraction* data were collected and refined by Prof. Weil (Institute of Chemical Technologies and Analytics, University of Vienna). *ESR spectra* were recorded on a Bruker EMX (X‐Band) with a

microwave frequency of 9.4 GHz (Institute of Inorganic Chemistry, University of Stuttgart) at 293 and 120 K.

Synthesis and characterization of DTB-containing compounds

5,5'-Bis(trimethylsilyl)-2,2'-bithiophene-3,3'-dicarboxaldehyde (**46**)



3,3'-Dibromo-5,5'-bis(trimethylsilyl)-2,2'-bithiophene **45** (7.00 g, 14.9 mmol) was dissolved in 140 mL dry THF and cooled to -78 °C. *n*-Butyl lithium (1.6 M in *n*-hexane, 21.5 mL, 34.4 mmol) was added within 15 min and the reaction was stirred for further 30 min. N,N'-dimethylformamide (3.28 g, 44.8 mmol) was added at the same temperature and stirring was continued for further 30 min. The mixture was quenched with 70 mL of a 2 M HCl solution and allowed to warm up to room temperature. The organic layer was separated and washed three times with water, once with brine and then dried over Na₂SO₄. The solvent was removed under vacuum. Purification via column chromatography using silica and DCM yielded bithiophene **46** (4.95 g, 13.5 mmol, 90%) as a yellow solid.

Mp: 93 – 94 °C.

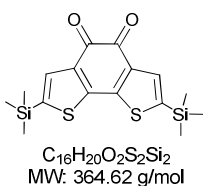
¹H NMR (400 MHz, CDCl₃): δ = 9.87 (s, 2H, CHO), 7.73 (s, 2H, Th-4,4'), 0.37 (s, 18H, TMS) ppm.

¹³C NMR (100 MHz, CDCl₃): δ = 184.80, 146.36, 144.89, 140.97, 133.73, -0.37 ppm.

MS (CI) *m/z*: calcd. for [M]⁺ (C₁₆H₂₂O₂S₂Si₂): 366; found: 367 [M+H]⁺.

Elemental analysis: calcd. for (C₁₆H₂₂O₂S₂Si₂): C, 52.41; H, 6.05; S, 17.49%; found: C, 52.29; H, 5.92; S, 17.43%.

2,7-Bis(trimethylsilyl)benzo[2,1-*b*:3,4-*b'*]dithiophene-4,5-dione (**47**)



Bithiophene **46** (4.50 g, 12.3 mmol), dry triethylamine (1.19 mL, 8.59 mmol) and 5-(2-hydroxyethyl)-4-methyl-3-(phenyl)-thiazoliumchloride (0.66 g, 2.45 mmol) were stirred in 250 mL dry *tert*-butanol

under exclusion of water and oxygen and the suspension was heated to 80 °C for 4.5 h. The resulting yellow solution was cooled down to 35 °C and air was blown through. Stirring was continued at 35 °C for 15 h. Afterwards, the solvent was removed under vacuum and the residue was dissolved in DCM. The organic phase was washed with water, dried over Na₂SO₄ and the solvent was evaporated under vacuum. Purification via column chromatography using silica and DCM afforded a deep red solid of **47** (3.63 g, 9.96 mmol, 81%).

Mp: 202 – 203 °C.

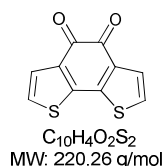
¹H NMR (400 MHz, CDCl₃): δ = 7.60 (s, 2H, DTB-3,6), 0.36 (s, 18H, TMS) ppm.

¹³C NMR (100 MHz, CDCl₃): δ = 175.21, 148.35, 142.46, 135.81, 134.36, -0.42 ppm.

MS (CI) *m/z*: calcd. for [M]⁺ (C₁₆H₂₀O₂S₂Si₂): 364; found: 365 [M+H]⁺.

Elemental analysis: calcd. for (C₁₆H₂₀O₂S₂Si₂): C, 52.70; H, 5.53; S, 17.59%; found: C, 52.75; H, 5.54; S, 17.38%.

Benzo[2,1-*b*:3,4-*b'*]dithiophene-4,5-dione (**44**)



Dione **47** (3.47 g, 9.52 mmol) was dissolved in THF (200 mL) and tetra-*n*-butylammonium fluoride trihydrate (6.90 g, 21.9 mmol) was added. The solution was stirred for 30 min at room temperature and quenched with water. The product was extracted with DCM and the combined organic layers were dried over Na₂SO₄. Removal of the solvent yielded the crude material which was purified by column chromatography using silica and DCM. Pure product **44** (1.28 g, 5.81 mmol, 61%) was obtained as a dark solid.

Mp: Sublimation at ca. 270 °C.

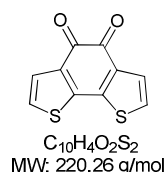
¹H NMR (400 MHz, DMSO): δ = 7.61 (d, ³*J* = 5.2 Hz, 2H, DTB-3,6), 7.44 (d, ³*J* = 5.2 Hz, 2H, DTB-2,7) ppm.

¹³C NMR (100 MHz, DMSO): δ = 174.01, 142.35, 135.29, 127.04, 127.03 ppm.

MS (CI) *m/z*: calcd. for [M]⁺ (C₁₀H₄O₂S₂): 220; found: 221 [M+H]⁺.

Elemental analysis: calcd. for (C₁₀H₄O₂S₂): C, 54.53; H, 1.83; S, 29.11%; found: C, 54.42; H, 1.91; S, 29.11%.

Analytical data were in accordance with literature data.^[2, 14]

Benzo[2,1-*b*:3,4-*b'*]dithiophene-4,5-dione (44**)**


2,2'-Bithiophene-3,3'-dicarboxyaldehyde **43** (600 mg, 2.70 mmol), dry triethylamine (0.26 mL, 1.89 mmol) and 5-(2-hydroxyethyl)-4-methyl-3-(phenyl)-thiazoliumchloride (146 mg, 0.54 mmol) were stirred in dry *tert*-butanol (40 mL) under exclusion of water and oxygen. The suspension was heated to 80 °C and stirred for 4 h. Atmospheric oxygen was not allowed to come in contact with the substance before completion of the benzoin condensation. The resulting yellow solution was cooled down to 35 °C and air was blown through. Dione **44** (560 mg, 2.54 mmol, 94%) precipitated overnight and could be collected by filtration.

Mp: Sublimation at ca. 270 °C.

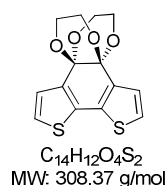
¹H NMR (400 MHz, DMSO-*d*₆): δ = 7.62 (d, ³*J* = 5.2 Hz, 2H, DTB-3,6), 7.44 (d, ³*J* = 5.1 Hz, 2H, DTB-2,7) ppm.

¹³C NMR (100 MHz, DMSO-*d*₆): δ = 174.02, 142.35, 135.30, 127.04, 127.03 ppm.

MS (CI) *m/z*: calcd. for [M]⁺ (C₁₀H₄O₂S₂): 220; found: 221 [M+H]⁺.

Elemental analysis: calcd. for (C₁₀H₄O₂S₂): C, 54.53; H, 1.83; S, 29.11%; found: C, 54.42; H, 1.91; S, 29.11%.

Analytical data were in accordance with literature data.^[2, 14]

Benzo[2,1-*b*:3,4-*b'*]dithiophene-4,5-ethylenedioxdane (48**)^[15-16]**


A round-bottomed flask was charged under argon with benzo[2,1-*b*:3,4-*b'*]dithiophene-4,5-dione **44** (1.31 g, 5.95 mmol) and 110 mL dry ethylene glycol. Chlorotrimethylsilane (4.00 mL, 31.3 mmol) was added in three portions at intervals of 2 days between each addition. After the addition of the third portion, the solution was stirred at room temperature for further 5 days. The solution was poured into 1 M NaOH solution and the product was extracted with DCM. The combined organic layers were washed with water and dried over Na₂SO₄. Afterwards, the solvent was evaporated and the resulting solid was crystallized from ethyl acetate to yield green crystals of **48** (1.57 g, 5.09 mmol, 86%).

Mp: 246 – 247 °C.

¹H NMR (400 MHz, CDCl₃): δ = 7.19 (m, 4H, DTB-2,3,6,7), 4.21-4.14 (m, 4H, O-CH₂), 3.75-3.69 (m, 4H, O-CH₂) ppm.

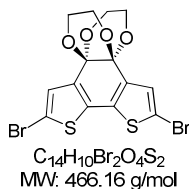
¹³C NMR (100 MHz, CDCl₃): δ = 135.50, 133.33, 125.26, 123.83, 93.70, 61.60 ppm.

MS (CI) *m/z*: calcd. for [M]⁺ (C₁₄H₁₂O₄S₂): 308; found: 309 [M+H]⁺.

Elemental analysis: calcd. for (C₁₄H₁₂O₄S₂): C, 54.53; H, 3.92; S, 20.80%; found: C, 54.71; H, 3.86; S, 20.79%.

Analytical data were in accordance with literature data.^[15-16]

2,7-Dibromo-benzo[2,1-*b*:3,4-*b'*]dithiophene-4,5-ethylenedioxiolane (**49**)



Benzo[2,1-*b*:3,4-*b'*]dithiophene-4,5-ethyleneoxolane **48** (1.40 g, 4.54 mmol) was dissolved in chloroform (100 mL), cooled to 0 °C and pyridine (1.10 mL, 13.6 mmol) was added. A solution of bromine (0.53 mL, 10.4 mmol), diluted 1:20 (vol.) in chloroform, was slowly dropped to the mixture. After complete addition, the reaction mixture was stirred overnight at room temperature and subsequently diluted with a sat. aqueous Na₂S₂O₃ solution. The organic layer was separated and washed with a sat. NaHCO₃ solution as well as with water. After drying over Na₂SO₄, the solvent was removed under vacuum. The obtained solid was crystallized from ethyl acetate to form yellow needles of **49** (1.95 g, 4.19 mmol, 92%).

Mp: 244 – 245 °C.

¹H NMR (400 MHz, CDCl₃): δ = 7.14 (s, 2H, DTB-3,6), 4.17-4.11 (m, 4H, O-CH₂), 3.73-3.67 (m, 4H, O-CH₂) ppm.

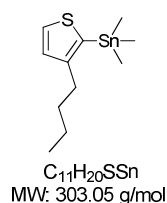
¹³C NMR (100 MHz, CDCl₃): δ = 135.97, 133.55, 128.17, 111.52, 92.86, 61.61 ppm.

MS (CI) *m/z*: calcd. for [M]⁺ (C₁₄H₁₀Br₂O₄S₂): 466; found: 466 [M]⁺.

Elemental analysis: calcd. for (C₁₄H₁₀Br₂O₄S₂): C, 36.07; H, 2.16; S, 13.76%; found: C, 36.19; H, 2.35; S, 13.85%.

Analytical data were in accordance with literature data.^[10]

3-Butyl-2-(trimethyltin)thiophene (52)



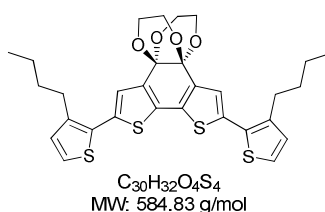
2-Bromo-3-butylthiophene (5.00 g, 22.8 mmol) in 100 mL dry THF were added slowly to magnesia turnings (0.58 g, 23.9 mmol) in a flame-dried flask. The reaction mixture was refluxed for 4 h. After cooling to room temperature, a solution of trimethyltin chloride (4.77 g, 23.9 mmol) in 15 mL dry THF was added and the suspension was stirred overnight at room temperature. The reaction mixture was poured onto ice water and extracted with diethyl ether. The combined organic layers were dried over Na_2SO_4 and the solvent was evaporated. The crude compound was purified by vacuum distillation (2.8×10^{-2} bar; 85 °C) to yield 3-butyl-2-(trimethyltin)thiophene **52** (5.65 g, 18.6 mol, 82%) as a colorless liquid.

1H NMR (400 MHz, $CDCl_3$): δ = 7.52 (d, 3J = 4.7 Hz, 1H, Th-5), 7.09 (d, 3J = 4.6 Hz, 1H, Th-4), 2.63 (t, 3J = 7.8 Hz, 2H, α - CH_2 -Bu), 1.61-1.53 (m, 2H, β - CH_2 -Bu), 1.41-1.32 (m, 2H, γ - CH_2 -Bu), 0.93 (t, 3J = 7.3 Hz, 3H, CH_3 -Bu), 0.37 (s, 9H, TMSn) ppm.

^{13}C NMR (100 MHz, $CDCl_3$): δ = 150.93, 131.42, 130.63, 129.47, 34.44, 32.35, 22.80, 14.15, -7.85 ppm.

MS (EI) m/z : calcd. for $[M]^+$ ($C_{11}H_{20}SSn$): 304; found: 304 $[M]^+$, 289 $[M-CH_3]^+$.

2,7-Bis(3-butylthien-2-yl)benzo[2,1-*b*:3,4-*b'*]dithiophene-4,5-ethylenedioxa-1,3-dioxane (53)



Benzodithiophene **49** (1.75 g, 3.75 mmol) and 3-butyl-2-(trimethyltin)thiophene **52** (2.73 g, 9.01 mmol) were dissolved in dry DMF (140 mL) and degassed. Tetrakis(triphenylphosphine)palladium(0) (216 mg, 187 μ mol) was added. The reaction mixture was heated at 80 °C for 2 d. After cooling to room temperature, the mixture was poured onto water and the product was extracted with DCM. The combined organic layers were dried over Na_2SO_4 and the solvent was evaporated. The residue was chromatographed on silica gel using a mixture of EE:*n*-hexane (1:4) as eluent to afford **53** (2.06 g, 3.53 mmol, 94%) as an orange solid.

Mp: 118 – 119 °C.

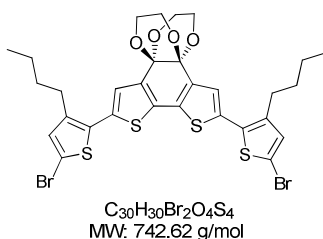
^1H NMR (400 MHz, CDCl_3): δ = 7.21 (s, 2H, DTB-3,6), 7.19 (d, 3J = 5.2 Hz, 2H, Th-5,5'), 6.94 (d, 3J = 5.2 Hz, 2H, Th-4,4'), 4.23-4.18 (m, 4H, O-CH₂), 3.82-3.76 (m, 4H, O-CH₂), 2.79 (t, 3J = 7.8 Hz, 4H, α -CH₂-Bu), 1.68-1.61 (m, 4H, β -CH₂-Bu), 1.45-1.36 (m, 4H, γ -CH₂-Bu), 0.94 (t, 3J = 7.3 Hz, 6H, CH₃-Bu) ppm.

^{13}C NMR (100 MHz, CDCl_3): δ = 139.74, 135.42, 134.84, 132.11, 129.75, 129.70, 123.82, 123.46, 93.13, 61.38, 32.40, 28.67, 22.29, 13.62, ppm.

MS (MALDI-TOF) m/z : calcd. for $[\text{M}]^+$ ($\text{C}_{30}\text{H}_{32}\text{O}_4\text{S}_4$): 584.1; found: 584.1 $[\text{M}]^+$.

Elemental analysis: calcd. for ($\text{C}_{30}\text{H}_{32}\text{O}_4\text{S}_4$): C, 61.61; H, 5.52; S, 21.93%; found: C, 61.93; H, 5.56; S, 21.77%.

2,7-Bis(5-bromo-3-butylthien-2-yl)-benzo[2,1-*b*:3,4-*b'*]dithiophene-4,5-ethylenedioxiolane (**54**)



DTB-containing quaterthiophene **53** (978 mg, 1.67 mmol) was dissolved in 100 mL chloroform, cooled to 0 °C and pyridine (0.41 mL, 5.02 mmol) was added. A solution of bromine (0.19 mL, 3.85 mmol), diluted 1:20 (vol.) in chloroform, was slowly added dropwise. After complete addition, the reaction mixture was stirred at rt for 5 h and subsequently diluted with a sat. aqueous $\text{Na}_2\text{S}_2\text{O}_3$ solution. The organic layer was separated and washed with a sat. NaHCO_3 solution and water. After drying over Na_2SO_4 , the solvent was removed in vacuum. The crude oil was purified by column chromatography using silica and a mixture of EE:*n*-hexane (1:4) as eluent to obtain **54** (1.19 g, 1.60 mmol, 96%) as a yellow film.

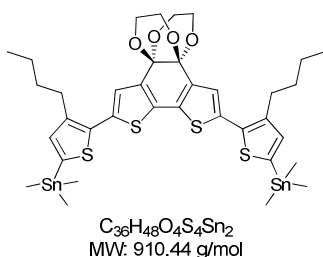
Mp: 68 – 69 °C.

^1H NMR (400 MHz, CDCl_3): δ = 7.14 (s, 2H, DTB-3,6), 6.90 (s, 2H, Th-4,4'), 4.22-4.18 (m, 4H, O-CH₂), 3.79-3.74 (m, 4H, O-CH₂), 2.72 (t, 3J = 7.7 Hz, 4H, α -CH₂-Bu), 1.64-1.58 (m, 4H, β -CH₂-Bu), 1.43-1.34 (m, 4H, γ -CH₂-Bu), 0.93 (t, 3J = 7.3 Hz, 6H, CH₃-Bu) ppm.

^{13}C NMR (100 MHz, CDCl_3): δ = 140.96, 136.22, 134.09, 132.93, 132.87, 131.56, 124.43, 111.23, 93.50, 77.39, 61.88, 32.77, 29.12, 22.70, 14.10 ppm.

MS (MALDI-TOF) m/z : calcd. for $[\text{M}]^+$ ($\text{C}_{30}\text{H}_{30}\text{Br}_2\text{O}_4\text{S}_4$): 741.9; found: 741.8 $[\text{M}]^+$.

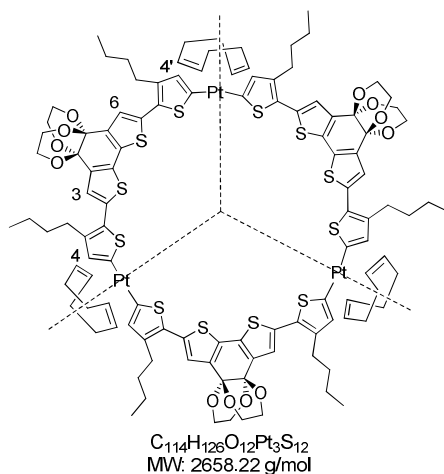
Elemental analysis: calcd. for ($\text{C}_{30}\text{H}_{30}\text{Br}_2\text{O}_4\text{S}_4$): C, 48.52; H, 4.07; S, 17.27%; found: C, 48.74; H, 4.04; S, 17.23%.

**2,7-Bis(3-butyl-5-trimethylstannylthien-2-yl)benzo[2,1-b:3,4-b']dithiophene-4,5-ethylenedioxi-
lane (55)**


To a solution of dibrominated quaterthiophene **54** (200 mg, 0.27 mmol) in 10 mL of dry THF was added dropwise *n*-butyl lithium (1.6 M in *n*-hexane, 0.39 mL, 0.63 mmol) at -78 °C within 25 min. After stirring between -75 °C and -65 °C for 65 min, trimethyltin chloride (134 mg, 0.67 mol) dissolved in dry THF (1.5 mL) was added quickly. The reaction mixture was allowed to warm up to room temperature overnight. After quenching with water, the product was extracted with dichloromethane and the combined organic layers were dried over Na₂SO₄. Crude product **55** (94% calcd. from ¹H NMR) was used without further purification in the next step.

¹H NMR (400 MHz, THF-d₈): δ = 7.13 (s, 2H, DTB-3,6), 7.04 (s, 2H, Th-4,4'), 4.11-4.07 (m, 4H, O-CH₂), 3.67-3.61 (m, 4H, O-CH₂), 2.81 (t, ³J = 7.8 Hz, 4H, α -CH₂-Bu), 1.69-1.61 (m, 4H, β -CH₂-Bu), 1.47-1.37 (m, 4H, γ -CH₂-Bu), 0.94 (t, ³J = 7.3 Hz, 6H, CH₃-Bu), 0.36 (s, 18H, TMSn) ppm.

MS (MALDI-TOF) *m/z*: calcd. for [M]⁺ (C₃₆H₄₈O₄S₄Sn₂): 910.0; found: 910.0 [M]⁺, 747.9 [M-TMSn]⁺, 583.8 [M-2xTMSn]⁺.

Pt(COD)[12]DTB (64a)


Distannylated quaterthiophene **55** (220 mg, 242 μ mol) and PtCl₂(COD) (96.1 mg, 257 μ mol) were dissolved in 230 mL DCM and refluxed for 7 days. The mixture was cooled to room temperature and

filtered through a column packed with alox IV using DCM as eluent. The solvent was evaporated and an orange-red solid (150 mg) was obtained. Isolation of the individual macrocycle **64a** (10.0 mg, 3.76 μmol , 23%) was achieved via SEC of one-fifth of the crude product with THF as eluent to yield an orange solid.

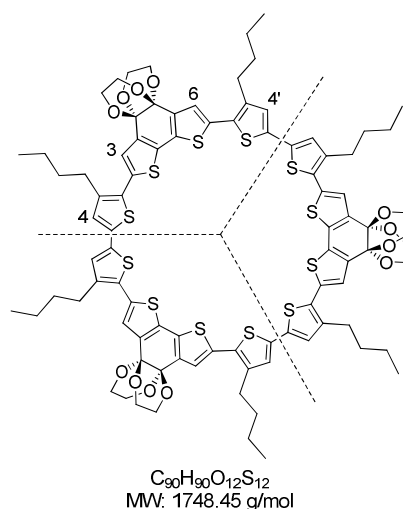
Mp: Decomposition at 230 °C.

^1H NMR (400 MHz, CDCl_3): δ = 7.05 (s, 6H, DTB-3,6), 6.60 (s, 6H, Th-4,4'), 5.55 (s, 12H, COD-CH), 4.14-4.10 (m, 12H, O-CH₂), 3.77-3.73 (m, 12H, O-CH₂), 2.72 (t, 3J = 7.6 Hz, 12H, α -CH₂-Bu), 2.61 (s, 24H, COD-CH₂), 1.64-1.57 (m, 12H, β -CH₂-Bu), 1.41-1.32 (m, 12H, γ -CH₂-Bu), 0.90 (t, 3J = 7.3 Hz, 18H, CH₃-Bu) ppm.

HRMS (MALDI-TOF) m/z : calcd. for $[\text{M}]^+$ ($\text{C}_{114}\text{H}_{126}\text{O}_{12}\text{Pt}_3\text{S}_{12}$): 2655.48410; found: 2655.44938 $[\text{M}]^+$, 2547.35194 $[\text{M}-\text{COD}]^+$, 2439.26204 $[\text{M}-2\times\text{COD}]^+$, 2244.30205 $[\text{M}-2\times\text{COD}-\text{Pt}]^+$, 1747.29777 $[\text{M}-3\times\text{COD}-3\times\text{Pt}]^+$.

^{13}C -NMR could not be measured due to poor solubility.

C[12]DTB (**67a**)



Distannylated quaterthiophene **55** (220 mg, 242 μmol) and $\text{PtCl}_2(\text{COD})$ (96.1 mg, 257 μmol) were dissolved in DCM (230 mL) and refluxed for 7 days. The mixture was cooled to room temperature and filtered through a column packed with alox IV using DCM as eluent. The solvent was evaporated under vacuum and an orange-red solid was obtained (150 mg).

The crude product (containing 169 μmol of $\text{Pt}(\text{COD})\text{DTB}$ -units) and 1,1'-bis(diphenylphosphino)-ferrocene (103 mg, 186 μmol) were dissolved in 30 mL of dry DCM and stirred at room temperature overnight. After the solvent was evaporated, 1,5-cyclooctadiene was removed under high vacuum and the obtained solid was dissolved in a sealed tube in 45 mL dry toluene and heated up at 140 °C

for 16 h. A red suspension was formed which was cooled to room temperature. The mixture was subsequently filtered through a short column filled with alox IV (DCM) and the solvent was evaporated to give a deep red residue. Isolation as well as purification of macrocycle **67a** (11.2 mg, 6.17 μ mol, 8%) was carried out by SEC eluting with THF to give a black solid.

Mp: Decomposition at 300 °C.

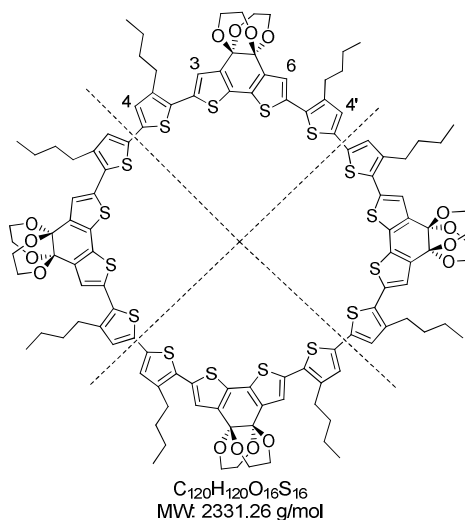
^1H NMR (400 MHz, CDCl_3): δ = 7.17 (s, 6H, DTB-3,6), 7.06 (s, 6H, Th-4,4'), 4.24-4.20 (m, 12H, O-CH₂), 3.83-3.79 (m, 12H, O-CH₂), 2.78 (t, 3J = 7.8 Hz, 12H, α -CH₂-Bu), 1.75-1.67 (m, 12H, β -CH₂-Bu), 1.50-1.41 (m, 12H, γ -CH₂-Bu), 0.98 (t, 3J = 7.3 Hz, 18H, CH₃-Bu) ppm.

^{13}C -NMR (125 MHz, CDCl_3): δ = 140.50, 136.64, 136.11, 134.86, 131.55, 131.45, 121.90, 120.55, 93.55, 61.58, 31.91, 29.18, 22.53, 13.83 ppm.

MS (MALDI-TOF) m/z : calcd. for $[\text{M}]^+$ ($\text{C}_{90}\text{H}_{90}\text{O}_{12}\text{S}_{12}$): 1746.3; found: 1747.0 $[\text{M}+\text{H}]^+$.

HRMS (MALDI-TOF) m/z : calcd. for $[\text{M}]^+$ ($\text{C}_{90}\text{H}_{90}\text{O}_{12}\text{S}_{12}$): 1746.30753; found: 1746.30699, $\delta_{m/m}$ = 0.3 ppm.

C[16]DTB (**67b**)



The synthetic and purification procedure followed the protocol described for macrocycle C[12]DTB **67a**. The larger analogue C[16]DTB **67b** (6.25 mg, 2.68 μ mol, 4%) was obtained as a black solid.

Mp: Decomposition at 300 °C.

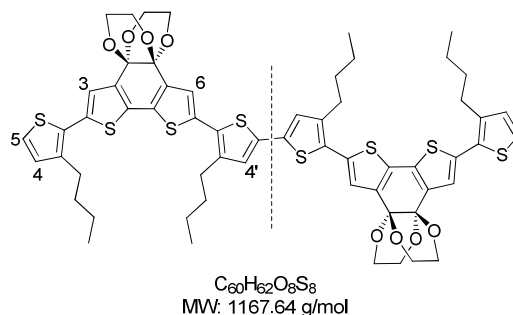
^1H NMR (400 MHz, CDCl_3): δ = 7.19 (s, 8H, DTB-3,6), 7.05 (s, 8H, Th-4,4'), 4.24-4.20 (m, 16H, O-CH₂), 3.83-3.78 (m, 16H, O-CH₂), 2.78 (t, 3J = 7.8 Hz, 16H, α -CH₂-Bu), 1.74-1.66 (m, 16H, β -CH₂-Bu), 1.50-1.40 (m, 16H, γ -CH₂-Bu), 0.98 (t, 3J = 7.3 Hz, 24H, CH₃-Bu) ppm.

MS (MALDI-TOF) m/z : calcd. for $[\text{M}]^+$ ($\text{C}_{120}\text{H}_{120}\text{O}_{16}\text{S}_{16}$): 2328.4; found: 2328.5 $[\text{M}]^+$.

HRMS (MALDI-TOF) m/z : calcd. for $[M]^+$ ($C_{120}H_{120}O_{16}S_{16}$): 2328.41022; found: 2328.40834, $\delta_{m/m} = 0.8$ ppm.

^{13}C -NMR could not be measured due to poor solubility.

L[8]DTB (79a)



DTB-containing quaterthiophene **53** (150 mg, 0.26 mmol) was dissolved in dry THF (8 mL), cooled to $-78\text{ }^{\circ}\text{C}$ and *n*-butyl lithium (1.6 M in *n*-hexane, 0.24 mL, 0.38 mmol) was added dropwise over a period of 15 min. The reaction mixture was stirred between $-78\text{ }^{\circ}\text{C}$ and $-65\text{ }^{\circ}\text{C}$ for 1 h and copper(II) chloride (51.7 mg, 0.38 mmol) was added in several portions under vigorous stirring. The mixture turned dark brown and some black solid deposit. After complete addition stirring was continued at $-70\text{ }^{\circ}\text{C}$ for 1 hour. The reaction mixture was allowed to warm up to $-10\text{ }^{\circ}\text{C}$ overnight and stirred for an additional hour at room temperature. Subsequent hydrolysis under ice cooling with a 2 N HCl solution and extraction of the aqueous phase with DCM were carried out. The combined organic layers were washed with water, dried over Na_2SO_4 and the solvent was removed under reduced pressure. An orange solid of linear oligomer L[8]DTB **79a** (30.0 mg, 29.1 μmol , 20%) was separated and purified by column chromatography using silica and DCM.

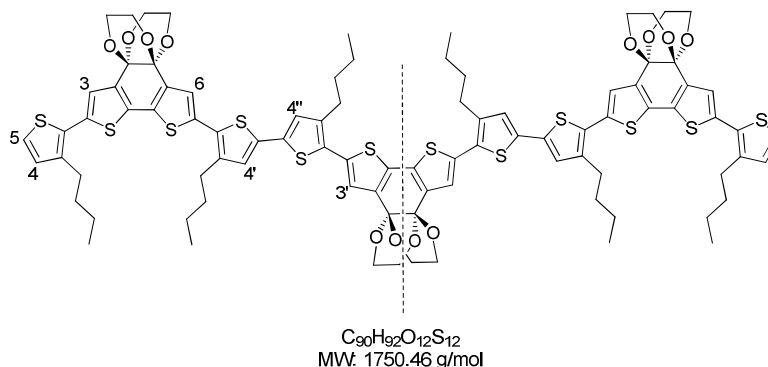
Mp: 253 – 254 $^{\circ}\text{C}$.

^1H NMR (400 MHz, CDCl_3): δ = 7.23 (s, 2H, DTB-3), 7.21 (s, 2H, DTB-6), 7.19 (d, $^3J = 5.2\text{ Hz}$, 2H, Th-5), 7.00 (s, 2H, Th-4'), 6.94 (d, $^3J = 5.2\text{ Hz}$, 2H, Th-4), 4.24-4.20 (m, 8H, O- CH_2), 3.82-3.78 (m, 8H, O- CH_2), 2.82-2.76 (m, 8H, $\alpha\text{-CH}_2\text{-Bu}$), 1.72-1.61 (m, 8H, $\beta\text{-CH}_2\text{-Bu}$), 1.47-1.38 (m, 8H, $\gamma\text{-CH}_2\text{-Bu}$), 0.99-0.93 (m, 12H, $\text{CH}_3\text{-Bu}$) ppm.

^{13}C NMR (125 MHz, CDCl_3): δ = 140.82, 140.12, 135.89, 135.32, 134.99, 134.74, 132.49, 132.34, 130.10, 130.03, 126.69, 124.48, 124.32, 124.18, 123.81, 123.65, 123.14, 122.98, 93.44, 61.73, 32.73, 32.51, 29.23, 29.02, 22.65, 22.63, 13.96 ppm.

MS (MALDI-TOF) m/z : calcd. for $[M]^+$ ($C_{60}H_{62}O_8S_8$): 1166.2; found: 1166.6 $[M]^+$.

HRMS (MALDI-TOF) m/z : calcd. for $[M]^+$ ($C_{60}H_{62}O_8S_8$): 1166.21995; found: 1166.22049, $\delta_{m/m} = 0.5$ ppm.

L[12]DTB (79b)


The synthetic and purification procedure followed the protocol described for L[8]DTB **79a**. The larger analogue L[12]DTB **79b** (12.0 mg, 6.86 μ mol, 8%) was obtained as a black solid.

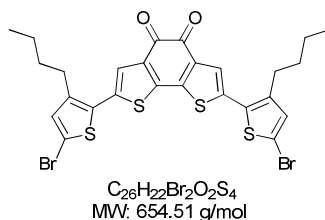
Mp: 257 – 259 °C.

1H NMR (400 MHz, $CDCl_3$): δ = 7.24 (s, 2H, DTB-3), 7.23 (s, 2H, DTB-6), 7.21 (s, 2H, DTB-3'), 7.19 (d, 3J = 5.3 Hz, 2H, Th-5), 7.01 (s, 4H, Th-4',4''), 6.94 (d, 3J = 5.2 Hz, 2H, Th-4), 4.22-4.20 (m, 12H, OCH_2), 3.82-3.78 (m, 12H, OCH_2), 2.82-2.77 (m, 12H, α - CH_2 -Bu), 1.72-1.61 (m, 12H, β - CH_2 -Bu), 1.47-1.38 (m, 12H, γ - CH_2 -Bu), 0.99-0.93 (m, 18H, CH_3 -Bu) ppm.

^{13}C NMR (125 MHz, $CDCl_3$): δ = 140.86, 140.83, 140.12, 136.06, 135.91, 135.89, 135.32, 135.03, 134.98, 134.89, 134.74, 132.50, 132.38, 132.34, 130.11, 130.03, 129.34, 129.31, 126.71, 124.19, 123.82, 123.66, 93.45, 93.43, 61.74, 32.74, 32.51, 29.25, 29.24, 29.02, 22.66, 22.63, 13.97 ppm.

MS (MALDI-TOF) m/z : calcd. for $[M]^+$ ($C_{90}H_{92}O_{12}S_{12}$): 1748.3; found: 1749.4 $[M+H]^+$.

HRMS (MALDI-TOF) m/z : calcd. for $[M]^+$ ($C_{90}H_{92}O_{12}S_{12}$): 1748.32318; found: 1748.32239, $\delta_{m/m}$ = 0.6 ppm.

2,7-Bis(5-bromo-3-butylthien-2-yl)-benzo[2,1-*b*:3,4-*b'*]dithiophene-4,5-dione (72)


Dibrominated quaterthiophene **54** (40.0 mg, 53.9 μ mol) was dissolved in 1.2 mL THF and 0.3 mL of a conc. HCl solution was added. The mixture was heated under reflux for 7 h. After cooling to room temperature, it was quenched with water and the product was extracted with DCM. The combined organic layers were dried over Na_2SO_4 and the solvent was removed under vacuum. Deprotected DTB **72** (35.3 mg, 53.9 μ mol, 100%) was obtained pure as a green solid.

Mp: 164 – 165 °C.

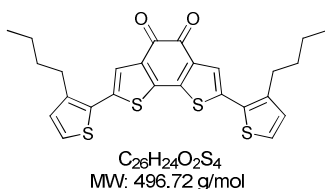
¹H NMR (400 MHz, CDCl₃): δ = 7.39 (s, 2H, DTB-3,6), 6.94 (s, 2H, Th-4,4'), 2.71 (t, ³J = 7.7 Hz, 4H, α-CH₂-Bu), 1.65-1.57 (m, 4H, β-CH₂-Bu), 1.44-1.34 (m, 4H, γ-CH₂-Bu), 0.94 (t, ³J = 7.3 Hz, 6H, CH₃-Bu) ppm.

¹³C NMR (100 MHz, CDCl₃): δ = 174.15, 142.61, 142.41, 135.82, 135.44, 132.98, 129.41, 125.66, 112.73, 32.51, 29.03, 22.47, 13.87 ppm.

MS (MALDI-TOF) *m/z*: calcd. for [M]⁺ (C₂₆H₂₂Br₂O₂S₄): 651.9; found: 651.6 [M]⁺.

HRMS (MALDI-TOF) *m/z*: calcd. for [M]⁺ (C₂₆H₂₂Br₂O₂S₄): 651.88639; found: 651.88718, δ_{m/m} = 1.2 ppm.

2,7-Bis(3-butylthien-2-yl)benzo[2,1-*b*:3,4-*b'*]dithiophene-4,5-dione (**71**)



DTB-containing quaterthiophene **53** (40.0 mg, 68.4 μmol) was dissolved in a solvent mixture of DCM (1 mL) and THF (0.5 mL). The solution was degassed and 0.8 mL of tetrafluoroboric acid (50% in diethyl ether), 0.4 mL of water and 0.2 mL of acetone were added. The mixture was intensely stirred overnight at room temperature, diluted with DCM and washed with water. The organic phase was dried over Na₂SO₄ and the solvent was evaporated. Purification of the crude product was performed via silica column chromatography with DCM as eluent and **71** (15.0 mg, 30.2 μmol, 44%) was obtained as a petroleum-colored solid.

Mp: 129 – 130 °C.

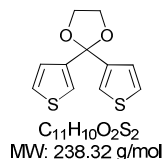
¹H NMR (400 MHz, CDCl₃): δ = 7.45 (s, 2H, DTB-3,6), 7.27 (d, ³J = 5.1 Hz, 2H, Th-5,5'), 6.98 (d, ³J = 5.1 Hz, 2H, Th-4,4'), 2.78 (t, ³J = 7.8 Hz, 4H, α-CH₂-Bu), 1.68-1.62 (m, 4H, β-CH₂-Bu), 1.45-1.37 (m, 4H, γ-CH₂-Bu), 0.95 (t, ³J = 7.4 Hz, 6H, CH₃-Bu) ppm.

¹³C NMR (100 MHz, CDCl₃): δ = 174.42, 142.62, 141.70, 137.19, 135.36, 130.33, 128.16, 125.49, 125.19, 32.67, 29.08, 22.57, 13.93 ppm.

MS (MALDI-TOF) *m/z*: calcd. for [M]⁺ (C₂₆H₂₄O₂S₄): 496.1; found: 496.2 [M]⁺.

HRMS (MALDI-TOF) *m/z*: calcd. for [M]⁺ (C₂₆H₂₄O₂S₄): 496.06536; found: 496.06610, δ_{m/m} = 1.5 ppm.

Synthesis and characterization of DCP-containing compounds

2,2-Bis(thien-3-yl)-1,3-dioxolane (57)^[17]


1,2-Bis(trimethylsilyloxy)ethane (16.5 mL, 67.4 mmol) and trimethylsilyl trifluoromethanesulfonate (3.19 mL, 17.6 mmol) were successively added to a cooled and stirred solution of bis(thien-3-yl)methanone **56** (5.70 g, 29.3 mmol) in 30 mL of DCM at 0 °C. The mixture was allowed to warm up to room temperature and stirred over the weekend. It was subsequently quenched by the addition of dry pyridine (6 mL), poured into a sat. NaHCO₃ solution and the product was extracted with Et₂O. The combined organic layers were dried over a 1:1-mixture of Na₂CO₃ and Na₂SO₄ and the solvent was evaporated. The crude product was purified by silica gel column chromatography eluting with a mixture of *n*-hexane:DCM (1:1) and dried under high vacuum. 2,2-Bis(thien-3-yl)-1,3-dioxolane **57** (5.99 g, 25.1 mmol, 86%) was obtained as colorless crystals.

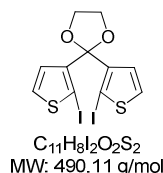
Mp: 114 – 115 °C.

¹H NMR (400 MHz, CDCl₃): δ = 7.32 (dd, ³*J* = 3.0 Hz, ⁴*J* = 1.2 Hz, 2H, Th-2,2'), 7.28 (dd, ³*J* = 5.0 Hz, 3.1 Hz, 2H, Th-5,5'), 7.11 (dd, ³*J* = 5.0 Hz, ⁴*J* = 1.2 Hz, 2H, Th-4,4'), 4.10 (s, 4H, O-CH₂) ppm.

¹³C NMR (100 MHz, CDCl₃): δ = 143.51, 126.29, 125.99, 123.05, 106.02, 65.05 ppm.

MS (EI) *m/z*: calcd. for [M]⁺ (C₁₁H₁₀O₂S₂): 238; found: 238 [M]⁺.

Elemental analysis: calcd. for (C₁₁H₁₀O₂S₂): C, 55.44; H, 4.23; S, 26.91%; found: C, 55.66; H, 4.17; S, 27.03%.

2,2-Bis(2-iodothien-3-yl)-1,3-dioxolane (58)^[19]


To a solution of 2,2-bis(thien-3-yl)-1,3-dioxolane **57** (5.73 g, 24.0 mmol) in dry diethyl ether (140 mL) was added dropwise *n*-butyl lithium (2.5 M in *n*-hexane, 20.7 mL, 51.7 mmol) at -28 °C. The reaction mixture was stirred for 1 h during which time it was allowed to warm up to -10 °C and a pale yellow suspension was formed. The cooling bath was removed and the reaction mixture was allowed to warm up to room temperature and was stirred for additional 1.5 h. After cooling to -20 °C, a solution

of iodine (14.0 g, 55.3 mmol) in dry diethyl ether (170 mL) was added dropwise. The resulting mixture was allowed to warm up to room temperature and was stirred overnight. It was subsequently quenched with a sat. aqueous $\text{Na}_2\text{S}_2\text{O}_3$ solution. The layers were separated and the product was extracted from the aqueous layer with Et_2O . The combined organic layers were washed with water, dried over Na_2SO_4 and the solvent was evaporated to afford a pale brown crystalline solid. Purification was carried out via silica column chromatography eluting with a mixture of *n*-hexane:DCM (1:1) to yield a colorless solid of dioxolane **58** (9.00 g, 18.4 mmol, 76%).

Mp: 125 – 126 °C.

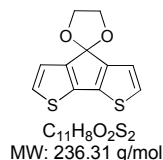
^1H NMR (400 MHz, CDCl_3): δ = 7.36 (d, 3J = 5.6 Hz, 2H, Th-5,5'), 6.98 (d, 3J = 5.6 Hz, 2H, Th-4,4'), 4.12 (s, 4H, O- CH_2) ppm.

^{13}C NMR (100 MHz, CDCl_3): δ = 144.17, 130.52, 129.27, 106.26, 73.34, 65.11 ppm.

MS (EI) m/z : calcd. for $[\text{M}]^+$ ($\text{C}_{11}\text{H}_8\text{I}_2\text{O}_2\text{S}_2$): 489; found: 490 $[\text{M}+\text{H}]^+$, 363 $[\text{M}-\text{I}]^+$.

Elemental analysis: calcd. for ($\text{C}_{11}\text{H}_8\text{I}_2\text{O}_2\text{S}_2$): C, 26.96; H, 1.65; S, 13.08%; found: C, 27.06; H, 1.70; S, 13.17%.

4,4-Ethylenedioxy-4*H*-cyclopenta[2,1-*b*:3,4-*b'*]dithiophene (**59**)^[20]



To a stirred solution of **58** (8.80 g, 17.9 mmol) in DMF (200 mL), copper powder (3.42 g, 53.9 mmol) was added at room temperature in one portion and the reaction mixture was heated under reflux overnight. After cooling down to ambient temperature, the solid was filtered off and washed with diethyl ether. The filtrate was washed thoroughly with brine and the organic layer was dried over Na_2SO_4 , filtered off and evaporation of the solvent followed. Purification via column chromatography using silica and a mixture of *n*-hexane:EE (4:1) afforded DCP **59** (3.87 g, 16.4 mmol, 91%) as a colorless solid.

Mp: 142 – 143 °C.

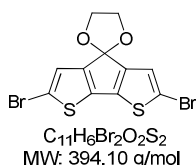
^1H NMR (400 MHz, CDCl_3): δ = 7.11 (d, 3J = 4.8 Hz, 2H, DCP-2,6), 6.96 (d, 3J = 4.8 Hz, 2H, DCP-3,5), 4.31 (s, 4H, O- CH_2) ppm.

^{13}C NMR (100 MHz, CDCl_3): δ = 150.13, 139.04, 126.19, 121.47, 107.28, 65.16 ppm.

MS (EI) m/z : calcd. for $[\text{M}]^+$ ($\text{C}_{11}\text{H}_8\text{O}_2\text{S}_2$): 235; found: 236 $[\text{M}+\text{H}]^+$.

Elemental analysis: calcd. for ($C_{11}H_8O_2S_2$): C, 55.91; H, 3.41; S, 27.14%; found: C, 56.16; H, 3.47; S, 26.95%.

2,6-Dibromo-4,4-ethylenedioxy-4*H*-cyclopenta[2,1-*b*:3,4-*b'*]dithiophene (**60**)



DCP **59** (3.90 g, 16.5 mmol) was dissolved in chloroform (230 mL), cooled to 0 °C and pyridine (4.00 mL, 49.5 mmol) was added. A solution of bromine (1.94 mL, 37.9 mmol), diluted 1:20 (vol.) in chloroform, was slowly added. After complete addition the reaction mixture was stirred for further 6 h at room temperature. The mixture was subsequently diluted with a sat. aqueous $Na_2S_2O_3$ solution and the organic layer was separated. The organic phase was washed with a sat. aqueous $NaHCO_3$ solution, dried over Na_2SO_4 and concentrated in vacuum. Purification was performed via silica column chromatography starting with a mixture of *n*-hexane:EE (4:1) as eluent which was gradually switched to pure EE to obtain dibrominated DCP **60** (5.84 g, 14.8 mmol, 90%) as a yellow solid.

Mp: 183 – 184 °C.

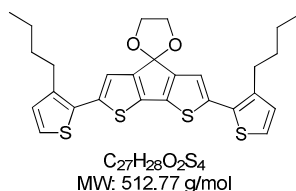
1H NMR (400 MHz, $CDCl_3$): δ = 6.96 (s, 2H, DCP-3,5), 4.26 (s, 4H, O-CH₂) ppm.

^{13}C NMR (100 MHz, $CDCl_3$): δ = 148.20, 138.59, 124.54, 112.82, 107.67, 65.43 ppm.

MS (CI) m/z : calcd. for $[M]^+$ ($C_{11}H_8Br_2O_2S_2$): 394; found: 394 $[M]^+$.

Elemental analysis: calcd. for ($C_{11}H_8Br_2O_2S_2$): C, 33.52; H, 1.53; S, 16.27%; found: C, 33.67; H, 1.64; S, 16.44%.

2,6-Bis(3-butylthien-2-yl)-4,4-ethylenedioxy-4*H*-cyclopenta[2,1-*b*:3,4-*b'*]dithiophene (**61**)



Dibrominated DCP **60** (960 mg, 2.44 mmol) and 3-butyl-2-(trimethyltin)thiophene **52** (1.77 g, 5.85 mmol) were dissolved in 50 mL of dry DMF, degassed and tetrakis(triphenylphosphine)palladium(0) (140 mg, 121 μ mol) was added. The reaction mixture was heated for 26 h at 80 °C. After cooling to room temperature the mixture was poured onto water and the product was extracted with DCM.

The combined organic layers were dried over Na_2SO_4 and the solvent was evaporated. The residue was purified by silica column chromatography eluting with a mixture of *n*-hexane:EE (4:1) to obtain an orange oil of **61** (1.08 g, 2.11 mmol, 86%) which crystallized in the cold.

Mp: 77 – 78 °C.

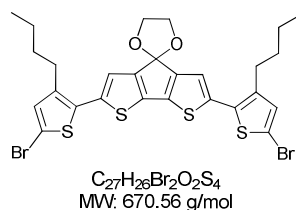
^1H NMR (400 MHz, CDCl_3): δ = 7.17 (d, 3J = 5.3 Hz, 2H, Th-5,5'), 6.98 (s, 2H, DCP-3,5), 6.93 (d, 3J = 5.3 Hz, 2H, Th-4,4'), 4.34 (s, 4H, O- CH_2), 2.76 (t, 3J = 7.8 Hz, 4H, α - CH_2 -Bu), 1.67-1.59 (m, 4H, β - CH_2 -Bu), 1.45-1.35 (m, 4H, γ - CH_2 -Bu), 0.94 (t, 3J = 7.3 Hz, 6H, CH_3 -Bu) ppm.

^{13}C NMR (100 MHz, CDCl_3): δ = 149.31, 139.50, 138.40, 137.44, 130.32, 129.62, 123.55, 120.13, 107.55, 64.98, 32.55, 28.63, 22.28, 13.63 ppm.

MS (MALDI-TOF) m/z : calcd. for $[\text{M}]^+$ ($\text{C}_{27}\text{H}_{28}\text{O}_2\text{S}_4$): 512.1; found: 512.3 $[\text{M}]^+$.

HRMS (MALDI-TOF): m/z : calcd. for $[\text{M}]^+$ ($\text{C}_{27}\text{H}_{28}\text{O}_2\text{S}_4$): 512.09666; found: 512.09641, $\delta_{m/m}$ = 0.5 ppm.

2,6-Bis(5-bromo-3-butylthien-2-yl)-4,4-ethylenedioxy-4H-cyclopenta[2,1-*b*:3,4-*b'*]dithiophene (**62**)



DCP-containing quaterthiophene **61** (5.79 g, 11.3 mmol) was dissolved in chloroform (250 mL), cooled to 0 °C and pyridine (2.73 mL, 33.8 mmol) was added. A solution of bromine (1.33 mL, 25.9 mmol), diluted 1:20 (vol.) in chloroform, was added within 60 min. After complete addition the mixture was stirred at room temperature for 4 h. The solution was subsequently diluted with a sat. aqueous $\text{Na}_2\text{S}_2\text{O}_3$ solution and the organic layer was separated. The organic phase was washed with a sat. NaHCO_3 solution, dried over Na_2SO_4 and concentrated in vacuum. The resulting oil was purified by silica column chromatography eluting with a mixture of *n*-hexane:EE (9:1) affording **62** (5.81 g, 8.67 mmol, 77%) as a yellow solid.

Mp: 121 – 122 °C.

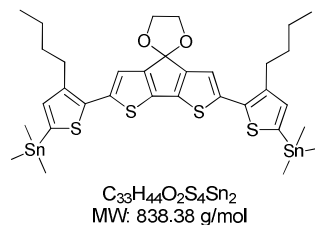
^1H NMR (400 MHz, CDCl_3): δ = 6.92 (s, 2H, DCP-3,5), 6.89 (s, 2H, Th-4,4'), 4.33 (s, 4H, O- CH_2), 2.69 (t, 3J = 7.8 Hz, 4H, α - CH_2 -Bu), 1.62-1.55 (m, 4H, β - CH_2 -Bu), 1.42-1.33 (m, 4H, γ - CH_2 -Bu), 0.93 (t, 3J = 7.3 Hz, 6H, CH_3 -Bu) ppm.

^{13}C NMR (100 MHz, CDCl_3): δ = 149.82, 140.58, 139.05, 136.49, 132.64, 131.98, 120.85, 110.71, 107.73, 65.42, 32.77, 28.92, 22.55, 13.98 ppm.

MS (MALDI-TOF) m/z : calcd. for $[\text{M}]^+$ ($\text{C}_{27}\text{H}_{26}\text{Br}_2\text{O}_2\text{S}_4$): 667.9; found: 668.0 $[\text{M}]^+$.

Elemental analysis: calcd. for (C₂₇H₂₆Br₂O₂S₄): C, 48.36; H, 3.91; S, 19.13%; found: C, 48.08; H, 3.71; S, 18.89%.

2,6-Bis(3-butyl-5-trimethylstannylthien-2-yl)-4,4-ethylenedioxy-4H-cyclopenta[2,1-*b*:3,4-*b'*]dithiophene (63)

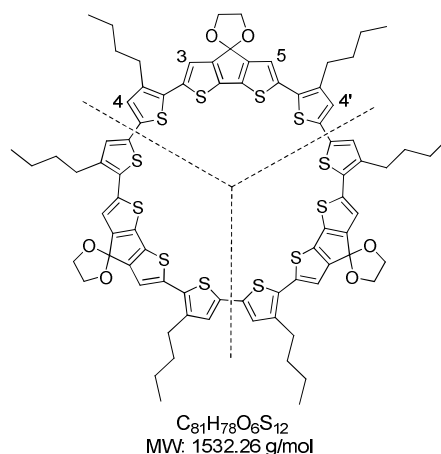


n-Butyl lithium (1.6 M in *n*-hexane, 0.66 mL, 1.05 mmol) was added dropwise to a solution of **62** (300 mg, 0.45 mmol) in dry THF (8 mL) at -78 °C within 20 min. After stirring between -75 and -65 °C for 65 min, Me₃SnCl (223 mg, 1.12 mmol) in dry THF (1 mL) was added at once. The reaction mixture was allowed to warm up to room temperature overnight. *n*-Hexane was added and lithium chloride precipitated as white solid. The separated organic phase was washed several times with water and dried over Na₂SO₄. The crude product was used without further purification in the next step. The conversion of distannylated quaterthiophene **63** (95%) was determined via ¹H NMR spectroscopy.

¹H NMR (400 MHz, CDCl₃): δ = 6.99 (s, 2H, Th-4,4'), 6.97 (s, 2H, DCP-3,5), 4.33 (s, 4H, O-CH₂), 2.78 (t, ³*J* = 7.9 Hz, 4H, α -CH₂-Bu), 1.67-1.60 (m, 4H, β -CH₂-Bu), 1.46-1.37 (m, 4H, γ -CH₂-Bu), 0.95 (t, ³*J* = 7.3 Hz, 6H, CH₃-Bu), 0.38 (s, 18H, TMSn) ppm.

MS (MALDI-TOF) *m/z*: calcd. for [M]⁺ (C₃₃H₃₄O₂S₄Sn₂): 840.0; found: 840.1 [M]⁺, 675 [M-TMSn]⁺.

C[12]DCP (70)



Distannylated quaterthiophene **63** (383 mg, 0.46 mmol) and $\text{PtCl}_2(\text{COD})$ (171 mg, 0.46 mmol) were dissolved in DCM (520 mL) and heated under reflux for 6 days. The mixture was cooled to room temperature and filtered through an alox IV column eluting with DCM. The solvent was evaporated and an orange-red solid (300 mg) was obtained.

50 mg of the crude product (containing 61.4 μmol of $\text{Pt}(\text{COD})\text{DCP}$ -units) and 1,1'-bis(diphenylphosphino)ferrocene (37.0 mg, 67.5 μmol) were dissolved in DCM (10 mL) at room temperature. The reaction mixture was stirred overnight. The solvent was subsequently evaporated and 1,5-cyclooctadiene was removed under high vacuum. The afforded solid was dissolved at rt in dry THF (12 mL) and silver triflate (36.0 mg, 139 μmol , 2.10 eq. per Pt) was added. The mixture was stirred overnight at room temperature. Afterwards, the organic suspension was diluted with DCM and washed successively with brine and water. The organic layer was dried over MgSO_4 and filtered through a short column packed with alox IV to remove precipitated platinum and silver. The solvent was evaporated to give a deep red residue and isolation as well as purification of DCP-macrocycle **70** (4.00 mg, 2.60 μmol , 10%) by SEC (THF) followed to give a black solid.

Mp: Decomposition at 250 °C.

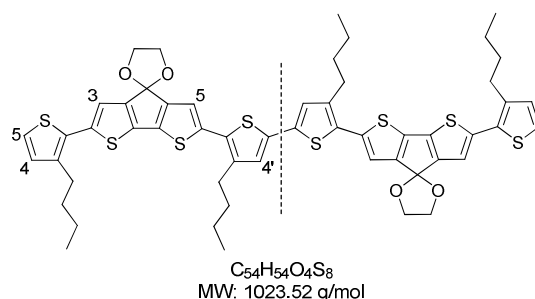
^1H NMR (400 MHz, CDCl_3): δ = 7.00 (s, 6H, DCP-3,5), 6.88 (s, 6H, Th-4,4'), 4.34 (s, 12H, O- CH_2), 2.73 (t, 3J = 7.7 Hz, 12H, α - CH_2 -Bu), 1.71-1.64 (m, 12H, β - CH_2 -Bu), 1.48-1.39 (m, 12H, γ - CH_2 -Bu), 0.97 (t, 3J = 7.3 Hz, 18H, CH_3 -Bu) ppm.

MS (MALDI-TOF) m/z : calcd. for $[\text{M}]^+$ ($\text{C}_{81}\text{H}_{78}\text{O}_6\text{S}_{12}$): 1530.2; found: 1531.0 $[\text{M}+\text{H}]^+$.

HRMS (MALDI-TOF) m/z : calcd. for $[\text{M}]^+$ ($\text{C}_{81}\text{H}_{78}\text{O}_6\text{S}_{12}$): 1530.24414; found: 1530.24226, $\delta_{m/m}$ = 1.3 ppm.

^{13}C -NMR could not be measured due to poor solubility.

L[8]DCP (80)



DCP-containing quaterthiophene **61** (300 mg, 0.59 mmol) was dissolved in 5 mL of dry THF, cooled to -78 °C and *n*-butyl lithium (1.6 M in *n*-hexane, 0.55 mL, 0.88 mmol) was added dropwise over a period of 15 min. The reaction mixture was stirred between -78 and -65 °C for 1.5 h and copper(II) chloride (118 mg, 0.88 mmol) was added in several portions under vigorous stirring. The mixture

turned dark brown and some black solid deposited. After complete addition, stirring was continued for 1 hour at -70 °C. The reaction mixture was allowed to warm up to -10 °C overnight and was then stirred for an additional hour at room temperature. Hydrolysis was subsequently performed under ice cooling with a 2 N HCl solution whereas the solid dissolved. After extraction with DCM the combined organic layers were washed with water, dried over Na₂SO₄ and the solvent was removed under reduced pressure. The oligomer was purified by silica column chromatography using *n*-hexane:EE (4:1) as eluent to afford a dark solid of **80** (30.0 mg, 29.3 μ mol, 10%).

Mp: 216 – 218 °C.

¹H NMR (400 MHz, CDCl₃): δ = 7.17 (d, ³*J* = 5.2 Hz, 2H, Th-5), 7.01 (s, 2H, DCP-3), 6.99 (s, 4H, DCP-5, Th-4'), 6.93 (d, ³*J* = 5.1 Hz, 2H, Th-4), 4.35 (s, 8H, O-CH₂), 2.79-2.73 (m, 8H, α -CH₂-*Bu*), 1.70-1.59 (m, 8H, β -CH₂-*Bu*), 1.48-1.36 (m, 8H, γ -CH₂-*Bu*), 0.98-0.92 (m, 12H, CH₃-*Bu*) ppm.

¹³C NMR (125 MHz, CDCl₃): δ = 149.69, 140.38, 139.86, 138.80, 137.89, 134.72, 130.58, 129.97, 126.45, 123.85, 121.08, 120.82, 120.35, 120.16, 119.67, 119.48, 107.76, 65.34, 32.87, 32.65, 29.20, 28.97, 22.65, 22.61, 13.98 ppm.

MS (MALDI-TOF) *m/z*: calcd. for [M]⁺ (C₅₄H₅₄O₄S₈): 1022.2; found: 1022.7 [M]⁺.

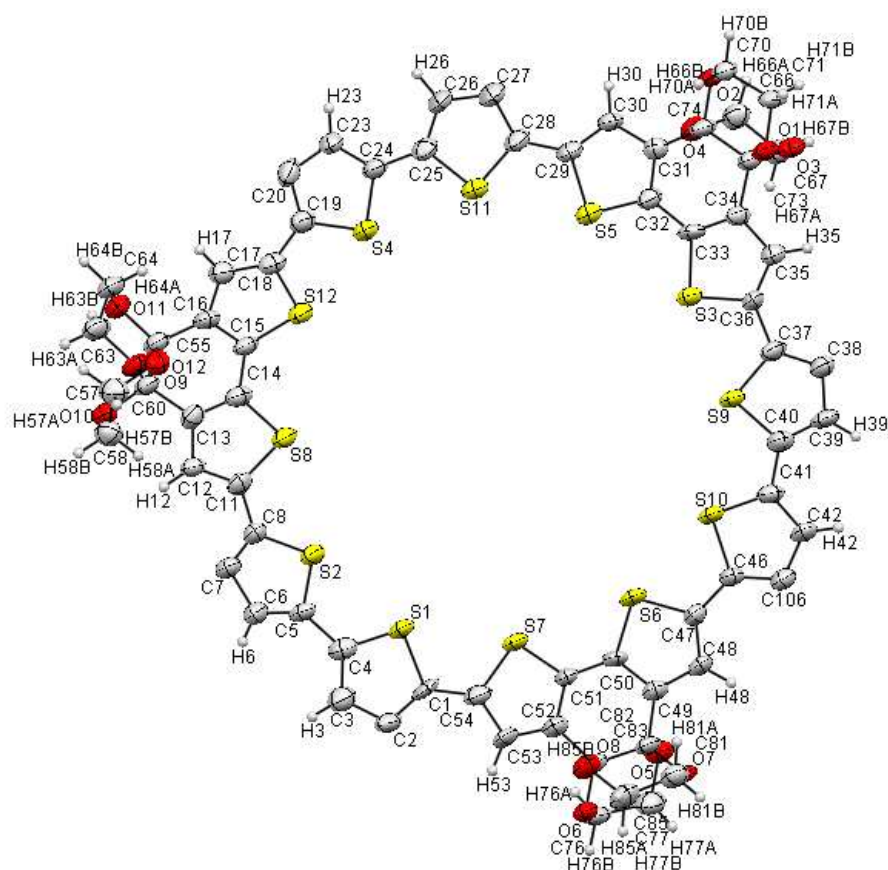
HRMS (MALDI-TOF) *m/z*: calcd. for [M]⁺ (C₅₄H₅₄O₄S₈): 1022.17724; found: 1022.17823, $\delta_{m/m}$ = 0.9 ppm.

3.13 Notes

[N1] X-ray structure analysis of macrocycle **67a**.

Table N1.1: Crystallographic and structural determination data for macrocycle **67a**.

formula	C ₉₀ H ₉₀ O ₁₂ S ₁₂
formula weight	1748.45
crystal system	triclinic
space group	P-1
a [Å]	15.3129(9)
b [Å]	16.9118(9)
c [Å]	17.5573(8)
α [°]	84.213(3)
β [°]	88.404(3)
γ [°]	66.308(3)
Z	2
R-factor	8.4
d [Å] ^{a)}	12.2 – 12.9

Table N1.2: Atomic coordinates of macrocycle **67a**.

number	label	x	y	z
1	S1	1.22039(14)	-0.14199(12)	0.20865(9)
2	S2	1.24206(13)	-0.06945(12)	0.36017(9)
3	S3	0.35370(13)	0.31768(12)	0.20892(9)
4	S4	0.71995(13)	0.32207(13)	0.59123(10)
5	S5	0.38085(14)	0.40011(12)	0.37903(10)
6	S6	0.84791(14)	-0.04426(13)	0.00129(9)
7	S7	1.07830(14)	-0.13449(13)	0.08471(10)
8	S8	1.12627(13)	0.02961(12)	0.50392(10)
9	S9	0.43847(13)	0.18399(13)	0.08612(10)
10	S10	0.62611(14)	0.05789(13)	0.00016(9)
11	S11	0.50857(14)	0.39448(12)	0.51828(10)
12	S12	0.93140(14)	0.17848(12)	0.59648(10)
13	O11	1.1678(4)	0.2201(3)	0.7554(3)
14	O2	0.0416(3)	0.4522(3)	0.4288(2)
15	O7	1.0045(3)	-0.1424(3)	-0.2427(2)
16	O12	1.2420(4)	0.0456(3)	0.7294(2)
17	O10	1.3318(3)	0.1093(3)	0.6671(3)
18	O3	0.0320(4)	0.3550(3)	0.3006(3)
19	O6	1.1971(4)	-0.2212(4)	-0.1715(3)
20	O1	0.0496(3)	0.4812(3)	0.2700(2)
21	O4	0.1504(4)	0.3133(3)	0.4303(3)
22	O8	1.1174(4)	-0.0769(4)	-0.1686(3)

23	O5	1.0300(4)	-0.2511(3)	-0.1476(3)
24	O9	1.1727(4)	0.2631(3)	0.6293(3)
25	C55	1.1613(5)	0.1984(5)	0.6802(4)
26	C60	1.2403(5)	0.1070(5)	0.6688(4)
27	C11	1.2500(5)	-0.0184(4)	0.5021(4)
28	C29	0.3274(5)	0.4336(4)	0.4665(4)
29	C46	0.6803(5)	0.0038(4)	-0.0796(4)
30	C74	0.1220(5)	0.3964(4)	0.3906(4)
31	C16	1.0637(5)	0.2029(4)	0.6637(4)
32	C50	0.9549(5)	-0.0995(5)	-0.0419(4)
33	C34	0.1847(5)	0.3554(4)	0.2578(4)
34	C25	0.5272(5)	0.4140(4)	0.6097(4)
35	C18	0.8978(5)	0.2620(4)	0.6561(4)
36	C47	0.7826(5)	-0.0404(5)	-0.0799(4)
37	C49	0.9391(5)	-0.1129(5)	-0.1156(4)
38	C14	1.1299(5)	0.0890(4)	0.5771(4)
39	C28	0.3858(5)	0.4399(5)	0.5266(4)
40	C42	0.5183(5)	0.0630(5)	-0.1095(4)
41	H42	0,4631	0,0764	-0,1401
42	C31	0.2088(5)	0.4163(4)	0.3985(4)
43	C8	1.2986(5)	-0.0811(4)	0.4468(4)
44	C73	0.0965(5)	0.3956(5)	0.3050(4)
45	C20	0.7500(6)	0.3636(5)	0.7219(4)
46	C5	1.3386(5)	-0.1542(4)	0.3268(4)
47	C70	0.0009(5)	0.5387(4)	0.3910(4)
48	H70A	0,0489	0,5644	0,3878
49	H70B	-0,0542	0,5756	0,4201
50	C83	1.1170(6)	-0.1577(5)	-0.1399(4)
51	C2	1.3648(5)	-0.2367(5)	0.1336(4)
52	C58	1.3376(6)	0.1756(5)	0.6123(4)
53	H58A	1,3252	0,1645	0,5602
54	H58B	1,4026	0,1748	0,6136
55	C32	0.2796(5)	0.3937(4)	0.3462(4)
56	C38	0.2694(5)	0.2283(5)	0.0296(4)
57	C7	1.3871(5)	-0.1476(5)	0.4511(4)
58	C15	1.0499(5)	0.1523(4)	0.6131(4)
59	C48	0.8428(5)	-0.0803(5)	-0.1367(4)
60	H48	0,8211	-0,0852	-0,1855
61	C53	1.2136(6)	-0.1886(5)	-0.0124(4)
62	H53	1,2747	-0,2116	-0,035
63	C82	1.0233(5)	-0.1641(5)	-0.1624(4)
64	C41	0.5144(5)	0.0917(5)	-0.0391(4)
65	C37	0.3163(5)	0.2399(5)	0.0909(4)
66	C64	1.1655(6)	0.1546(5)	0.8138(4)
67	H64A	1,1051	0,147	0,8097
68	H64B	1,1689	0,1728	0,8651
69	C52	1.1281(5)	-0.1627(5)	-0.0537(4)
70	C23	0.6506(5)	0.4022(5)	0.7074(4)
71	H23	0,6064	0,437	0,7421
72	C33	0.2676(5)	0.3608(5)	0.2763(4)

73	C106	0.6111(5)	0.0119(5)	-0.1330(4)
74	C51	1.0480(5)	-0.1300(5)	-0.0095(4)
75	C4	1.3307(5)	-0.1798(5)	0.2511(4)
76	C66	0.0841(6)	0.2748(5)	0.4240(4)
77	H66A	0,0231	0,3099	0,4477
78	H66B	0,1093	0,2159	0,4516
79	C40	0.4294(5)	0.1464(5)	0.0006(4)
80	C17	0.9771(5)	0.2652(5)	0.6881(4)
81	H17	0,9739	0,3054	0,7233
82	C13	1.2203(5)	0.0707(5)	0.5991(4)
83	C81	1.0049(6)	-0.0597(5)	-0.2684(4)
84	H81A	0,9532	-0,0139	-0,2432
85	H81B	0,9928	-0,0478	-0,3244
86	C12	1.2898(5)	0.0107(4)	0.5556(4)
87	H12	1,3566	-0,0074	0,5628
88	C6	1.4098(5)	-0.1880(5)	0.3812(4)
89	H6	1,4692	-0,2343	0,3733
90	C26	0.4426(6)	0.4546(5)	0.6437(4)
91	H26	0,4385	0,4723	0,6938
92	C35	0.1893(5)	0.3144(4)	0.1906(4)
93	H35	0,1373	0,3053	0,171
94	C3	1.3999(6)	-0.2283(5)	0.2042(4)
95	H3	1,4657	-0,254	0,2179
96	C19	0.7976(5)	0.3157(5)	0.6630(4)
97	C63	1.2485(6)	0.0704(5)	0.8041(4)
98	H63A	1,3091	0,0774	0,8097
99	H63B	1,2472	0,025	0,8438
100	C39	0.3362(6)	0.1751(5)	-0.0214(4)
101	H39	0,3172	0,1607	-0,0673
102	C1	1.2670(6)	-0.1916(5)	0.1265(4)
103	C77	1.1132(6)	-0.3138(5)	-0.1824(5)
104	H77A	1,1086	-0,302	-0,2388
105	H77B	1,1169	-0,3733	-0,1686
106	C67	0.0671(6)	0.2694(5)	0.3400(4)
107	H67A	0,1275	0,2321	0,3168
108	H67B	0,0201	0,2435	0,3355
109	C24	0.6237(5)	0.3859(4)	0.6405(4)
110	C76	1.2007(6)	-0.3059(6)	-0.1533(4)
111	H76A	1,2058	-0,32	-0,097
112	H76B	1,2581	-0,3482	-0,1762
113	C71	-0.0305(5)	0.5339(5)	0.3126(4)
114	H71A	-0,079	0,5089	0,3162
115	H71B	-0,0599	0,5931	0,2857
116	C36	0.2762(5)	0.2895(5)	0.1570(4)
117	C27	0.3605(6)	0.4690(6)	0.5996(5)
118	C85	1.0978(6)	-0.0578(6)	-0.2505(4)
119	H85A	1,149	-0,1011	-0,2783
120	H85B	1,0967	3E-4	-0,2675
121	C57	1.2665(6)	0.2618(5)	0.6300(5)
122	H57A	1,2808	0,2742	0,6811

123	H57B	1,2702	0,3074	0,5916
124	C30	0.2349(5)	0.4407(5)	0.4662(4)
125	H30	0,1926	0,4602	0,5074
126	C54	1.2001(6)	-0.1774(5)	0.0653(4)

Table N1.3: Bond angles in macrocycle **67a**.

The butyl side chains were omitted for clarity. Nevertheless, all atoms are listed in the table below. Thus, some of the listed bond angles cannot be found in the depicted figure.

number	start label	middle label	end label	angle [°]
1	C4	S1	C1	92.1(4)
2	C8	S2	C5	92.0(3)
3	C33	S3	C36	91.6(4)
4	C19	S4	C24	91.8(4)
5	C29	S5	C32	91.9(3)
6	C50	S6	C47	92.2(4)
7	C51	S7	C54	92.4(4)
8	C11	S8	C14	90.9(3)
9	C37	S9	C40	92.2(4)
10	C46	S10	C41	92.4(4)
11	C25	S11	C28	93.1(4)
12	C18	S12	C15	91.7(3)
13	C55	O11	C64	112.5(6)
14	C74	O2	C70	112.8(5)
15	C82	O7	C81	112.3(5)
16	C60	O12	C63	114.6(6)
17	C60	O10	C58	112.8(6)
18	C73	O3	C67	112.5(6)
19	C83	O6	C76	112.2(6)
20	C73	O1	C71	113.2(5)
21	C74	O4	C66	113.7(6)
22	C83	O8	C85	112.6(6)
23	C82	O5	C77	112.7(6)
24	C55	O9	C57	113.9(6)
25	O11	C55	O9	106.7(6)
26	O11	C55	C60	110.1(6)
27	O11	C55	C16	111.4(6)
28	O9	C55	C60	111.2(6)
29	O9	C55	C16	105.8(6)
30	C60	C55	C16	111.5(6)
31	O12	C60	O10	106.7(6)
32	O12	C60	C55	111.2(6)
33	O12	C60	C13	103.6(6)
34	O10	C60	C55	110.8(6)
35	O10	C60	C13	112.4(6)
36	C55	C60	C13	111.8(6)
37	S8	C11	C8	120.2(5)
38	S8	C11	C12	111.6(5)
39	C8	C11	C12	128.2(7)
40	S5	C29	C28	118.5(5)
41	S5	C29	C30	109.8(5)

42	C28	C29	C30	131.3(7)
43	S10	C46	C47	118.7(5)
44	S10	C46	C106	109.9(5)
45	C47	C46	C106	131.4(7)
46	O2	C74	O4	106.9(5)
47	O2	C74	C31	112.9(6)
48	O2	C74	C73	110.6(6)
49	O4	C74	C31	102.5(6)
50	O4	C74	C73	111.1(6)
51	C31	C74	C73	112.4(6)
52	C45	C44	C106	114.5(6)
53	C55	C16	C15	121.5(7)
54	C55	C16	C17	125.5(7)
55	C15	C16	C17	112.4(7)
56	S6	C50	C49	110.2(6)
57	S6	C50	C51	127.6(6)
58	C49	C50	C51	122.2(7)
59	C73	C34	C33	120.4(7)
60	C73	C34	C35	125.5(6)
61	C33	C34	C35	114.0(7)
62	S11	C25	C26	110.0(6)
63	S11	C25	C24	120.7(5)
64	C26	C25	C24	129.2(7)
65	S12	C18	C17	110.3(5)
66	S12	C18	C19	118.6(5)
67	C17	C18	C19	131.1(7)
68	S6	C47	C46	119.1(6)
69	S6	C47	C48	110.3(6)
70	C46	C47	C48	130.5(7)
71	C50	C49	C48	114.0(7)
72	C50	C49	C82	118.9(7)
73	C48	C49	C82	127.0(7)
74	S8	C14	C15	127.3(6)
75	S8	C14	C13	111.8(6)
76	C15	C14	C13	120.9(7)
77	S11	C28	C29	119.3(6)
78	S11	C28	C27	110.2(6)
79	C29	C28	C27	130.1(7)
80	H42	C42	C41	122.7(8)
81	H42	C42	C106	122.9(8)
82	C41	C42	C106	114.4(7)
83	C74	C31	C32	121.2(6)
84	C74	C31	C30	124.2(6)
85	C32	C31	C30	113.2(7)
86	S2	C8	C11	117.9(5)
87	S2	C8	C7	112.3(6)
88	C11	C8	C7	129.7(7)
89	O3	C73	O1	106.3(6)
90	O3	C73	C74	110.3(6)
91	O3	C73	C34	112.6(6)

92	O1	C73	C74	110.6(6)
93	O1	C73	C34	104.9(6)
94	C74	C73	C34	111.9(6)
95	C23	C20	C19	110.9(7)
96	C23	C20	C21	126.2(8)
97	C19	C20	C21	122.9(8)
98	S2	C5	C4	118.2(5)
99	S2	C5	C6	110.3(5)
100	C4	C5	C6	131.4(7)
101	C9	C10	C89	113.2(7)
102	O2	C70	H70A	110.1(6)
103	O2	C70	H70B	110.1(6)
104	O2	C70	C71	108.2(6)
105	H70A	C70	H70B	108.4(7)
106	H70A	C70	C71	110.1(6)
107	H70B	C70	C71	110.1(6)
108	O6	C83	O8	106.0(6)
109	O6	C83	C82	111.6(6)
110	O6	C83	C52	111.0(7)
111	O8	C83	C82	110.8(6)
112	O8	C83	C52	105.5(6)
113	C82	C83	C52	111.7(7)
114	C3	C2	C1	112.1(7)
115	C3	C2	C75	124.9(7)
116	C1	C2	C75	123.0(7)
117	C44	C45	C86	112.8(7)
118	O10	C58	H58A	109.7(7)
119	O10	C58	H58B	109.6(7)
120	O10	C58	C57	109.9(7)
121	H58A	C58	H58B	108.2(8)
122	H58A	C58	C57	109.7(7)
123	H58B	C58	C57	109.7(7)
124	S5	C32	C31	111.8(5)
125	S5	C32	C33	127.5(6)
126	C31	C32	C33	120.4(7)
127	C37	C38	C39	110.4(7)
128	C37	C38	C95	126.3(7)
129	C39	C38	C95	123.2(7)
130	C8	C7	C9	124.3(7)
131	C8	C7	C6	111.1(7)
132	C9	C7	C6	124.6(7)
133	S12	C15	C16	112.1(5)
134	S12	C15	C14	127.0(6)
135	C16	C15	C14	120.8(7)
136	C47	C48	C49	113.2(7)
137	C47	C48	H48	123.3(8)
138	C49	C48	H48	123.4(8)
139	H53	C53	C52	123.4(8)
140	H53	C53	C54	123.3(8)
141	C52	C53	C54	113.3(7)

142	O7	C82	O5	105.3(6)
143	O7	C82	C49	112.1(6)
144	O7	C82	C83	111.0(6)
145	O5	C82	C49	103.4(6)
146	O5	C82	C83	111.1(6)
147	C49	C82	C83	113.4(6)
148	S10	C41	C42	111.1(6)
149	S10	C41	C40	121.4(6)
150	C42	C41	C40	127.5(7)
151	S9	C37	C38	111.9(6)
152	S9	C37	C36	118.9(6)
153	C38	C37	C36	129.1(7)
154	O11	C64	H64A	109.8(7)
155	O11	C64	H64B	109.9(7)
156	O11	C64	C63	109.4(6)
157	H64A	C64	H64B	108.3(8)
158	H64A	C64	C63	109.8(7)
159	H64B	C64	C63	109.7(7)
160	C83	C52	C53	126.6(7)
161	C83	C52	C51	119.4(7)
162	C53	C52	C51	113.5(7)
163	C20	C23	H23	122.7(8)
164	C20	C23	C24	114.5(7)
165	H23	C23	C24	122.8(8)
166	C10	C9	C7	111.1(6)
167	S3	C33	C34	110.8(6)
168	S3	C33	C32	126.8(6)
169	C34	C33	C32	122.3(7)
170	C46	C106	C44	122.9(7)
171	C46	C106	C42	112.2(7)
172	C44	C106	C42	124.8(7)
173	S7	C51	C50	127.5(6)
174	S7	C51	C52	111.1(6)
175	C50	C51	C52	121.3(7)
176	S1	C4	C5	118.5(6)
177	S1	C4	C3	111.3(6)
178	C5	C4	C3	130.2(7)
179	O4	C66	H66A	109.7(7)
180	O4	C66	H66B	109.6(7)
181	O4	C66	C67	109.8(6)
182	H66A	C66	H66B	108.1(8)
183	H66A	C66	C67	109.7(7)
184	H66B	C66	C67	109.8(7)
185	S9	C40	C41	121.2(6)
186	S9	C40	C39	110.5(6)
187	C41	C40	C39	128.3(7)
188	C16	C17	C18	113.5(7)
189	C16	C17	H17	123.2(7)
190	C18	C17	H17	123.3(8)
191	C60	C13	C14	120.8(7)

192	C60	C13	C12	125.4(7)
193	C14	C13	C12	113.6(7)
194	O7	C81	H81A	109.6(7)
195	O7	C81	H81B	109.6(7)
196	O7	C81	C85	110.4(7)
197	H81A	C81	H81B	108.0(8)
198	H81A	C81	C85	109.7(7)
199	H81B	C81	C85	109.6(7)
200	C11	C12	C13	112.1(7)
201	C11	C12	H12	124.0(7)
202	C13	C12	H12	123.9(7)
203	C5	C6	C7	114.3(7)
204	C5	C6	H6	123.0(8)
205	C7	C6	H6	122.8(8)
206	C25	C26	H26	122.2(8)
207	C25	C26	C27	115.6(8)
208	H26	C26	C27	122.2(8)
209	C34	C35	H35	123.6(7)
210	C34	C35	C36	112.8(7)
211	H35	C35	C36	123.6(7)
212	C2	C3	C4	113.8(7)
213	C2	C3	H3	123.1(8)
214	C4	C3	H3	123.2(8)
215	S4	C19	C18	119.0(6)
216	S4	C19	C20	111.4(6)
217	C18	C19	C20	129.6(7)
218	O12	C63	C64	108.6(6)
219	O12	C63	H63A	110.0(7)
220	O12	C63	H63B	110.0(7)
221	C64	C63	H63A	109.9(7)
222	C64	C63	H63B	109.9(7)
223	H63A	C63	H63B	108.4(8)
224	C38	C39	C40	115.0(7)
225	C38	C39	H39	122.5(8)
226	C40	C39	H39	122.5(8)
227	S1	C1	C2	110.7(6)
228	S1	C1	C54	116.4(6)
229	C2	C1	C54	132.9(8)
230	O5	C77	H77A	110.1(7)
231	O5	C77	H77B	110.1(7)
232	O5	C77	C76	108.1(7)
233	H77A	C77	H77B	108.4(8)
234	H77A	C77	C76	110.1(8)
235	H77B	C77	C76	110.1(8)
236	O3	C67	C66	109.1(6)
237	O3	C67	H67A	109.8(7)
238	O3	C67	H67B	109.9(7)
239	C66	C67	H67A	109.8(7)
240	C66	C67	H67B	109.9(7)
241	H67A	C67	H67B	108.3(8)

242	S4	C24	C25	120.6(5)
243	S4	C24	C23	111.3(6)
244	C25	C24	C23	128.1(7)
245	O6	C76	C77	111.4(7)
246	O6	C76	H76A	109.3(8)
247	O6	C76	H76B	109.4(8)
248	C77	C76	H76A	109.3(8)
249	C77	C76	H76B	109.4(8)
250	H76A	C76	H76B	108.0(8)
251	O1	C71	C70	110.1(6)
252	O1	C71	H71A	109.7(6)
253	O1	C71	H71B	109.6(6)
254	C70	C71	H71A	109.7(7)
255	C70	C71	H71B	109.6(7)
256	H71A	C71	H71B	108.2(7)
257	S3	C36	C37	116.9(6)
258	S3	C36	C35	110.7(6)
259	C37	C36	C35	132.3(7)
260	C28	C27	C26	111.0(8)
261	C28	C27	C91	126.7(8)
262	C26	C27	C91	122.1(8)
263	O8	C85	C81	110.2(7)
264	O8	C85	H85A	109.6(7)
265	O8	C85	H85B	109.5(7)
266	C81	C85	H85A	109.7(8)
267	C81	C85	H85B	109.7(8)
268	H85A	C85	H85B	108.1(8)
269	O9	C57	C58	110.1(7)
270	O9	C57	H57A	109.6(7)
271	O9	C57	H57B	109.7(7)
272	C58	C57	H57A	109.7(8)
273	C58	C57	H57B	109.7(8)
274	H57A	C57	H57B	108.1(8)
275	C2	C75	C88A	110(1)
276	C2	C75	C88B	113(1)
277	C88A	C75	C88B	27(1)
278	C29	C30	C31	113.4(7)
279	C29	C30	H30	123.2(8)
280	C31	C30	H30	123.4(7)
281	C22B	C22A	C21	76(2)
282	C22B	C22A	C107	59(1)
283	C21	C22A	C107	120(2)
284	C22A	C22B	C21	47(1)
285	C22A	C22B	C107	75(1)
286	C21	C22B	C107	111(1)
287	C20	C21	C22A	134(2)
288	C20	C21	C22B	114.9(9)
289	C22A	C21	C22B	57(1)
290	S7	C54	C53	109.7(6)
291	S7	C54	C1	118.9(6)

292	C53	C54	C1	131.4(8)
293	C10	C89	C90	110.6(7)
294	C45	C86	C87	114.0(7)
295	C38	C95	C96	111.5(8)
296	C92	C93	C94	109.6(8)
297	C93	C92	C91	112.0(8)
298	C27	C91	C92	112.8(8)
299	C95	C96	C97A	116(2)
300	C95	C96	C97B	104(1)
301	C97A	C96	C97B	29(2)
302	C96	C97A	C97B	61(3)
303	C96	C97A	C98A	138(3)
304	C96	C97A	C98B	100(2)
305	C97B	C97A	C98A	104(4)
306	C97B	C97A	C98B	87(3)
307	C98A	C97A	C98B	38(2)
308	C96	C97B	C97A	90(3)
309	C96	C97B	C98B	102(2)
310	C97A	C97B	C98B	65(3)
311	C75	C88A	C88B	64(3)
312	C75	C88A	C1A	96(2)
313	C75	C88A	C1B	95(2)
314	C88B	C88A	C1A	61(3)
315	C88B	C88A	C1B	33(3)
316	C1A	C88A	C1B	66(2)
317	C75	C88B	C88A	89(3)
318	C75	C88B	C1A	114(2)
319	C75	C88B	C1B	141(3)
320	C88A	C88B	C1A	94(3)
321	C88A	C88B	C1B	123(4)
322	C1A	C88B	C1B	87(3)
323	C97A	C98A	C98B	77(4)
324	C97A	C98B	C97B	28(2)
325	C97A	C98B	C98A	65(3)
326	C97B	C98B	C98A	80(3)
327	C22A	C107	C22B	46(1)
328	C22A	C107	C99B	109(2)
329	C22A	C107	C105	147(2)
330	C22B	C107	C99B	122(2)
331	C22B	C107	C105	105(1)
332	C99B	C107	C105	100(2)
333	C88A	C1A	C88B	25(1)
334	C88A	C1B	C88B	23(2)

Table N1.4: Bond lengths in macrocycle **67a**.

The butyl side chains were omitted for clarity. Nevertheless, all atoms are listed in the table below. Thus, some of the listed bond lengths cannot be found in the depicted figure.

number	start label	end label	length [Å]
1	S1	C4	1.710(7)
2	S1	C1	1.732(7)
3	S2	C8	1.726(8)
4	S2	C5	1.732(6)
5	S3	C33	1.727(7)
6	S3	C36	1.752(9)
7	S4	C19	1.722(8)
8	S4	C24	1.710(7)
9	S5	C29	1.756(7)
10	S5	C32	1.716(9)
11	S6	C50	1.725(7)
12	S6	C47	1.745(8)
13	S7	C51	1.716(7)
14	S7	C54	1.746(9)
15	S8	C11	1.737(7)
16	S8	C14	1.724(8)
17	S9	C37	1.728(7)
18	S9	C40	1.718(8)
19	S10	C46	1.752(7)
20	S10	C41	1.711(8)
21	S11	C25	1.725(8)
22	S11	C28	1.730(7)
23	S12	C18	1.743(7)
24	S12	C15	1.712(8)
25	O11	C55	1.422(9)
26	O11	C64	1.44(1)
27	O2	C74	1.416(7)
28	O2	C70	1.436(7)
29	O7	C82	1.428(8)
30	O7	C81	1.43(1)
31	O12	C60	1.403(9)
32	O12	C63	1.434(9)
33	O10	C60	1.42(1)
34	O10	C58	1.43(1)
35	O3	C73	1.42(1)
36	O3	C67	1.434(9)
37	O6	C83	1.410(9)
38	O6	C76	1.41(1)
39	O1	C73	1.414(8)
40	O1	C71	1.436(8)
41	O4	C74	1.406(8)
42	O4	C66	1.42(1)
43	O8	C83	1.41(1)
44	O8	C85	1.454(9)
45	O5	C82	1.43(1)
46	O5	C77	1.457(9)

47	O9	C55	1.40(1)
48	O9	C57	1.43(1)
49	C55	C60	1.562(9)
50	C55	C16	1.50(1)
51	C60	C13	1.51(1)
52	C11	C8	1.468(9)
53	C11	C12	1.36(1)
54	C29	C28	1.44(1)
55	C29	C30	1.37(1)
56	C46	C47	1.44(1)
57	C46	C106	1.39(1)
58	C74	C31	1.51(1)
59	C74	C73	1.57(1)
60	C44	C45	1.54(1)
61	C44	C106	1.51(1)
62	C16	C15	1.37(1)
63	C16	C17	1.410(9)
64	C50	C49	1.38(1)
65	C50	C51	1.42(1)
66	C34	C73	1.51(1)
67	C34	C33	1.36(1)
68	C34	C35	1.41(1)
69	C25	C26	1.35(1)
70	C25	C24	1.46(1)
71	C18	C17	1.37(1)
72	C18	C19	1.444(9)
73	C47	C48	1.37(1)
74	C49	C48	1.40(1)
75	C49	C82	1.508(9)
76	C14	C15	1.444(9)
77	C14	C13	1.35(1)
78	C28	C27	1.41(1)
79	C42	H42	0.949(8)
80	C42	C41	1.36(1)
81	C42	C106	1.410(9)
82	C31	C32	1.36(1)
83	C31	C30	1.41(1)
84	C8	C7	1.368(8)
85	C20	C23	1.41(1)
86	C20	C19	1.38(1)
87	C20	C21	1.50(1)
88	C5	C4	1.46(1)
89	C5	C6	1.37(1)
90	C10	C9	1.57(1)
91	C10	C89	1.52(1)
92	C70	H70A	0.991(9)
93	C70	H70B	0.990(6)
94	C70	C71	1.49(1)
95	C83	C82	1.55(1)
96	C83	C52	1.52(1)

97	C2	C3	1.41(1)
98	C2	C1	1.38(1)
99	C2	C75	1.52(1)
100	C45	C86	1.55(1)
101	C58	H58A	0.990(8)
102	C58	H58B	0.99(1)
103	C58	C57	1.48(1)
104	C32	C33	1.44(1)
105	C38	C37	1.38(1)
106	C38	C39	1.42(1)
107	C38	C95	1.51(1)
108	C7	C9	1.50(1)
109	C7	C6	1.43(1)
110	C48	H48	0.951(8)
111	C53	H53	0.950(8)
112	C53	C52	1.40(1)
113	C53	C54	1.39(1)
114	C41	C40	1.465(9)
115	C37	C36	1.47(1)
116	C64	H64A	0.99(1)
117	C64	H64B	0.990(8)
118	C64	C63	1.50(1)
119	C52	C51	1.38(1)
120	C23	H23	0.951(7)
121	C23	C24	1.34(1)
122	C4	C3	1.36(1)
123	C66	H66A	0.990(7)
124	C66	H66B	0.990(7)
125	C66	C67	1.52(1)
126	C40	C39	1.36(1)
127	C17	H17	0.950(8)
128	C13	C12	1.410(9)
129	C81	H81A	0.990(7)
130	C81	H81B	0.991(7)
131	C81	C85	1.48(1)
132	C12	H12	0.951(7)
133	C6	H6	0.950(6)
134	C26	H26	0.950(7)
135	C26	C27	1.42(1)
136	C35	H35	0.949(8)
137	C35	C36	1.36(1)
138	C3	H3	0.950(8)
139	C63	H63A	0.99(1)
140	C63	H63B	0.990(8)
141	C39	H39	0.950(8)
142	C1	C54	1.44(1)
143	C77	H77A	0.989(9)
144	C77	H77B	0.990(9)
145	C77	C76	1.51(1)
146	C67	H67A	0.991(7)

147	C67	H67B	0.99(1)
148	C76	H76A	0.991(7)
149	C76	H76B	0.989(8)
150	C71	H71A	0.989(9)
151	C71	H71B	0.991(7)
152	C27	C91	1.51(1)
153	C85	H85A	0.989(8)
154	C85	H85B	0.99(1)
155	C57	H57A	0.991(9)
156	C57	H57B	0.990(9)
157	C75	C88A	1.65(3)
158	C75	C88B	1.49(2)
159	C30	H30	0.950(7)
160	C22A	C22B	1.30(3)
161	C22A	C21	1.15(3)
162	C22A	C107	1.76(3)
163	C22B	C21	1.52(2)
164	C22B	C107	1.56(2)
165	C89	C90	1.56(1)
166	C87	C86	1.54(1)
167	C95	C96	1.51(2)
168	C93	C92	1.53(2)
169	C93	C94	1.60(1)
170	C92	C91	1.52(1)
171	C96	C97A	1.68(4)
172	C96	C97B	1.47(2)
173	C97A	C97B	0.81(5)
174	C97A	C98A	1.45(5)
175	C97A	C98B	1.56(4)
176	C97B	C98B	1.72(3)
177	C88A	C88B	0.75(4)
178	C88A	C1A	1.77(4)
179	C88A	C1B	1.57(6)
180	C88B	C1A	1.56(3)
181	C88B	C1B	1.03(5)
182	C98A	C98B	0.99(5)
183	C107	C99B	1.32(2)
184	C107	C105	1.62(3)

Table N1.5: Torsion angles of macrocycle **67a**.

number	start label	middle label	middle label	end label	torsion [°]
1	S3	C36	C37	S9	20.3(9)
2	S9	C40	C41	S10	4(1)
3	S10	C46	C47	S6	4.0(9)
4	S6	C50	C51	S7	11(1)
5	S7	C54	C1	S1	-14.4(9)
6	S1	C4	C5	S2	-13.9(8)
7	S2	C8	C11	S8	30.0(8)
8	S8	C14	C15	S12	5(1)
9	S12	C18	C19	S4	-22.2(8)
10	S4	C24	C25	S11	-7.7(9)
11	S11	C28	C29	S5	-12.8(9)
12	S5	C32	C33	S3	1(1)

Table N1.6: Diameter of macrocycle **67a**.

number	start label	end label	distance [Å]
1	S3	S2	12.724(3)
2	S1	S5	12.921(3)
3	S11	S7	12.704(3)
4	S9	S8	12.243(3)
5	S10	S12	12.261(3)
6	S4	S6	12.311(3)

3.14 References

- [1] H. Ohnishi, M. Kozaki, K. Okada, *Synth. Met.* **2003**, *135-136*, 85-86.
- [2] F. A. Arroyave, C. A. Richard, J. R. Reynolds, *Org. Lett.* **2012**, *14*, 6138-6141.
- [3] J. Z. Brzezinski, J. R. Reynolds, *Synthesis* **2002**, *8*, 1053-1258.
- [4] Y. A. Getmanenko, C. Risko, P. Tongwa, E.-G. Kim, H. Li, B. Sandhu, T. Timofeeva, J.-L. Brédas, S. R. Marder, *J. Org. Chem.* **2011**, *76*, 2660-2671.
- [5] J. A. Letizia, S. Cronin, R. P. Ortiz, A. Facchetti, M. A. Ratner, T. J. Marks, *Chem. Eur. J.* **2010**, *16*, 1911-1928.
- [6] P. Espinet, A. M. Echavarren, *Angew. Chem.* **2004**, *116*, 4808-4839; *Angew. Chem. Int. Ed.* **2004**, *43*, 4704-4734.
- [7] T. N. Mitchell, *Synthesis* **1992**, *9*, 803-815.
- [8] J. K. Stille, *Angew. Chem.* **1986**, *98*, 504-519; *Angew. Chem. Int. Ed.* **1986**, *25*, 508-524.
- [9] M. C. Gallazzi, F. Toscano, D. Paganuzzi, C. Bertarelli, A. Farina, G. Zotti, *Macromol. Chem. Phys.* **2001**, *202*, 2074-2085.
- [10] R. Rieger, *PhD Thesis, University of Mainz, Germany* **2009**.
- [11] D. Enders, T. Balensiefer, *Acc. Chem. Res.* **2004**, *37*, 534-541.
- [12] R. Mondal, H. A. Becerril, E. Verploegen, D. Kim, J. E. Norton, S. Ko, N. Miyaki, S. Lee, M. F. Toney, J.-L. Bredas, M. D. McGehee, Z. Bao, *J. Mater. Chem.* **2010**, *20*, 5823-5834.
- [13] Y. A. Getmanenko, P. Tongwa, T. V. Timofeeva, S. R. Marder, *Org. Lett.* **2010**, *12*, 2136-2139.

- [14] Y. Zhang, J. Zou, H.-L. Yip, K.-S. Chen, J. A. Davies, Y. Sun, A. K. Y. Jen, *Macromolecules* **2011**, *44*, 4752-4758.
- [15] T. H. Chan, M. A. Brook, T. Chaly, *Synthesis* **1983**, 203-205.
- [16] M. Kozaki, K. Sugimura, H. Ohnishi, K. Okada, *Org. Lett.* **2006**, *8*, 5235-5238.
- [17] P. Lucas, N. El Mehdi, H. A. Ho, D. Bélager, L. Breau, *Synthesis* **2000**, *9*, 1253-1258.
- [18] R. Beyer, M. Kalaji, G. Kingscote-Burton, P. J. Murphy, V. M. S. C. Pereira, D. M. Taylor, G. O. Willians, *Synth. Met.* **1998**, *92*, 25-29.
- [19] P. Jordens, G. Rawson, H. Wynberg, *J. Chem. Soc. (C)* **1970**, 273-277.
- [20] B. Pal, W.-C. Yen, J.-S. Yang, C.-Y. Chao, Y.-C. Hung, S.-T. Lin, C.-H. Chuang, C.-W. Chen, W.-F. Su, *Macromolecules* **2008**, *41*, 6664-6671.
- [21] G. Fuhrmann, *PhD Thesis, University of Ulm, Germany* **2006**.
- [22] F. Zhang, P. Bäuerle, *J. Am. Chem. Soc.* **2007**, *129*, 3090-3091.
- [23] A. Meyer, E. Sigmund, F. Luppertz, G. Schnakenburg, I. Gadaczek, T. Bredow, S.-S. Jester, S. Höger, *Beilstein J. Org. Chem.* **2010**, *6*, 1180-1187.
- [24] L. Boymond, M. Rottländer, G. Cahiez, P. Knochel, *Angew. Chem.* **1998**, *110*, 1801-1803; *Angew. Chem. Int. Ed.* **1998**, *37*, 1701-1703.
- [25] X.-j. Wang, X. Sun, L. Zhang, Y. Xu, D. Krishnamurthy, C. H. Senanayake, *Org. Lett.* **2006**, *8*, 305-307.
- [26] E. Mena-Osteritz, F. Zhang, G. Götz, P. Reineker, P. Bäuerle, *Beilstein J. Nanotechnol.* **2011**, *2*, 720-726.
- [27] F. Zhang, G. Götz, H. D. F. Winkler, Christoph A. Schalley, P. Bäuerle, *Angew. Chem.* **2009**, *121*, 6758-6762; *Angew. Chem. Int. Ed.* **2009**, *48*, 6632-6635.
- [28] M. Bednarz, P. Reineker, E. Mena-Osteritz, P. Bäuerle, *J. Lumin.* **2004**, *110*, 225-231.
- [29] S. S. Zade, M. Bendikov, *J. Org. Chem.* **2006**, *71*, 2972-2981.
- [30] M. Bednarz, J. Knoester, *J. Phys. Chem. B* **2001**, *105*, 12913-12923.
- [31] F. Zhang, *unpublished results*.
- [32] H. Jiang, W. Lin, *J. Am. Chem. Soc.* **2003**, *125*, 8084-8085.
- [33] L. Zhang, Y.-H. Niu, A. K. Y. Jen, W. Lin, *Chem. Commun.* **2005**, 1002-1004.
- [34] I. Stengel, *PhD Thesis, University of ulm* **2011**.
- [35] T. Sakai, T. Satou, T. Kaikawa, K. Takimiya, T. Otsubo, Y. Aso, *J. Am. Chem. Soc.* **2005**, *127*, 8082-8089.
- [36] J. A. E. H. van Haare, E. E. Havinga, J. L. J. van Dongen, R. A. J. Janssen, J. Cornil, J.-L. Brédas, *Chem. Eur. J.* **1998**, *4*, 1509-1521.
- [37] F. Zhang, G. Götz, E. Mena-Osteritz, M. Weil, B. Sarkar, W. Kaim, P. Bäuerle, *Chem. Sci.* **2011**, *2*, 781-784.
- [38] P. Bäuerle, U. Segelbacher, A. Maier, M. Mehring, *J. Am. Chem. Soc.* **1993**, *115*, 10217-10223.
- [39] J. Guay, P. Kasai, A. Diaz, R. Wu, J. M. Tour, L. H. Dao, *Chem. Mater.* **1992**, *4*.
- [40] J. Guay, A. Diaz, R. Wu, J. M. Tour, *J. Am. Chem. Soc.* **1993**, *115*, 1869-1874.
- [41] T. Nishinaga, A. Wakamiya, D. Yamazaki, K. Komatsu, *J. Am. Chem. Soc.* **2004**, *126*, 3163-3174.
- [42] M. Tateno, M. Takase, M. Iyoda, K. Komatsu, T. Nishinaga, *Chem. Eur. J.* **2013**, *19*, 5457-5467.
- [43] V. M. Geskin, J.-L. Brédas, *ChemPhysChem* **2003**, *4*, 498-504.
- [44] A. W. J. Tol, *Chem. Phys.* **1996**, *208*, 73-79.
- [45] Y. Gao, C.-G. Liu, Y.-S. Jiang, *J. Phys. Chem. A* **2002**, *106*, 5380-5384.
- [46] A. W. J. Tol, *Synth. Met.* **1995**, *74*, 95-98.
- [47] K. Fesser, A. R. Bishop, D. K. Campbell, *Phys. Rev. B* **1983**, *27*, 4804-4825.

- [48] J. Cornil, D. Beljonne, J. L. Brédas, *J. Chem. Phys.* **1995**, *103*, 842-849.
- [49] H. Plenio, *Angew. Chem.* **1997**, *109*, 358-360; *Angew. Chem. Int. Ed.* **1997**, *46*, 348-350.
- [50] R. Azumi, E. Mena-Osteritz, R. Boese, J. Benet-Buchholz, P. Bäuerle, *J. Mater. Chem.* **2006**, *16*, 728-735.
- [51] *Pd(PPh₃)₄ was prepared from PdCl₂ and PPh₃ in DMSO at 140 °C with addition of hydrazine*
- [52] J. X. McDermott, J. F. White, G. M. Whitesides, *J. Am. Chem. Soc.* **1976**, *98*, 6521-6528.
- [53] P. Kreitmeier, *Einführung in die präparativen Methoden in der Organischen Chemie, Ein Tutorium zum Organischen Praktikum als Hypertextsystem, Kapitel 9: Trocknung von Feststoffen, Lösungen und Lösemitteln, Universität Regensburg* **2001**.
- [54] A. B. Pangborn, M. A. Giardello, R. H. Grubbs, R. K. Rosen, F. J. Timmers, *Organometallics* **1996**, *15*, 1518-1520.
- [55] G. R. Fulmer, A. J. M. Miller, N. H. Sherden, H. E. Gottlieb, A. Nudelman, B. M. Stoltz, J. E. Bercaw, K. I. Goldberg, *Organometallics* **2010**, *29*, 2176-2179.

CHAPTER 4

Donor-Functionalized α -Conjugated Cyclo[n]thiophenes

4.1 Design of a donor-substituted oligothiienyl precursor

The elaborate molecular design concept to modify C[n]Ts and advance their photophysical properties focuses besides the introduction of acceptor core units (Chapter 3) on the incorporation of donor units into the cyclic backbone. The modification process to generate thiophene-based, donor-functionalized macrocycles is shown schematically in Chart 4.1. Thus, a dithienopyrrole-(DTP) containing oligomer 4T-DTP was chosen as precursor and several aspects, which will be explained in the following, were considered.

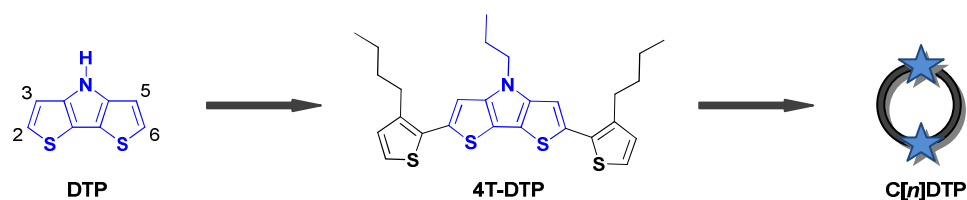


Chart 4.1: Structure of the fused DTP moiety with corresponding quaterthiophene unit 4T-DTP and prospective macrocycle series C[n]DTP.

The electron-donating DTP unit is supposed to influence the electronic properties of the ring and to cause different optoelectronic results in comparison to the acceptor- and non-functionalized cyclo[n]thiophenes **67a**, **70**, and **81**.

The DTP-unit possess a rigid and stiff structure and is meant to improve π -conjugation along the cyclic backbone and enhance π - π stacking of the molecules. The effective assembly into potential channels might enhance charge mobilities and is particularly interesting for the field of organic nanoelectronics. In literature, the DTP moiety has recently attracted particular interest as donor functionality for polymeric and oligomeric π -conjugated systems to gain high charge carrier mobilities. As the bridging electron donor amino group provides a planar inflexible structure, it usually improves hole-transport properties of the material in the bulk. DTP-containing materials were already applied in organic light emitting diodes, organic photovoltaic cells, and field effect transistors.^[1-12]

According to the DTB and DCP acceptor units, the donor moiety is elongated at both sides of the fused DTP core system with one additional thiophene unit. Hence, quaterthiophene precursor 4T-DTP provides a hemicyclic shape if adopting an all-*syn* conformation that should support the cyclization process itself and aid to form one preferred ring size. Inserted butyl side chains are supposed to direct the external thiophene units into this *syn*-conformation to gain the mentioned hemicyclic shape. They are also meant to provide sufficient solubility of the molecule. The geometry of the molecule was optimized via semiempirical calculations using the Austin Model 1 (AM1) with defined Hartree Fock-conditions to get more information about the inner angle of the bent monomer

unit. The value of the inner angle was determined by drawing manually straight lines through the molecule parallel to terminal CH-bonds as depicted in Chart 4.2 and yielded an angle of about 96°. Since the building block shows an axial-symmetry, highly symmetric macrocycles are expected.

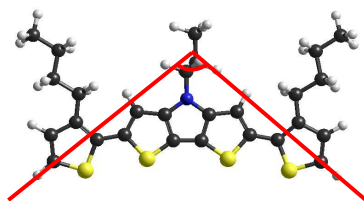


Chart 4.2: Calculated structure of 4T-DTP.

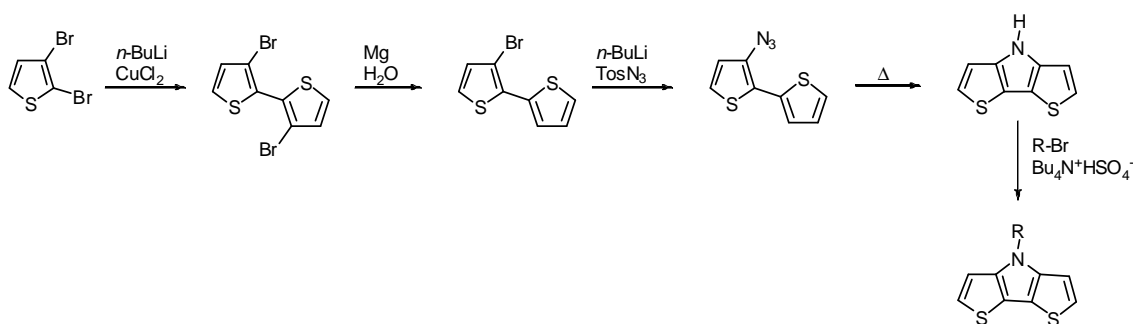
All synthetic steps towards desired DTP-containing precursor 4T-DTP as well as cyclization reactions are described and discussed in the following sections.

4.2 Synthesis of donor-substituted oligothieryl macrocycles

4.2.1. Synthesis of a donor-substituted oligothieryl precursor

4.2.1.1 General introduction of the synthesis of *N*-alkylated DTPs

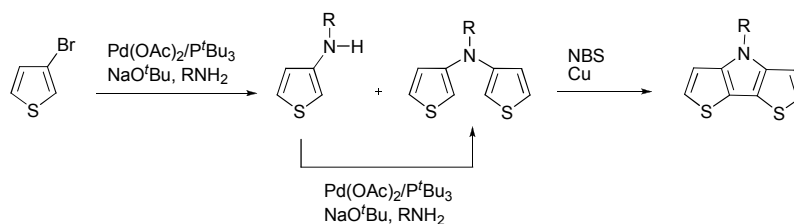
Three routes to prepare *N*-alkyl-DTPs have already been described in literature. A first approach was performed by Zanirato and co-workers in 1983^[13] and starts from 2,3-dibromothiophene (Scheme 4.1). Four reaction steps are necessary to gain the parent DTP-unit which is clearly a drawback of this elaborated method. The synthesis was extended by Zotti et al.^[14], who added a further alkylation step to generate desired *N*-alkyl DTPs.



Scheme 4.1: First route to *N*-functionalized DTPs by Zanirato and Zotti.^[13-14]

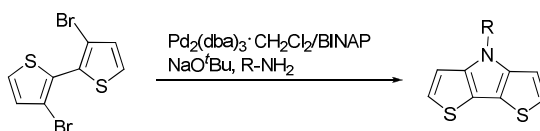
Rasmussen et al. developed a second approach which reduced the total number of reaction steps significantly and resulted additionally in an increase of the overall yield (Scheme 4.2).^[15] They synthesized secondary and tertiary aminothiophenes via a Buchwald-Hartwig reaction and treated primary amines with 3-bromothiophene. Thereby, a mixture of *N*-functionalized 3-aminothiophenes

and *N*-functionalized *N*-(3'-thienyl)-3-aminothiophenes was obtained. A second Buchwald-Hartwig coupling reaction had to be performed to convert incomplete reacted 3-aminothiophene into desired *N*-(3'-thienyl)-3-aminothiophene. Ring closure was performed by a one-pot two-step reaction consisting of bromination with NBS, followed by a Cu-mediated coupling to afford DTP products in an average yield of 70%.^[16] However, there exist still a few drawbacks. The secondary and tertiary aminothiophenes are rather unstable and scaling up of the reaction proved to be difficult due to a considerable decrease in yields. In addition, the whole reaction sequence has to be repeated from the beginning if one would like to introduce another *N*-alkyl substituent.



Scheme 4.2: Synthesis of *N*-alkylated DTPs via ring closure of aminothiophenes published by Rasmussen et al.^[15-16]

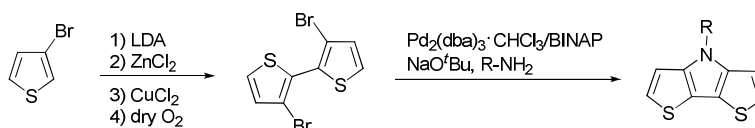
Koeckelberghs et al. reported a third approach for the synthesis of *N*-alkyl DTPs via a Buchwald-Hartwig reaction with 3,3'-dibromo-2,2'-bithiophene and various *n*-alkyl amines achieving yields up to 80% (Scheme 4.3).^[17-18] They were the first to prepare alkylated DTPs in high yields and on a large scale by testing different Pd-catalysts, ligands, and solvents. In addition to the efficiency, this synthetic route allows the introduction of a variety of different *N*-substituents by the simple selection of the primary amine. The most promising results were obtained with the dichloromethane adduct $\text{Pd}_2(\text{dba})_3 \cdot \text{CH}_2\text{Cl}_2$ and bidentate ligand BINAP as catalyst system. In the case of monodentate ligands such as $\text{P}(\text{tert-Bu})_3$, Koeckelberghs described β -hydride elimination in the catalytic cycle instead of reductive elimination. Buchwald^[19] and Hartwig^[20-21] showed that the observed β -hydride elimination could be suppressed by utilizing bidentate ligands such as BINAP or dppf.



Scheme 4.3: Efficient Pd-catalyzed amination of dibromobithiophene reported by Koeckelberghs et al.^[17-18]

In 2010, Evenson and Rasmussen^[1] published an optimized strategy for the efficient synthesis of *N*-alkylated DTPs by combining the presented method of Koeckelberghs et al.^[17-18] and a high yielding reaction towards 3,3'-dibromo-2,2'-bithiophene starting from inexpensive 3-bromothiophene (Scheme 4.4). The desired bithiophene was obtained in 85-90% yield by lithiation with LDA, transmetalation with ZnCl_2 and oxidatively induced homocoupling with CuCl_2 . The amination

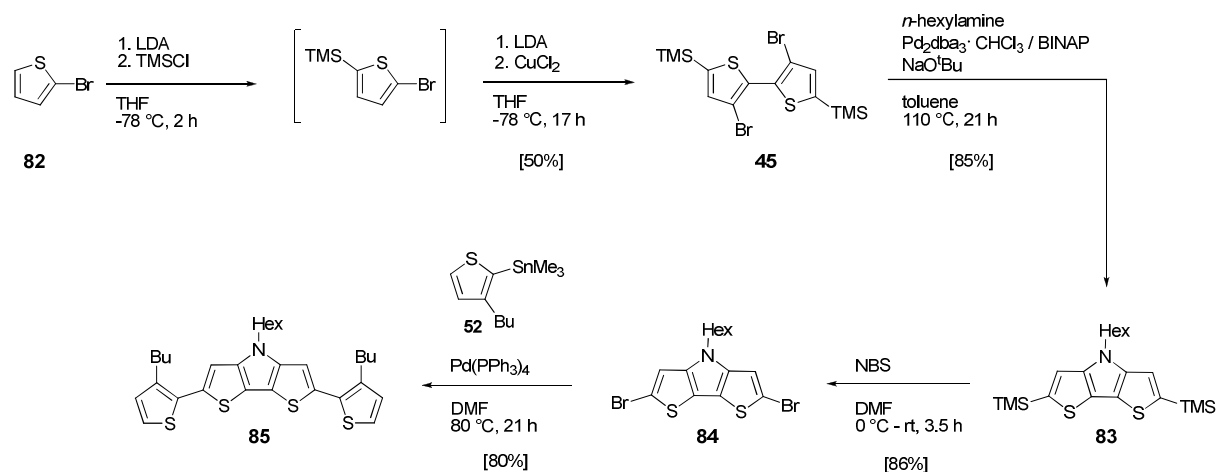
reaction was then performed via a Buchwald-Hartwig reaction with $\text{Pd}_2(\text{dba})_3 \cdot \text{CHCl}_3$ and BINAP. Thus, a prosperous and versatile method to produce *N*-alkylated DTPs in a good overall yield and only two reaction steps was elaborated.



Scheme 4.4: Effective synthesis of *N*-alkylated DTPs presented by Rasmussen et al.^[1]

4.2.1.2 Access to *N*-hexyl 4T-DTP (**85**)

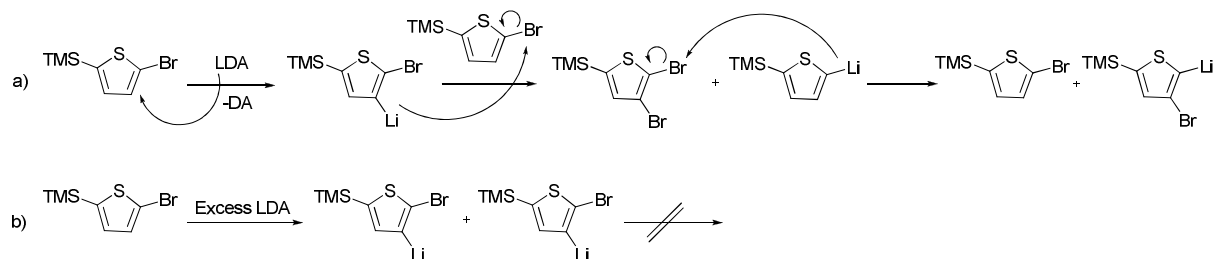
Commercially available 2-bromothiophene **82** was reacted after a protocol by Marder et al. with LDA and TMSCl to introduce a TMS-protecting group at the 5'-position.^[22] The 'base-catalyzed halogen dance reaction'^[23-28] was initialized by a second equivalent of LDA and bithiophene derivative **45** was subsequently formed via oxidatively induced C-C-coupling with copper(II)chloride (Scheme 4.5). Purification was carried out by filtration over silica gel and bithiophene **45** was obtained as a yellow solid in 50% yield. The analytical data were consistent with the literature but the yield was somewhat lower.^[22]



Scheme 4.5: Synthesis of DTP-oligothiophene precursor **85**.

In general, α -halogen aryl compounds are transformed into α -lithium- β -halogen aryl species via base-catalyzed halogen dance reactions and represent the reactive intermediates for an oxidatively induced coupling (Scheme 4.6). One of the crucial steps leading to the desired reactive intermediates is a slow addition of LDA. Thus, the simultaneous existence of already deprotonated and still protonated species is provided in which the molecules can undergo a successful halogen-exchange to generate the anion at the more stable 2'-position. If the base is added too fast, the halogen dance

reaction is inhibited since the deprotonated species exists in an excess and no halogen-exchange between the molecules can occur.



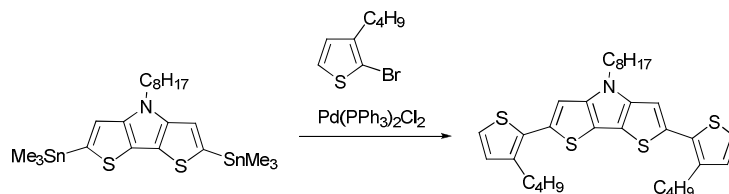
Scheme 4.6: a) Reaction mechanism for the base-catalyzed halogen dance reaction with slow addition of LDA.
b) No halogen dance reaction in the case of a fast addition of LDA.

The DTP core unit was synthesized via a palladium-catalyzed Buchwald-Hartwig cross-coupling reaction^[29-33] with primary *n*-hexylamine and bithiophene **45** (Scheme 4.5). The reaction was performed in degassed toluene at 110 °C for 21 h with the addition of NaO^tBu as organic base. After purification of the crude product using alox column chromatography, literature unknown DTP-derivative **83** was isolated in 85% yield. In literature, DTPs are often purified using silica column chromatography and were described to be stable under these purification method. However, when DTP **83** came into contact with silica gel decomposition could be observed through a ring opening of the pyrrole moiety which was observed via ¹H-NMR spectroscopy. In general, both TMS-protecting groups of **83** did not cleave off when stored under argon in the fridge.

The third reaction step included an *ipso*-substitution reaction of both α -trimethylsilyl groups into bromine atoms by reacting DTP **83** with NBS in DMF at 0 °C. After filtrating the crude material over aluminium oxide, dibrominated DTP **84** was obtained as a colorless solid in 86% yield and stored under argon in the fridge. The instability of *N*-alkyl substituted DTPs after a bromination reaction with NBS in chloroform/acetic acid is known in literature, in which no dibromo derivatives are described.^[34] Barlow et al. assumed that the presence of the CH₂ group next to the nitrogen in the *N*-alkyl derivatives plays a crucial role for the decomposition, but they did not give any further more detailed explanation for this problem.^[34] However, bromination reactions with NBS in DMF/chloroform are known to generate stable *N*-alkylated DTP core units in good yields.^[35-36]

Finally, a Stille cross-coupling reaction was performed under general Pd-catalyzed conditions with dibrominated DTP core unit **84** and 3-butyl-2-(trimethyltin)thiophene **52**. The reaction was carried out in DMF at 80 °C for 21 h and *N*-hexyl 4T-DTP **85** was isolated in 80% yield after column chromatography with aluminium oxide. In 2005, Rasmussen et al. published the synthesis of a *N*-octyl DTP-containing quaterthiophene analogue (Scheme 4.7).^[5, 37] The molecule was as well prepared via

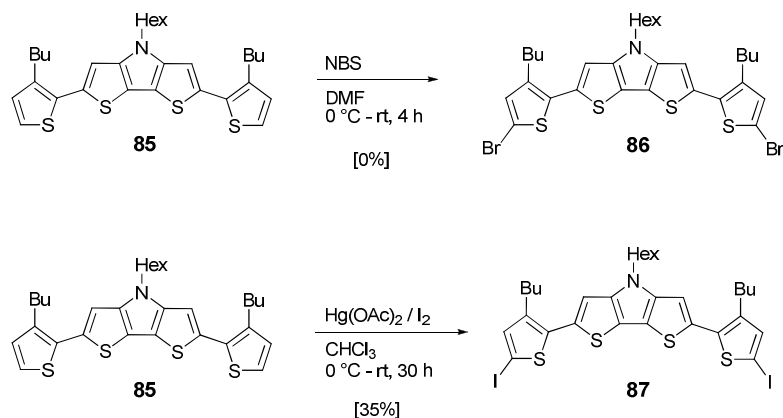
a Pd-catalyzed aryl-aryl coupling under standard Stille-conditions, but started from a distannylated DTP intermediate and the corresponding oligomer was obtained in 40-45% yield.



Scheme 4.7: Synthesis of a DTP-based oligothiophene via Stille cross-coupling by Rasmussen et al.

4.2.1.3 Attempts to halogenate 4T-DTP (**85**)

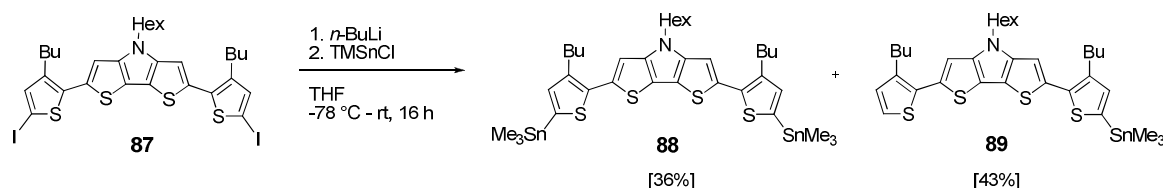
Several experiments were carried out to introduce halides into the free α -positions of 4T-DTP **85** in order to provide a clean metal-halogen exchange with *n*-BuLi in the following stannylation step. Thus, **85** was reacted with NBS in DMF/chloroform at 0 °C, whereby a dark suspension resulted after warming up to room temperature (Scheme 4.8). Neither starting material nor dibrominated target quaterthiophene **86** could be isolated. In a second attempt, elemental bromine in chloroform at 0 °C was used as reagent and the solution changed its color to dark blue. Also in this case, desired 4T-DTP **86** was not formed. Therefore, quaterthiophene **85** was transferred into a mercury intermediate by the addition of Hg(OAc)₂, which was consecutively reacted with elemental iodine. After purification via column chromatography on alox, target diiodooligothiophene **87** was obtained in 35% yield as a yellow oil.



Scheme 4.8: Synthetic reactions towards dibrominated and diiodinated oligothiophenes **86** and **87**.

4.2.1.4 Stannylation reaction of diiodinated 4T-DTP (**87**)

Oligothiophene **87** was treated with *n*-BuLi at -78 °C to generate a metal-halogen exchange to obtain a twofold lithiated species. The formed dianion was subsequently trapped with trimethyltin chloride to achieve distannylated DTP **88** (Scheme 4.9). ^1H NMR analysis exhibited the coexistence of three different derivatives. Their yields were calculated via integration of the corresponding signals in the proton NMR spectrum and showed for distannylated quaterthiophene **88** a content of only 36%, whereas monostannylated derivative **89** occurred to 43%. Dehalogenated starting material **85** was observed in 21% yield.



Scheme 4.9: Synthesis of distannylated DTP-oligothiophene **88**.

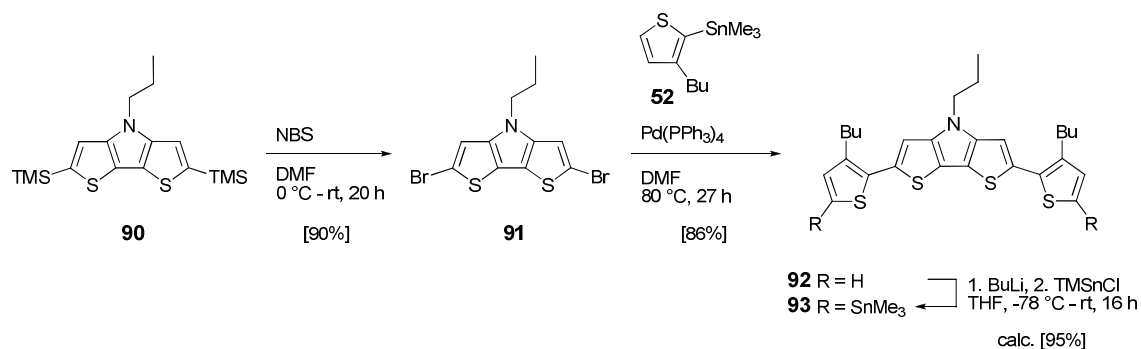
The structures were also proven by mass spectrometry. Attempts to vary the reaction conditions of the metal-halogen exchange did not improve the ratio of conversion. Investigations of a direct stannylation reaction through a proton-metal exchange seemed more promising and are described in the following section.

4.2.1.5 Access to *N*-propyl 4T-DTP (**93**)

A second DTP-containing oligothiophene **93** comprising a propyl chain at the nitrogen atom was synthesized. In contrast to the oily hexyl analogue, the propyl-substituted oligothiophene was crystalline and more facile to handle (Scheme 4.10).

The synthetic pathway started from TMS-protected DTP **90** which has been prepared via the two-step synthesis described in Scheme 4.5. *n*-Propylamine was utilized as primary amine in the Buchwald-Hartwig amination reaction.

Subsequent introduction of bromine atoms at the DTP core was achieved by an *ipso*-substitution reaction of **90** with NBS in DMF at 0 °C. Dihalogenated DTP **91** was isolated in 90% yield after filtration through a short column filled with aluminium oxide (Scheme 4.10).



Scheme 4.10: Synthesis of distannylated 4T-DTP precursor **93**.

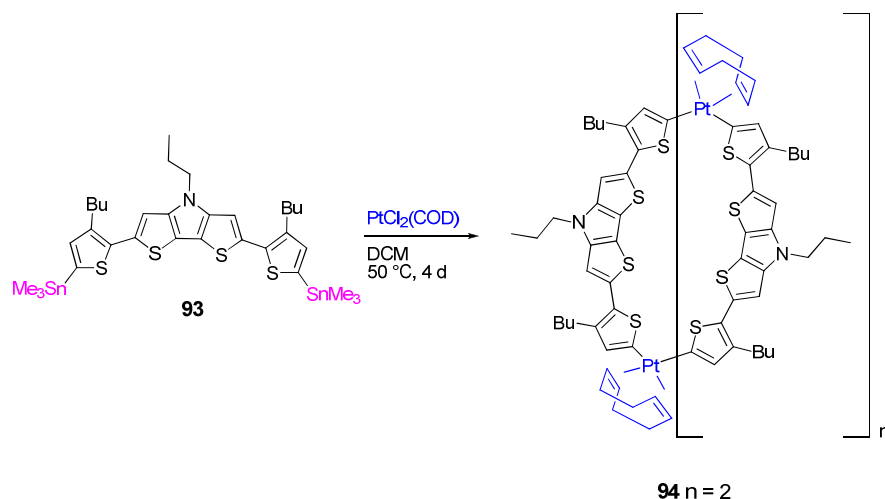
The following step included a Stille cross-coupling reaction of **91** and 3-butyl-2-(trimethyltin)thiophene **52** in DMF at 80 °C which was performed under general Pd-catalyzed conditions. Desired oligothiophene **92** was isolated in 86% yield after silica column chromatography.

Finally, a direct stannylation reaction was carried out under highly concentrated conditions (0.3 M). The proton-metal exchange was initiated by *n*-BuLi with subsequent trapping of the dilithiated species with TMSnCl. After aqueous work-up, precursor **93** was obtained in 95% yield which was calculated via integration of the corresponding signals in the proton NMR spectrum. Tin compound **93** was also confirmed by mass analysis and a monostannylated derivative occurred as byproduct. The crude product was not further purified and was used directly in the next macrocyclization step.

4.2.2 Macrocyclization via the ‘metal-assisted template method’

4.2.2.1 DTP-containing macrocyclic Pt^{II} oligothiényl complexes

Distannylated precursor **93** was reacted with PtCl₂(COD) under reflux for 4 d in DCM and multinuclear macrocyclic Pt^{II}(COD)oligothiényl complex **94** was obtained (Scheme 4.11). Reaction control was performed via proton NMR spectroscopy after three and four days. The reaction was stopped after four days since nearly no starting material was left.



Scheme 4.11: Synthesis of multinuclear macrocyclic $\text{Pt}^{\text{II}}(\text{COD})$ oligothienyl complex **94** via the ‘metal-assisted template method’.

Figure 4.1 shows the comparison of the proton NMR spectrum of precursor **93** (bottom) and a reaction sample after three days (top). To calculate the conversion to the formed metalla intermediate **94**, the intensity of the singlet signal of the tin groups in starting material **93** at $\delta = 0.36$ ppm was compared to the singlet signal of cleaved off trimethyltin chloride at $\delta = 0.57$ ppm. At the same time, a broad signal appeared at $\delta = 5.50$ ppm which can be attributed to the protons of the double bond of the COD ligand ($\text{HC}=\text{CH}$) in symmetric metallacycles. The broad signal at $\delta = 2.63$ ppm belongs as well to the COD ligand and corresponds to the CH_2 -groups. The triplet and multiplet signals of the butyl side chains were located in both spectra at similar chemical shifts at around $\delta = 2.80, 1.60, 1.40$, and 0.90 ppm for the $\alpha\text{-CH}_2$, $\beta\text{-CH}_2$, $\gamma\text{-CH}_2$, and CH_3 -groups, respectively. The same behaviour was observed for the signals of the *N*-propyl chain at around $\delta = 4.20, 1.90$, and 0.90 ppm for the $\alpha'\text{-CH}_2$, $\beta'\text{-CH}_2$, and CH_3' -groups, respectively. COD signals which can be assigned to linear asymmetric products and are usually located at around $\delta = 5.70$ and 5.60 ppm (see Chapter 3.3.3.1) did not appear, which gave a hint for the formation of a high amount of cyclic products and a low amount of linear byproducts. No aromatic signals of the thiophene protons of distannylated DTP precursor **63** at $\delta = 7.14$ and 7.03 ppm were left in the spectrum of the reaction sample. Instead, two singlets at $\delta = 6.89$ and 6.63 ppm occurred which can be assigned to the aromatic thiophene protons of one macrocycle size. The remaining signals belong to different ring sizes and byproducts.

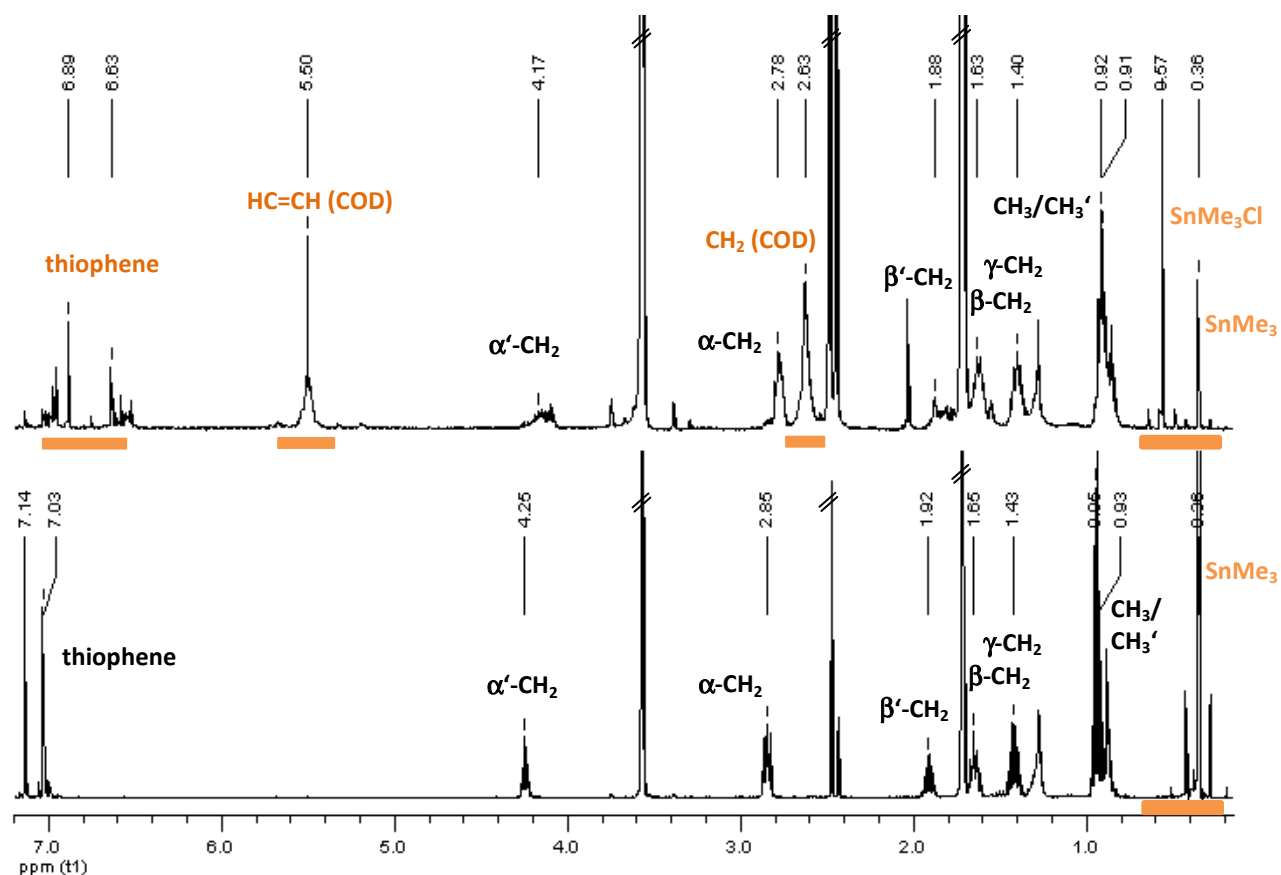


Figure 4.1: ^1H NMR spectra of a reaction sample after three days (top) and distannylated precursor **93** (bottom), measured in THF- d_8 (400 MHz).

The reaction product **94**, containing a mixture of both cyclic and little linear material, was filtered through a short plug of deactivated aluminium oxide to remove trimethyltin chloride from the reaction mixture.

Purification of the $\text{Pt}^{\text{II}}(\text{COD})$ oligothienyl complex **94** (Chart 4.3) was performed extensively via SEC with THF as eluent and **94** was obtained pure in 28% yield and investigated via proton NMR spectroscopy and mass spectrometry.

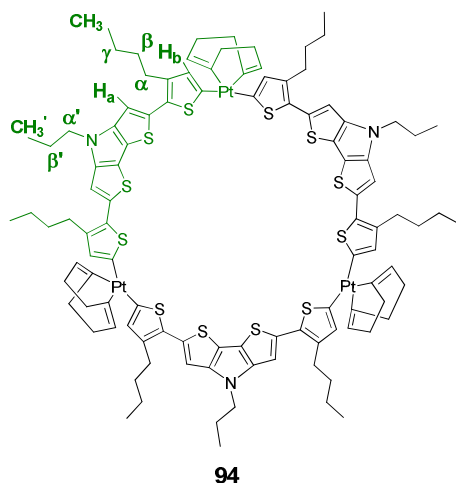


Chart 4.3: Structure of the trimeric metallacycle $\text{Pt}(\text{COD})[12]\text{DTP}$ **94**.

In the ^1H NMR spectrum (Figure 4.2), characteristic signals of the aromatic protons H_a and H_b of the cyclic backbone were found at $\delta = 6.89$ (H_a) and 6.64 ppm (H_b). Multiplet signals of the COD ligand were observed at $\delta = 5.50$ ($\text{HC}=\text{CH}$) and 2.64 ppm (CH_2). Triplet and multiplet signals belonging to the attached butyl side chains were located in the aliphatic region of the spectrum at $\delta = 2.79$, 1.65, 1.42, and 0.92 ppm for the $\alpha\text{-CH}_2$, $\beta\text{-CH}_2$, $\gamma\text{-CH}_2$, and CH_3 -groups, respectively. The signals for the *N*-propyl chain occurred at $\delta = 4.10$ ($\alpha'\text{-CH}_2$), 1.82 ($\beta'\text{-CH}_2$), and 0.87 ppm (CH_3').

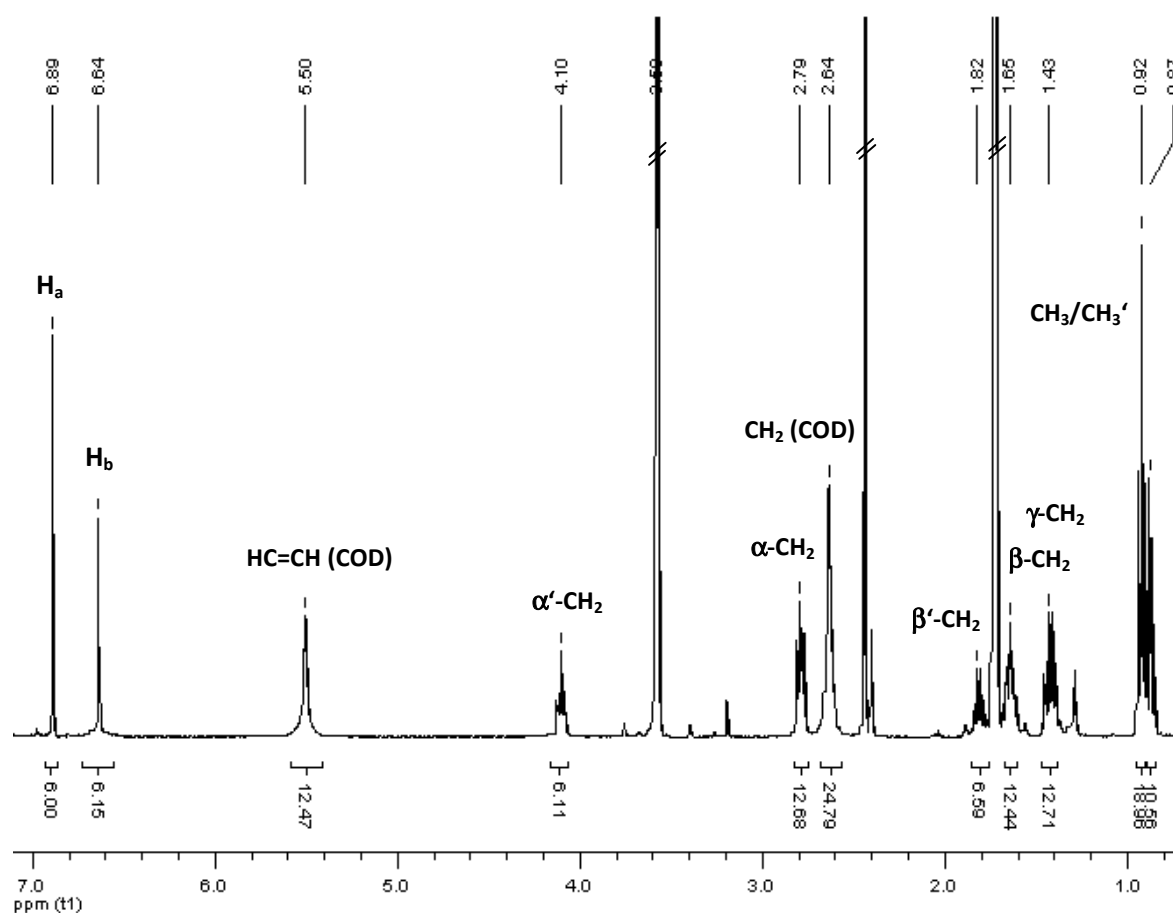
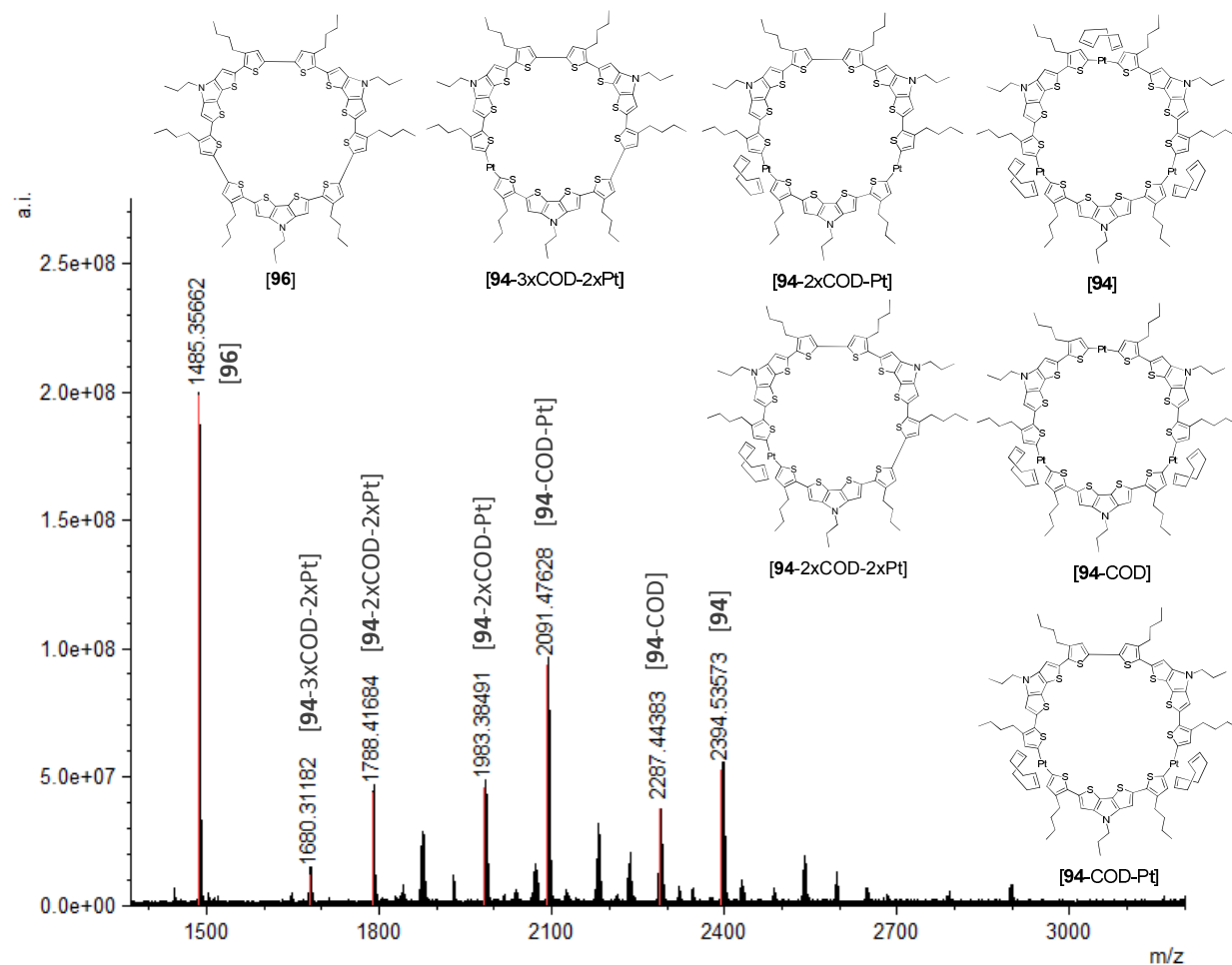


Figure 4.2: ^1H NMR spectrum of highly symmetric metallacycle **94**, measured in THF-d_8 (400 MHz).

Several signals were detected in mass analysis (MALDI-TOF) which showed not only the expected and calculated value for the isolated trimeric metallacycle **94** with $m/z = 2394.5$, but also fragments which followed a defined decomposition process that was triggered through the strength of ionization during the MALDI-TOF measurement. The data are summarized in Table 4.1. It can be regarded as a successive elimination of the COD ligands and platinum atoms until a fully α -conjugated C[12]DTP was obtained. The high resolution mass spectrum of **94** is depicted in Figure 4.3.

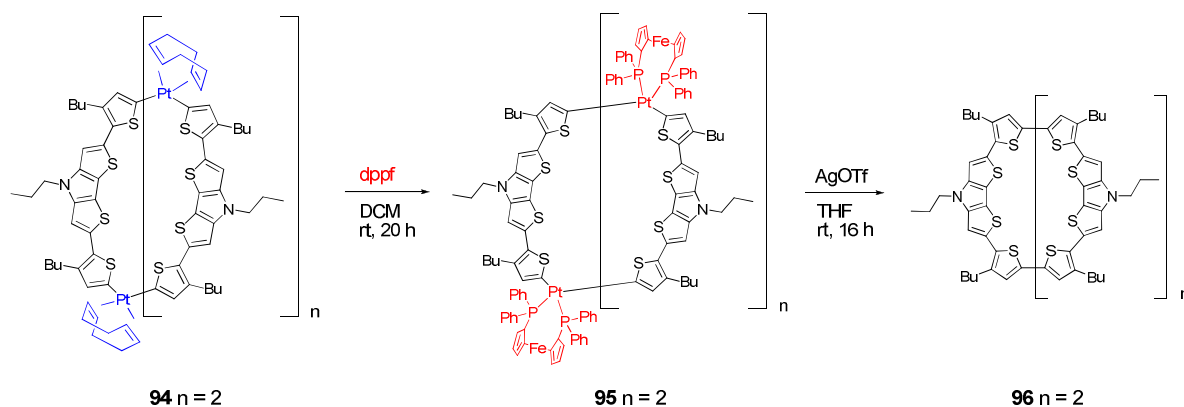
Table 4.1: Summarized data of the successive fragmentation of **94** during mass analysis.

metallacycle	<i>m/z</i>
[94]	[M] ⁺ calcd. (C ₁₀₅ H ₁₂₃ N ₃ Pt ₃ S ₁₂): 2394.53087 / found [M] ⁺ : 2394.53573
[94 -COD]	[M] ⁺ calcd. (C ₉₇ H ₁₁₁ N ₃ Pt ₃ S ₁₂): 2287.43838 / found [M] ⁺ : 2287.44383
[94 -COD-Pt]	[M] ⁺ calcd. (C ₉₇ H ₁₁₁ N ₃ Pt ₂ S ₁₂): 2091.47220 / found [M] ⁺ : 2091.47628
[94 -2xCOD-Pt]	[M] ⁺ calcd. (C ₈₉ H ₉₉ N ₃ Pt ₂ S ₁₂): 1983.37830 / found [M] ⁺ : 1983.38491
[94 -2xCOD-2xPt]	[M] ⁺ calcd. (C ₈₉ H ₉₉ N ₃ Pt ₂ S ₁₂): 1788.41352 / found [M] ⁺ : 1788.41684
[94 -3xCOD-2xPt]	[M] ⁺ calcd. (C ₈₉ H ₉₉ N ₃ Pt ₂ S ₁₂): 1680.31962 / found [M] ⁺ : 1680.31182
[96]	[M] ⁺ calcd. (C ₈₁ H ₈₇ N ₃ S ₁₂): 1485.35485 / found [M] ⁺ : 1485.35662

**Figure 4.3:** MALDI-TOF mass spectrum of Pt(COD)[12]DTB **94** and detected fragments.

4.2.2.2 Fully α -conjugated DTP-functionalized cyclo[n]thiophenes via oxidatively induced reductive elimination

The crude $\text{Pt}^{\text{II}}(\text{COD})$ metallacycle **94** was first converted via ligand exchange reaction into $\text{Pt}^{\text{II}}(\text{dppf})$ complex **95** (Scheme 4.12). The reaction was performed overnight at ambient temperature in DCM by adding 1,1'-bis(diphenylphosphino) ferrocene as solid. The ligand exchange was followed via proton NMR spectroscopy due to typical signals of inserted dppf (multiplets at 7.40 and 4.30 ppm) and eliminated COD (singlets at 5.58 and 2.38 ppm). The crude $\text{Pt}^{\text{II}}(\text{dppf})$ oligothienyl complex **95** was not further purified nor investigated and used directly for the next step, the oxidatively induced reductive elimination which was carried out in THF at ambient temperature with the one-electron oxidant silver triflate (AgOTf) (Scheme 4.12).



Scheme 4.12: Synthesis of fully α -conjugated DTP-macrocycle **96** via oxidatively induced reductive elimination.

After aqueous work-up, reaction mixture **96** was filtered through a short plug of aluminium oxide to remove eliminated metal and then transferred to a SEC column. The macrocycle was separated and purified and linear oligomers were removed. C[12]DTP **96** (Chart 4.4) was obtained pure as a black powder in an overall yield of 29% calculated from distannylated quaterthiophene **93**. The macrocycle was characterized by mass- and proton NMR-analysis and investigated with respect to its optical and electronic properties.

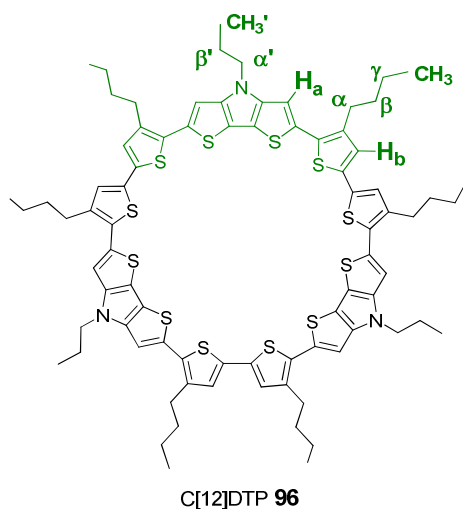


Chart 4.4: Structure of macrocycle C[12]DTP **96**.

The mass analysis confirmed the structure of C[12]DTP **96** with a value of $m/z = 1486.2$ (calcd. $m/z = 1485.3$). High resolution mass analysis provided an accuracy of $\delta_{m/m} = 0.3$ ppm, whereby the obtained experimental isotopic distribution pattern was in a very good agreement with the theoretical one. Figure 4.4 shows the MALDI-TOF mass spectrum of **96**.

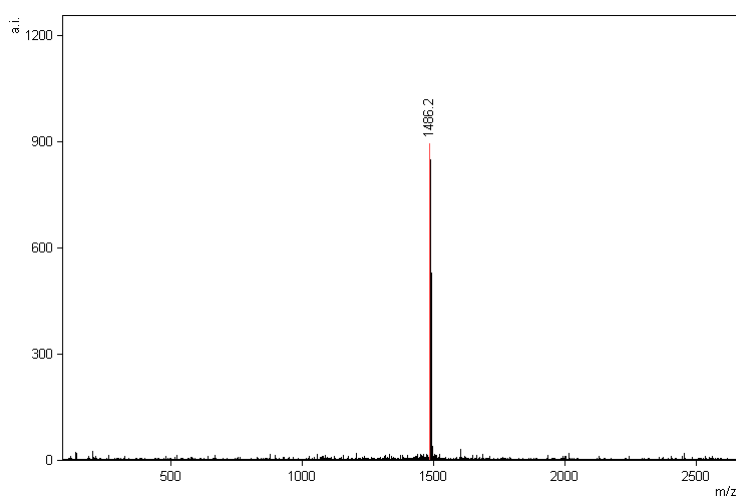


Figure 4.4: MALDI-TOF mass spectrum of C[12]DTP **96**.

The proton NMR spectrum of macrocycle **96** (Figure 4.5) revealed two typical downfield shifted singlets of the aromatic protons of the highly symmetric cyclic backbone with $\delta = 7.14$ for H_a and 7.08 ppm for H_b . The triplet and multiplet signals of the *N*-propyl chains were present in the aliphatic region of the spectrum at $\delta = 4.21$, 1.90, and 0.98 ppm for the α' -CH₂, β' -CH₂, and CH₃'-groups, respectively. The signals corresponding to the butyl side chains were located at $\delta = 2.85$ (α -CH₂), 1.75 (β -CH₂), 1.47 (γ -CH₂), and 0.98 ppm (CH₃).

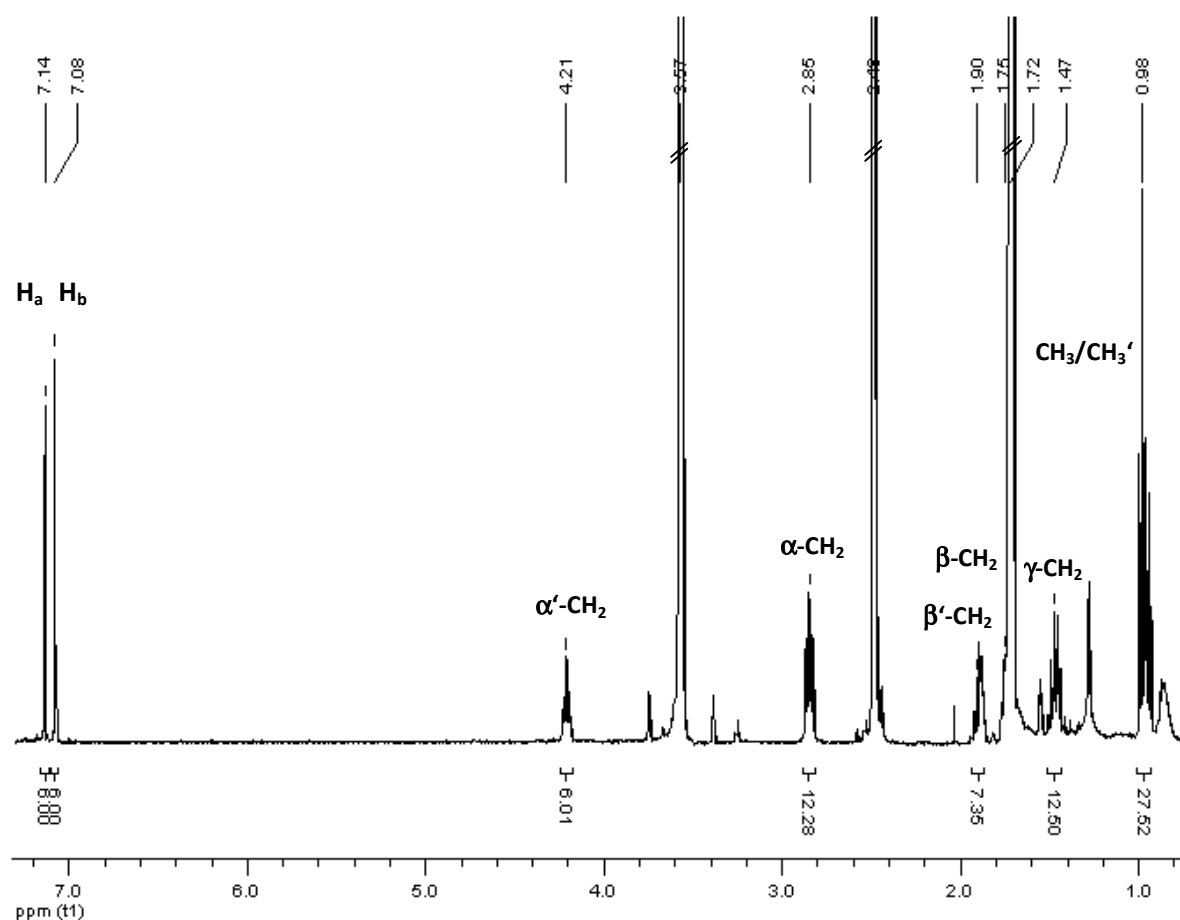
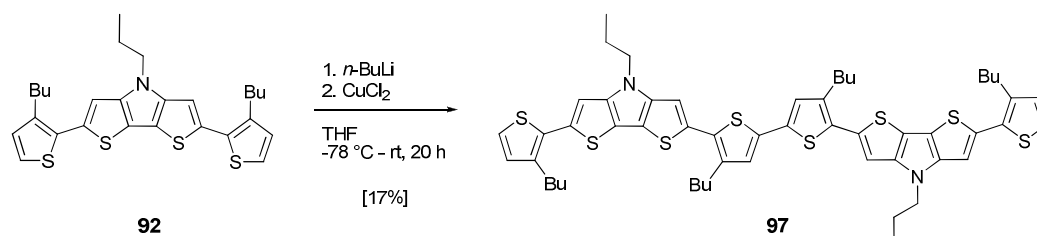


Figure 4.5: ^1H NMR spectrum of the highly symmetric macrocycle C[12]DTP **96**, measured in THF- d_8 (400 MHz).

4.3 Synthesis of a linear DTP-containing oligothiophene as model compound

A linear DTP-containing oligothiophene was synthesized in order to investigate its optical and electronic properties and to compare these to the macrocycle since a previously obtained comparison between only thiophene-based linear and cyclic systems showed interesting effects.^[38-40]



Scheme 4.13: Synthesis of linear octithiophene L[8]DTP **97**.

DTP-quaterthiophene **92** was reacted with *n*-butyl lithium (1.5 eq.) in THF at -78°C to generate a proton-lithium exchange and was subsequently trapped with copper(II)chloride to initiate oxidative C-C-bond formation (Scheme 4.13). Octithiophene L[8]DTP **97** was obtained as an orange solid in 17%

yield after column chromatography. Threefold coupled dodecithiophene L[12]DTP was as well formed, but could not be isolated in pure form even after several purification attempts using either column chromatography or precipitation. Yields were not the main issue in this reaction, but rather the short synthetic route which provides the two linear oligomers in one reaction step starting from DTP **92**.

4.4 Optical properties of donor-functionalized C[12]DTP (**96**)

The photophysical properties of the isolated fully π -conjugated ring system C[12]DTP **96** were analyzed by absorption and fluorescence spectroscopy and compared to the optical data of metallacycle Pt(COD)[12]DTP **94**, linear derivative L[8]DTP **97** and DTP-quaterthiophene **92**. The absorption and emission spectra are illustrated in Figure 4.6 and summarized in Table 4.2.

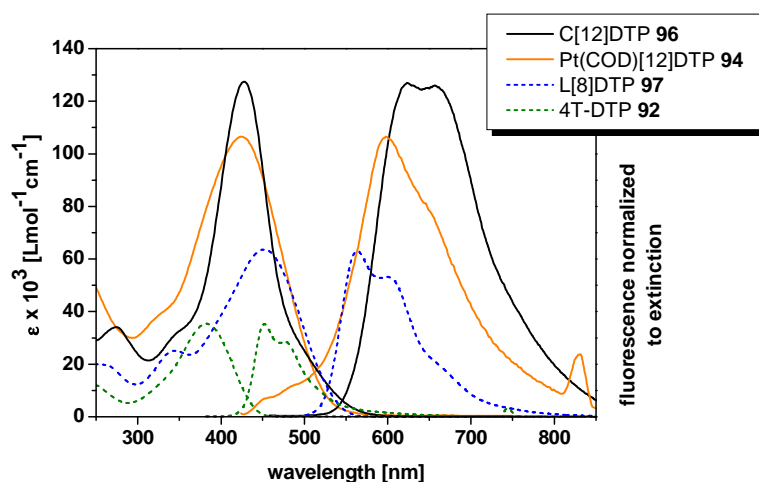


Figure 4.6: UV/vis absorption and emission spectra of DTP-macrocycle **96**, metallacycle **94**, linear octithiophene **97** and quaterthiophene **92**, measured in chloroform.

Macrocycle **96** exhibited an absorption maximum for the π - π^* transition at $\lambda = 428$ nm with an extinction coefficient of $127.000 \text{ Lmol}^{-1}\text{cm}^{-1}$. This electronic excitation can be assigned to the preferred and symmetry allowed $S_0 \rightarrow S_2$ transition. The transition into the S_1 -state is theoretically forbidden due to the required, but missing dipole moment perpendicular to the plane as a consequence of the selection rules for highly symmetric systems. All thiophene units are mainly oriented into the plane with a dipole moment parallel to the x-y-axis, why the main excitation follows the $S_0 \rightarrow S_2$ transition. Nevertheless, some of the thiophene moieties are slightly twisted out of the plane and show some transition dipole moment for the first excitation. Thus, the observed shoulder at $\lambda = 492$ nm can be ascribed to the $S_0 \rightarrow S_1$ transition (see also Chapter 3).^[38-40]

The absorption maximum of metallacycle **94** is mainly dominated by the π - π^* transition of the oligothiophene subunits. An additional electron transfer from the platinum centers to the ligands is likely as well as an enhanced electron distribution through the platinum cores. The maximum of the absorption band occurred at $\lambda = 424$ nm and is red-shifted in contrast to the monomer unit 4T-DTP **92** ($\lambda = 382$ nm). The extinction coefficient of the metallacycle ($\epsilon = 104.000 \text{ Lmol}^{-1}\text{cm}^{-1}$) is tripled compared to that of 4T-DTP ($\epsilon = 35.000 \text{ Lmol}^{-1}\text{cm}^{-1}$), because of the three oligomeric subunits. Octithiophene L[8]DTP **97** showed an absorption band for the π - π^* transition at $\lambda = 451$ nm which is ascribed to the $S_0 \rightarrow S_1$ transition. Due to the elongated π -system, the red-shift of 69 nm was expected in comparison to quaterthiophene 4T-DTP **92**. The observed higher energy shoulders at around $\lambda = 330, 340$ nm can be assigned to excitations of the parent DTP unit.^[1, 22]

The emission bands of the cyclic and linear oligothiophenes showed vibronic splitting up to three distributions indicating a more planar and quinoidal structure in the excited state. Metallacycle **94** tend to gain a more stiff structure with an increased double bonding character especially for the carbon-platinum bond to enhance π -conjugation along the complete molecule. Its emission maximum occurred at $\lambda = 598$ nm and is blue-shifted compared to the fully α -conjugated macrocycle **96** with $\lambda = 623$ nm. Since the emission of the linear derivative L[8]DTP takes place from the S_1 -state and is located at a shorter wavelength ($\lambda = 563$ nm), strained system **96** is expected to emit from a potentially lower-lying level (T_1 - or excimer state) which leads to the bathochromic shift. Fluorescence life-time measurements should be performed to determine a potential triplet state. To investigate the excimer state, fluorescence/excitation studies of concentrated solutions should be carried out.

Table 4.2: Summary of the optical data of cyclic systems **96**, **94** and linear oligothiophenes **97**, **92**.

oligothiophene	$\lambda_{\text{abs, max}}$ [nm]	ϵ [$\text{Lmol}^{-1}\text{cm}^{-1}$]	$\lambda_{\text{em, max}}$ [nm]
C[12]DTP 96	428 ^{a)} /492 ^{b)}	127.000	623/656
Pt(COD)[12]DTP 94	424	104.000	598
L[8]DTP 97	451	63.000	563
4T-DTP 92	382	35.000	452

^{a)} assigned to the $S_0 \rightarrow S_2$ transition.

^{b)} assigned to the $S_0 \rightarrow S_1$ transition, exact value calculated via Gaussian Fit (originPro 7.0).

To investigate the electronic influence of the electron-withdrawing and electron-donating units, a comparison of the photophysical properties of acceptor-macrocycles C[12]DTB **67a** and C[12]DCP **70**, donor-macrocycle C[12]DTP **69** and non-functionalized C[12]T **81** should be of great interest (Chart

4.5). The absorption and emission spectra of all four fully α -conjugated macrocycles are illustrated in Figure 4.7 (left). The figure on the right shows the appropriate normalized absorption curves. The spectrum of the non-functionalized system was recorded in DCM whereas these for the modified macrocycles were recorded in chloroform.

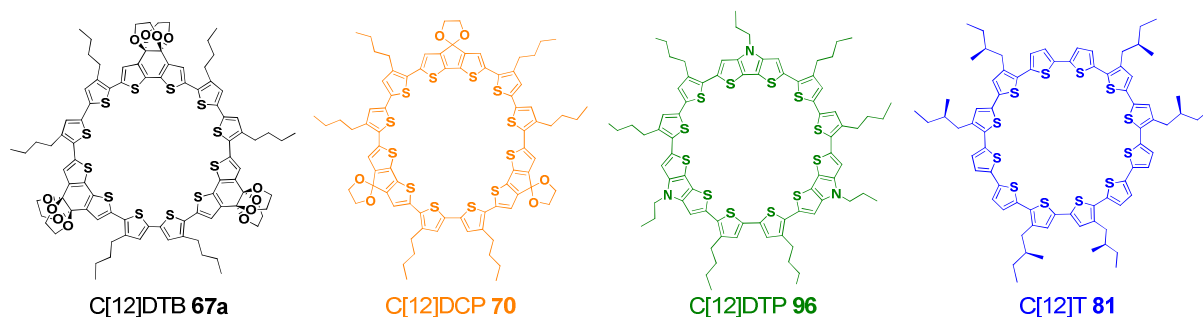


Chart 4.5: Structures of the four fully α -conjugated acceptor-, donor- and non-functionalized macrocycles **67a**, **70**, **96**, and **81**.

All absorption spectra revealed next to the main absorption band for the π - π^* transition a clear shoulder at higher wavelengths which belongs to the theoretically forbidden $S_0 \rightarrow S_1$ transition. This band is not observable for the corresponding higher homologues, since the main absorption band overlaps this ring-size independent transition. The absorption maxima for the $S_0 \rightarrow S_2$ transition of the acceptor-functionalized macrocycles C[12]DTB **67a** and C[12]DCP **70** were located at similar wavelengths at $\lambda = 453$ and 450 nm, respectively, and donor-macrocycle C[12]DTP **96** absorbed blue-shifted at $\lambda = 428$ nm. The acceptor-containing ring systems possess in contrast to the electron-donating ring a smaller optical band gap due to a stronger influence of the electron withdrawing moieties which lowers the LUMO and results the absorption red-shifted. The main absorption band of the non-functionalized macrocycle C[12]T **81** occurred at the shortest wavelength at $\lambda = 427$ nm. Since the absorption was nearly the same value as for **96**, the DTP-unit seems not to strongly influence the optical behaviour. A summary of the photophysical data is given in Table 4.3.

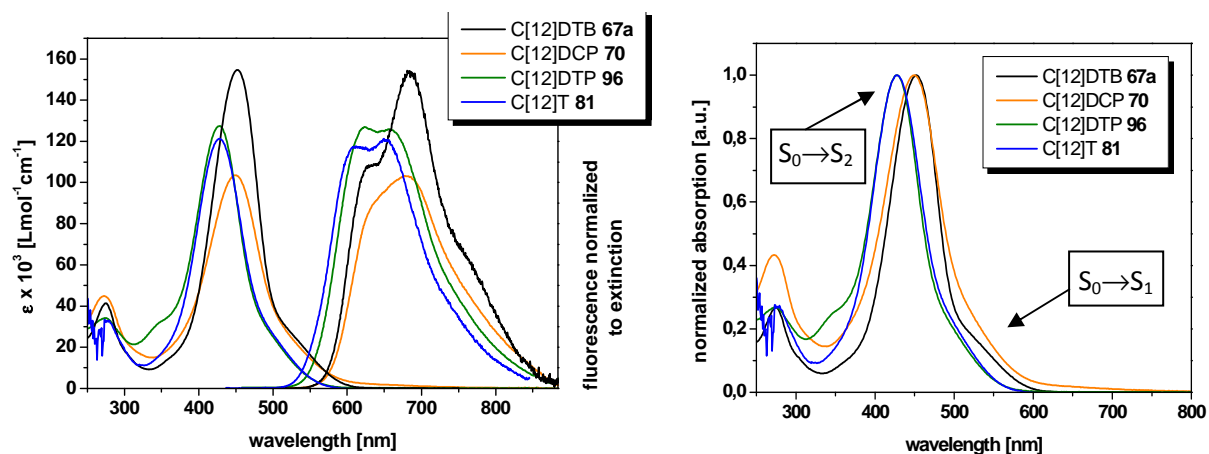


Figure 4.7 UV/vis absorption and emission spectra (left) of macrocycles **67a**, **70**, **96**, and **81**. Normalized absorption curves (right) of the four macrocycles, measured in chloroform (**81** measured in DCM).

All emission curves exhibited a vibronic splitting, indicating a planar geometry in the excited state. The shape of the emission bands for C[12]DTB **67a** and C[12]DCP **70** revealed strongly red-shifted maxima due to an assumed high ring strain. The emission maxima of the cycles C[12]DTP **96** and C[12]T **81** exhibited maxima at $\lambda = 656$ and 650 nm, respectively.

Table 4.3: Summary of the optical data of macrocycles **67a**, **70**, **96**, and **81**.

macrocycle	$\lambda_{\text{abs,max}}$ [nm]	ϵ [Lmol ⁻¹ cm ⁻¹]	$\lambda_{\text{em,max}}$ [nm]
C[12]DTB 67a	453 ^{a)} /512 ^{b)}	153.000	684
C[12]DCP 70	450 ^{a)} /526 ^{b)}	103.000	678
C[12]DTP 96	428 ^{a)} /492 ^{b)}	127.000	656
C[12]T 81	427 ^{a)} /516 ^{b)}	121.000	650

^{a)} assigned to the $S_0 \rightarrow S_2$ transition.

^{b)} assigned to the $S_0 \rightarrow S_1$ transition, exact values calculated via Gaussian Fit (originPro 7.0).

4.5 Characterization of different redox states of donor-functionalized C[12]DTP (**96**)

4.5.1 Electrochemical properties of donor-functionalized C[12]DTP (**96**)

The redox properties of macrocycle C[12]DTP **96** were investigated by cyclic voltammetry and the results compared to those of acceptor-functionalized macrocycle C[12]DTB **67a** and non-functionalized C[12]T **81**.

The cyclic voltammograms were recorded in benzonitrile as solvent at ambient temperature. The polar solvent should prevent adsorption of charged species at the electrode. TBAPF₆ (0.1 M) was used as supporting electrolyte and ferrocene as internal standard. Since the measurements were carried out at low substrate concentrations of 0.1 mM, a Pt-working electrode with a relatively large diameter of 3.4 mm was utilized to obtain well resolved redox waves.

The cyclic and deconvoluted voltammograms of the donor-functionalized ring system **96** are depicted in Figure 4.8 and the electrochemical data are summarized in Table 4.4. Several reversible redox waves were observed which indicate stable, multiply charged species during the oxidation processes. No oligomerization took place due to the lack of free α -positions. By comparing the integrals of the redox waves of the deconvoluted voltammogram of **96** to the oxidation wave of ferrocene, which was used as standard and measured under consistent conditions (295 K, 0.1 mM, benzonitrile), the

number of transferred electrons for **96** could be determined in a good approximation (Figure 4.8, right). Ferrocene is well known as one-electron transfer reagent and the transferred electrons within the redox waves of the DTP-macrocycle were calculated to $1.08e^-:1.03e^-:1.3e^-$. Thus, three reversible one-electron transfer processes were detectable at $E_{ox1}^0-E_{ox3}^0$ (-0.01 V, 0.30/0.36/0.58/0.66 V, 0.81/1.03 V) with a very sharp and intense first oxidation and a strongly structured second and third oxidation step (Figure 4.8, bottom). Upon increasing the scan range to 1.2 V, an additional wave occurred within the reductive backscan negatively located towards the first oxidation wave. The formation of non-reversible aggregates was assumed.

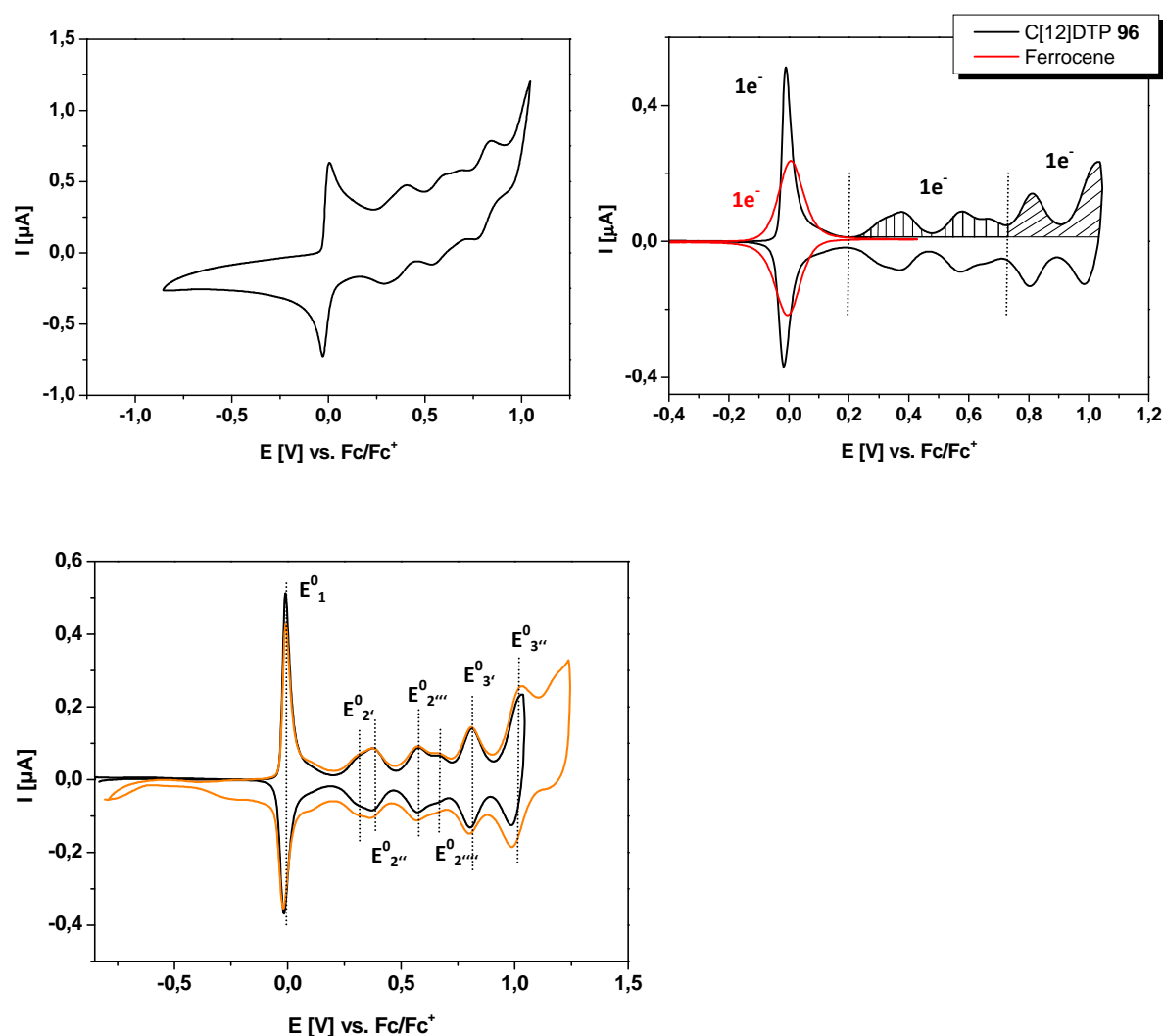
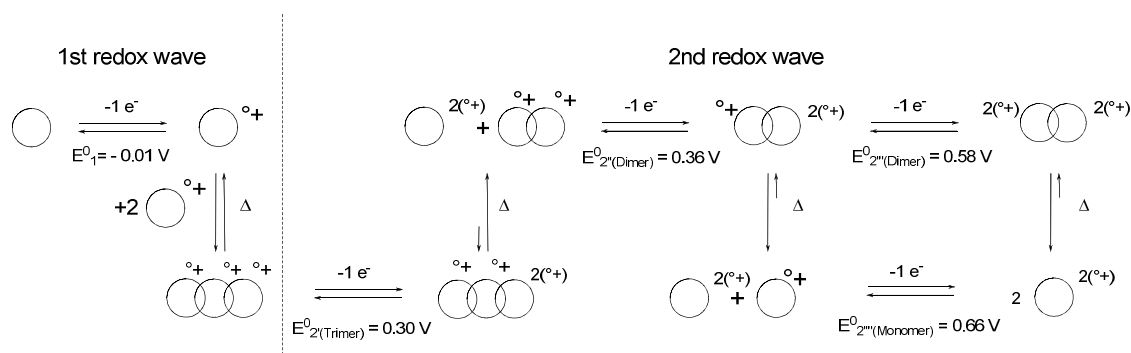


Figure 4.8: CV of C[12]DTP **96** (top, left), comparison of the calculated integrals of ferrocene as standard and **96** (top, right), deconvoluted voltammogram of **96** (bottom), measured at 295 K in benzonitrile/TBAPF₆ (0.1M) vs. Fc/Fc^+ , 20 mV/s, $c = 1.0 \times 10^{-4}$ M, respectively.

The formation of reversible dimers via π - π interactions during electrochemical analysis is very likely, as this fact has already been detected and discussed for the acceptor-functionalized cycle C[12]DTB **67a** in Chapter 3.8.1. Furthermore, dimerization of charged species of a previously synthesized and characterized non-functionalized cycle C[10]T has already been published in literature.^[40] A

schematic presentation for suggested oxidation processes of C[12]DTP **96** is illustrated in Scheme 4.14 for the first two redox waves. Since the first oxidation wave at -0.01 V did not reveal any splitting, a clear one-electron transfer from the neutral species into a radical cation structure is assigned. Within the second single-electron transfer, four oxidation potentials $E_{2'}^0$ - $E_{2'''}^0$ were visible and are attributed to four oxidation processes. Presumably, a trimer species consisting of three radical cations was formed, which was oxidized at $E_{2'}^0 = 0.30$ V and subsequently deaggregates to yield one dication and one dimer with two monoradical cations. The DTP-macrocycles are expected to adopt an almost planar geometry and thus allow the facile piling of several molecules into multiple charged assemblies. No rejection between the charged cycles is supposed, as they would aggregate antiparallel with respect to their charges. Further oxidation processes would follow: An oxidation of the dimer at $E_{2''}^0 = 0.36$ V with subsequent deaggregation to a dication and one monomeric radical cation, followed by the oxidation of the radical cation species into a twofold charged cation at $E_{2'''}^0 = 0.66$ V. The dimer can also undergo an one-electron transition at $E_{2'''}^0 = 0.58$ V to yield a dimer of two dicationic species, that equilibrates with two monomeric dications.



Scheme 4.14: Schematic presentation of assumed oxidation processes of C[12]DTP **96** on a molecular level.

To investigate the influence of the incorporated acceptor- and donor-functionalities on the electrochemical property, **96** was compared to C[12]DTB **67a** and C[12]T **81**. The deconvoluted cyclic voltammograms are depicted in Figure 4.9. Due to the high electron density, electrochemical oxidation was more facile for the electron rich DTP-cycle **96** compared to the electron-withdrawing DTB-derivative **67a**. This is reflected in the first oxidation potentials with $E_1^0 = -0.01$ V for DTP **96** and $E_1^0 = 0.19$ V for DTB **67a**. The electronically unaffected C[12]T **81** exhibited its first oxidation potential in-between at $E_1^0 = 0.09$ V. In total, six oxidation processes occurred for **81** (0.09 V, 0.26 V, 0.53 V, 0.71 V, 0.90 V, 1.26 V). It is not clarified if the processes for **81** are one-electron or multiple-electron transfer steps, but dimerization of charged species for this kind of cycle is likely, too. The scan range was not elongated beyond 1.1 V, as measurements upon higher voltages showed irreversible waves within the negative backscan for both functionalized macrocycles. Instead, no irreversible waves were detected for C[12]T when measured up to a potential of 1.4 V. Presumably, multiple charged

species on the cyclic backbone of simple, only thiophene-based macrocycles are more stable at higher voltages than on electronical influenced systems.

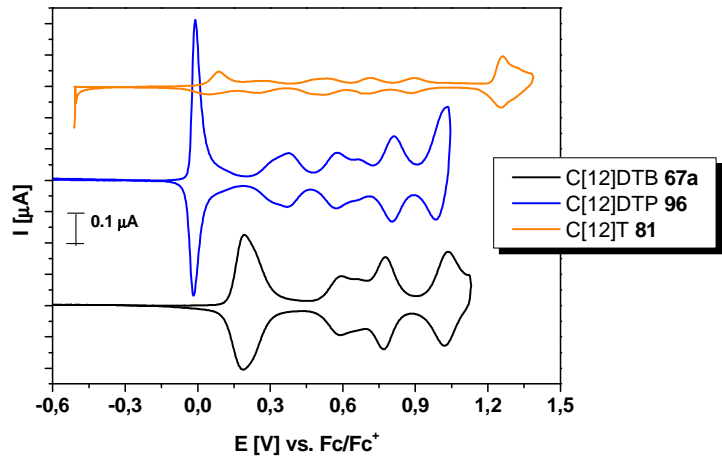


Figure 4.9: Cyclic voltammograms of **67a**, **96**, and **81**, measured at 295 K in DCM/TBAPF₆ (0.1M) and benzonitrile/TBAPF₆ (0.1M) vs. Fc/Fc⁺.

Table 4.4: Summary of the oxidation potentials of the three one-electron oxidation steps.

oligothiophene	E^0_{ox1} [V]	E^0_{ox2} [V]	E^0_{ox3} [V]
C[12]DTB 67a	0.19	0.59 / 0.66 / 0.77	1.03
C[12]DTP 96	-0.01	0.30 / 0.36 / 0.58 / 0.66	0.81 / 1.03
C[12]T 81	0.09	_{a)}	_{a)}

^{a)} Internal measurement; determination of the amount of transferred electrons per oxidation wave was not performed, E^0_{ox} values cannot be assigned to a defined wave.^[41]

4.5.2 Characterization of different redox states of C[12]DTP (96) via UV/vis/NIR absorption spectroscopy

During electrochemical analysis by means of cyclic voltammetry, C[12]DTP **96** was multiply oxidized and showed several reversible redox waves. These stable oxidized states can be investigated via UV/vis/NIR absorption spectroscopy to gain more information about the electronic states (Chart 4.6). The measurements were carried out according to acceptor-functionalized macrocycle C[12]DTB **67a** already described and discussed in Chapter 3.8.2 and non-functionalized C[10]T, published by Zhang et al.^[42] The oxidation was performed with the chemical oxidant tris(2,4-dibromophenyl)aminium hexachloroantimonat (TDBPA⁺SbCl₆⁻) to guide partial oxidation with a defined range of 0.5 equivalents and to exhibit the stepwise oxidation process in more detail. All spectra were recorded in dichloromethane and the samples were prepared from stock solutions of the macrocycle and the

oxidant, whereby defined and increasing amounts of oxidant were added to a consistent concentration of the macrocycle.

Absorption spectra through the stepwise addition of oxidant up to 1.0 eq. are shown in Figure 4.10 (left). The corresponding cyclic voltammogram is depicted on the right and presents a sharp one-electron oxidation wave at $E_1^0 = -0.01$ V for the first oxidation process.

Macrocycle **96** in its neutral state revealed a main absorption band at $\lambda = 428$ nm for the allowed $S_0 \rightarrow S_2$ transition and an unresolved shoulder at $\lambda = 492$ nm for the forbidden $S_0 \rightarrow S_1$ transition. Upon increasing the amount of oxidant up to 1.0 eq., the band of the neutral state decreased with a simultaneous appearance of several novel absorption bands. The two main bands were located red-shifted at $\lambda = 561$ nm and in the NIR-region with a broad band at $\lambda = 2269$ nm. Both can be ascribed to the formed singly charged radical cationic species $C[12]DTP^+$. The band at lower wavelength occurred due to the excitation of an electron from the singly occupied level to the first unoccupied one, whereas the band in the NIR-region can be assigned to the transition of an electron from the highest doubly occupied level into the singly occupied level.

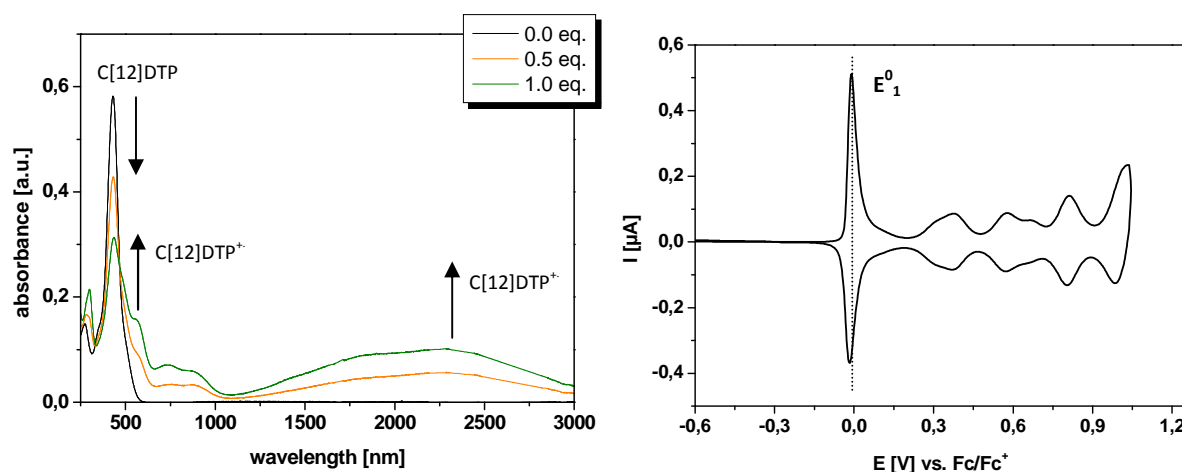
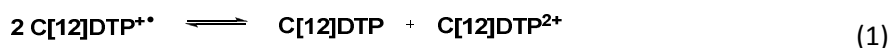


Figure 4.10: Absorption spectra of C[12]DTP **96** with the successive addition of oxidant TDBPA⁺SbCl₆⁻ up to 1.0 eq. (left) and deconvoluted voltammogram of **96**, both measured in DCM.

The detected absorption bands inbetween can be assigned to dimeric species which are formed via π - π -interactions of the π -conjugated, charged systems. The suggested dimers were investigated via temperature-dependent measurements for C[12]DTB **67a** (Chapter 3.8.2), pure thiophene-based macrocycle C[10]T^[42] and linear end-capped oligothiophenes.^[43] A change in the intensity of the absorption bands was observed when measured at different temperatures, supporting the assumption of formed dimeric structures which deaggregate at elevated temperatures and are more prominent upon cooling. In this case, no temperature-dependent measurements were carried out for C[12]DTP **96**.

Even after the addition of 1.0 equivalent of oxidant some amount of neutral compound C[12]DTP was still left. This could be observed by the diminishing but not vanishing absorption band at $\lambda = 492$ nm. The fact might be explained by a disproportionation equilibrium described in equation (1).^[44] The absorption of the appearing dicationic species in equation (1) is probably overlapped by a dimeric one.



The increasing absorption band below 300 nm belongs to the reduced triarylamine of the utilized oxidant.

Upon further oxidation with 1.5, 2.0, and 2.5 eqs. of $\text{TDBPA}^+\text{SbCl}_6^-$, three sharp absorption bands appeared with a simultaneous decrease of the bands for the neutral and radical cation species (Figure 4.11). The absorption maxima at $\lambda = 696$ and 1832 nm can be assigned to the dicationic species C[12]DTP^{2+} , the bands located inbetween at $\lambda = 1426$ and 1594 nm probably correspond to the formation of charged aggregates, which would be consistent with the results obtained from cyclic voltammetry for the second single-electron transfer ($E_{2^0}^0 - E_{2^{\bullet+}}^0$). The lack of isosbestic points, typically an indication of a clean conversion from one charged species into the next higher oxidized one, can be ascribed to the coexistence of several charged species and the assumed tendency towards dimerization.

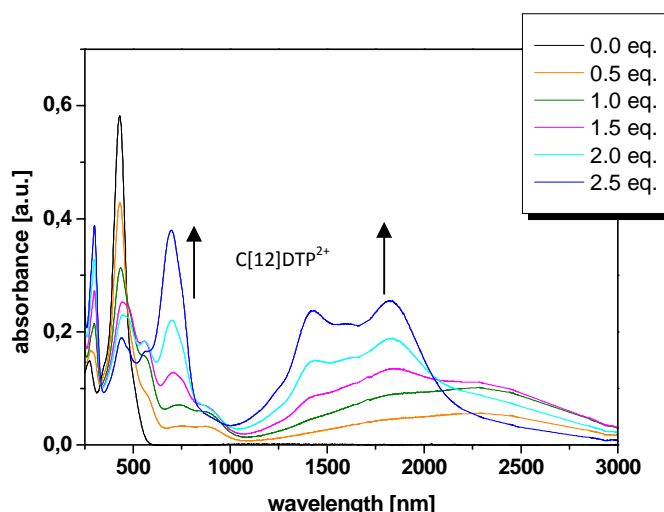


Figure 4.11: Absorption spectra of C[12]DTP **96** with the successive addition of oxidant $\text{TDBPA}^+\text{SbCl}_6^-$ up to 3.0 eqs., measured in DCM.

Upon the addition of further equivalents of oxidant, two absorption bands occurred at $\lambda = 736$ and 1118 nm with a clear decrease and overlapping of the bands of the lower oxidized species (Figure 4.12). The mentioned new absorption maxima appeared due to a triply oxidized macrocycle C[12]DTP^{3+} . The unresolved shoulders at higher energies at around $\lambda = 671$ and 958 nm can be a hint

of aggregation processes of charged species or rather vibrational splitting.^[43] The oxidation up to a trication was also observed in the recorded cyclic voltammogram.

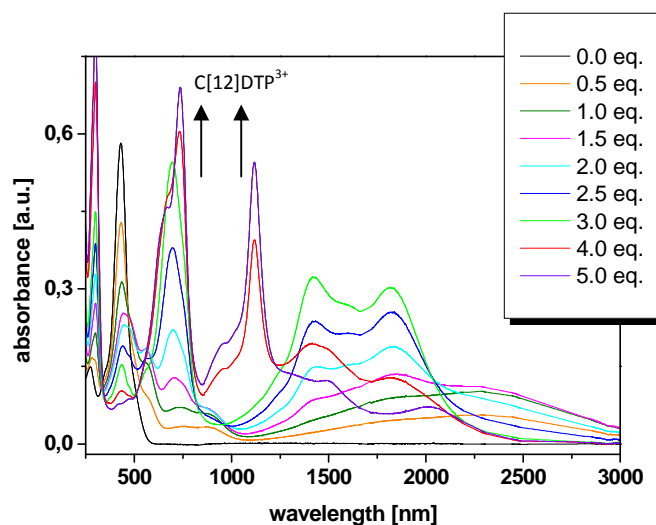


Figure 4.12: Absorption spectra of C[12]DTP **96** with the successive addition of oxidant TDBPA⁺SbCl₆⁻ up to 5.0 eqs., measured in DCM.

All absorption maxima of the different oxidation states are given in Table 4.5.

Table 4.5: Summary of the absorption maxima of **96** for the respective oxidized states.

	C[12]DTP	C[12]DTP ⁺	(C[12]DTP ⁺) ₂	C[12]DTP ²⁺	C[12]DTP ³⁺
λ_{max} [nm]	428, 492	561, 2269	737, 876, 1830	696, 1832 (1425, 1595)	736 (671), 1118 (958)

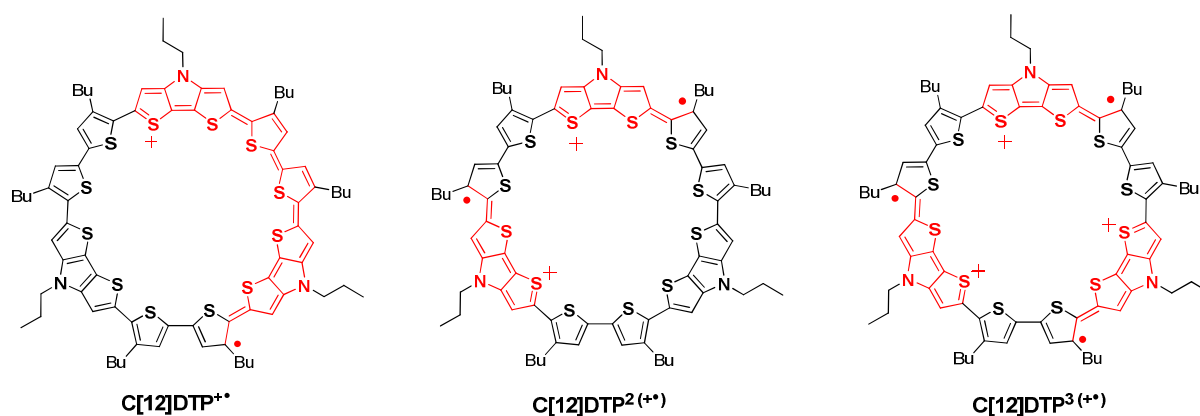


Chart 4.6: Structures of the singly, doubly and triply oxidized macrocyclic DTP-species.

4.6 Characterization of doubly oxidized species C[12]DTP²⁽⁺⁾ via electron spin resonance

Electron spin resonance analysis (ESR) was carried out at ambient temperature and at 120 K for the singly and doubly oxidized species of C[12]DTP **96**. The same measurements were performed for DTB-substituted macrocycle **67a** (Chapter 3.9) and non-functionalized cyclo[10]thiophene.^[42] This method should give an insight into the electronic structure of a doubly oxidized cyclic species, since configurations of a bipolaronic or polaronic pair structure are possible (Figure 4.13).

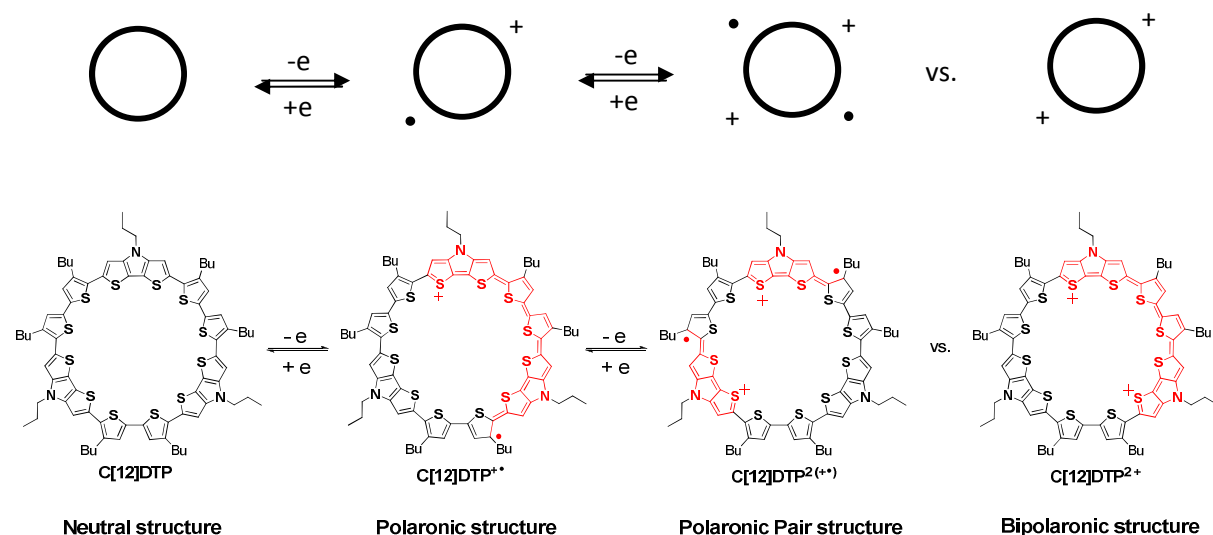


Figure 4.13: Electronic structures of macrocycle C[12]DTP **96** in the neutral, singly and doubly oxidized state.

In the case of a bipolaronic structure, no visible ESR signal is expected to occur since a closed-shell with no unpaired electrons exist. Instead, a signal should be obtained for the polaronic pair-like arrangement with two individual polarons on one macrocycle. The spins of the radicals can exist as singlet or triplet state. Depending on the strength of the exchange interaction between two singlet electrons, the intensity of the recorded signal for a polaronic pair can vary notably.^[44] A strongly stabilized singlet ground state can even cause the absence of an ESR signal.^[45]

The samples for the ESR-measurements were prepared according to the procedure for the UV/vis/NIR absorption spectroscopy. 1.0 Eq. and 2.5 eqs. of the chemical oxidant TDBPA⁺SbCl₆⁻ were added to a defined concentration of the macrocycle, respectively.

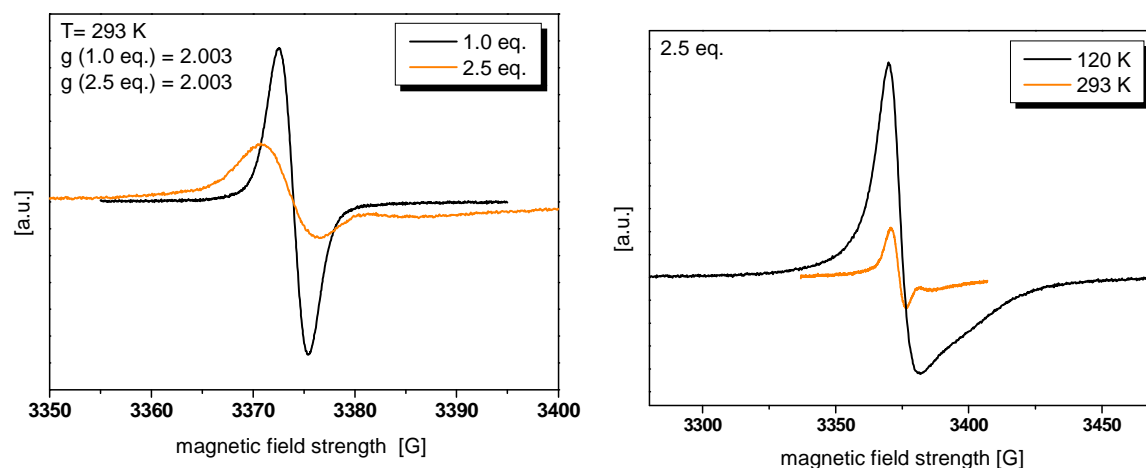


Figure 4.14 ESR-spectra of the singly and doubly oxidized species of **96** at 293 K (left). ESR-spectrum of the doubly oxidized species of **96** at 120 and 293 K (right), measured in DCM.

The obtained ESR spectra for **96** in general reflect the same observations as obtained for the DTB-modified macrocycle **67a**. A sharp and intense signal for the singly oxidized $\text{C}[12]\text{DTP}^{+\cdot}$ and a diminished signal for the doubly oxidized species $\text{C}[12]\text{DTP}^{2+}$ probably due to a thermodynamical equilibrium between triplet and singlet configuration or an interaction between the singlet states of the unpaired electrons, which leads to an average signal (Figure 4.14, left). With a decrease of the temperature to 120 K, an amplification of the ESR signal for $\text{C}[12]\text{DTP}^{2(+\cdot)}$ occurred presumably because of the preference for one of the possible spin states (Figure 4.14, right). The asymmetric shape of the signal might be due to the influence of a slight excess of oxidant $\text{TDBPA}^+\text{SbCl}_6^-$ (2.5 eq.), which itself exists as a radical cation. Upon increasing the concentration of the oxidant from 1.0 to 2.5 eqs., the g factor does not change and remains constant at 2.003 which is a slight deviation from the literature value of a free electron ($g = 2.0023$). This deviation can be caused by spin-orbit couplings or strong intramolecular interactions of the radicals.

Based on a positive ESR signal, a polaronic pair configuration $\text{C}[12]\text{DTP}^{2(+\cdot)}$ for the doubly oxidized species is very likely. The result is also in accordance with the investigations for $\text{C}[12]\text{DTB}$ **67a** and $\text{C}[10]\text{T}$.

4.7 Summary

The synthesis of the shape-persistent, donor-functionalized macrocycle $\text{C}[12]\text{DTP}$ **96** applying the well established ‘metal-assisted template method’ was finally achieved and described within this chapter. The required precursor 4T-DTP **92** was synthesized by using a Stille cross-coupling reaction of a corresponding dihalogenated DTP-core unit and a tin-compound. The final macrocyclization step

was carried out by means of $\text{PtCl}_2(\text{COD})$. Due to extensive purification, $\text{Pt}(\text{COD})[12]\text{DTP}$ **94** was successfully isolated and characterized by proton NMR spectroscopy and mass spectrometry. Fully α -conjugated cyclotrimer $\text{C}[12]\text{DTP}$ **96** was isolated in 29% yield after oxidatively induced reductive elimination with AgOTf and purification via SEC. Characterization, photophysical and electrochemical investigations have been performed and results were compared to acceptor-substituted and non-functionalized macrocycles. Recorded absorption spectra revealed in comparison to the acceptor-analogues $\text{C}[12]\text{DTB}$ **67a** and $\text{C}[12]\text{DCP}$ **70** a blue-shifted maximum for the $S_0 \rightarrow S_2$ transition which appeared at nearly the same absorption wavelength than macrocycle $\text{C}[12]\text{T}$ **81**. It is obvious that the optical band gap is less influenced by the electron-donating DTP unit than by the electron-withdrawing DTB and DCP moieties. As it would have been expected for an electron-rich functionality, **96** showed the lowest first oxidation potential due to a high electron density. Several reversible one-electron transfer steps occurred upon oxidation, which additionally indicate the aggregation of charged species. A polaronic pair-like configuration for doubly oxidized $\text{C}[12]\text{DTP}^{2(+)}$ was determined by ESR-measurements. The synthesis of $\text{C}[12]\text{DTP}$ **96** is a further success for the 'metal-assisted template method' towards tailored and tunable macrocycles.

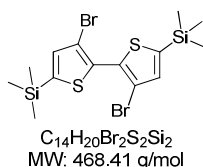
4.8 Experimental section

General remarks about chemicals, synthesis, analytical data, and performed measurements

Remarks given in the experimental part in Chapter 3 are generally as well valid in this section. The experimental setup of the photophysical, electrochemical, and ESR-measurements is given in the experimental part in Chapter 3. Additionally, 2-bromothiophene, tris(dibenzylideneacetone) dipalladium (Pd_2dba_3), and 2,2'-bis(diphenylphosphino)-1,1'-binaphthyl (BINAP) were purchased from Aldrich. Mercury acetate was purchased from Alfa Aesar and sodium *tert*-butoxide, *n*-hexylamine, and *N*-bromosuccinimide were purchased from Merck.

Synthesis and characterization

3,3'-Dibromo-5,5'-bis(trimethylsilyl)-2,2'-bithiophene (45**)**^[22]



2-Bromothiophene (8.15 g, 50.0 mmol) was dissolved in 100 mL dry THF and cooled to $-78\text{ }^{\circ}\text{C}$. LDA (1.2 M in THF, 41.6 mL, 50.0 mmol) was added dropwise and the clear yellow solution was stirred for 1 h. Chlorotrimethylsilane (5.43 g, 50.0 mmol) was added dropwise, the colorless suspension was stirred for 1 h and a clean formation of 2-bromo-5-trimethylsilylthiophene was confirmed by GC-MS analysis. LDA (1.20 M in THF, 45.8 mL, 55.0 mmol) was added within 30 min and the mixture was stirred for further 30 min, whereby a thick suspension was formed. Anhydrous CuCl_2 (7.39 g, 55.0 mmol) was added in several portions to keep the temperature low. The mixture was allowed to slowly warm up to room temperature overnight. *n*-Hexane and water were added (copper salts partially precipitated) and the organic phase was carefully concentrated under vacuum. The aqueous phase was extracted with *n*-hexane and the combined organic layers were dried over Na_2SO_4 . Upon filtration, the solvent was partially removed under vacuum and the brown solution was filtered through a silica gel plug with *n*-hexane as eluent. Removal of the solvent yielded a yellow oil which partially solidified overnight. The crystals of bithiophene **45** (6.40 g, 13.7 mmol, 55%) were collected by filtration.

Mp.: 88 – 89 $^{\circ}\text{C}$.

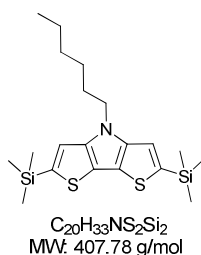
^1H NMR (400 MHz, CDCl_3): δ = 7.15 (s, 2H, Th-4,4'), 0.34 (s, 18H, TMS) ppm.

^{13}C NMR (100 MHz, CDCl_3): δ = 142.93, 137.01, 133.96, 112.95, -0.38 ppm.

MS (EI) m/z : calcd. for $[\text{M}]^+$ ($\text{C}_{14}\text{H}_{20}\text{Br}_2\text{S}_2\text{Si}_2$): 468; found: 468 $[\text{M}]^+$.

Elemental analysis: calcd. for ($\text{C}_{14}\text{H}_{20}\text{Br}_2\text{S}_2\text{Si}_2$): C, 35.90; H, 4.30; S, 13.69%; found: C, 36.03; H, 4.26; S, 13.69%.

2,6-Bis(trimethylsilyl)-*N*-hexyldithieno[3,2-*b*:2',3'-*d*]pyrrole (**83**)^[18]



A solution of 3,3'-dibromo-5,5'-bis(trimethylsilyl)-2,2'-bithiophene **45** (4.00 g, 8.54 mmol), NaO^tBu (1.97 g, 20.5 mmol), Pd_2dba_3 (0.22 g, 0.21 mmol), and BINAP (0.53 g, 0.85 mmol) in dry toluene (50 mL) was purged with argon for 20 min. Hexylamine (0.86 g, 8.54 mmol) was added and the mixture was stirred for 21 h at $110\text{ }^{\circ}\text{C}$. After cooling to room temperature, water was added and the layers were separated. The product was extracted twice from the aqueous phase with diethyl ether. The combined organic layers were dried over Na_2SO_4 , filtered off and the solvent was removed under

vacuum. The crude compound was further purified by column chromatography using aluminium oxide II and *n*-hexane to afford a colorless solid of DTP **83** (2.97 g, 7.28 mmol, 85%).

Mp: 94 – 95 °C.

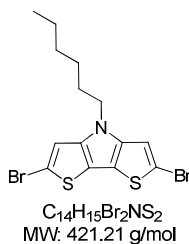
¹H NMR (CDCl₃, 400 MHz): δ = 7.05 (s, 2H, DTP-3,5), 4.18 (t, ³J = 7.1 Hz, 2H, α-CH₂-Hex), 1.91-1.84 (m, 2H, β-CH₂-Hex), 1.38-1.26 (m, 6H, 3xCH₂-Hex), 0.88 (t, ³J = 7.0 Hz, 3H, CH₃-Hex), 0.36 (s, 18H, TMS) ppm.

¹³C NMR (CDCl₃, 100 MHz): δ = 147.68, 138.30, 119.57, 116.46, 47.10, 31.20, 30.20, 26.48, 22.36, 13.78, -0.20 ppm.

MS (CI) *m/z*: calcd. for [M]⁺ (C₂₀H₃₃NS₂Si₂): 407; found: 407 [M]⁺.

Elemental analysis: calcd. for (C₂₀H₃₃NS₂Si₂): C, 58.91; H, 8.16; N, 3.43%; found: C, 59.14; H, 7.95; N, 3.63%.

2,6-Dibromo-*N*-hexyldithieno[3,2-*b*:2',3'-*d*]pyrrole (**84**)



In the absence of light, a solution of *N*-bromosuccinimide (2.49 g, 14.0 mmol) in 80 mL DMF was added dropwise to a solution of DTP **83** (2.60 g, 6.38 mmol) in 160 mL DMF at 0 °C. The reaction mixture was allowed to warm up slowly to room temperature within 2.5 h and stirred overnight. After diluting with DCM, the organic phase was washed with water and a sat. NaHCO₃ solution before being dried over Na₂SO₄. The solvent was concentrated in vacuum and the residue was diluted with *n*-hexane. The solution was filtered through a short pad of aluminium oxide II and eluted with *n*-hexane. Dibrominated DTP **84** (2.30 g, 5.46 mmol, 86%) was obtained as a colorless solid.

Mp: 80 - 82 °C.

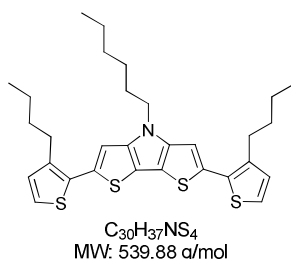
¹H NMR (CDCl₃, 400 MHz): δ = 7.02 (s, 2H, DTP-3,5), 4.08 (t, ³J = 7.1 Hz, 2H, α-CH₂-Hex), 1.84-1.77 (m, 2H, β-CH₂-Hex), 1.31-1.25 (m, 6H, 3xCH₂-Hex), 0.87 (t, ³J = 6.8 Hz, 3H, CH₃-Hex) ppm.

¹³C NMR (CDCl₃, 100 MHz): δ = 141.16, 114.44, 113.91, 109.42, 47.26, 31.03, 29.90, 26.25, 22.14, 13.64 ppm.

MS (CI) *m/z*: calcd. for [M]⁺ (C₁₄H₁₅Br₂NS₂): 421; found: 421 [M]⁺.

Elemental analysis: calcd. for ($C_{14}H_{15}NS_2Si_2$): C, 39.92; H, 3.59; N, 3.33%; found: C, 39.86; H, 3.59; N, 3.46%.

2,6-Bis(3-butylthien-2-yl)-*N*-hexyldithieno[3,2-*b*:2',3'-*d*]pyrrole (85)



Brominated DTP **84** (2.10 g, 4.99 mmol) and 3-butyl-2-(trimethyltin)thiophene **52** (3.77 g, 12.5 mmol) were dissolved in dry DMF (100 mL), degassed and $Pd(PPh_3)_4$ (0.28 g, 0.25 mmol) was added. The reaction mixture was heated at 80 °C for 21 h. Water was added and the product was extracted with DCM. The combined organic layers were dried over Na_2SO_4 , filtered off and the solvent was removed under vacuum. The crude product was purified by column chromatography using aluminium oxide II and *n*-hexane to obtain quaterthiophene **85** (2.14 g, 3.97 mmol, 80%) as a yellow oil.

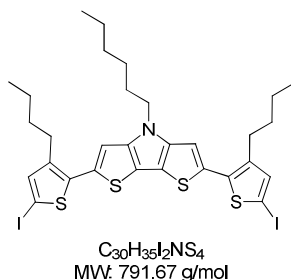
1H NMR ($CDCl_3$, 400 MHz): δ = 7.18 (d, 3J = 5.1 Hz, 2H, Th-5,5'), 7.02 (s, 2H, DTP-3,5), 6.95 (d, 3J = 5.1 Hz, 2H, Th-4,4'), 4.20 (t, 3J = 7.0 Hz, 2H, α -CH₂-Hex), 2.83 (t, 3J = 7.9 Hz, 4H, α -CH₂-Bu), 1.93-1.86 (m, 2H, β -CH₂-Hex), 1.69-1.62 (m, 4H, β -CH₂-Bu), 1.46-1.37 (m, 6H, 3xCH₂-Hex), 1.35-1.25 (m, 4H, γ -CH₂-Bu), 0.94 (t, 3J = 7.3 Hz, 6H, CH₃-Bu), 0.89 (t, 3J = 6.7 Hz, 3H, CH₃-Hex) ppm.

^{13}C NMR ($CDCl_3$, 100 MHz): δ = 144.00, 139.45, 133.60, 131.90, 130.08, 123.63, 114.84, 109.71, 47.41, 32.99, 31.41, 30.31, 29.00, 26.70, 22.66, 22.51, 13.98 ppm.

MS (MALDI-TOF) m/z : calcd. for $[M]^+$ ($C_{30}H_{37}NS_4$): 539.2; found: 539.4 $[M]^+$.

Elemental analysis: calcd. for ($C_{30}H_{37}NS_4$): C, 66.74; H, 6.91; N, 2.59%; found: C, 66.73; H, 6.91; N, 2.49%.

2,6-Bis(3-butyl-5-iodothiien-2-yl)-*N*-hexyldithieno[3,2-*b*:2',3'-*d*]pyrrole (87)

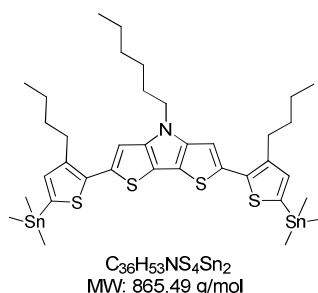


DTP-derivative **85** (160 mg, 0.30 mmol) was dissolved in dry CHCl_3 (10 mL) at 0 °C under exclusion of light. $\text{Hg}(\text{OAc})_2$ (189 mg, 0.60 mmol) was added and the mixture was stirred for 24 h at room temperature. The mixture was subsequently cooled to 0 °C and iodine (150 mg, 0.60 mmol) was added. The suspension was allowed to warm up to rt and was stirred for further 6 h. The resulting mixture was concentrated under vacuum and purified by column chromatography using aluminium oxide II and *n*-hexane (gradual addition of DCM) to obtain diiodinated DTP **87** (83.0 mg, 0.10 mmol, 35%) as an orange oil.

^1H NMR (CDCl_3 , 400 MHz): δ = 7.09 (s, 2H, DTP-3,5), 6.95 (s, 2H, Th-4,4'), 4.17 (t, 3J = 7.0 Hz, 2H, $\alpha\text{-CH}_2\text{-Hex}$), 2.77 (t, 3J = 7.8 Hz, 4H, $\alpha\text{-CH}_2\text{-Bu}$), 1.91-1.83 (m, 2H, $\beta\text{-CH}_2\text{-Hex}$), 1.65-1.58 (m, 4H, $\beta\text{-CH}_2\text{-Bu}$), 1.44-1.34 (m, 6H, 3x $\text{CH}_2\text{-Hex}$), 1.33-1.28 (m, 4H, $\gamma\text{-CH}_2\text{-Bu}$), 0.93 (t, 3J = 7.3 Hz, 6H, $\text{CH}_3\text{-Bu}$), 0.87 (t, 3J = 6.7 Hz, 3H, $\text{CH}_3\text{-Hex}$) ppm.

MS (MALDI-TOF) m/z : calcd. for $[\text{M}]^+$ ($\text{C}_{30}\text{H}_{35}\text{I}_2\text{NS}_4$): 790.9; found: 791.3 $[\text{M}]^+$.

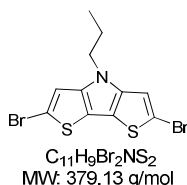
2,6-Bis(3-butyl-5-trimethylstannylthien-2-yl)-*N*-hexyldithieno[3,2-*b*:2',3'-*d*]pyrrole (**88**)



To a solution of DTP **87** (91.3 mg, 0.12 mmol) in dry THF (10 mL) was added dropwise *n*-BuLi (1.6 M in *n*-hexane, 0.16 mL, 0.25 mmol) at -78 °C within 20 min. After stirring between -75 and -65 °C for 40 min, Me_3SnCl (54.0 mg, 0.27 mmol) in dry THF (5 mL) was added slowly within 20 min. The reaction mixture was allowed to warm up to room temperature overnight. After quenching with water, the product was extracted with DCM and the combined organic layers were dried over Na_2SO_4 . The solvent was removed under vacuum and the crude distannylated DTP **88** (36% yield calcd. from ^1H -NMR) was not further purified.

^1H NMR (CDCl_3 , 400 MHz): overlapping signals of distannylated DTP **88**, monostannylated derivative **89** and quaterthiophene **85**.

MS (MALDI-TOF) m/z : calcd. for $[\text{M}]^+$ ($\text{C}_{36}\text{H}_{53}\text{NS}_4\text{Sn}_2$): 865.1; found: 865.1 $[\text{M}]^+$, 703.0 $[\text{M-TMSn}]^+$, 538.8 $[\text{M-2xTMSn}]^+$.

2,6-Dibromo-N-propyldithieno[3,2-*b*:2',3'-*d*]pyrrole (91)

In the absence of light, a solution of N-bromosuccinimide (2.14 g, 12.0 mmol) in 40 mL DMF was added dropwise to a solution of DTP **90** (2.14 g, 12.0 mmol) in 80 mL DMF at 0 °C. The reaction mixture was allowed to warm up slowly to room temperature and stirred overnight. Subsequently, it was poured onto a sat. $NaHCO_3$ /ice-solution whereby a solid precipitated. DCM was added and the organic layer was separated, dried over Na_2SO_4 and the solvent was removed under vacuum. The residue was filtered through a short pad of aluminium oxide II eluting with *n*-hexane. Dibrominated DTP **91** (1.85 g, 4.90 mmol, 90%) was obtained as a slightly yellow solid.

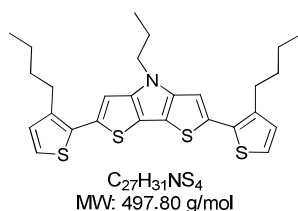
Mp: decomposition at 50 °C.

1H NMR (400 MHz, $CDCl_3$): δ = 7.03 (s, 2H, DTP-3,5), 4.06 (t, 3J = 7.0 Hz, 2H, α - CH_2 -Pr), 1.90-1.81 (m, 2H, β - CH_2 -Pr), 0.91 (t, 3J = 7.4 Hz, 3H, CH_3 -Pr) ppm.

^{13}C NMR (100 MHz, $THF-d_8$): δ = 142.57, 115.58, 110.03, 49.30, 24.16, 11.35 ppm.

MS (CI) m/z : calcd. for $[M]^+$ ($C_{11}H_9Br_2NS_2$): 379; found: 379 $[M]^+$.

Elemental analysis: calcd. for ($C_{11}H_9Br_2NS_2$): C, 34.85; H, 2.39; N, 3.69; S, 16.91%; found: C, 34.84; H, 2.45; N, 3.79; S, 16.83%.

2,6-Bis(3-butylthien-2-yl)-N-propyldithieno[3,2-*b*:2',3'-*d*]pyrrole (92)

DTP-derivative **91** (300 mg, 0.79 mmol) and 3-butyl-2-(trimethyltin)thiophene **52** (599 mg, 1.98 mmol) were dissolved in dry DMF (16 mL), degassed and tetrakis(triphenylphosphine) palladium(0) (45.7 mg, 39.6 μ mol) was added. The reaction mixture was heated for 27 h at 80 °C. After cooling to room temperature, water was added and the product was extracted with DCM. The combined organic layers were dried over Na_2SO_4 and the solvent was evaporated. The crude product was chromatographed on aluminium oxide II with a mixture of *n*-hexane:DCM (4:1) to obtain a yellow solid of quaterthiophene **92** (338 mg, 0.68 mmol, 86%).

Mp: 73 – 74 °C.

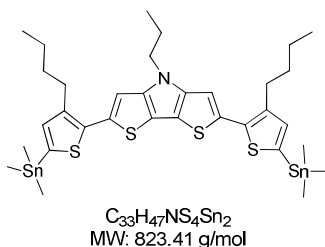
¹H NMR (400 MHz, CDCl₃): δ = 7.18 (d, ³J = 5.3 Hz, 2H, Th-5,5'), 7.03 (s, 2H, DTP-3,5), 6.95 (d, ³J = 5.4 Hz, 2H, Th-4,4'), 4.18 (t, ³J = 6.9 Hz, 2H, α-CH₂-Pr), 2.83 (t, ³J = 7.8 Hz, 4H, α-CH₂-Bu), 1.98-1.89 (m, 2H, β-CH₂-Pr), 1.70-1.62 (m, 4H, β-CH₂-Bu), 1.47-1.37 (m, 4H, γ-CH₂-Bu), 0.99 (t, ³J = 7.3 Hz, 3H, CH₃-Pr), 0.95 (t, ³J = 7.3 Hz, 6H, CH₃-Bu) ppm.

¹³C NMR (100 MHz, CDCl₃): δ = 144.05, 139.44, 133.60, 131.87, 130.08, 123.61, 114.84, 109.71, 49.03, 32.98, 29.00, 23.72, 22.66, 13.98, 11.70 ppm.

MS (MALDI-TOF) *m/z*: calcd. for [M]⁺ (C₂₇H₃₁NS₄): 497.1; found: 497.3 [M]⁺.

HRMS (MALDI-TOF) *m/z*: calcd. for [M]⁺ (C₂₇H₃₁NS₄): 497.13338; found: 497.13326 [M]⁺, δ_{m/m} = 0.2 ppm.

2,6-Bis(3-butyl-5-trimethylstannylthien-2-yl)-*N*-propyldithieno[3,2-*b*:2',3'-*d*]pyrrole (93)

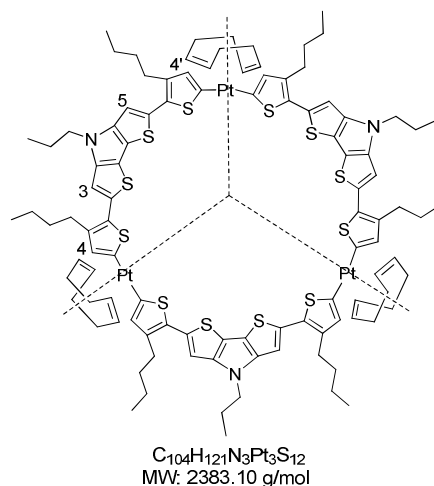


n-Butyl lithium (1.6 M in *n*-hexane, 0.89 mL, 1.42 mmol) was added dropwise to a solution of DTP-derivative **92** (300 mg, 0.60 mmol) in dry THF (2 mL) at -78 °C within 20 min. The mixture was stirred between -75 and -65 °C for 1 h. Afterwards, the cooling bath was removed and Me₃SnCl (294 mg, 1.48 mmol) in dry THF (0.5 mL) was added at once. Stirring was continued overnight during which time the mixture was allowed to warm up to room temperature. *n*-Hexane was added and lithium chloride precipitated as a white solid. The organic phase was washed several times with water and dried over Na₂SO₄. The solvent was removed under vacuum and the crude distannylated DTP **93** (95% calcd. from ¹H-NMR) was used without further purification in the next step.

¹H NMR (400 MHz, THF-*d*₈): δ = 7.14 (s, 2H, DTP-3,5), 7.03 (s, 2H, Th-4,4'), 4.25 (t, ³J = 6.9 Hz, 2H, α-CH₂-Pr), 2.85 (t, ³J = 7.8 Hz, 4H, α-CH₂-Bu), 1.96-1.87 (m, 2H, β-CH₂-Pr), 1.69-1.61 (m, 4H, β-CH₂-Bu), 1.46-1.37 (m, 4H, γ-CH₂-Bu), 0.97-0.92 (m, 9H, CH₃-Pr, CH₃-Bu), 0.36 (s, 18H, TMSn) ppm.

¹³C NMR (100 MHz, THF-*d*₈): δ = 145.06, 140.79, 139.00, 138.50, 136.86, 134.49, 115.37, 110.11, 49.16, 33.97, 32.35, 29.56, 23.46, 14.15, 11.64, -8.67 ppm.

MS (MALDI-TOF) *m/z*: calcd. for [M]⁺ (C₃₃H₄₇NS₄Sn₂): 823.1; found: 823.4 [M]⁺, 661.1 [M-TMSn]⁺.

Pt(COD)[12]DTP (94)

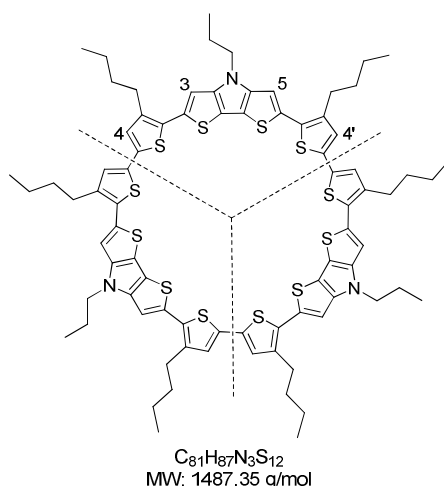
Distannylated quaterthiophene **93** (185 mg, 225 μ mol) and $PtCl_2(COD)$ (84.2 mg, 225 μ mol) were dissolved in dichloromethane (200 mL) and refluxed for 4 days. The mixture was cooled to room temperature and filtered through a column packed with aluminium oxide IV (DCM as eluent). The solvent was evaporated and a red-orange solid was obtained. Isolation of macrocyclic **94** (50 mg, 20.8 μ mol, 28%) was achieved by SEC with THF as eluent.

Mp: decomposition at 210 $^{\circ}C$.

1H NMR (400 MHz, THF- d_8): δ = 6.89 (s, 6H, DTP-3,5), 6.94 (s, 6H, Th-4,4'), 5.50 (s, 12H, COD-CH), 4.10 (t, 3J = 6.9 Hz, 6H, α -CH $_2$ -Pr), 2.79 (t, 3J = 7.7 Hz, 12H, α -CH $_2$ -Bu), 2.64 (s, 24 H, COD-CH $_2$), 1.86-1.77 (m, 6H, β -CH $_2$ -Pr), 1.68-1.61 (m, 12H, β -CH $_2$ -Bu), 1.46-1.37 (m, 12H, γ -CH $_2$ -Bu), 0.92 (t, 3J = 7.3 Hz, 18H, CH $_3$ -Bu), 0.87 (t, 3J = 7.4 Hz, 9H, CH $_3$ -Pr) ppm.

HRMS (MALDI-TOF) m/z : calcd. for $[M]^+$ ($C_{105}H_{123}N_3Pt_3S_{12}$): 2394.52926; found: 2394.53569 $[M]^+$ ($\delta_{m/m}$ = 2.6 ppm), 2287.44417 $[M-COD]^+$, 2091.47637 $[M-COD-Pt]^+$, 1982.38387 $[M-2xCOD-Pt]^+$, 1788.41685 $[M-2xCOD-2xPt]^+$, 1485.35664 $[M-3xCOD-3xPt]^+$.

^{13}C NMR could not be measured due to poor solubility.

C[12]DTP (96)

Distannylated quaterthiophene **93** (458 mg, 557 μ mol) and PtCl₂(COD) (219 mg, 586 μ mol) were dissolved in dichloromethane (700 mL) and refluxed for 5 days. The mixture was cooled to room temperature and filtered through a column packed with aluminium oxide IV (DCM as eluent). The solvent was evaporated and a red-orange solid (447 mg) was obtained.

50.0 mg of the crude product (containing 62.5 μ mol of Pt(COD)DTP-units) and 1,1'-bis(diphenylphosphino) ferrocene (38.0 mg, 68.8 μ mol) were dissolved in 20 mL dry dichloromethane at room temperature. The reaction mixture was stirred overnight. Subsequently, the solvent was evaporated and 1,5-cyclooctadiene was removed under high vacuum. The obtained solid was dissolved in dry THF (30 mL) at room temperature and silver triflate (36.3 mg, 141 μ mol, 2.10 eq. per Pt) was added. The mixture was stirred overnight and the organic suspension was diluted with DCM and washed successively with brine and water. The organic layer was dried over MgSO₄ and filtered through a short pad of aluminium oxide IV to remove precipitated platinum and silver. The solvent was evaporated to provide a deep red residue and isolation as well as purification of DTP-macrocyclic **96** (9.00 mg, 6.04 μ mol, 29%) was performed by SEC (THF) to obtain a redbrown solid.

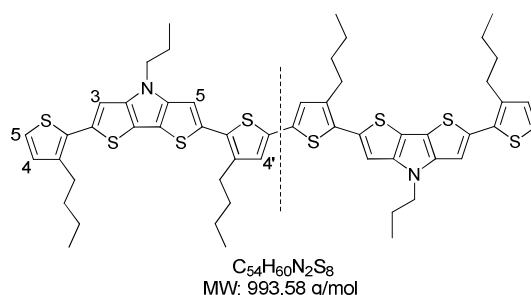
Mp: decomposition at 250 °C.

¹H NMR (400 MHz, THF-d₈): δ = 7.14 (s, 6H, DTP-3,5), 7.08 (s, 6H, Th-4,4'), 4.21 (t, ³J = 6.8 Hz, 6H, α -CH₂-Pr), 2.85 (t, ³J = 7.6 Hz, 12H, α -CH₂-Bu), 1.92-1.87 (m, 6H, β -CH₂-Pr), 1.77-1.72 (m, 12H, β -CH₂-Bu), 1.51-1.42 (m, 12H, γ -CH₂-Bu), 0.98 (t, ³J = 7.3 Hz, 18H, CH₃-Bu), 0.94 (t, ³J = 7.0 Hz, 9H, CH₃-Pr) ppm.

MS (MALDI-TOF) m/z : calcd. for [M]⁺ (C₈₁H₈₇N₃S₁₂): 1485.3; found: 1486.2 [M+H]⁺.

HRMS (MALDI-TOF) m/z : calcd. for [M]⁺ (C₈₁H₈₇N₃S₁₂): 1485.35430; found: 1485.35385, $\delta_{m/m}$ = 0.3 ppm.

¹³C NMR could not be measured due to poor solubility.

L[8]DTP (97)

DTP-quaterthiophene **92** (100 mg, 0.20 mmol) was dissolved in dry THF (1.4 mL) and cooled to -78 °C. *n*-Butyl lithium (1.6 M in *n*-hexane, 0.18 mL, 0.30 mmol) was added dropwise over a period of 5 min at this temperature. The reaction mixture was stirred between -78 and -65 °C for 1 h and copper(II) chloride (66.0 mg, 0.49 mmol) was added in several portions under vigorous stirring. The mixture turned dark brown and some black solid deposited. After complete addition, stirring was continued for 1 hour at -70 °C. The reaction mixture was allowed to warm up to -10 °C overnight and stirring was continued for an additional hour at rt. Subsequent hydrolysis with a 2 N HCl-solution was carried out under ice-cooling, whereas the solid dissolved. The layers were separated and extraction of the aqueous phase with DCM followed. The combined organic layers were washed with water, dried over Na₂SO₄ and the solvent was removed under reduced pressure. The oligomer was purified by column chromatography using aluminium oxide II and a mixture of *n*-hexane:DCM (7:3) to obtain an orange solid of L[8]DTP **97** (17.0 mg, 17.1 μmol, 17%).

Mp: 152 – 154 °C.

¹H NMR (400 MHz, THF-d₈): δ = 7.25 (d, ³J = 5.2 Hz, 2H, Th-5), 7.23 (s, 2H, DTP-3), 7.18 (s, 2H, DTP-5), 7.12 (s, 2H, Th-4'), 6.95 (d, ³J = 5.3 Hz, 2H, Th-4), 4.28 (t, ³J = 6.9 Hz, 4H, α-CH₂-Pr), 2.88-2.83 (m, 8H, α-CH₂-Bu), 1.96-1.90 (m, 4H, β-CH₂-Pr), 1.75-1.62 (m, 8H, β-CH₂-Bu), 1.51-1.36 (m, 8H, γ-CH₂-Bu), 0.98-0.91 (m, 18H, CH₃-Bu, CH₃-Pr) ppm.

¹³C NMR (125 MHz, THF-d₈): δ = 145.33, 145.12, 140.53, 139.92, 135.31, 134.46, 133.71, 132.64, 131.91, 130.60, 127.15, 124.42, 115.61, 115.45, 110.69, 110.47, 49.16, 33.77, 33.49, 29.84, 29.61, 24.40, 23.36, 23.30, 14.13, 14.11, 11.62 ppm.

MS (MALDI-TOF) *m/z*: calcd. for [M]⁺ (C₅₄H₆₀N₂S₈): 992.3; found: 992.8 [M]⁺.

HRMS (MALDI-TOF) *m/z*: calcd. for [M]⁺ (C₅₄H₆₀N₂S₈): 992.25167; found: 992.25095, δ_{m/m} = 0.7 ppm.

4.9 References

- [1] S. J. Evenson, S. C. Rasmussen, *Org. Lett.* **2010**, *12*, 4054-4057.
- [2] K. Ogawa, S. C. Rasmussen, *Macromolecules* **2006**, *39*, 1771-1778.
- [3] K. Ogawa, J. A. Stafford, S. D. Rothstein, D. E. Tallman, S. C. Rasmussen, *Synth. Met.* **2005**, *152*, 137-140.
- [4] S. C. Price, A. C. Stuart, W. You, *Macromolecules* **2010**, *43*, 797-804.
- [5] K. R. Radke, K. Ogawa, S. C. Rasmussen, *Org. Lett.* **2005**, *7*, 5253-5256.
- [6] W. Vanormelingen, K. Van den Bergh, G. Koeckelberghs, *Macromolecules* **2008**, *41*, 5582-5589.
- [7] A. Yassin, P. Leriche, J. Roncali, *Macromol. Rapid Commun.* **2010**, *31*, 1467-1472.
- [8] X. Zhang, T. T. Steckler, R. R. Dasari, S. Ohira, W. J. Potscavage, S. P. Tiwari, S. Coppée, S. Ellinger, S. Barlow, J. L. Brédas, B. Kippelen, J. R. Reynolds, S. R. Marder, *J. Mater. Chem.* **2010**, *20*, 123-134.
- [9] E. Zhou, J. Cong, K. Hashimoto, K. Tajima, *Energy Environ. Sci.* **2012**, *5*, 9756-9759.
- [10] A. Yassin, P. Leriche, M. Allain, J. Roncali, *New J. Chem.* **2013**, *37*, 502-507.
- [11] R. Gisorio, G. Allegretta, G. P. Suranna, P. Mastroilli, A. Loiudice, A. Rizzo, M. Mazzeo, G. Gigli, *J. Mater. Chem.* **2012**, *22*, 19752-19760.
- [12] S. C. Rasmussen, S. J. Evenson, *Prog. Polym. Sci.* **2013**, *38*, 1773-1804.
- [13] P. Zanirato, P. Spagnolo, G. Zanardi, *J. Chem. Soc., Perkin Trans. 1* **1983**, 2551-2554.
- [14] A. Berlin, G. Pagani, G. Zotti, G. Schiavon, *Makromol. Chem.* **1992**, *193*, 399-409.
- [15] K. Ogawa, K. R. Radke, S. D. Rothstein, S. C. Rasmussen, *J. Org. Chem.* **2001**, *66*, 9067-9070.
- [16] K. Ogawa, S. C. Rasmussen, *J. Org. Chem.* **2003**, *68*, 2921-2928.
- [17] G. Koeckelberghs, L. De Cremer, A. Persoons, T. Verbiest, *Macromolecules* **2007**, *40*, 4173-4181.
- [18] G. Koeckelberghs, L. De Cremer, W. Vanormelingen, W. Dehaen, T. Verbiest, A. Persoons, C. Samyn, *Tetrahedron* **2005**, *61*, 687-691.
- [19] J. P. Wolfe, S. Wagaw, S. L. Buchwald, *J. Am. Chem. Soc.* **1996**, *118*, 7215-7216.
- [20] M. S. Driver, J. F. Hartwig, *J. Am. Chem. Soc.* **1996**, *118*, 7217-7218.
- [21] J. F. Hartwig, *Angew. Chem.* **1998**, *110*, 2154-2177; *Angew. Chem. Int. Ed.* **1998**, *37*, 2046-2067.
- [22] Y. A. Getmanenko, P. Tongwa, T. V. Timofeeva, S. R. Marder, *Org. Lett.* **2010**, *12*, 2136-2139.
- [23] M. Schnürch, M. Spina, A. F. Khan, M. D. Mihovilovic, P. Stanetty, *Chem. Soc. Rev.* **2007**, *36*, 1046-1057.
- [24] J. Fröhlich, W. Kalt, *J. Org. Chem.* **1990**, *55*, 2993-2995.
- [25] J. Fröhlich, C. Hametner, W. Kalt, *Monatsh. Chem.* **1996**, *127*, 435-443.
- [26] J. Fröhlich, *Bull. Soc. Chim. Belg.* **1996**, *105*, 615-634.
- [27] J. F. Bunnett, *Acc. Chem. Res.* **1972**, *5*, 139-147.
- [28] E. Lukevics, P. Arsenyan, S. Belyakov, J. Popelis, O. Pudova, *Tetrahedron Lett.* **2001**, *42*, 2039-2041.
- [29] M. S. Driver, J. F. Hartwig, *J. Am. Chem. Soc.* **1997**, *119*, 8232-8245.
- [30] J. F. Hartwig, *Synlett* **1997**, *4*, 329-340.
- [31] J. F. Hartwig, *Acc. Chem. Res.* **1998**, *31*, 852-860.
- [32] D. S. Surry, S. L. Buchwald, *Angew. Chem. Int. Ed.* **2008**, *47*, 6338-6361.
- [33] J. P. Wolfe, S. L. Buchwald, *J. Org. Chem.* **1996**, *61*, 1133-1135.

- [34] Susan A. Odom, K. Lancaster, L. Beverina, Kelly M. Lefler, Natalie J. Thompson, V. Coropceanu, J.-L. Brédas, Seth R. Marder, S. Barlow, *Chem. Eur. J.* **2007**, *13*, 9637-9646.
- [35] R. Grisorio, G. Allegretta, G. P. Suranna, P. Mastrorilli, A. Loiudice, A. Rizzo, M. Mazzeo, G. Gigli, *J. Mater. Chem.* **2012**, *22*, 19752-19760.
- [36] P. Imin, M. Imit, A. Adronov, *Macromolecules* **2011**, *44*, 9138-9145.
- [37] H. Mo, K. R. Radke, K. Ogawa, C. L. Heth, B. T. Erpelding, S. C. Rasmussen, *Phys. Chem. Chem. Phys.* **2010**, *12*, 14585-14595.
- [38] M. Bednarz, P. Reineker, E. Mena-Osteritz, P. Bäuerle, *J. Lumin.* **2004**, *110*, 225-231.
- [39] E. Mena-Osteritz, F. Zhang, G. Götz, P. Reineker, P. Bäuerle, *Beilstein J. Nanotechnol.* **2011**, *2*, 720-726.
- [40] F. Zhang, G. Götz, H. D. F. Winkler, Christoph A. Schalley, P. Bäuerle, *Angew. Chem. Int. Ed.* **2009**, *48*, 6632-6635.
- [41] F. Zhang, *unpublished results*.
- [42] F. Zhang, G. Götz, E. Mena-Osteritz, M. Weil, B. Sarkar, W. Kaim, P. Bäuerle, *Chem. Sci.* **2011**, *2*, 781-784.
- [43] P. Bäuerle, U. Segelbacher, A. Maier, M. Mehring, *J. Am. Chem. Soc.* **1993**, *115*, 10217-10223.
- [44] J. A. E. H. van Haare, E. E. Havinga, J. L. J. van Dongen, R. A. J. Janssen, J. Cornil, J.-L. Brédas, *Chem. Eur. J.* **1998**, *4*, 1509-1521.
- [45] V. M. Geskin, J.-L. Brédas, *ChemPhysChem* **2003**, *4*, 498-504.

CHAPTER 5

Peripherically Functionalized π -Conjugated Cyclo[n]thiophenes

5.1. Introduction

The second molecular design concept focuses on the attachment of functional groups to the periphery of macrocyclic systems to create shape-persistent, fully π -conjugated C[n]Ts with external reactive centers for potential chemical reactions or self-aggregation processes into well defined two-dimensional pattern. Improved charge mobilities are supposed and might make the macrocycles attractive candidates for a possible application in electronic nanotechnology. The modification process to realize macrocycles which comply the demands for that concept is depicted schematically in Chart 5.1. Thus, a dendritic terthiophene moiety CHO-3T with an aldehyde group was selected as target precursor. The aldehyde unit should give access to the potential introduction of various organic functionalities to the outer sphere of the prospective macrocycles which might influence the electronic properties or self-aggregation behaviour.

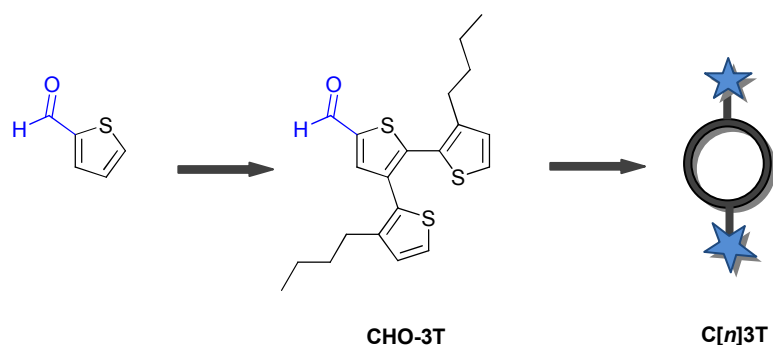


Chart 5.1: Structure of selected terthiophene moiety CHO-3T and prospective macrocycle series C[n]3T.

Further aspects were taken into account for the build-up of CHO-3T: The inserted butyl side chains are supposed to provide solubility of the precursor and induce the external thiophene units in a position with the sulfur atoms facing each other. This conformation should support the macrocyclization step since its bent in a crescent shape. To gain more information about the special molecular configuration of the precursor, the geometry of CHO-3T was optimized via Austin Model 1 (AM1) calculations with defined Hartree Fock conditions. Any functionality on the remaining α -positions was not taken into account for the computational optimization in order to facilitate the calculation process. This fact should not influence the geometry of the conjugated backbone. The value of the inner angle was determined by drawing manually straight lines through print-outs of the molecule like depicted in Figure 5.1 and revealed a value of 25°. Such a small angle should be predestinated to form one defined macrocycle with two monomer moieties and diminish side reactions drastically. A high conversion to a cyclic dimer is expected. It is worth to mention, that the resulting macrocycles will end up in constitutional isomers, since the presented dendritic terthiophene precursor CHO-3T is asymmetric (see Chart 5.2).

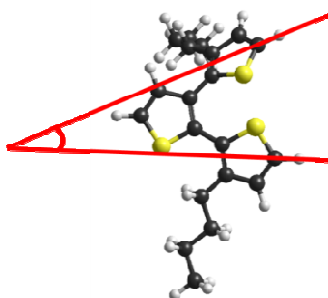


Figure 5.1: Calculated structure of dendritic CHO-3T.

Synthetic details, characterizations (proton NMR spectroscopy, mass spectrometry), and information about photophysical properties (UV/vis absorption and fluorescence spectroscopy, cyclic voltammetry) of the peripherically functionalized π -conjugated macrocycles are presented in the following sections.

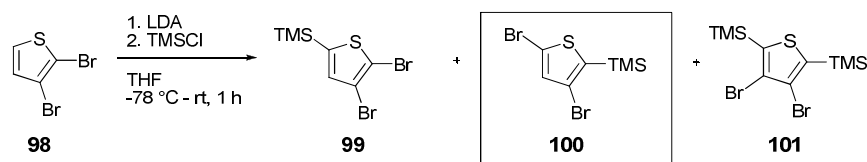
5.2 Synthesis of aldehyde-substituted oligothieryl macrocycles

5.2.1. Synthesis of aldehyde-substituted oligothieryl precursors

5.2.1.1 Synthesis of dendritic terthiophene TMS-3T (**99**)

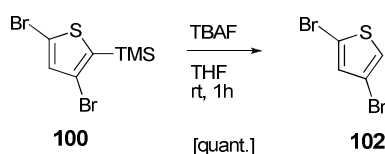
Instead of the final aldehyde group, a first idea was to attach a trimethylsilyl group at the α -position of the core thiophene unit in the dendritic target oligomer CHO-3T. The TMS group displays a versatile functionality which can easily be transferred through an *ipso*-reaction for example into a halogen atom and further be replaced by other reactive organic substituents.

The synthetic pathway is depicted in Scheme 5.1 and starts from 2,3-dibromothiophene **98**, which was slowly added to LDA (1.0 eq.) at $-78\text{ }^{\circ}\text{C}$ in THF after a protocol of Seconi et al.^[1] The metalated species was quenched after a period of 5 min with chlorotrimethylsilane and the crude product was characterized by GC-MS analysis. Only one signal with a mass of $m/z = 314$ appeared that fitted to the desired compound **99**. Seconi mentioned in his publication the occurrence of regioisomers, but declared 2,3-dibromo-5-trimethylsilylthiophene **99** to be the main product.^[1] The potential regioisomer **100** would emerge due to a ‘base-catalyzed halogen dance reaction’ during which the anion is formed at the more stable 2-position between the sulfur and adjacent bromine atom. Subsequent addition of TMSCl would lead to the undesired 2,4-dibromo-5-trimethylsilylthiophene **100**.



Scheme 5.1: Unsuccessful synthesis of target molecule **99**.

Investigations of the isolated main reaction product by proton and carbon NMR spectroscopy did not allow a defined determination of the structure since both regioisomers **99** and **100** would show the same spectroscopic characteristics. To gain more information about the present material, a deprotection of the crude reaction product was carried out under general standard conditions with tetra-*n*-butylammonium fluoride (Scheme 5.2).



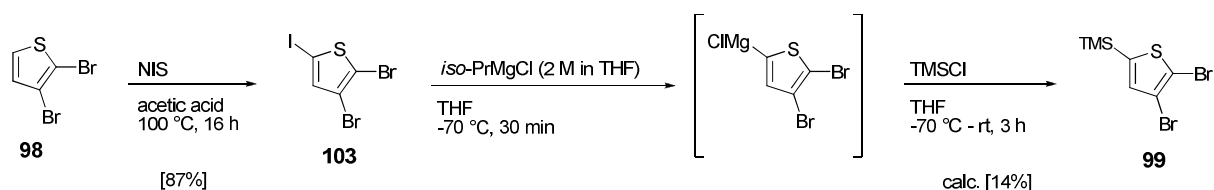
Scheme 5.2: Deprotection of regioisomer **100** with TBAF.

Investigations of the deprotected crude material via ^1H NMR spectroscopy revealed regioisomer **100** to be the real main product. The deprotection generated thiophene **102** with a 2,4-substitution pattern for the bromine atoms exhibiting two singlet signals in the recorded proton NMR spectrum. If target compound **99** would have been formed, two dublet signals for the deprotected regained starting material **98** would have been expected. The NMR results confirmed the wrongly ascribed main product by Seconi since a halogen dance rearrangement caused by LDA took clearly place. Some examples for regioselective halogen migrations at thiophene and phenyl derivatives have been published in literature.^[2-8] It is described that the halogen dance reaction can be diminished by a fast addition of the organic base to obtain an excess of deprotonated molecules whereby no halogen exchange can occur.

Thus, in a second experiment, the amount of utilized organic base LDA was increased to 1.6 equivalents with otherwise constant reaction conditions. Investigations during the reaction via GC-MS revealed two very narrow (0.2 min distance), but baseline separated signals with an identical mass of $m/z = 314$ which were ascribed to **99** and **100**. A ratio of 33%:36% was calculated via GC-analysis. Attempts to separate both TMS-functionalized isomers via column chromatography or distillation failed. Additionally, a signal at higher retention time with a mass of $m/z = 386$ appeared, which was assigned to the twofold functionalized TMS-molecule **101**. Unknown byproducts appeared as well. A third experiment with 2.5 equivalents of LDA resulted in no improvement.

Since a direct introduction of the TMS group turned out to be problematic, an alternative synthetic route was elaborated, in which the same starting material as above, 2,3-dibromothiophene **98**, was iodinated with NIS in acetic acid at 100 °C (Scheme 5.3). After crystallization from *n*-hexane, iodothiophene **103** was obtained in 87% yield.

It was further reacted with *iso*-PrMgCl to form the corresponding Grignard-intermediate. Reaction control was carried out via GC-MS and GC-analysis of aqueous worked-up samples, which proved a complete conversion after 30 min. The far better reactivity of iodine towards the Grignard reagent in contrast to bromine was exploited during this reaction.^[9] However, a reaction of the Grignard intermediate with TMSCl to target thiophene **99** was hardly observed. Besides retrieved starting material **98** as main product, TMS-substituted thiophene **99** was obtained in 14% yield. The value was calculated via GC-analysis from the crude mixture since the molecule could not be isolated. A too weak electrophilicity of TMSCl was assumed to be the reason for the poor reactivity.

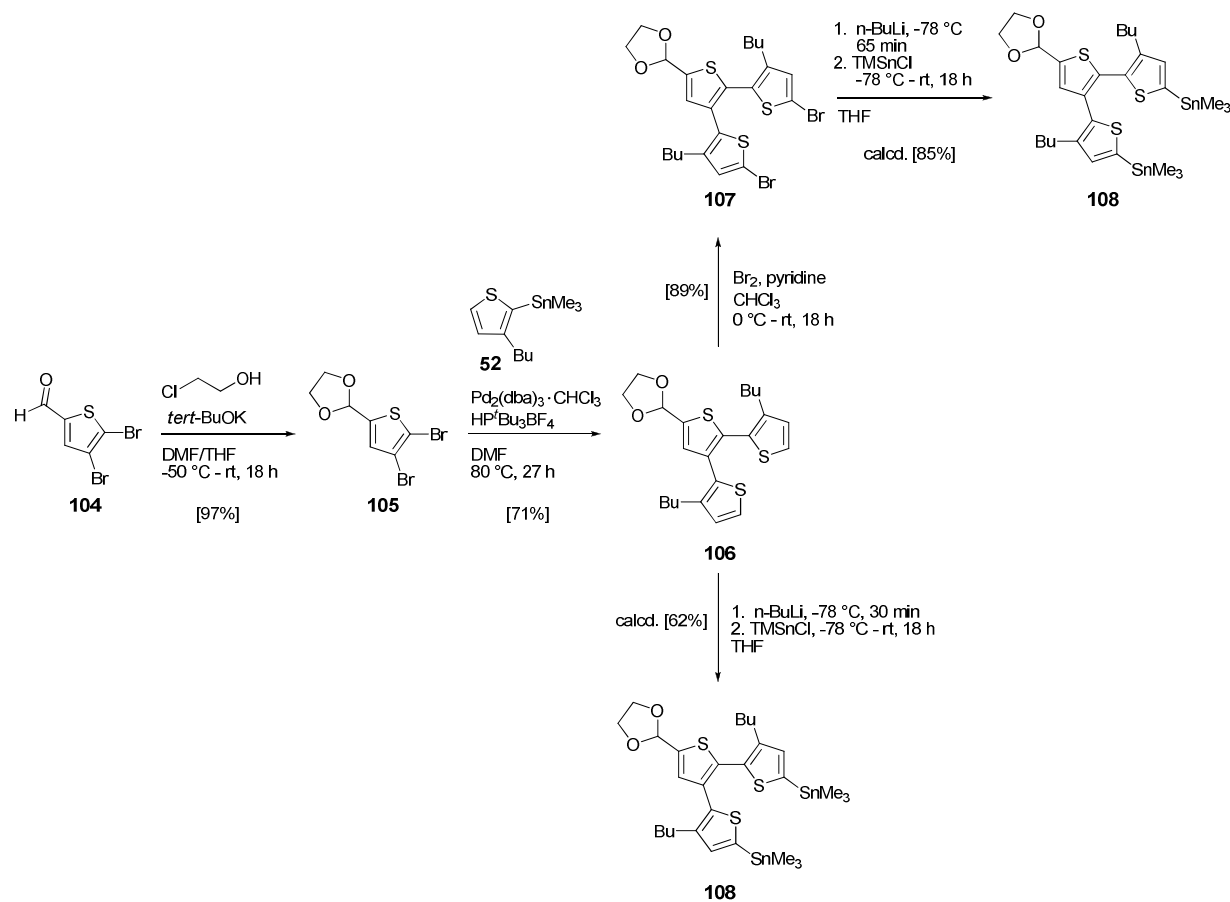


Scheme 5.3: Alternative synthetic route towards **99** via a Grignard reaction with *iso*-PrMgCl.

Since both synthetic attempts to introduce a functional TMS group resulted in dissatisfying results, an aldehyde-group as organic functionality was chosen instead. The elaborate synthesis towards the aldehyde-functionalized dendritic terthiophene is described in the following chapter and outlined in Scheme 5.4.

5.2.1.2 Synthesis of dendritic terthiophene CHO-3T (**106**)

Commercially available 4,5-dibromothiophene-2-carboxaldehyde **104** was protected with chloroethanol under basic conditions in a mixture of DMF and THF at -50 °C after a protocol of Makosza.^[10] The protection of the aldehyde group was essential due to a later lithiation with *n*-BuLi, which would otherwise attack the aldehyde group. Protected thiophene **105** was isolated in 97% yield and subsequently reacted in a palladium-catalyzed Stille cross-coupling reaction with 3-butyl-(2-trimethyltin)thiophene **52** to generate 4,5-linked terthiophene **106**. After purification via column chromatography, branched terthiophene **106** was obtained pure in 71% yield.



Scheme 5.4: Synthesis of dendritic precursor **108**.

The following proton-metal exchange was carried out with *n*-butyl lithium and the formed ionized species was trapped afterwards with trimethyltin chloride to provide distannylated terthiophene **108**. The conversion of the stannylation reaction yielded 62% (calcd. from ^1H NMR) and is insufficient for a consecutive macrocyclization step. The corresponding monostannylated derivative was observed as the only byproduct in 38% yield. The lithiation of branched thiophene **106** was as well performed under highly concentrated conditions and elevated temperatures at $0\text{ }^{\circ}\text{C}$. However, an improved conversion of the double lithiated species was not obtained.

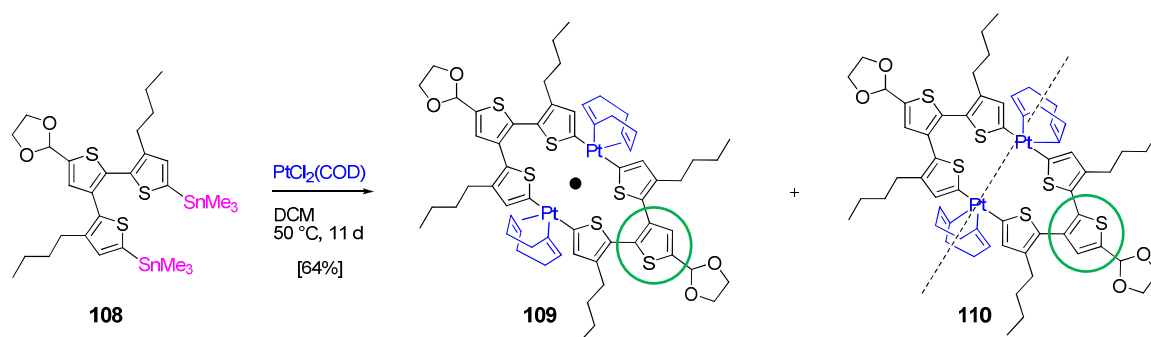
Terthiophene **106** was then subjected to a bromination reaction with elemental bromine in chloroform at $0\text{ }^{\circ}\text{C}$ under exclusion of light. Pyridine was added as an organic base to trap arising acidic HBr and prevent elimination of the acetal protecting group. Dihalogenated terthiophene **107** was obtained in 89% yield after purification using silica column chromatography. The introduction of bromine atoms at both available α -positions should increase the conversion of the following stannylation reaction, since a halogen-metal exchange is known to react more selective and fast than a comparable proton-metal exchange which was investigated prior.

Eventually, the stannylation reaction was carried out under consistent reaction conditions with *n*-butyl lithium and TMSnCl to afford target oligothiophene **108** in 85% yield (calcd. from ^1H NMR). The observed 15% byproduct were ascribed to the monostannylated analogue.

The obtained acetal-functionalized dendritic terthiophene unit **108** presents the desired precursor in the following macrocyclization reaction.

5.2.1.3 π -Conjugated peripherally functionalized cyclo[*n*]thiophenes via oxidatively induced reductive elimination

Distannylated terthiophene **108** was converted into shape-persistent and stable Pt^{II} -metallacycles **109** and **110** by refluxing it with transition metal complex $\text{PtCl}_2(\text{COD})$ for 7 days (Scheme 5.5). The progressing conversion of the starting material into the Pt^{II} complexes was monitored via proton NMR spectroscopy, as already described for the acceptor and donor-functionalized macrocycles. The decrease of the singlet signal of the tin-groups of precursor **108** was compared to the increase of the arising chlorotrimethyl stannane signal. Additionally, typical signals of reacted, thus inserted COD ligands, occurred. The crude reaction mixture was filtered through a plug of aluminium oxide to remove cleaved-off Me_3SnCl and the product was purified afterwards via SEC (THF). One visible main fraction was obtained and characterized by mass spectrometry indicating the isolation of a metallamacrocycle consisting of six thiophene units in 64% yield. Due to the asymmetry of the utilized precursor **108**, the existence of two regioisomeric pretemplated rings within this fraction was expected and confirmed by proton NMR spectroscopy (Figures 5.2 and 5.3). Thus, the formation of cyclic metalladimer species proceeded highly selective to point-symmetric macrocycle **109** and axial-symmetric ring **110**. No higher analogues were detected.



Scheme 5.5: Synthesis of cyclic metalladimers **109** and **110**.

It is clearly visible that the assumed and possible mixture of the two regioisomers **109** and **110** was formed, since in the ^1H NMR spectrum of the separated main fraction an exact double set of

expected signals for a single ring occurred (Figures 5.2 and 5.3). By calculating the integrals of the signals, a statistical 1:1 mixture of both isomers is observed.

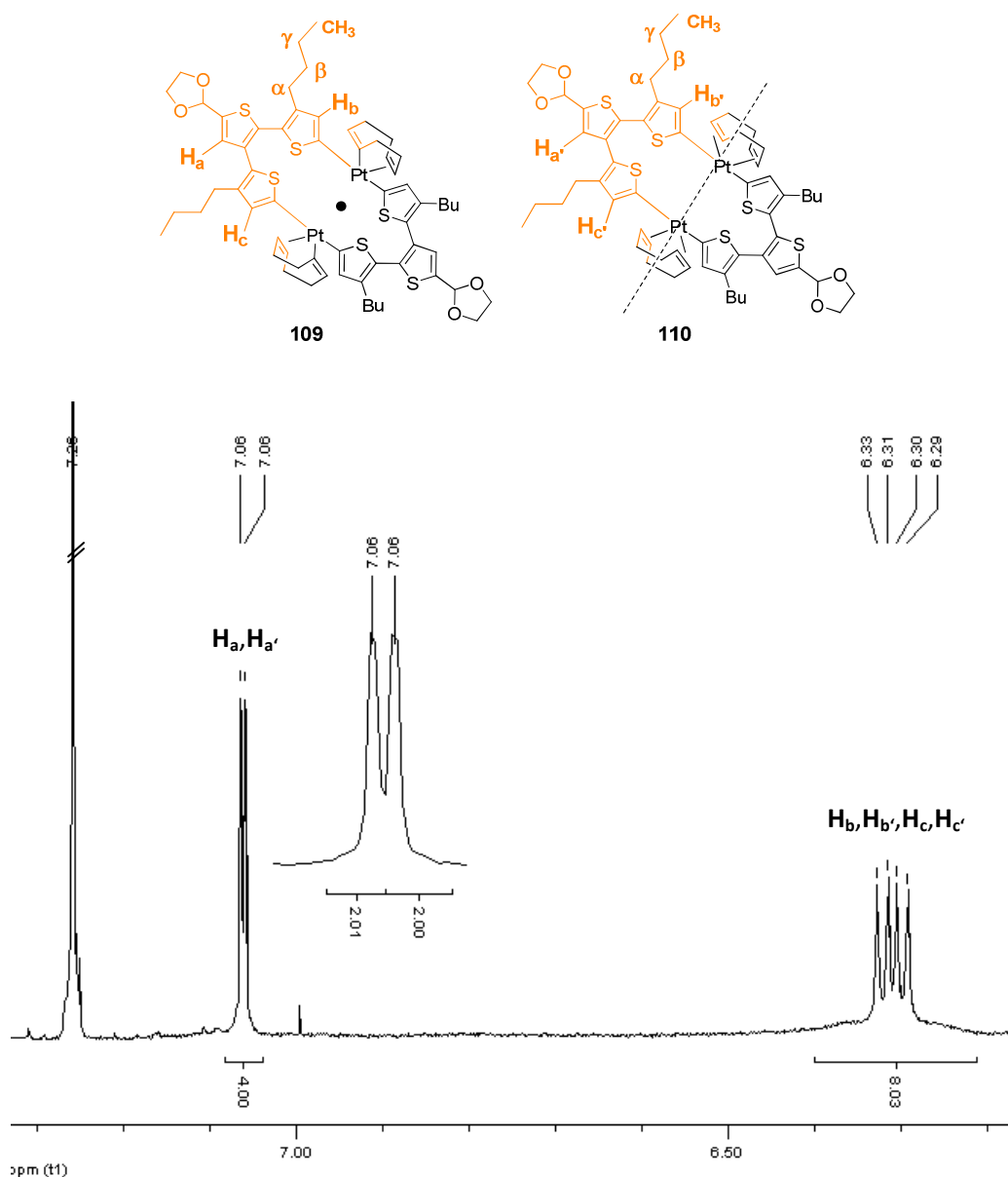


Figure 5.2: Aromatic region of the ^1H NMR spectrum of a 1:1-mixture of metallaregioisomers **109:110**, measured in CDCl_3 (400 MHz).

The two singlets at $\delta = 7.06$ ppm are assigned to $\text{H}_a, \text{H}_{a'}$ and the four singlets at $\delta = 6.33$ - 6.29 ppm to $\text{H}_b, \text{H}_{b'}$ and $\text{H}_c, \text{H}_{c'}$ and belong to the protons of the terthiophene subunits. The signal at $\delta = 6.08$ ppm can be ascribed to the proton of the acetal-protecting group (OCH). The multiplets of the OCH_2 -groups of the ethylene glycol bridges were located at $\delta = 4.14$ and 4.01 ppm. The signals of the COD ligands occurred at $\delta = 5.47$ ppm ($\text{HC}=\text{CH}$) and at $\delta = 2.62$ ppm (CH_2). Multiplet signals for the butyl side chains are upfield shifted at $\delta = 2.46$ - 2.36 , 1.44 , 1.21 , and 0.82 ppm for the α - CH_2 , β - CH_2 , γ - CH_2 , and CH_3 -groups, respectively.

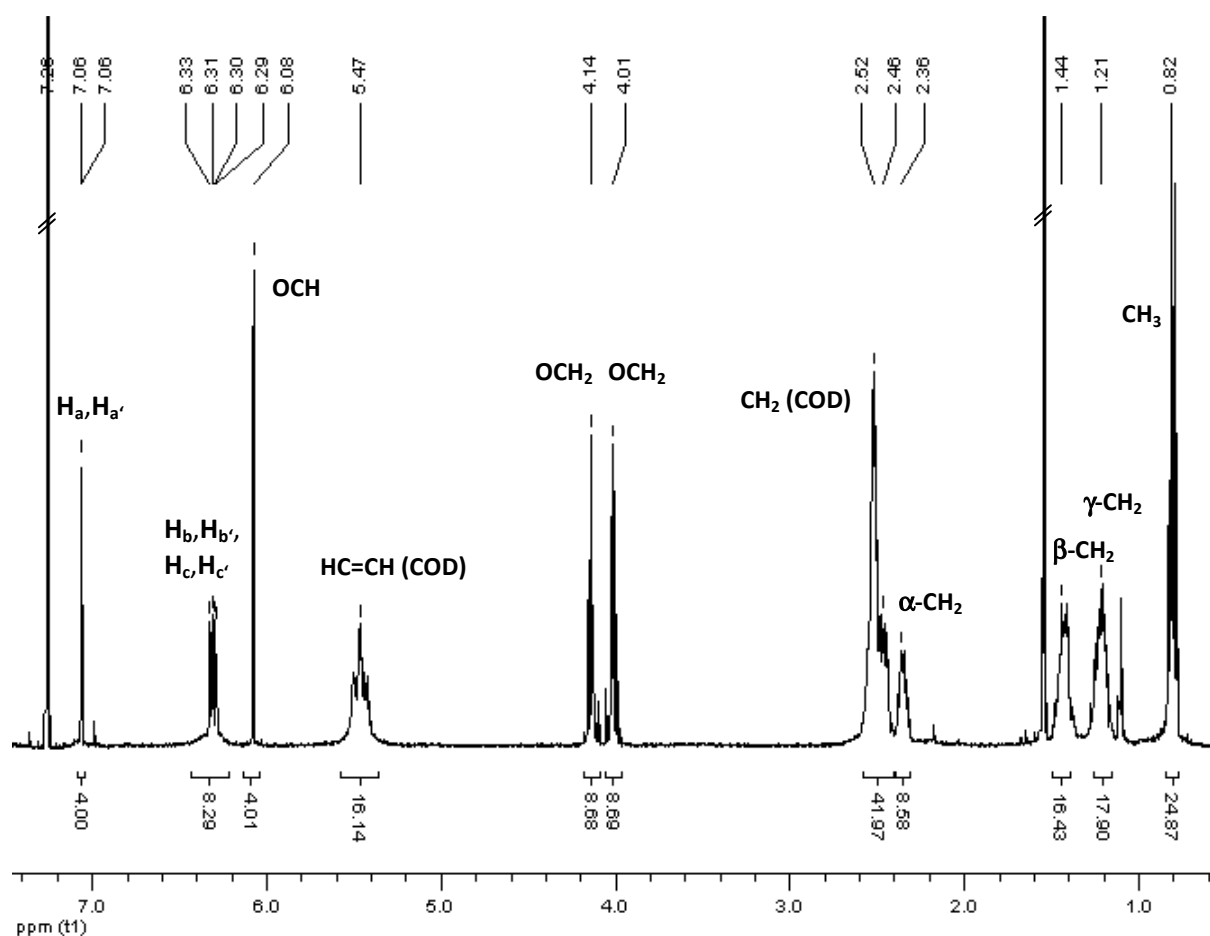
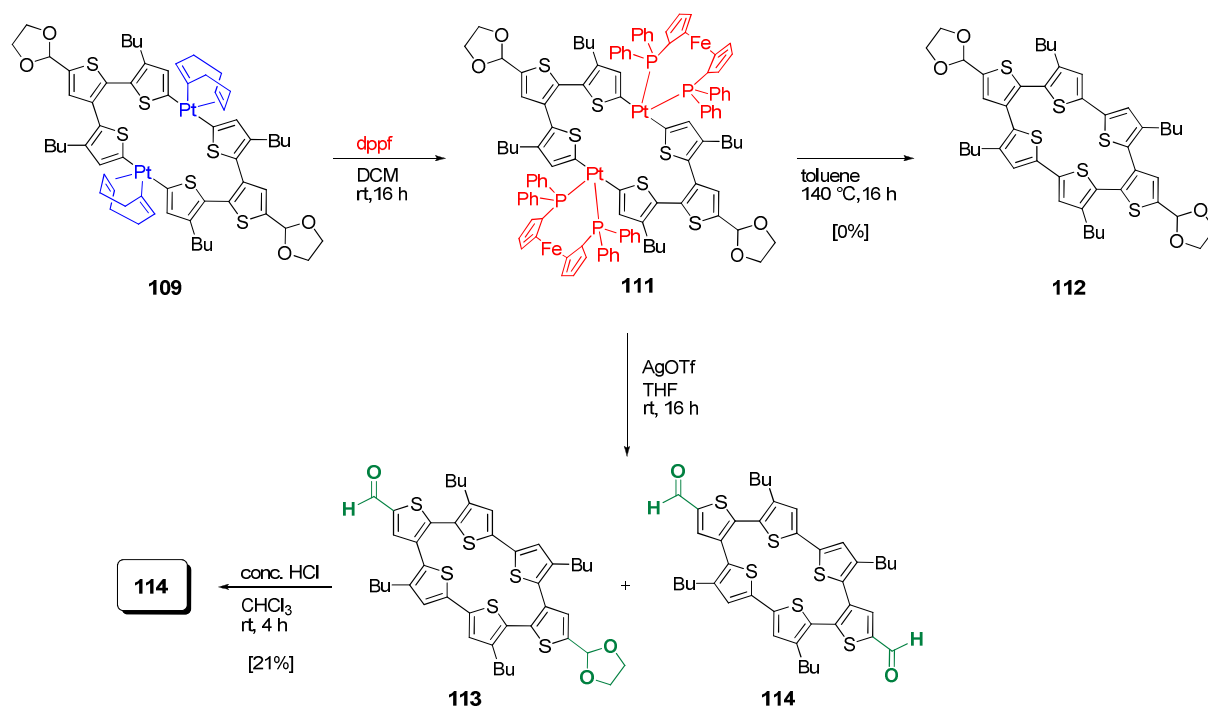


Figure 5.3: ^1H NMR spectrum of a 1:1-mixture of metallaregioisomers **109:110**, measured in CDCl_3 (400 MHz). Impurities of water and *n*-hexane belong to the solvent.

The mixture of the regioisomers was also examined by mass spectrometry. Only one signal was detected which belongs to the Pt^{II} complexes with one COD ligand cleaved off; $m/z = 1358.4$ (calcd. $m/z = 1358.2$). The exact mass of **109:110** was not observed. Presumably, the intensity of the laser was too strong and induced the elimination of the dative linked COD ligand, which has been previously observed for the acceptor and donor-functionalized Pt^{II} oligothiophenyl complexes as well. However, the intensities of the integrals concerning the COD ligands matched exactly in the proton NMR spectrum, reflecting a successful formation of metallacycles **109:110**.

The consecutive reaction steps, the ligand exchange reaction and elimination process, are displayed in Scheme 5.6. The ligand exchange of **109** at the Pt-centers from COD to dppf was carried out overnight at room temperature and resulted in metallacycle **111**, which was not further purified. The exchange was followed via ^1H NMR spectroscopy according to typical signals of the dppf ligand (multiplets at around 7.40 and 4.20 ppm) and eliminated COD (singlets at 5.57 and 2.35 ppm).



Scheme 5.6: Synthesis of π -conjugated aldehyde-substituted macrocycle **114**. The scheme is valid for the 1:1 mixture of **109:110**. Regioisomer **110** was omitted for clarity in order to facilitate the reaction scheme.

A first attempt to the reductive elimination towards π -conjugated, platinum-free macrocycles was carried out in toluene at 140 °C. The high temperature should induce reductive elimination under simultaneous C-C bond formation. Investigations via both proton NMR- and mass-analysis indicated still existing metallacycles next to several unidentifiable byproducts, but desired macrocycle **112** was not detected. Dppf-signals were still present in the NMR-spectrum and signals of fragmented Pt-metallacycles were observed in the recorded mass spectrum.

An oxidatively induced reductive elimination of Pt^{II} metallacycles with the one-electron oxidant AgOTf was then performed in a second attempt. The reaction was carried out overnight at ambient temperature and thus mild reaction conditions were applied (Scheme 5.6). The crude reaction mixture was filtered through a short plug of aluminium oxide IV after aqueous work-up to remove precipitated elemental metal. Subsequent purification via size exclusion chromatography eluting with dichloromethane afforded one main fraction, which contained completely unprotected macrocycle **114** besides mono-aldehyde species **113**. Both macrocycles proved to be inseparable after several chromatographic attempts. To gain complete deprotected material, the mixture was subjected to concentrated hydrochloric acid, whereat only aldehyde-functionalized macrocycle **114** resulted. Further collected fractions of the SEC process revealed unidentifiable byproducts next to dppf. Since the syntheses in Scheme 5.6 were performed for a 1:1 mixture of regioisomers **109:110** (**110** was omitted for clarity), isomeric macrocycle **115** was formed besides **114** (Chart 5.2). The 1:1 mixture was obtained pure as a yellow powder in an overall yield of 21% which was calculated from

dibrominated dendritic terthiophene **107**. It was characterized via proton NMR spectroscopy and mass spectrometry and was investigated with respect to the photophysical and electrochemical properties.

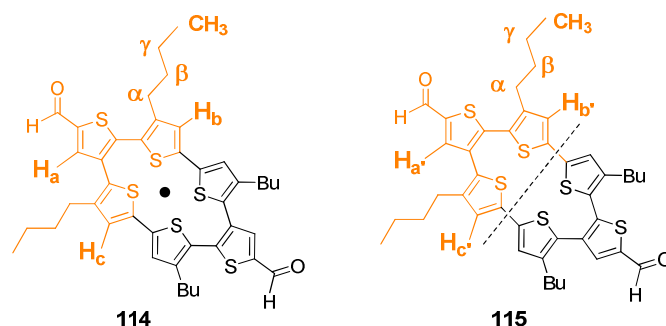


Chart 5.2: Structures of the regioisomeric π -conjugated macrocycles **114** and **115**.

The ^1H NMR spectrum of the 1:1 mixture of **114:115** is depicted in Figures 5.4 and 5.5. The two singlets at $\delta = 7.81$ and 7.80 ppm are assigned to $\text{H}_a, \text{H}_{a'}$ and the four singlets at $\delta = 6.81$ – 6.76 ppm to $\text{H}_b, \text{H}_{b'}$ and $\text{H}_c, \text{H}_{c'}$ and belong to the protons of the terthiophene subunits. The signal for the aldehyde protons (CHO) was shifted downfield to $\delta = 9.98$ ppm. The signals for the butyl side chains were located at $\delta = 2.64$ ($\alpha\text{-CH}_2$), 2.48 ($\alpha\text{-CH}_2$), 1.59 ($\beta\text{-CH}_2$), 1.39 ($\gamma\text{-CH}_2$), and 0.92 ppm (CH_3).

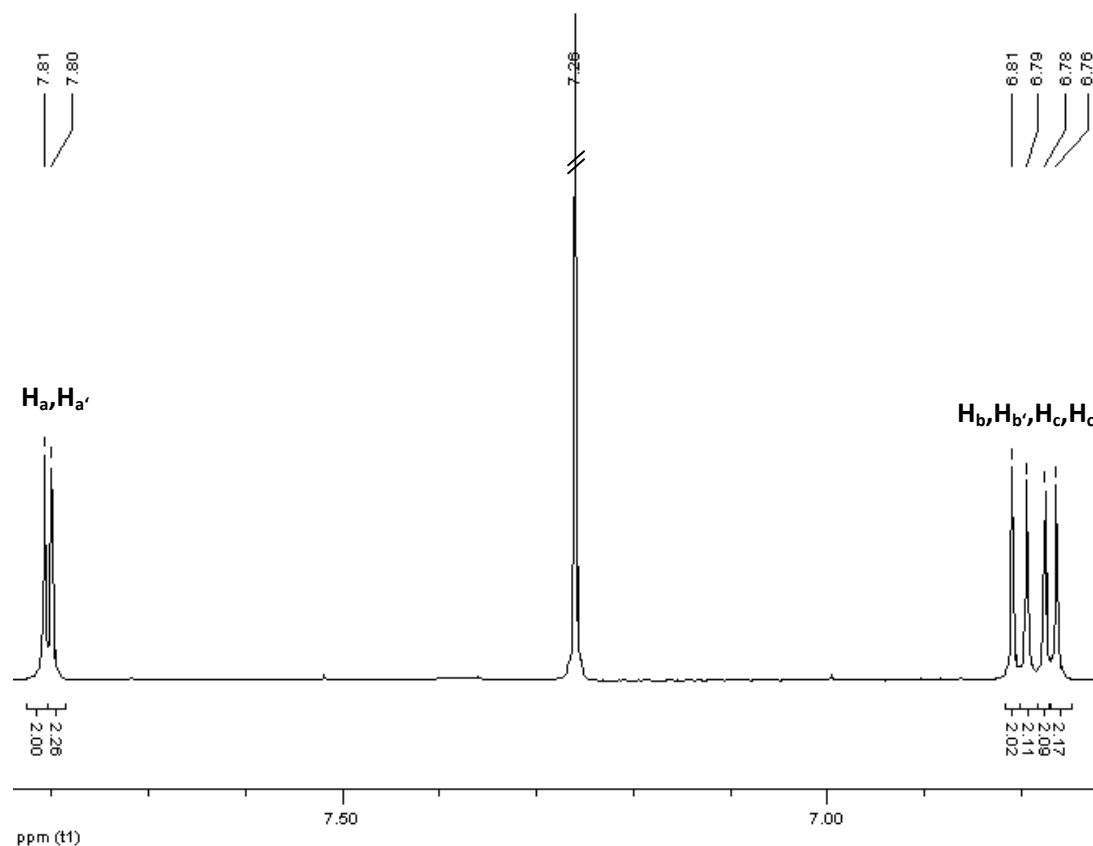


Figure 5.4: Aromatic region of the ^1H NMR spectrum of the 1:1 mixture of macrocycles **114:115**, measured in CDCl_3 (400 MHz).

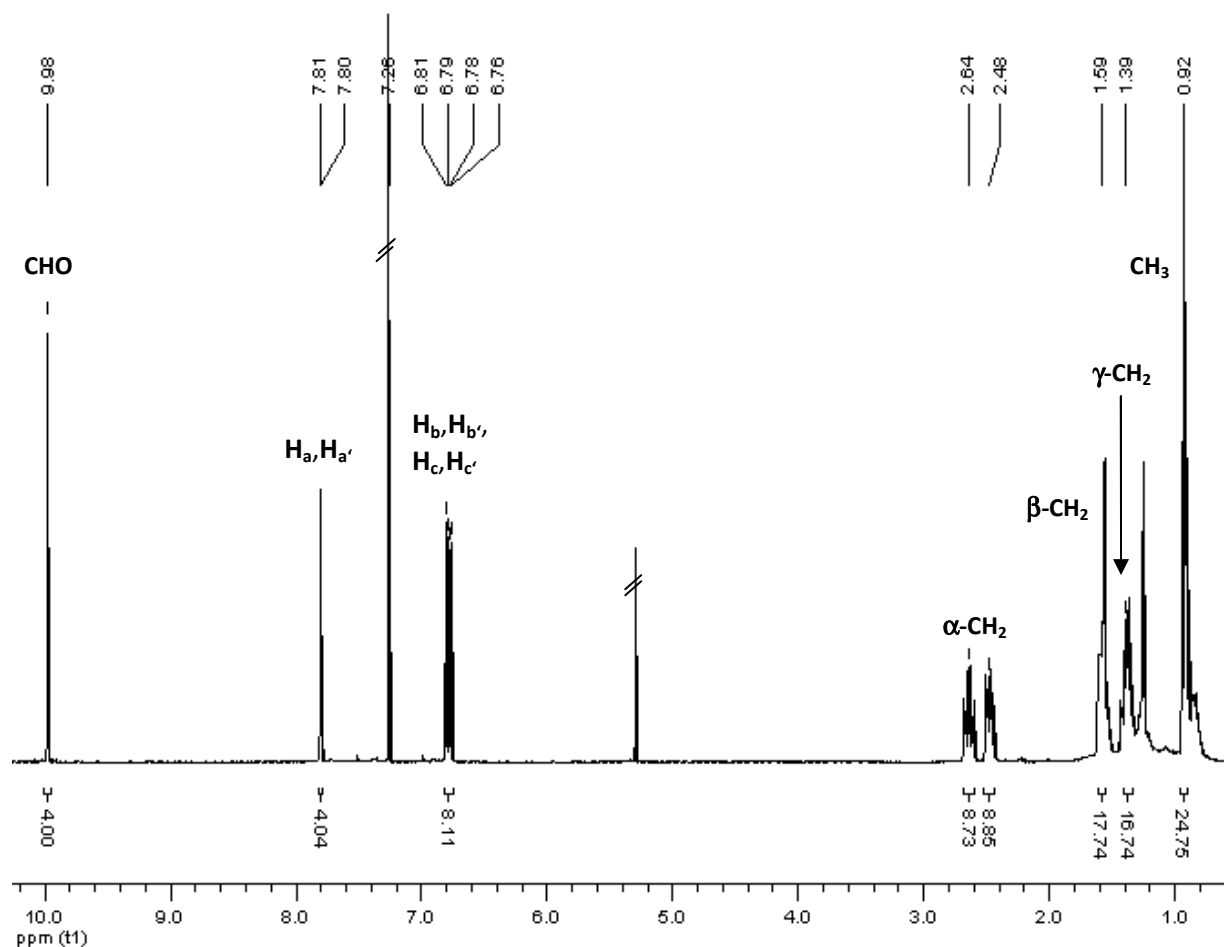


Figure 5.5: ^1H NMR spectrum of the 1:1 mixture of macrocycles **114:115**, measured in CDCl_3 (400 MHz). The spectrum contains signals of DCM and *n*-hexane.

Mass analysis revealed a value of $m/z = 772.1$, which exactly corresponds to the calculated mass (calcd. $m/z = 722.1$) and to the theoretical isotopic pattern. The MALDI-TOF mass spectrum is given in Figure 5.6.

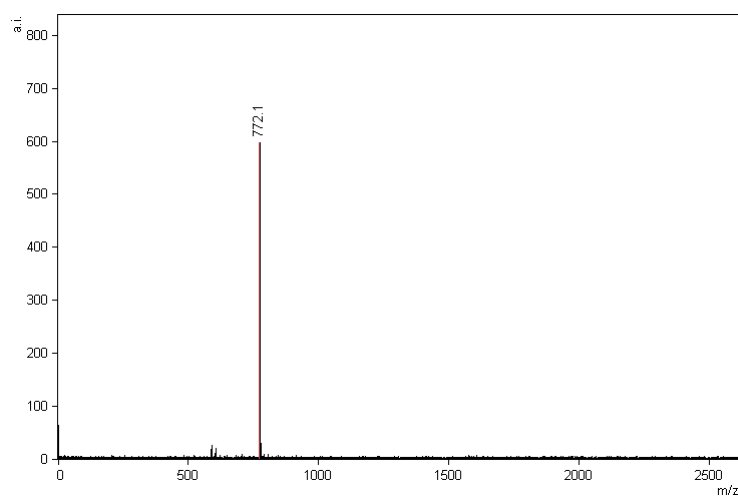


Figure 5.6: MALDI-TOF mass spectrum of the 1:1 mixture of macrocycles **114:115**.

An isomeric 1:1 mixture of peripherally functionalized macrocycles with a π -conjugated backbone was synthesized ready to undergo potential further chemical reactions. It is worth to mention that probably due to the geometry and predetermined inner angle of the precursor CHO-3T **106** an exclusive formation of only one ring size comprising of six thiophene units was observed.

5.3 Optical properties of peripherally functionalized macrocycles

The photophysical properties of the 1:1 mixture of regioisomers **114:115** were investigated by means of UV/vis absorption and fluorescence spectroscopy. The analytical data were opposed to the isomeric mixture of metalla-analogues **109:110** and dendritic oligomer CHO-3T **106**. It is noteworthy that the metal free cyclic systems are deprotected, whereat both comparative compounds still possess ethylene glycol protecting groups. Since the functionalization is located at the periphery, the electronic influence of the free aldehyde groups should not be too influential on the optical properties. The UV/vis and fluorescence curves are shown in Figure 5.7 and the data of the optoelectronic measurements are summarized in Table 5.1.

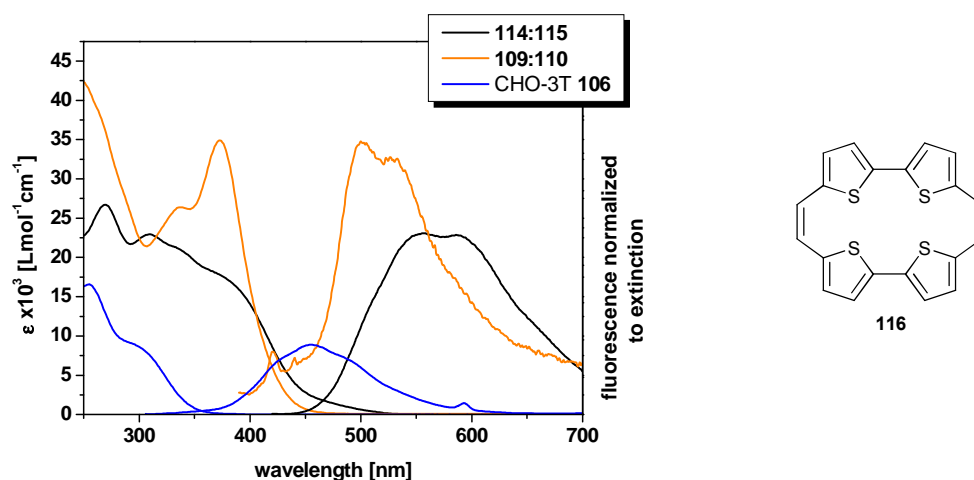


Figure 5.7: (left) UV/vis absorption and emission spectra of the 1:1 mixture of macrocycles **114:115** and metallacycles **109:110** as well as linear dendritic terthiophene **106**, measured in chloroform. (right) Structure of oligothiényl macrocycle **116**, published by Cava et al.^[11]

The shape of the absorption spectrum of **114:115** revealed a very broad and unstructured band with a maximum for the π - π^* -transition at $\lambda = 309$ nm and an extinction coefficient of $\epsilon = 23.000 \text{ Lmol}^{-1}\text{cm}^{-1}$. The blue-shifted maximum at $\lambda = 269$ nm can be attributed to n - π^* -transitions. A macrocycle with a similar assembly of the delocalized π -system has already been published by Cava et al. (Figure 5.7, **116**).^[11] Cava described the UV/vis absorption behaviour of the macrocycle as a composition of four different maxima postulating a moderate conjugation between the thiophene units due to a non-planarity of the strained system. The non-planarity was confirmed by X-ray structure analysis in

a study of Ellinger.^[12] Based on this research, it is assumed that the broadness of the absorption band of **114:115** is due to an overlapping of different absorption bands derived from conjugated, but disrupted subunits and not from the complete annulene. The quoted absorption values for **116** are all blue-shifted in contrast to **114:115** probably as a consequence of the lack of electron-influencing groups. The herein introduced aldehyde functionality lowers the optical band gap and results in a red-shift of the observed UV/vis data.

The platinum metallacycles **109:110** revealed an absorption maximum at $\lambda = 373$ nm for the π -conjugated systems with an extinction coefficient of $\epsilon = 34.000 \text{ Lmol}^{-1}\text{cm}^{-1}$. The red-shift compared to the metal-free macrocycle can probably be assigned to an additional electron transfer from the transition metals to the ligands which increases the extend of conjugation. Nevertheless, an overlapping of different absorptions derived from variable oligothiophene subunits similar to the behaviour of **114:115** is expected.

The maximum for the α,α - and α,β -linked precursor **106** is located at $\lambda = 254$ nm. A composition of the observed broad absorption band of a terthiophene- and a bithiophene-unit ($\lambda = 296$ nm) is assumed. Ward and co-workers ascertained a maximum for the optical properties of bithiophene in chloroform at $\lambda = 307$ nm.^[13]

All emission spectra exhibited a vibronic splitting indicating a more planar and stiff structure in the excited state. The maximum of the emission of the Pt^{II} oligothienyl complexes **109:110** was blue-shifted ($\lambda = 500$ nm) compared to macrocycles **114:115** ($\lambda = 557$ nm). The emission of the terthiophene monomer unit **106** with the shortest conjugation length was located at $\lambda = 455$ nm.

Table 5.1: Summary of the optical data of 1:1 mixtures of macrocycles **114:115** and **109:110** and linear oligomer **106**.

oligothiophene	$\lambda_{\text{abs,max}}$ [nm]	ϵ [$\text{Lmol}^{-1}\text{cm}^{-1}$]	$\lambda_{\text{em,max}}$ [nm]
114:115	309	23.000	557
109:110	373	34.000	500
CHO-3T 106	254	16.000	455

The geometry of the isomeric macrocycles **114** and **115** was theoretically calculated and optimized via Austin Model 1 (AM1) calculations with defined Hartree Fock-conditions to get an insight into the thiophene arrangement. The theoretical determination of the geometry was performed with ethyl side chains instead of the actual butyl ones. This should facilitate the optimization process but not affect the results. The obtained structures are presented in Chart 5.3 and proof the expected non-

planarity of both rings due to a strong ring strain. Expanded conjugation is therefore diminished since single thiophene units are twisted out of the plane and cause only a low overlap of the π -orbitals.^[14]

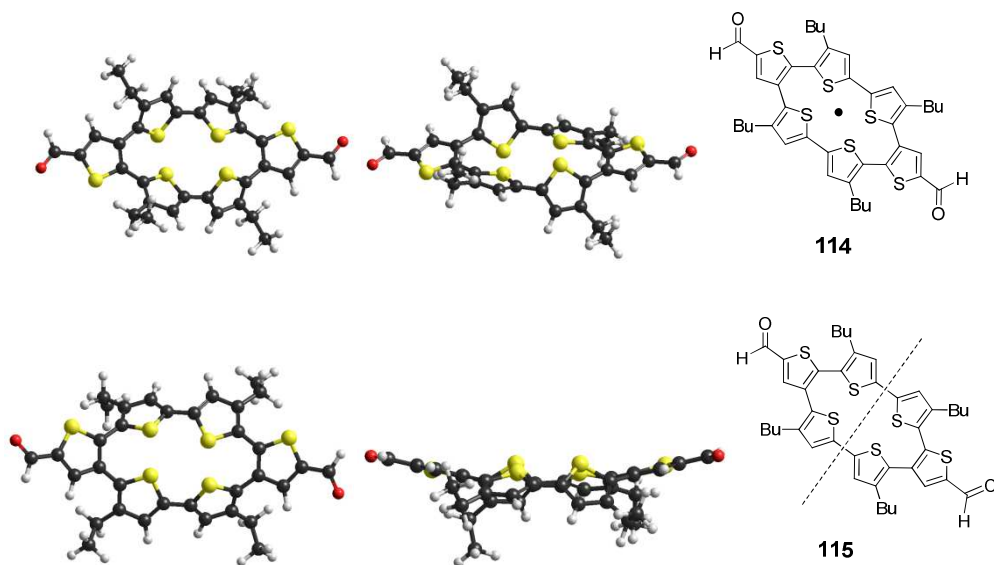


Chart 5.3: Calculated structures of the cyclic regioisomers **114** and **115**.

For regioisomer **114** with a point-symmetry, the opposed thiophene units are arranged in different directions. Three of them face the sulfur atoms upwards, three of them downwards, similar to a cyclic wave motion. The geometry of **115** with an axial-symmetry exhibits rather a boat conformation with the inner thiophene moieties twisted in the same direction.

5.4 Electrochemical properties of peripherally functionalized macrocycles

The 1:1 isomeric mixture **114:115** was also characterized by means of cyclic voltammetry. The voltammograms were recorded in benzonitrile at ambient temperature and TBAPF₆ (0.1 M) was used as supporting electrolyte and ferrocene as internal standard. Since the measurements were carried out at low substrate concentrations of 0.1 mM, a Pt-working electrode with a relatively large surface ($\phi = 3.4$ mm) was utilized to obtain well resolved redox waves. The voltammograms were recorded at a low scan rate of 20 mV/s to keep the disturbance currents low.

The cyclic voltammogram and the deconvoluted voltammograms are depicted in Figure 5.8. With increasing voltage range, three quasi-reversible one-electron redox waves occurred at E_1^0 - E_3^0 (0.75 V, 0.87 V, 1.01 V). One additional wave appeared in the negative backscan at around -0.1 V and increased as well as shifted to lower potentials by rising reversal potential. Since the macrocycles do not represent a completely closed system due to the introduced aldehyde functionalities, a formation of reversible, dimeric σ -complexes of multiple charged cycles as follow-up products is

likely and might have caused the broad extra wave. The electrochemical potentials are listed in Table 5.2.

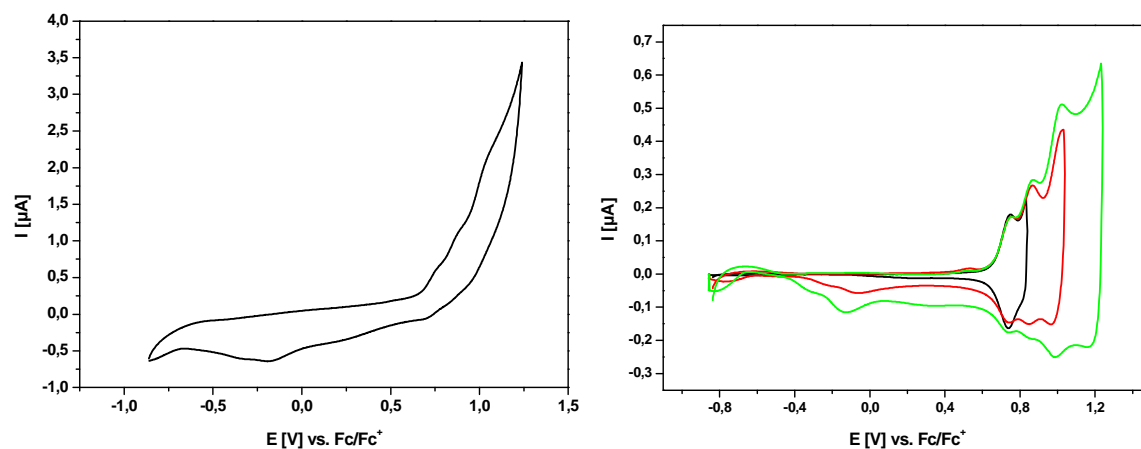


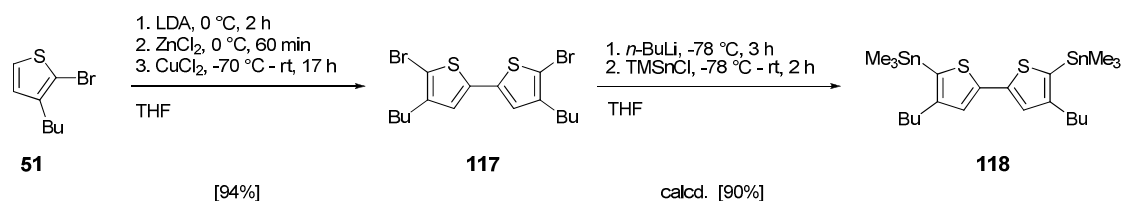
Figure 5.8: Cyclic voltammogram (left) and deconvoluted voltammograms (right) of the 1:1 mixture **114:115**, measured in benzonitrile/TBAPF₆ (0.1M) vs. Fc/Fc⁺, 20 mV/s, $c = 1.0 \times 10^{-4}$ M.

Table 5.2: Summary of the oxidation potentials.

macrocycle	E^0_{ox1} [V]	E^0_{ox2} [V]	E^0_{ox3} [V]
114:115	0.75	0.87	1.01

5.5 Synthesis of a non-isomeric, peripherically functionalized macrocycle

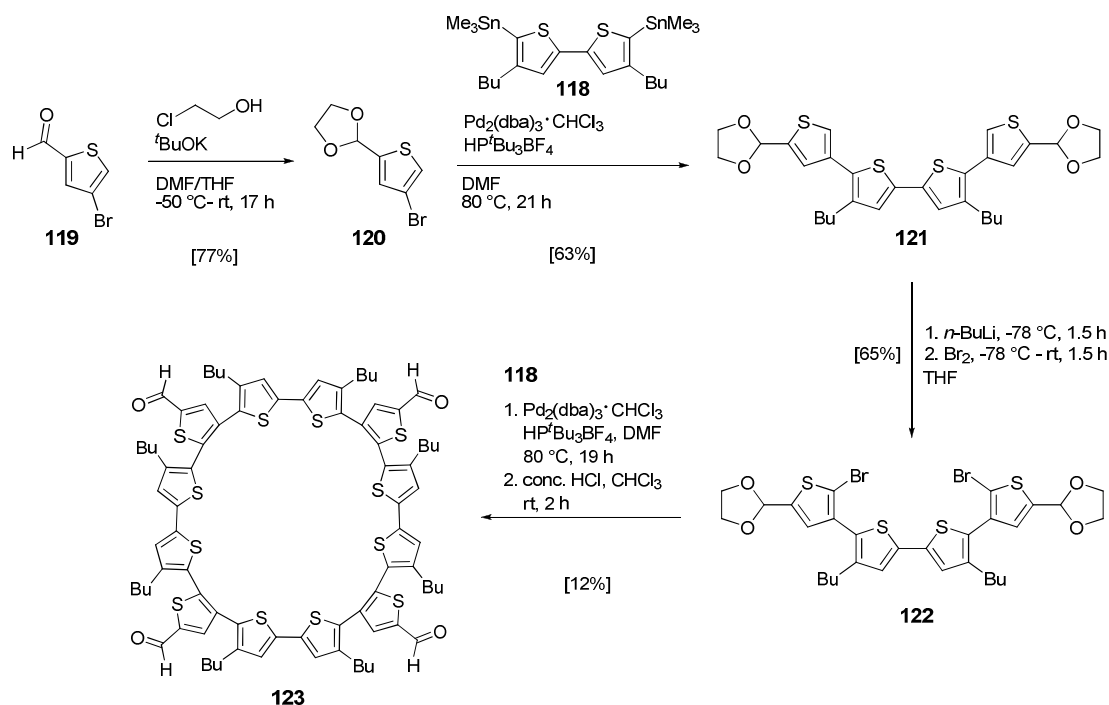
It is more elegant and satisfying to investigate pure compounds instead of isomeric mixtures by methods like NMR spectroscopy, absorption and emission spectroscopy as well as electrochemistry. Thus, an alternative synthetic route was developed to produce non-isomeric, peripherically functionalized macrocycles. The synthetic pathway is outlined in Scheme 5.7. It started from 2-bromo-3-butylthiophene **51** which was lithiated via a metal-proton exchange with LDA at 0 °C and treated with zinc(II)chloride to stabilize the formed anion at the 5-position. The zinc intermediate was oxidatively coupled by means of copper(II)chloride to generate C-C bond formation to bithiophene derivative **117** which was gained in 94% yield after filtration over a silica gel plug.



Scheme 5.7: Synthesis of α,α' -distannylated bithiophene derivative **118**.

The following reaction step included a halogen-metal exchange with *n*-butyl lithium at -78 °C. The doubly lithiated species was reacted with Me₃SnCl and distannylated bithiophene **118** was obtained in 90% yield and not further purified by chromatographic methods to avoid elimination of the tin containing groups. The yield was calculated from the corresponding proton NMR spectrum of the crude material after work-up.

In a parallel synthetic route, an acetal-functionalized quaterthiophene **122** was built up (Scheme 5.8). It started from commercially available 4-bromothiophene-2-carboxyaldehyde **119**, which was protected under basic conditions via chloroethanol in a mixture of DMF and THF at -50 °C following a procedure by Makosza.^[10] Dioxolane **120** was purified by column chromatography with silica and obtained in 77% yield. The analytical data are consistent with the literature in which the protection was carried out with ethylene glycol and *p*-TsOH.^[15]



Scheme 5.8: Synthesis of non-isomeric, peripherally functionalized macrocycle **123**.

Dioxolane **120** and previously synthesized α,α' -distannylated bithiophene **118** were coupled in a Stille cross-coupling reaction under common palladium-catalyzed conditions. After purification via silica gel column chromatography, quaterthiophene **121** comprising an α,β -linkage was obtained in 63% yield as yellow solid.

The remaining protons at the free α -positions of the external thiophene units were transformed into bromine atoms by means of *n*-butyl lithium at $-78\text{ }^{\circ}\text{C}$. The doubly lithiated intermediate was subsequently reacted with elemental bromine. A pale yellow oil of halogenated quaterthiophene **122** was isolated in 65% yield after purification using column chromatography. The bromination with NBS in DMF at $0\text{ }^{\circ}\text{C}$ failed since the bromine atoms were introduced at the less reactive β -positions of the inner bithiophene moiety.

Inspired by the selective synthesis of cycloparaphenylene via a Suzuki-Miyaura cross-coupling reaction performed by Itami and co-workers^[16], a standard palladium-catalyzed Stille cross-coupling reaction of halogenated quaterthiophene **122** and distannylated bithiophene **118** was carried out for the final cyclization step. After aqueous work-up and purification via SEC with DCM as eluent, the collected main fraction was treated in a follow-up reaction with concentrated HCl in chloroform to eliminate all acetal protecting groups. Macrocycle **123**, including twelve thiophene units within the cyclic backbone, was obtained in 12% yield. The expected smaller analogue, cyclic hexamer **114**, composed of only six thiophene moieties was only observed in traces. The isolated macrocycle **123** (Chart 5.4) was investigated by proton NMR spectroscopy (Figure 5.9 and 5.10).

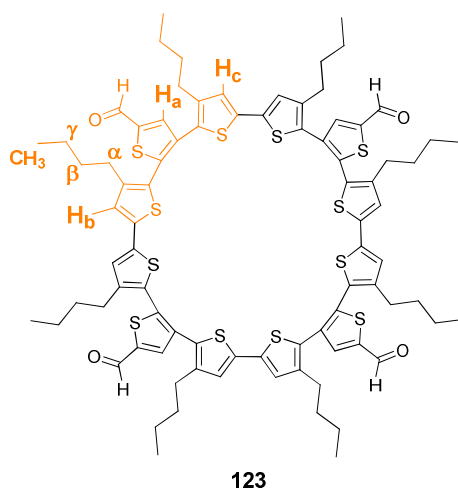


Chart 5.4: Structure of the non-isomeric, peripherically functionalized macrocycle **123**.

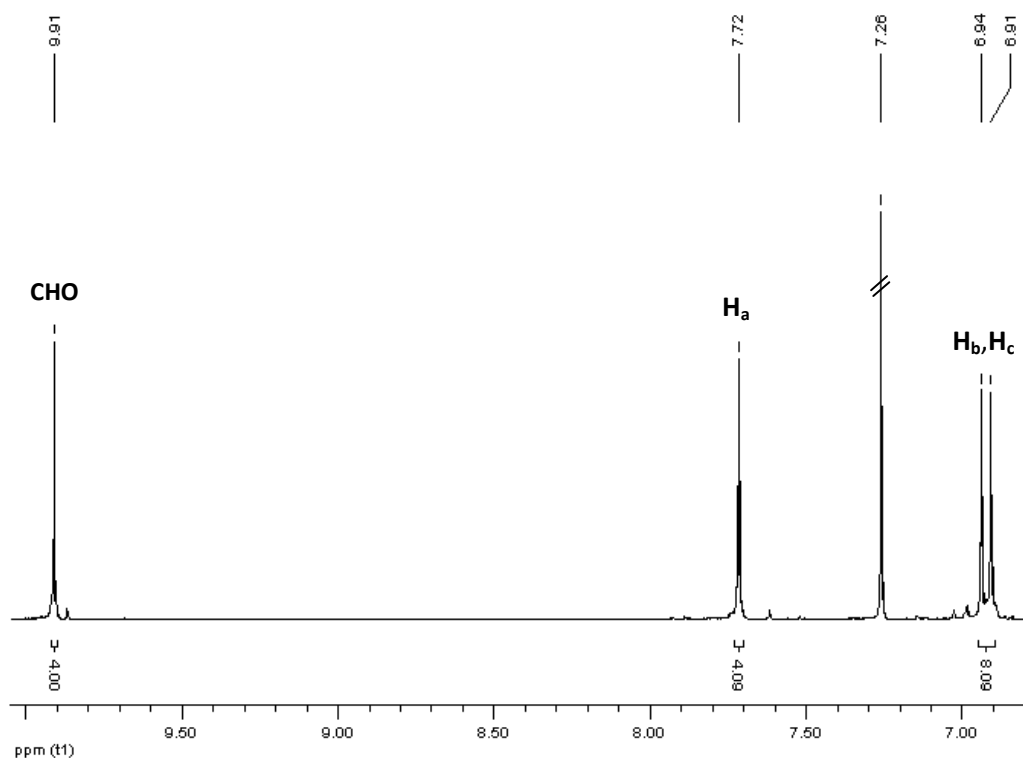


Figure 5.9: Aromatic region of the ^1H NMR spectrum of macrocycle **123**, measured in CDCl_3 (400 MHz).

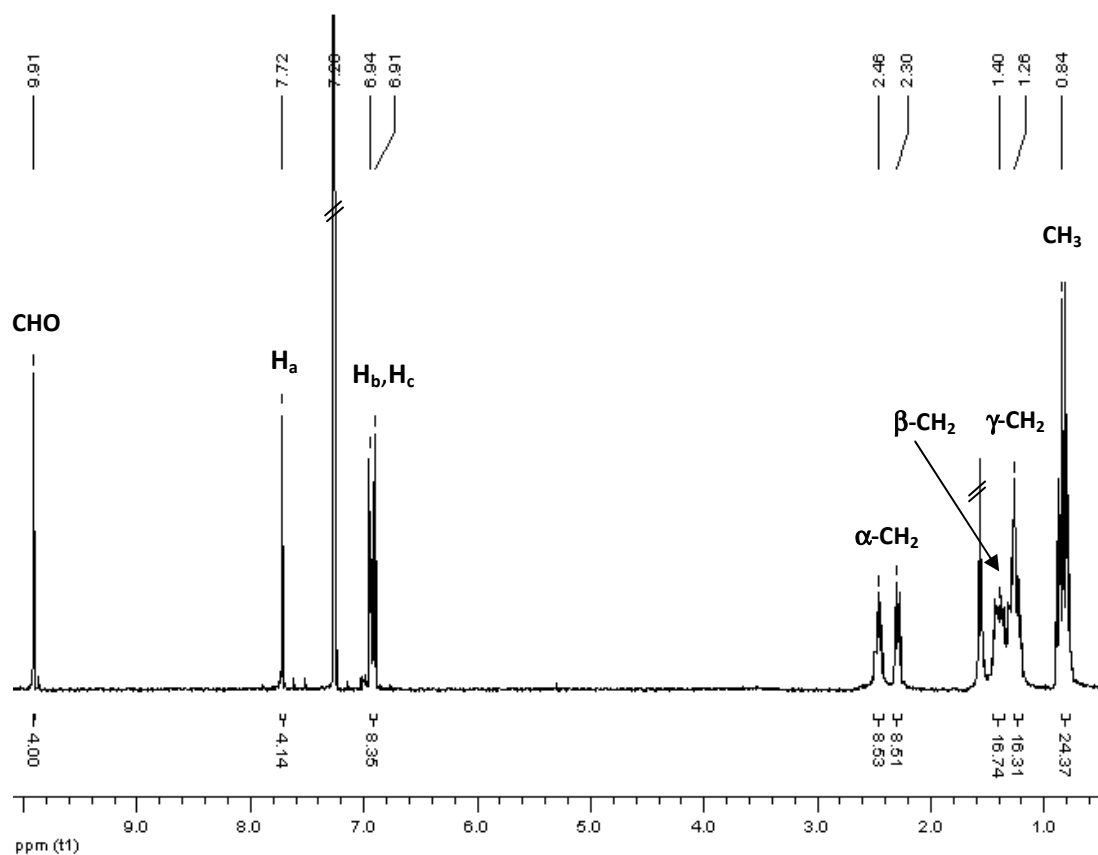


Figure 5.10: ^1H NMR spectrum of macrocycle **123**, measured in CDCl_3 (400 MHz). The spectrum contains signals of water and *n*-hexane.

Since macrocycle **123** is highly symmetric three singlet signals are expected for the aromatic protons, which appear at $\delta = 7.72$ for H_a , 6.94 and 6.91 ppm for H_b and H_c . The signal of the aldehyde group (CHO) was located downfield shifted at $\delta = 9.91$ ppm and the signals of the butyl side chains were present in the aliphatic region of the spectrum at $\delta = 2.46$ (α -CH₂), 2.30 (α -CH₂), 1.40 (β -CH₂), 1.26 (γ -CH₂), and 0.84 ppm (CH₃).

The existence of the macrocycle was as well determined by mass spectrometry with a value of $m/z = 1545.0$, which is in good agreement with the theoretical determined mass of $m/z = 1544.3$ (Figure 5.11).

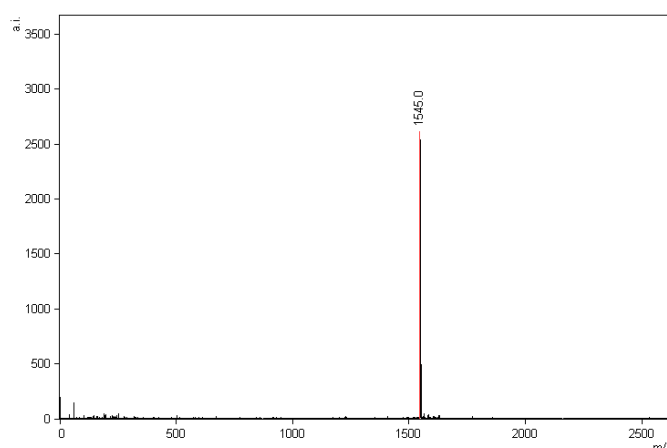


Figure 5.11: MALDI-TOF mass spectrum of **123**.

A shape-persistent, structurally defined macrocycle could be generated via a Stille cross-coupling reaction. The introduced aldehyde functionalities serve as potential reactive positions for further chemistry. The Stille reaction could be regarded as a future option next to the elaborated Pt^{II}-assisted template method.

5.5.1 Optical properties of non-isomeric peripherally functionalized macrocycle (**123**)

The photophysical properties of macrocycle **123** were investigated by means of UV/vis absorption and fluorescence spectroscopy and the results were compared to the data of the 1:1 isomeric mixture **114:115** (Figure 5.12). The shape of the absorption curves for both classes of macrocycles follows the trend towards a broad and unstructured band. Since the broadness in the case of **114:115** has already been suggested to be an overlapping of different conjugated, but disrupted oligomeric subunits due to an existing non-planarity of the ring-plane, this is very likely to be the case for **123** as well. The maximum of macrocycle **123** was located at $\lambda = 353$ nm with an extinction coefficient of $\epsilon = 63.000 \text{ Lmol}^{-1}\text{cm}^{-1}$. The extinction of **123** is clearly higher than for the isomeric mixture **114:115** since **123** possess a twice as large chromophoric system. The emission curves of both substances exhibit a

very similar shape and the maximum of **123** was red-shifted to a very low range of 7 nm in contrast to **114:115** (557 nm vs. 550 nm, respectively). The data are summarized in Table 5.3.

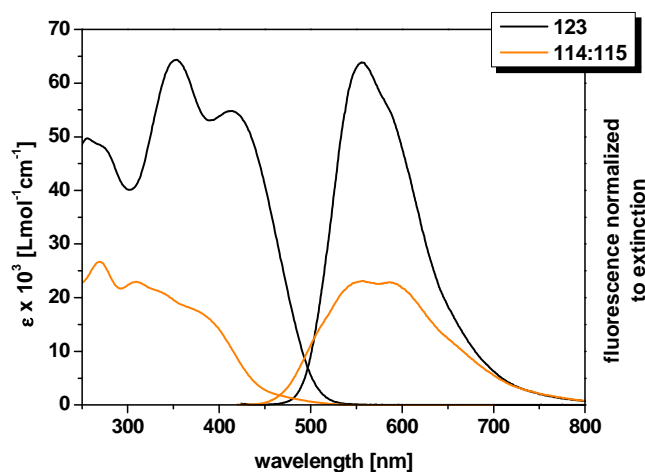


Figure 5.12: UV/vis absorption and emission spectra of macrocycle **123** and 1:1 mixture **114:115**, measured in chloroform.

Table 5.3: Summary of the photophysical data of **123** and 1:1 mixture **114:115**.

macrocycle	$\lambda_{\text{abs,max}}$ [nm]	ϵ [Lmol ⁻¹ cm ⁻¹]	$\lambda_{\text{em,max}}$ [nm]
114:115	309	23.000	557
123	353	63.000	550

5.6 Summary

The synthesis, characterization, and photophysical studies of peripherally functionalized, shape-persistent macrocycles were described within this chapter. The preparation of an aldehyde-substituted macrocycle via the ‘metal-assisted template method’ caused two regioisomers **114** and **115** composed of six thiophene units, respectively, in 21% yield. The formation of the inseparable mixture was caused by the usage of an asymmetric dendritic precursor **108**, which initialized the formation of only one defined ring size due to its particularly strongly bent, hemicyclic shape. The structure of the 1:1 mixture **114:115** was confirmed by ¹H NMR spectroscopy and analyzed consecutively by means of absorption spectroscopy. A broad and unstructured absorption band indicated a non-planarity of the strained system which was proven via computational calculations. The twist of the single thiophene units out of the plane led to an overlap of different absorption bands derived from disrupted π -conjugated subunits. Electrochemical measurements up to high voltages caused dimeric σ -complexes of multiple charged species via the reactive aldehyde groups.

Macrocycle **123** with 12 thiophene units was prepared as final main ring from an alternative synthetic approach towards a non-isomeric peripherically functionalized analogue of **114**. Stille cross-coupling reaction was utilized as the crucial macrocyclization step and **123** was isolated in 12% yield and investigated via UV/vis absorption spectroscopy. A broad and unstructured absorption band led as well to the assumption of a non-planar macrocycle and the overlap of different absorption bands of disrupted π -conjugated subunits.

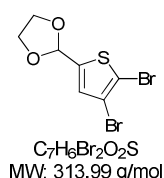
5.7 Experimental section

General remarks about chemicals, synthesis, analytical data and performed measurements

Remarks given in the experimental part in Chapter 3 are generally valid in this section, as well. The experimental setup of the photophysical and electrochemical measurements is given in the experimental part in Chapter 3. Additionally, tri(*tert*-butyl)phosphonium tetrafluoroborate ($\text{HP}^t\text{Bu}_3\text{BF}_4$) was purchased from Aldrich and 4,5-dibromo-thiophene-2-carbaldehyde and 4-bromothiophene-2-carbaldehyde were purchased from Alfa Aesar. 2-Chloroethanol, potassium *tert*-butoxide, and zinc(II)chloride were purchased from Merck.

Synthesis and characterization

2-(4,5-Dibromothien-2-yl)-1,3-dioxolane (105)



To a vigorously stirred solution of 4,5-dibromothiophene-2-carboxaldehyde **104** (3.00 g, 11.1 mmol) and 2-chloroethanol (1.12 mL, 16.7 mmol) in a mixture of DMF (30 mL) and THF (15 mL) at -50 °C, a solution of $t\text{BuOK}$ (1.87 g, 16.7 mmol) in DMF (18 mL) was added dropwise over 45 min. The mixture was stirred for 90 min at this temperature and at room temperature overnight. Afterwards, brine and water were added. The organic product was extracted with DCM and the combined organic layers were washed with water and dried over Na_2SO_4 . The solvent was removed under reduced pressure and a brown liquid of **105** (3.39 g, 10.8 mmol, 97%) was obtained.

$^1\text{H NMR}$ (400 MHz, CDCl_3): δ = 6.96 (s, 1H, Th-3), 6.01 (s, 1H, O-CH), 4.10-4.05 (m, 2H, O-CH₂), 4.04-3.99 (m, 2H, O-CH₂) ppm.

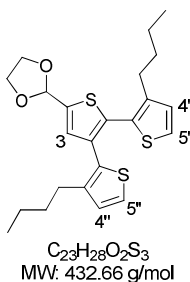
$^{13}\text{C NMR}$ (100 MHz, CDCl_3): δ = 143.35, 128.57, 113.29, 112.23, 99.37, 65.25 ppm.

MS (EI) m/z : calcd. for $[M]^+$ ($C_7H_6Br_2O_2S$): 312; found: 313 $[M+H]^+$.

Elemental analysis: calcd. for ($C_7H_6Br_2O_2S$): C, 26.78; H, 1.93; S, 10.21%; found: C, 26.99; H, 2.00; S, 10.15%.

Analytical data were in accordance with the literature.^[15]

2-[4,5-Bis(3-butylthien-2-yl)thien-2-yl]-1,3-dioxolane (**106**)



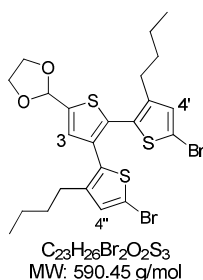
Dioxolane **105** (1.00 g, 3.18 mmol) and 3-butyl-2-(trimethyltin)thiophene **52** (2.32 g, 7.64 mmol) were dissolved in dry DMF (50 mL) and degassed. Afterwards, $Pd_2(dba)_3$ (165 mg, 159 μ mol) and $HP^tBu_3BF_4$ (92.4 mg, 0.32 mmol) were added. The reaction mixture was heated for 24 h at 80 °C. After cooling to room temperature, the mixture was poured onto water and the product was extracted with DCM. The combined organic layers were dried over Na_2SO_4 and the solvent was evaporated. The residue was purified by column chromatography using silica gel with a mixture of *n*-hexane:EE (9:1) to obtain terthiophene **106** (1.12 g, 2.58 mmol, 81%) as a yellow oil.

1H NMR (400 MHz, $CDCl_3$): δ = 7.21 (d, 3J = 5.2 Hz, 1H, Th-5'), 7.17 (d, 3J = 5.2 Hz, 1H, Th-5''), 7.15 (s, 1H, Th-3), 6.85 (d, 3J = 5.2 Hz, 1H, Th-4'), 6.84 (d, 3J = 5.2 Hz, 1H, Th-4''), 6.10 (s, 1H, O-CH), 4.20-4.17 (m, 2H, O-CH₂), 4.07-4.04 (m, 2H, O-CH₂), 2.39 (t, 3J = 7.7 Hz, 2H, α -CH₂-Bu), 2.33 (3J = 7.6 Hz, 2H, α -CH₂-Bu), 1.41-1.31 (m, 4H, β -CH₂-Bu), 1.29-1.20 (m, 4H, γ -CH₂-Bu), 0.84 (t, 3J = 7.2 Hz, 3H, CH₃-Bu), 0.83 (t, 3J = 7.2 Hz, 3H, CH₃-Bu) ppm.

^{13}C NMR (100 MHz, $CDCl_3$): δ = 142.01, 140.66, 140.41, 133.57, 132.68, 131.19, 129.69, 128.60, 128.58, 128.28, 125.93, 124.69, 100.18, 65.33, 32.45, 28.62, 28.51, 22.68, 13.95 ppm.

MS (EI) m/z : calcd. for $[M]^+$ ($C_{23}H_{28}O_2S_3$): 432; found: 432 $[M]^+$.

Elemental analysis: calcd. for ($C_{23}H_{28}O_2S_3$): C, 63.85; H, 6.52; S, 22.23%; found: C, 63.70; H, 6.35; S, 22.06%.

2-[4,5-Bis(5-bromo-3-butylthien-2-yl)thien-2-yl]-1,3-dioxolane (107)

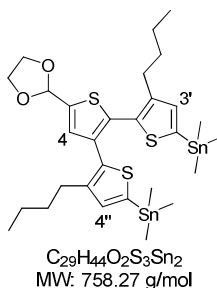
Dendritic dioxolane **106** (720 mg, 1.66 mmol) was dissolved in chloroform (25 mL), cooled to 0 °C and pyridine (0.47 mL, 5.82 mmol) was added. A solution of bromine (0.21 mL, 4.16 mmol) diluted 1:20 (vol.) in chloroform was slowly added within 15 min. After complete addition, the reaction mixture was stirred for 15 min at 0 °C and at room temperature overnight. The solution was diluted with an aqueous $Na_2S_2O_3$ solution and the organic layer was separated and washed successively with an aqueous sat. $NaHCO_3$ solution and water, dried over Na_2SO_4 and concentrated in vacuum. Purification of the resulted solid via silica column chromatography followed, eluting with a mixture of *n*-hexane:EE (9:1) to achieve a colorless oil of terthiophene **107** (870 mg, 1.47 mmol, 89%).

1H NMR (400 MHz, THF- d_8): δ = 7.12 (s, 1H, Th-3), 6.97 (s, 1H, Th-4'), 6.93 (s, 1H, Th-4''), 6.00 (s, 1H, O-CH), 4.07-4.01 (m, 2H, O-CH₂), 3.99-3.93 (m, 2H, O-CH₂), 2.39 (t, 3J = 7.7 Hz, 2H, α -CH₂-Bu), 2.33 (3J = 7.6 Hz, 2H, α -CH₂-Bu), 1.42-1.32 (m, 4H, β -CH₂-Bu), 1.29-1.19 (m, 4H, γ -CH₂-Bu), 0.85 (t, 3J = 7.2 Hz, 3H, CH₃-Bu), 0.84 (t, 3J = 7.3 Hz, 3H, CH₃-Bu) ppm.

^{13}C NMR (100 MHz, THF- d_8): δ = 145.26, 144.88, 143.28, 134.42, 133.77, 133.74, 133.67, 133.37, 131.76, 130.73, 114.30, 112.98, 101.51, 66.95, 34.09, 34.05, 30.46, 30.36, 24.38, 15.13 ppm.

MS (EI) m/z : calcd. for $[M]^+$ ($C_{23}H_{26}Br_2O_2S_3$): 590; found: 591 $[M+H]^+$.

Elemental analysis: calcd. for ($C_{23}H_{26}Br_2O_2S_3$): C, 46.79; H, 4.44; S, 16.29%; found: C, 46.63; H, 4.53; S, 16.09%.

(4-Butyl-5-{3-[3-butyl-5-(trimethylstannyl)thien-2-yl]-5-(1,3-dioxolan-2-yl)thien-2-yl}thien-2-yl)trimethylstannane (108)

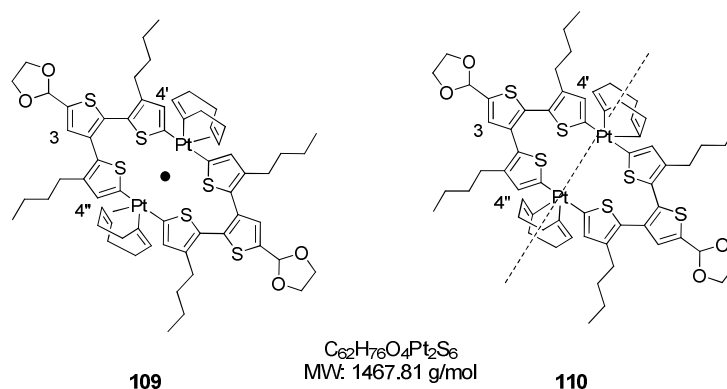
n-Butyl lithium (1.6 M in *n*-hexane, 0.94 mL, 1.56 mmol) was added dropwise to a solution of dibrominated terthiophene **107** (400 mg, 0.68 mmol) in dry THF (12 mL) at -78 °C within 20 min. After stirred between -75 and -65 °C for 65 min, Me₃SnCl (324 mg, 1.63 mmol) in dry THF (1 mL) was added at once. The reaction mixture was allowed to warm up to room temperature overnight. *n*-Hexane was added and lithium chloride precipitated as a white solid. The organic phase was washed several times with water and dried over Na₂SO₄. After evaporation of the solvent a yellow oil was obtained. The conversion of distannylated **108** (98%) was calculated via ¹H-NMR-spectroscopy. The compound was used without further purification for the next step.

¹H NMR (400 MHz, CDCl₃): δ = 7.13 (s, 1H, Th-4), 6.88 (s, 2H, Th-3',4''), 6.09 (s, 1H, O-CH), 4.19-4.13 (m, 2H, O-CH₂), 4.08-4.02 (m, 2H, O-CH₂), 2.29 (t, ³J = 8.0 Hz, 2H, α-CH₂-Bu), 2.23 (t, ³J = 7.8 Hz, 2H, α-CH₂-Bu), 1.31-1.15 (m, 8H, β-CH₂-Bu, γ-CH₂-Bu), 0.81 (t, ³J = 7.1 Hz, 3H, CH₃-Bu), 0.80 (t, ³J = 7.1 Hz, 3H, CH₃-Bu), 0.32 (s, 18H, TMSn) ppm.

¹³C NMR (100 MHz, CDCl₃): δ = 142.80, 141.50, 140.25, 138.37, 137.41, 136.81, 136.67, 136.57, 134.68, 133.53, 132.23, 129.98, 100.28, 65.28, 32.38, 32.35, 28.49, 28.41, 22.90, 22.86, 14.12, 14.03, -8.27 ppm.

MS (MALDI-TOF) *m/z*: calcd. for [M]⁺ (C₂₉H₄₄O₂S₃Sn₂): 758.0; found: 758.2 [M]⁺, 596.2 [M-TMSn]⁺.

1:1 mixture of Pt^{II}-metallacycles (**109:110**)



Distannylated terthiophene **108** (495 mg, 0.65 mmol) and PtCl₂(COD) (244 mg, 0.65 mmol) were dissolved in dry dichloromethane (750 mL) and degased. The reaction mixture was heated under reflux for 10.5 days. The mixture was cooled to room temperature and filtered through a short column packed with alox IV (DCM as eluent). The solvent was removed under vacuum and a yellow solid was obtained (450 mg). Separation and isolation of the individual compounds of 40 mg of the crude product was achieved by SEC, eluting with THF and the 1:1 mixture of regioisomers **109:110** (27.0 mg, 18.3 mmol, 64%) was obtained pure as a yellow solid.

Mp: 219 – 220 °C, decomposition.

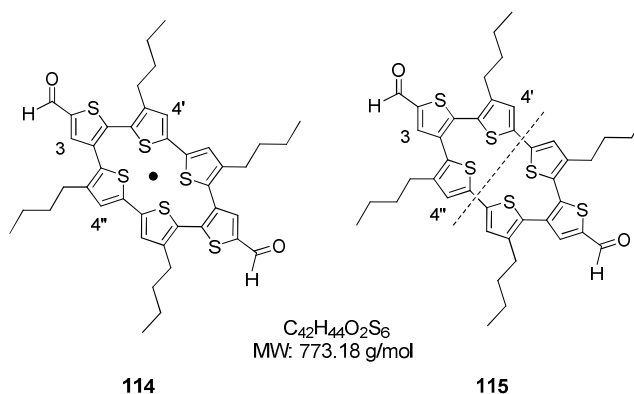
^1H NMR (400 MHz, CDCl_3): δ = 7.06 [7.06] (s, 4H, Th-3), 6.33 [6.31] (s, 4H, Th-4'), 6.30 [6.29] (s, 4H, Th-4''), 6.08 (s, 4H, O-CH), 5.47 (s, 16H, COD-CH), 4.16-4.10 (m, 8H, O-CH₂), 4.06-3.99 (m, 8H, O-CH₂), 2.52 (s, 32H, COD-CH₂), 2.48-2.43 (m, 8H, α -CH₂-Bu), 2.33-2.38 (m, 8H, α -CH₂-Bu), 1.48-1.37 (m, 16H, β -CH₂-Bu), 1.25-1.17 (m, 16H, γ -CH₂-Bu), 0.83-0.78 (m, 24H, CH₃-Bu) ppm. *Signals of the isomer are given in square brackets. Values of the integrals are given for the isomeric mixture.*

MS (MALDI-TOF) m/z : calcd. for $[\text{M}]^+$ ($\text{C}_{62}\text{H}_{76}\text{O}_4\text{Pt}_2\text{S}_6$): 1466.3; found: 1358.4 $[\text{M-COD}]^+$.

HRMS (MALDI-TOF) m/z : calcd. for $[\text{M}]^+$ ($\text{C}_{62}\text{H}_{76}\text{O}_4\text{Pt}_2\text{S}_6$): 1466.33521; found: 1466.33587 $[\text{M}]^+$, 1358.23965 $[\text{M-COD}]^+$.

^{13}C NMR could not be measured due to poor solubility.

1:1 mixture of macrocycles (114:115)



Distannylated terthiophene **108** (495 mg, 0.65 mmol) and $\text{PtCl}_2(\text{COD})$ (244 mg, 0.65 mmol) were dissolved in dry dichloromethane (750 mL) and degased. The reaction mixture was heated under reflux for 10.5 days. The mixture was cooled to room temperature and filtered through a short column packed with alox IV (DCM as eluent). The solvent was removed under vacuum and a yellow solid was obtained (450 mg). 34.0 mg of the crude product (containing 46.3 μmol of $\text{Pt}(\text{COD})_3\text{T}$ -units) and 1,1'-bis(diphenylphosphino)ferrocene (28.3 mg, 50.9 μmol) were dissolved in 8 mL of dry dichloromethane at room temperature. The reaction mixture was stirred overnight. The solvent was subsequently evaporated and 1,5-cyclooctadiene was removed under high vacuum. The afforded solid was dissolved in 10 mL dry THF at room temperature and silver triflate (31.1 mg, 121 μmol , 2.10 eq. per Pt) was added. The mixture was stirred overnight. Afterwards, the organic suspension was diluted with DCM and successively washed with brine and water. The organic layer was dried over MgSO_4 and filtered through a short pad of alox IV eluting with DCM to remove precipitated platinum and silver. The solvent was evaporated to give an orange residue which was dissolved in chloroform (3 mL) and 4 drops of conc. HCl were added. The solution was stirred at room temperature for 4 h

and a sat. aqueous NaHCO_3 solution was added. Extraction with DCM followed. The combined organic layers were washed with water, dried over MgSO_4 and the solvent was evaporated under reduced pressure. Isolation as well as purification of the macrocycles was prepared by SEC (DCM) and the 1:1 mixture of regioisomers **114:115** (8.00 mg, 10.3 μmol , 42%) was obtained pure as a yellow solid.

Mp: 150 – 151 $^\circ\text{C}$.

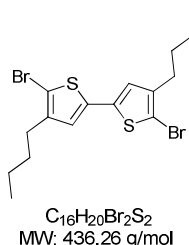
^1H NMR (400 MHz, CDCl_3): δ = 9.98 (s, 4H, COH), 7.81 [7.80] (s, 4H, Th-3), 6.81 [6.79] (s, 4H, Th-4'), 6.78 [6.76] (s, 4H, Th-4''), 2.67-2.60 (m, 8H, $\alpha\text{-CH}_2\text{-Bu}$), 2.51-2.45 (m, 8H, $\alpha\text{-CH}_2\text{-Bu}$), 1.59-1.53 (m, 16H, $\beta\text{-CH}_2\text{-Bu}$), 1.42-1.33 (m, 16H, $\gamma\text{-CH}_2\text{-Bu}$), 0.95-0.90 (m, 24H, $\text{CH}_3\text{-Bu}$) ppm. *Signals of the isomer are given in square brackets. Values of the integrals are given for the isomeric mixture.*

MS (MALDI-TOF) m/z : calcd. for $[\text{M}]^+$ ($\text{C}_{42}\text{H}_{44}\text{O}_2\text{S}_6$): 772.2; found: 772.1 $[\text{M}]^+$.

HRMS (MALDI-TOF) m/z : calcd. for $[\text{M}]^+$ ($\text{C}_{42}\text{H}_{44}\text{O}_2\text{S}_6$): 772.16259; found: 772.16601 $[\text{M}]^+$, $\delta_{m/m}$ = 4.4 ppm.

^{13}C NMR could not be measured due to poor solubility.

5,5'-Dibromo-4,4'-dibutyl-2,2'-bithiophene (**117**)^[17]



n-Butyl lithium (1.6 M in *n*-hexane, 3.14 mL, 5.02 mmol) was added dropwise via syringe to a solution of diisopropylamine (0.71 mL, 5.02 mmol) in 40 mL of dry THF at 0 $^\circ\text{C}$ and stirred for 45 min. 2-bromo-3-butylthiophene **51** (1.00 g, 4.56 mmol) was added at 0 $^\circ\text{C}$ and the mixture was stirred for 2 h. Anhydrous ZnCl_2 (0.68 g, 5.02 mmol) was added at this temperature and stirring was continued for one hour. Anhydrous CuCl_2 (0.92 g, 6.84 mmol) was added in portions at -70 $^\circ\text{C}$ and stirring was maintained for further 60 min under cooling and then allowed to slowly warm up to room temperature overnight. Silica gel was added and the solvent was carefully removed under vacuum. The mixture was filtered over a silica gel plug eluting with *n*-hexane:DCM (95:5) and a pale yellow oil of bithiophene **117** (937 mg, 2.15 mmol, 94%) was obtained.

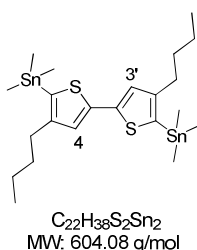
^1H NMR (400 MHz, CDCl_3): δ = 6.77 (s, 2H, Th-3,3'), 2.53 (t, 3J = 7.6 Hz, 4H, $\alpha\text{-CH}_2\text{-Bu}$), 1.60-1.53 (m, 4H, $\beta\text{-CH}_2\text{-Bu}$), 1.41-1.32 (m, 4H, $\gamma\text{-CH}_2\text{-Bu}$), 0.94 (t, 3J = 7.3 Hz, 6H, $\text{CH}_3\text{-Bu}$) ppm.

^{13}C NMR (100 MHz, CDCl_3): δ = 142.90, 136.11, 124.45, 107.85, 31.76, 29.25, 22.29, 13.88 ppm.

MS (CI) m/z : calcd. for $[M]^+$ ($C_{16}H_{20}Br_2S_2$): 436; found: 437 $[M+H]^+$.

Elemental analysis: calcd. for ($C_{16}H_{20}Br_2S_2$): C, 44.05; H, 4.62; S, 14.70%; found: C, 43.88; H, 4.53; S, 14.76%.

{3-Butyl-5-[4-butyl-5-(trimethylstannyl)thien-2-yl]thien-2-yl}trimethylstannane (118)



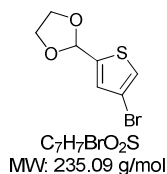
To a solution of bithiophene **117** (480 mg, 1.10 mmol) in dry THF (4.5 mL) was added dropwise *n*-butyl lithium (1.6 M in *n*-hexane, 1.58 mL, 2.53 mmol) at -78 °C within 30 min. The mixture was stirred between -75 and -50 °C for 3.5 h. Afterwards the cooling bath was removed and a solution of Me_3SnCl (526 mg, 2.4 mmol) in THF (1 mL) was added at once. Stirring was continued for 2.5 h during which time the mixture was allowed to warm up to room temperature. *n*-Hexane was added and lithium chloride precipitated as a white solid. The organic phase was washed several times with water and dried over Na_2SO_4 . Crude distannylated bithiophene **118** (618 mg, 90% calcd. from 1H -NMR) was used without further purification in the next step.

1H NMR (400 MHz, $CDCl_3$): δ = 7.11 (s, 2H, Th-4,3'), 2.55 (t, 3J = 7.8 Hz, 4H, α - CH_2 -Bu), 1.61-1.55 (m, 4H, β - CH_2 -Bu), 1.41-1.34 (m, 4H, γ - CH_2 -Bu), 0.93 (t, 3J = 7.3 Hz, 6H, CH_3 -Bu), 0.37 (s, 18H, TMSn) ppm.

^{13}C NMR (100 MHz, $CDCl_3$): δ = 151.51, 142.65, 130.91, 125.96, 34.13, 32.52, 22.64, 14.04, -7.89 ppm.

MS (MALDI-TOF) m/z : calcd. for $[M]^+$ ($C_{22}H_{38}S_2Sn_2$): 606.0; found: 606.4 $[M]^+$.

2-(4-Bromothiophen-2-yl)-1,3-dioxolane (120)



To a vigorously stirred solution of 4-bromothiophene-2-carbaldehyde **119** (1.00 g, 5.23 mmol) and 2-chloroethanol (632 mg, 7.85 mmol) in a solvent mixture of DMF (14 mL) and THF (7 mL) at -50 °C, a solution of *tert*-BuOK (881 mg, 7.85 mmol) in DMF (9 mL) was added dropwise over 30 min. The mixture was stirred for 90 min at this temperature and at room temperature overnight. Afterwards brine and water were added. The product was extracted with DCM and the combined organic layers

were washed again with water and dried over Na_2SO_4 . The solvent was removed under reduced pressure and the crude product was purified by column chromatography using silica and a mixture of *n*-hexane:EE (9:1) to obtain dioxolane **120** (952 mg, 4.05 mmol, 77%) as a colorless liquid.

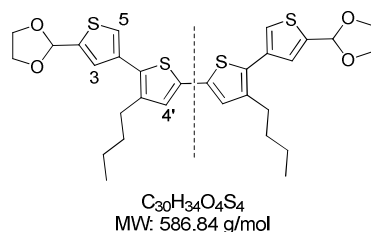
$^1\text{H NMR}$ (400 MHz, CDCl_3): δ = 7.22 (d, 4J = 1.4 Hz, 1H, Th-3), 7.08 (d, 4J = 1.2 Hz, 1H, Th-5), 6.07 (s, 1H, O-CH), 4.13-4.07 (m, 2H, O-CH₂), 4.06-4.00 (m, 2H, O-CH₂) ppm.

$^{13}\text{C NMR}$ (100 MHz, CDCl_3): δ = 143.21, 128.64, 123.50, 109.27, 99.39, 65.24 ppm.

MS (CI) m/z : calcd. for $[\text{M}]^+$ ($\text{C}_7\text{H}_7\text{BrO}_2\text{S}$): 236; found: 237 $[\text{M}+\text{H}]^+$.

Analytical data were in accordance with literature data.^[15]

2-[4-(3-Butyl-5-{4-butyl-5-[5-(1,3-dioxolan-2-yl)thien-3-yl]thien-2-yl}thien-2-yl)thien-2-yl]-1,3-dioxolane (**121**)



Distannylated bithiophene **118** (180 mg, 0.30 mmol) and 2-(4-bromothiophen-2-yl)-1,3-dioxolane **120** (161 mg, 0.69 mmol) were dissolved in dry DMF (5 mL), degassed and $\text{Pd}_2(\text{dba})_3$ (15.4 mg, 14.9 μmol) and $\text{HP}^t\text{Bu}_3\text{BF}_4$ (8.65 mg, 29.8 μmol) were added. The reaction mixture was heated for 21 h at 80 °C. After cooling to room temperature, the mixture was poured onto water and the product was extracted with DCM. The combined organic layers were dried over Na_2SO_4 and the solvent was evaporated. The residue was purified by silica gel column chromatography with a mixture of *n*-hexane:EE (9:1) to obtain quaterthiophene **121** (110 mg, 0.19 mmol, 63%) as a yellow solid.

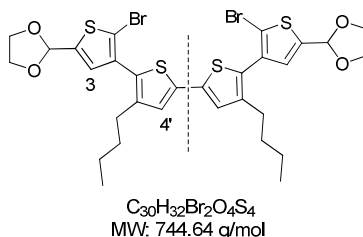
Mp: 103 – 104 °C.

$^1\text{H NMR}$ (400 MHz, CDCl_3): δ = 7.28-7.27 (m, 4H, Th-3,5), 6.98 (s, 2H, Th-4'), 6.13 (s, 2H, O-CH), 4.19-4.12 (m, 4H, O-CH₂), 4.09-4.03 (m, 4H, O-CH₂), 2.65 (t, 3J = 7.8 Hz, 4H, α -CH₂-Bu), 1.66-1.58 (m, 4H, β -CH₂), 1.43-1.33 (m, 4H, γ -CH₂), 0.92 (t, 3J = 7.3 Hz, 6H, CH₃-Bu) ppm.

$^{13}\text{C NMR}$ (100 MHz, CDCl_3): δ = 142.11, 139.67, 134.63, 134.22, 131.06, 127.28, 125.91, 122.90, 100.03, 65.29, 32.74, 28.86, 22.61, 13.96 ppm.

MS (MALDI-TOF) m/z : calcd. for $[\text{M}]^+$ ($\text{C}_{30}\text{H}_{34}\text{O}_4\text{S}_4$): 586.1; found: 586.1 $[\text{M}]^+$, 542.2 $[\text{M}-\text{C}_2\text{H}_4\text{O}]^+$, 498.2 $[\text{M}-2\times\text{C}_2\text{H}_4\text{O}]^+$.

HRMS (MALDI-TOF) m/z : calcd. for $[\text{M}]^+$ ($\text{C}_{30}\text{H}_{34}\text{O}_4\text{S}_4$): 586.13358; found: 586.13344, $\delta_{m/m}$ = 0.2 ppm.

2-[5-Bromo-4-(5-{5-[2-bromo-5-(1,3-dioxolan-2-yl)thien-3-yl]-4-butylthien-2-yl}-3-butylthien-2-yl)thien-2-yl]-1,3-dioxolane (122)

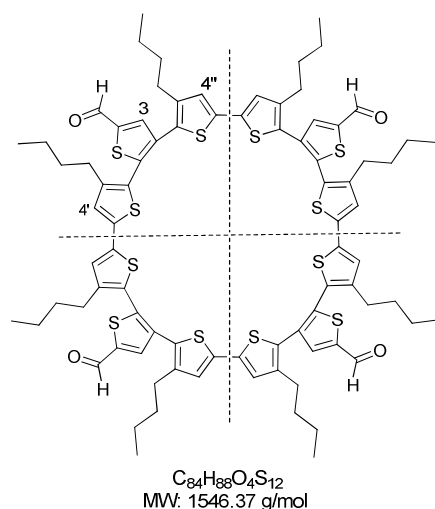
n-Butyl lithium (1.6 M in *n*-hexane, 0.34 mL, 0.55 mmol) was added dropwise to a solution of quaterthiophene **121** (140 mg, 0.24 mmol) in dry THF (2.8 mL) at -60 °C within 20 min. The mixture was stirred between -65 and -50 °C for 2 h. Bromine (28.1 μ L, 0.55 mmol) was added and the mixture was quickly warmed up to room temperature. Stirring was continued for 2 h and the reaction was quenched by the addition of water. The organic phase was separated and the aqueous layer extracted with DCM. The combined organic layers were washed with water and dried over Na₂SO₄. After removal of the solvent, the crude product was purified by silica gel column chromatography with a mixture of DCM:*n*-hexane (7:3) to obtain halogenated quaterthiophene **122** (115 mg, 0.15 mmol, 65%) as a pale yellow oil.

¹H NMR (400 MHz, CDCl₃): δ = 7.03 (s, 2H, Th-3), 7.00 (s, 2H, Th-4'), 6.05 (s, 2H, O-CH), 4.16-4.10 (m, 4H, O-CH₂), 4.07-4.01 (m, 4H, O-CH₂), 2.46 (t, ³*J* = 7.7 Hz, 4H, α -CH₂-*Bu*), 1.58-1.50 (m, 4H, β -CH₂-*Bu*), 1.33-1.24 (m, 4H, γ -CH₂-*Bu*), 0.86 (t, ³*J* = 7.3 Hz, 6H, CH₃-*Bu*) ppm.

¹³C NMR (100 MHz, THF-*d*₈): δ = 144.16, 143.02, 137.43, 134.84, 129.49, 129.31, 125.83, 113.83, 100.47, 65.93, 33.34, 29.48, 23.09, 14.07 ppm.

MS (MALDI-TOF) *m/z*: calcd. for [M]⁺ (C₃₀H₃₂Br₂O₄S₄): 742.0; found: 742.0 [M]⁺, 664.0 [M-Br]⁺.

HRMS (MALDI-TOF) *m/z*: calcd. for [M]⁺ (C₃₀H₃₂Br₂O₄S₄): 741.95447; found: 741.95399, $\delta_{m/m}$ = 0.5 ppm.

Macrocycle (123)

Dibrominated quaterthiophene **122** (106 mg, 0.14 mmol) and distannylated bithiophene **118** (86.0 mg, 0.14 mmol) were dissolved in dry DMF (140 mL), degassed and $Pd_2(dba)_3$ (14.7 mg, 14.2 μ mol) and $HP^tBu_3BF_4$ (8.26 mg, 28.5 μ mol) were added. The reaction mixture was heated at 80 °C for 19 h. After cooling to room temperature, the mixture was poured onto water and the product was extracted with DCM. The combined organic layers were dried over Na_2SO_4 and the solvent was evaporated. The residue was dissolved in DCM and filtered through a short pad of alox IV. Isolation and purification was achieved by SEC (DCM). The isolated material was dissolved in little chloroform and a few drops of conc. HCl were added. The solution was stirred at room temperature for 2 h. It was subsequently quenched with water and the organic phase was separated. After dried over Na_2SO_4 , the solvent was evaporated to yield macrocycle **123** (16.2 mg, 10.5 μ mol, 12%) pure as a yellow solid.

Mp: 249 – 250 °C.

1H NMR (400 MHz, $CDCl_3$): δ = 9.91 (s, 4H, COH), 7.72 (s, 4H, Th-3), 6.94 (s, 4H, Th-4'), 6.91 (s, 4H, Th-4''), 2.46 (t, 3J = 7.8 Hz, 8H, α -CH₂-Bu), 2.30 (t, 3J = 7.8 Hz, 8H, α -CH₂-Bu), 1.46-1.34 (m, 16H, β -CH₂-Bu), 1.31-1.21 (m, 16H, γ -CH₂-Bu), 0.84 (t, 3J = 7.2 Hz, 12H, CH₃-Bu), 0.81 (t, 3J = 7.2 Hz, 12H, CH₃-Bu) ppm.

^{13}C NMR (125 MHz, $CDCl_3$): δ = 182.55, 144.15, 142.26, 142.07, 141.96, 139.32, 138.02, 136.93, 133.19, 128.69, 126.97, 126.39, 125.22, 32.35, 32.27, 29.20, 28.79, 22.74, 22.71, 13.97, 13.92 ppm.

MS (MALDI-TOF) m/z : calcd. for $[M]^+$ ($C_{84}H_{88}O_4S_{12}$): 1544.3; found: 1545.0 $[M+H]^+$.

HRMS (MALDI-TOF) m/z : calcd. for $[M]^+$ ($C_{84}H_{88}O_4S_{12}$): 1544.33311; found: 1544.33176, $\delta_{m/m}$ = 0.9 ppm.

5.8 References

- [1] G. Seconi, C. Eaborn, J. G. Stamper, *J. Organomet. Chem.* **1981**, *204*, 153-168.
- [2] Y. A. Getmanenko, P. Tongwa, T. V. Timofeeva, S. R. Marder, *Org. Lett.* **2010**, *12*, 2136-2139.
- [3] M. Schnürch, M. Spina, A. F. Khan, M. D. Mihovilovic, P. Stanetty, *Chem. Soc. Rev.* **2007**, *36*, 1046-1057.
- [4] J. Fröhlich, W. Kalt, *J. Org. Chem.* **1990**, *55*, 2993-2995.
- [5] J. Fröhlich, C. Hametner, W. Kalt, *Monatsh. Chem.* **1996**, *127*, 435-443.
- [6] J. Fröhlich, *Bull. Soc. Chim. Belg.* **1996**, *105*, 615-634.
- [7] J. F. Bunnett, *Acc. Chem. Res.* **1972**, *5*, 139-147.
- [8] E. Lukevics, P. Arsenyan, S. Belyakov, J. Popelis, O. Pudova, *Tetrahedron Lett.* **2001**, *42*, 2039-2041.
- [9] L. Boymond, M. Rottländer, G. Cahiez, P. Knochel, *Angew. Chem.* **1998**, *110*, 1801-1803; *Angew. Chem. Int. Ed.* **1998**, *37*, 1701-1703.
- [10] M. Barbasiewicz, M. Makosza, *Org. Lett.* **2006**, *8*, 3745-3748.
- [11] Z. Hu, J. L. Atwood, M. P. Cava, *J. Org. Chem.* **1994**, *59*, 8071-8075.
- [12] F. Ellinger, A. Gieren, T. Hübner, J. Lex, F. Lucchesini, A. Merz, R. Neidlein, J. Salbeck, *Monatsh. Chem.* **1993**, *124*, 931-943.
- [13] A. C. Soegiarto, A. Comotti, M. D. Ward, *J. Am. Chem. Soc.* **2010**, *132*, 14603-14616.
- [14] J. L. Brédas, G. B. Street, B. Thémans, J. M. André, *J. Chem. Phys.* **1985**, *83*, 1323-1329.
- [15] A. L. Johnson, *J. Org. Chem.* **1976**, *41*, 1320-1324.
- [16] H. Takaba, H. Omachi, Y. Yamamoto, J. Bouffard, K. Itami, *Angew. Chem.* **2009**, *121*, 6228-6232; *Angew. Chem. Int. Ed.* **2009**, *48*, 6112-6116.
- [17] L. U. Lehmann, *U.S. Pat. Appl. Publ.*, US 20080262183 A1 20081023 **2008**.

Summary

The thesis outlined the synthesis, characterization, and optoelectronic properties of functionalized, fully π -conjugated cyclo[*n*]thiophenes.

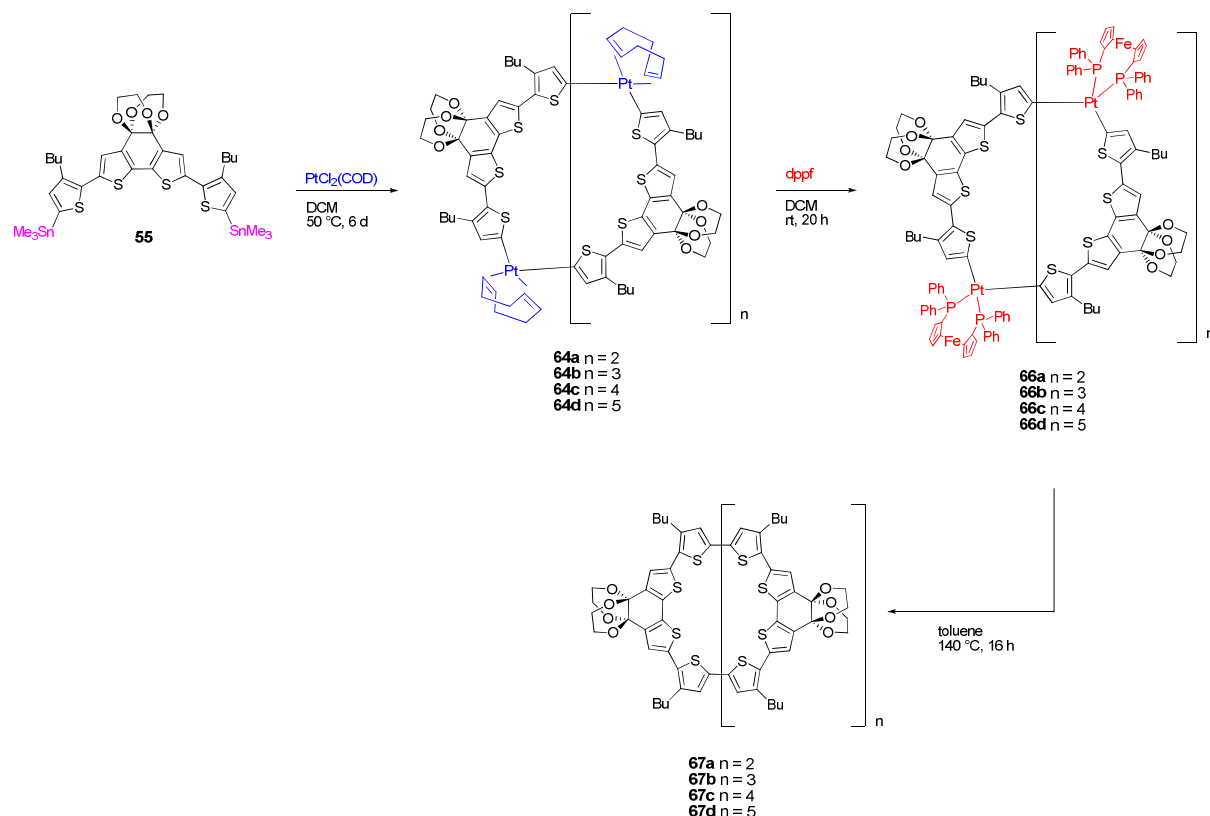
The main focus laid on the expansion of the 'metal-assisted template method' to functionalized precursors that give entry into advanced, shape-persistent macrocycles. Attention was given to two possible molecular design concepts: 1) the introduction of functionalized groups within the cyclic conjugated backbone to influence the electronic properties of the macrocycles, and 2) the attachment of organic modules to the periphery of the rings to provide reactive positions for potential further organic chemistry or possible assembly into well-defined ordered structures.

For the first concept, dithienobenzoquinone (DTB)- and dithienocyclopentanone (DCP)-electron-accepting moieties as well as a dithienopyrrole (DTP)-electron-donating unit have been incorporated into the monomer building blocks to provide modified macrocycles during the crucial macrocyclization step (see Chapters 3 and 4). The synthetic strategy towards the series of substituted macrocycles is depicted in Scheme S1 using the example of the DTB-functionalized series. The synthetic procedure is similar for the DCP- and DTP-cycles. Mixtures of cyclic, multinuclear Pt^{II}metallacomplexes **64a-d** evolved from the reaction between distannylated precursor **55** and transition metal complex PtCl₂(COD). Two trimeric, stable complexes Pt(COD)[12]DTB **64a** and Pt(COD)[12]DTP **94** have been isolated using size exclusion chromatography and characterized by proton NMR spectroscopy and mass spectrometry (Chart S1).

A ligand exchange reaction of the crude mixture **64a-d** with the bulky phosphine 1,1'-bis(diphenylphosphino)ferrocene (dppf) must be carried out prior to reductive elimination, which can be induced thermally or, in the case of the DCP- and DTP-Pt^{II}metallacycles, by addition of the oxidizing reagent AgOTf. The 1,1-concerted reductive elimination forms a crude mixture of different ring sizes of fully α -conjugated macrocycles **67a-d**.

Four functionalized macrocycles were isolated after extensive purification processes using size exclusion chromatography and precipitation method; C[12]DTB **67a** (8%), C[16]DTB **67b** (4%), C[12]DCP **70** (11%), and C[12]DTP **96** (29%) (Chart S1). The values expressed as percentages in brackets refer to the respective overall yields calculated from the appropriate distannylated starting

material. Higher homologues were formed in traces and could not be isolated pure due to low availability of the material.



Scheme S1: Synthesis of functionalized fully α -conjugated macrocycles using the example of the DTB-containing series **67a-d**. The synthetic procedure is similar for the DCP- and DTP-containing macrocycles **70** and **96**.

The isolated macrocycles have been characterized via ^1H NMR spectroscopy and mass spectrometry and optoelectronic properties have been investigated by means of UV/vis absorption and fluorescence spectroscopy. The macrocycles exhibited an absorption maximum for the π - π^* transition, which can be ascribed to the $S_0 \rightarrow S_2$ transition and one weak shoulder at longer wavelengths, which can be assigned to the symmetry forbidden, ring size dependent $S_0 \rightarrow S_1$ transition. Due to the stronger influence of the electron-withdrawing moieties on the optical band gap, the absorption maxima of the acceptor-substituted trimeric rings **67a** and **70** are significantly bathochromically shifted in comparison to the donor-substituted trimeric ring **96**. In comparison to a purely thiophene-containing model macrocycle C[12]T **81** (Chart S2), the rather weak influence of the electron-rich DTP-functionality on the optical band gap in **96** is obvious, since both rings show nearly identical absorption maxima. An expected red-shift of the absorption maximum for the larger macrocycle C[16]DTB **67b** in comparison to the smaller analogue C[12]DTB **67a** was observed due to the expanded π -system.

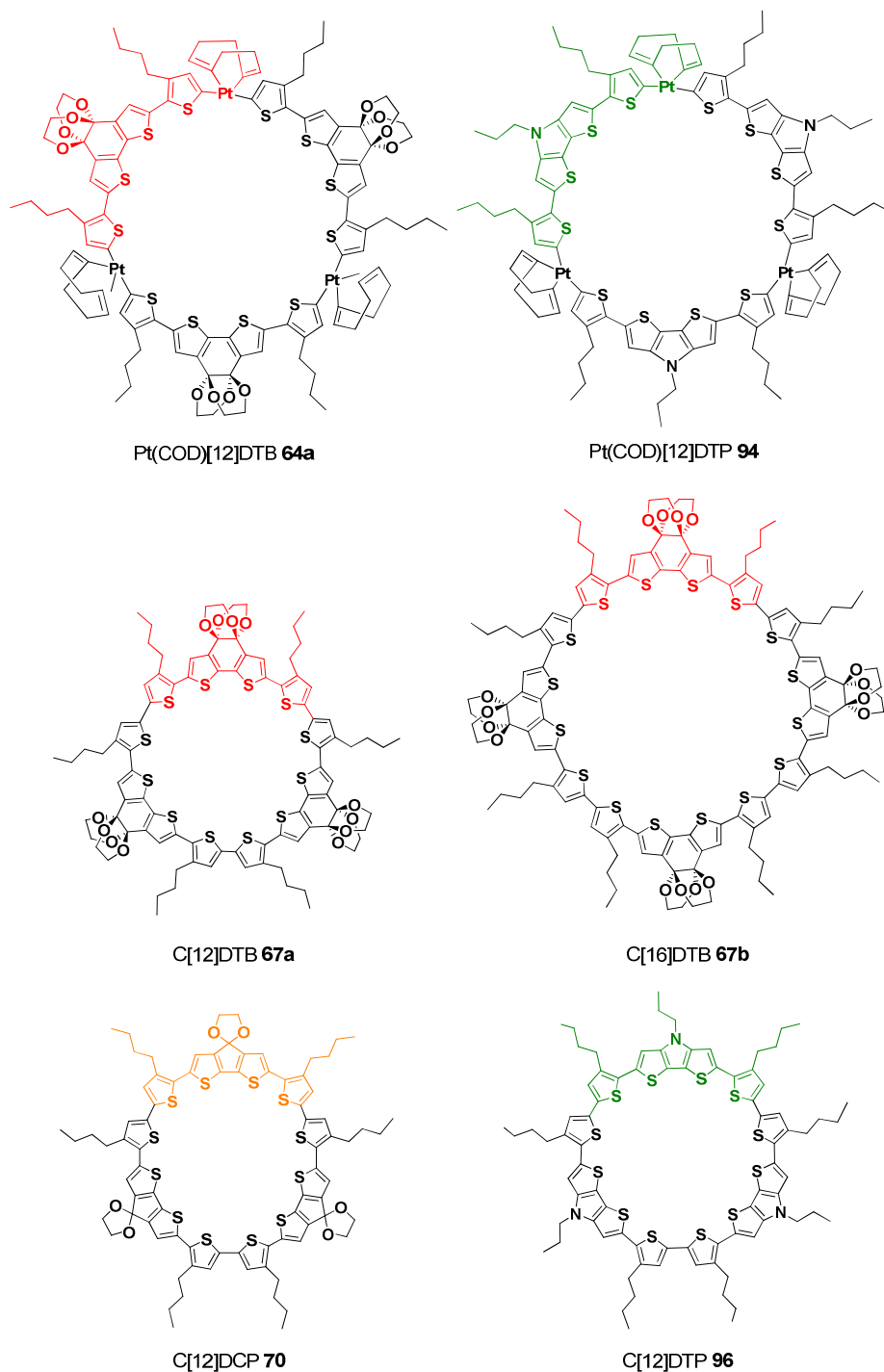


Chart S1: Structures of the successfully isolated macrocycles **64a**, **94**, **67a**, **67b**, **70**, and **96**.

Further investigations in comparison to linear oligomers were undertaken, whereupon the absorption of the rings were found to correspond approximately to the absorption of appropriate linear oligomers with half the number of thiophene molecules. This was observed by opposing the absorption maxima of the linear homologues **79a**, **79b** and **97** (Chart S2) to the corresponding substituted macrocycles. The fact can as well be explained by theoretical analysis, since the energy

levels for the $S_0 \rightarrow S_2$ transition are degenerate, which leads in addition to extremely high extinction coefficients.

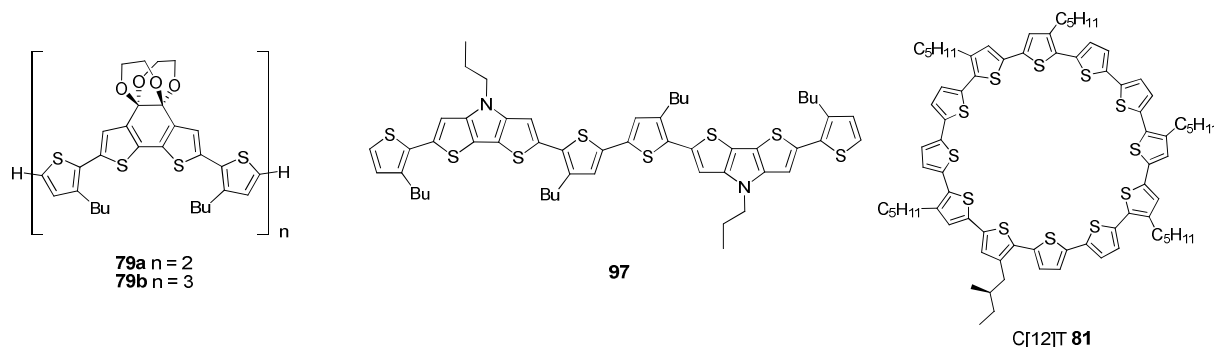


Chart S2: Structures of the linear oligomers **79a**, **79b** and **97** as well as the pure, thiophene-based macrocycle **81**.

All macrocycles showed vibronic fine structure for the emission bands since they adopt a more quinoidal and stiff structure in the excited state. The emission spectra of **67a** and **67b** differ greatly, both in the position of the maxima and the shape of the peaks. Macrocycle **67b** is blue-shifted compared to that of **67a** and is rather similar to the emission spectra of linear oligomers. Presumably, the emission of **67b** takes place from the S_1 -state, whereas the strained trimeric macrocycle **67a** emits from an energetically low-lying excited state.

The macrocycles C[12]DTB **67a** and C[12]DTP **96** were investigated by cyclic voltammetry (CV) and exhibited several reversible one-electron redox waves. Some one-electron transition processes are split into multiple oxidation processes indicating the formation of dimeric charged aggregates via intermolecular π - π -interactions which are oxidized as well. This has been proven by temperature-dependent CV-measurements for macrocycle **67a**, during which most of the splits disappeared and the shape of the waves turned into a rather Gaussian-form, indicating the decomposition of the aggregates. A comparison between all four functionalized macrocycles revealed a very low first oxidation potential for DTP-macrocycle **96** due to the high electron density inside the ring. In contrast, a high first oxidation potential can be observed for DTB-macrocycle **67a**, since the electron density is reduced because of the electron withdrawing DTB-moieties. Upon oxidation of the macrocycles, stable charged species arose. These stable oxidized states have also been investigated by means of UV/vis/NIR spectroscopy to gain insight into the electronic states of the charged species. A chemical oxidant ($\text{TDBPA}^+\text{SbCl}_6^-$) was added stepwise to solutions of the macrocycles C[12]DTB **67a** and C[12]DTP **96** in order to generate different oxidized states, which were surveyed for their optoelectronic properties. Two main absorption bands for the doubly oxidized species were observed, which are a hint for a polaronic pair structure with two individual polarons and an distorted geometry of the conjugated backbone. The presence of a polaronic pair configuration and

not a bipolaronic configuration was confirmed as well by positive signals at electron spin resonance (ESR)-measurements.

The cyclic structure of macrocycle C[12]DTB **67a** was determined by X-ray crystallographic analysis of a single-crystal grown from chloroform/*n*-hexane. All thiophene moieties adopt a *syn*-conformation with each sulfur atom directed into the inside of the cavity. The cycles present a nearly planar, slightly curved structure. They pack into stacks in which one cycle lays slightly displaced on top of each other with an interdigitation behaviour between adjacent stacks.

The second molecular design concept examined in this thesis focused on the attachment of organic functionalities to the periphery of the macrocycles. The synthesis also followed the 'metal-assisted template method' of a distannylated precursor and PtCl₂(COD) as described in Scheme S1. The preparation of aldehyde-substituted macrocycles resulted in a 1:1 mixture of regioisomers **114** and **115** in an overall yield of 21% (Chart S3). The formation of the inseparable mixture was caused by the use of an asymmetric monomer unit **108**. The macrocyclization succeeded in the formation of only one defined ring size composed of six thiophene units, due to the strongly bent structure of **108** with a very small inner angle. The 1:1 mixture **114**:**115** was characterized via proton NMR spectroscopy and mass spectrometry and was investigated for their optical and electrochemical properties.

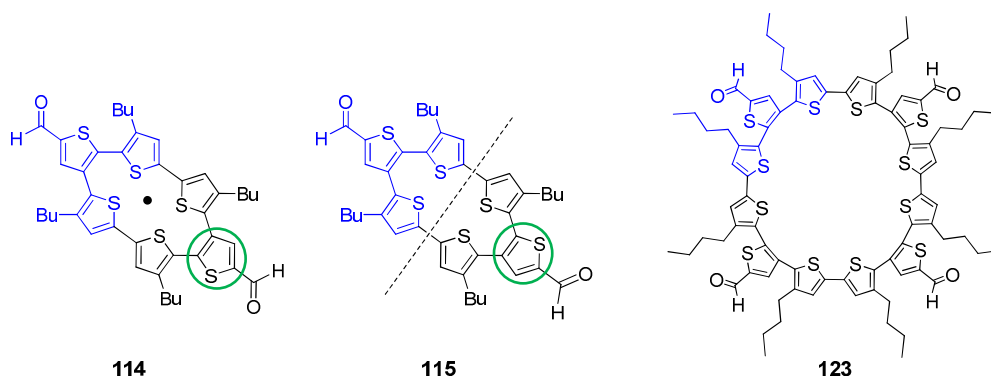


Chart S3: Structures of the 1:1 isomeric mixture **114**:**115** and the non-isomeric macrocycle **123**.

A broad and unstructured absorption band indicated a non-planarity of the macrocycles **114** and **115** which was confirmed by computational calculations. The twisting of single thiophene moieties out of the plane resulted in an overlap of different absorption bands of disrupted π -conjugated subunits.

Macrocycle **123** was synthesized as a non-isomeric, peripherically functionalized analogue in an alternative synthetic route via a Stille cross-coupling reaction and isolated in 12% yield. Absorption spectroscopic investigations led to the assumption of a curved and strained system as well, since the recorded absorption band showed a broad and structured shape which was caused by the overlap of

several disrupted conjugated subunits. Thus, the utilized Stille-cross coupling reaction can be regarded as another synthetic pathway into shape-persistent macrocycles.

Both classes of aldehyde-substituted macrocycles provide reactive centers for potential subsequent chemical reactions to influence either electronic properties or self-organize the cycles into well-ordered structures on surfaces or in the solid phase.

To conclude, the platinum-assisted method gives access to tailored macrocyclic compounds with tunable optoelectronic properties. The possibility of a defined electronic modification of the cyclic systems and the application in the field of electronic nanotechnology exists through the selection of certain functionalities. Attachment of self-organizing groups, intermolecular interactions or chemical reactions between the macrocycles can potentially direct the molecules into well structured one- and two-dimensional networks on surfaces or in the solid phase. This may improve charge mobilities and make the cycles attractive candidates for electronic devices such as organic field effect transistors (OFETs).

Besides, an elaborated synthetic pathway utilizing the Stille cross-coupling reaction as crucial cyclization step led to a π -conjugated macrocycle and can be regarded as an alternative strategy to shape-persistent macrocycles.

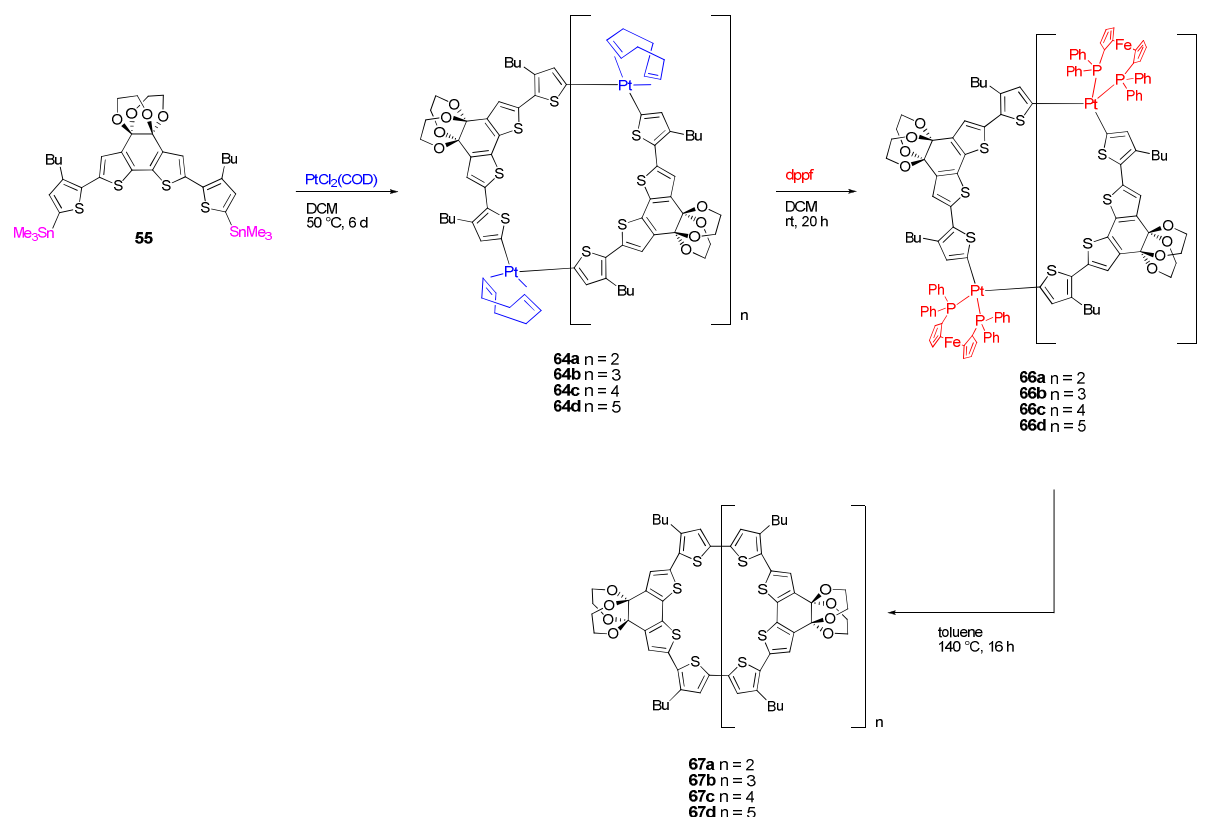
Zusammenfassung

Die vorliegende Arbeit beschäftigt sich mit der Synthese, Charaktisierung und Untersuchung der optoelektronischen Eigenschaften funktionalisierter, vollständig π -konjugierter Cyclo[n]thiophene.

Dabei stand die Erforschung der Erweiterung des Einsatzgebietes der entwickelten "Metall-assistierten Templatierungsmethode" zur Darstellung formstabiler Makrocyclen auf Basis substituierter Bausteine im Vordergrund. Hierzu wurden zwei mögliche Konzepte bearbeitet: 1) Den Einbau funktioneller Gruppen innerhalb des konjugierten cyclischen Rückgrates zur Beeinflussung der elektronischen Eigenschaften makrocyclischer Systeme, und 2) die Anbringung organischer Module innerhalb der Peripherie der Ringsysteme zur Gewährleistung reaktiver Stellen für potentielle weiterführende chemische Reaktionen oder die Anordnung von Cyclen in übergeordneten Strukturen.

Als funktionelle Gruppen wurden im ersten Konzept gezielt Dithienobenz^oquinon (DTB)- und Dithienocyclopentan^on (DCP)-Elektronen-Akzeptorbausteine sowie eine Dithienopyrrol (DTP)-Elektronen-Donoreinheit in die Monomerkomponenten eingebracht, um im entscheidenden Reaktionsschritt der Cyclisierung modifizierte Ringsysteme zu erzielen (Vergleich Kapitel 3 und 4). Die Darstellung makrocyclischer Serien ist in Schema 1 an Hand der DTB-Makrocyclenserie abgebildet. Die Synthese der DCP- und DTP-Serien erfolgt vergleichbar. Durch Reaktion des zweifach stannylierten Startmaterials **55** mit dem Platin-Komplex PtCl₂(COD) entstanden entsprechende Gemische aus cyclischen, mehrkernigen Pt^{II}-Metallverbindungen **64a-d**. Mittels Größenausschlusschromatographie konnten zwei trimere, stabile Komplexe Pt(COD)[12]DTB **64a** und Pt(COD)[12]DTP **94** isoliert und über ¹H-NMR- und Massenanalyse charakterisiert werden (Abbildung 1). Im weiteren Reaktionsschritt erfolgte der Ligandenaustausch des Gemischs **64a-d** mit dem sterisch anspruchsvollen Phosphinliganden 1,1'-bis(diphenylphosphino)ferrocen (dppf) zu **66a-d**, bevor die reduktive Eliminierung auf thermisch induziertem Wege durchgeführt wurde. Im Falle der DCP- und DTP-Platincyclen erfolgte die reduktive Eliminierung oxidativ induziert mittels AgOTf. Bei der 1,1-konzertierten Eliminierung entstanden Rohgemische unterschiedlicher Cyclengrößen der vollständig π -konjugierten Makrocyclen. Durch aufwändige Aufreinigungsprozesse über Größenausschlusschromatographie und Präzipitation konnten insgesamt vier funktionalisierte Makrocyclen rein isoliert werden; C[12]DTB **67a** [8%], C[16]DTB **67b** [4%], C[12]DCP **70** [11%] und C[12]DTP **96** [29%]

(Abbildung 1). Die in Klammern angegebenen Prozentwerte beziehen sich auf die jeweiligen Gesamtausbeuten über drei Stufen, ausgehend des entsprechend bisstannylierten Startmaterials. Die höheren Homologen entstanden nur in Spuren und konnten auf Grund der wenigen Substanzmenge nicht rein isoliert werden.



Schema 1: Schema zur Darstellung funktionalisierter Makrocyclen am Beispiel der DTB-Serie **67a-d**. Die Synthese der DCP- und DTP-Makrocyclen **70** und **96** erfolgt auf vergleichbarem Wege.

Die isolierten Makrocyclen wurden über ^1H -NMR-Spektroskopie und Massenspektrometrie charakterisiert und auf ihre optoelektronischen Eigenschaften mittels UV/vis Absorptions- und Fluoreszenzspektroskopie hin untersucht. Dabei zeigten die Cyclen ein Absorptionsmaximum für den π - π^* -Übergang, das dem $\text{S}_0 \rightarrow \text{S}_2$ -Übergang zuzuschreiben ist, sowie eine schwache Schulter im langwelligen Bereich, die dem symmetrieverbotenen $\text{S}_0 \rightarrow \text{S}_1$ -Übergang angehört und in Abhängigkeit von der Ringgröße steht. Die Maxima der trimeren Akzeptor-substituierten Ringe **67a** und **70** zeigten im Vergleich zum trimeren Donor-Ring **96** eine deutliche bathochrome Verschiebung, welche durch den stärkeren Einfluss der elektronenziehenden Gruppe auf die optische Bandlücke ausgelöst wird. In Gegenüberstellung der modifizierten Makrocyclen mit einem vergleichbaren 12-gliedrigen rein Thiophen-basierenden Makrocyclus C[12]T **81** (Abbildung 2) wird ersichtlich, dass die elektronenschiebende DTP-Funktionalität in **96** einen eher schwachen Einfluss auf die optische Bandlücke ausübt, da beide Absorptionsmaxima fast identische Werte aufwiesen. Bei einem Vergleich der DTB-Cyclen **67a** und **67b** innerhalb einer Serie, kann eine erwartete Rotverschiebung

des Absorptionsmaximum des höheren Homologen gegenüber dem kleineren Ring auf Grund des erweiterten π -Systems beobachtet werden.

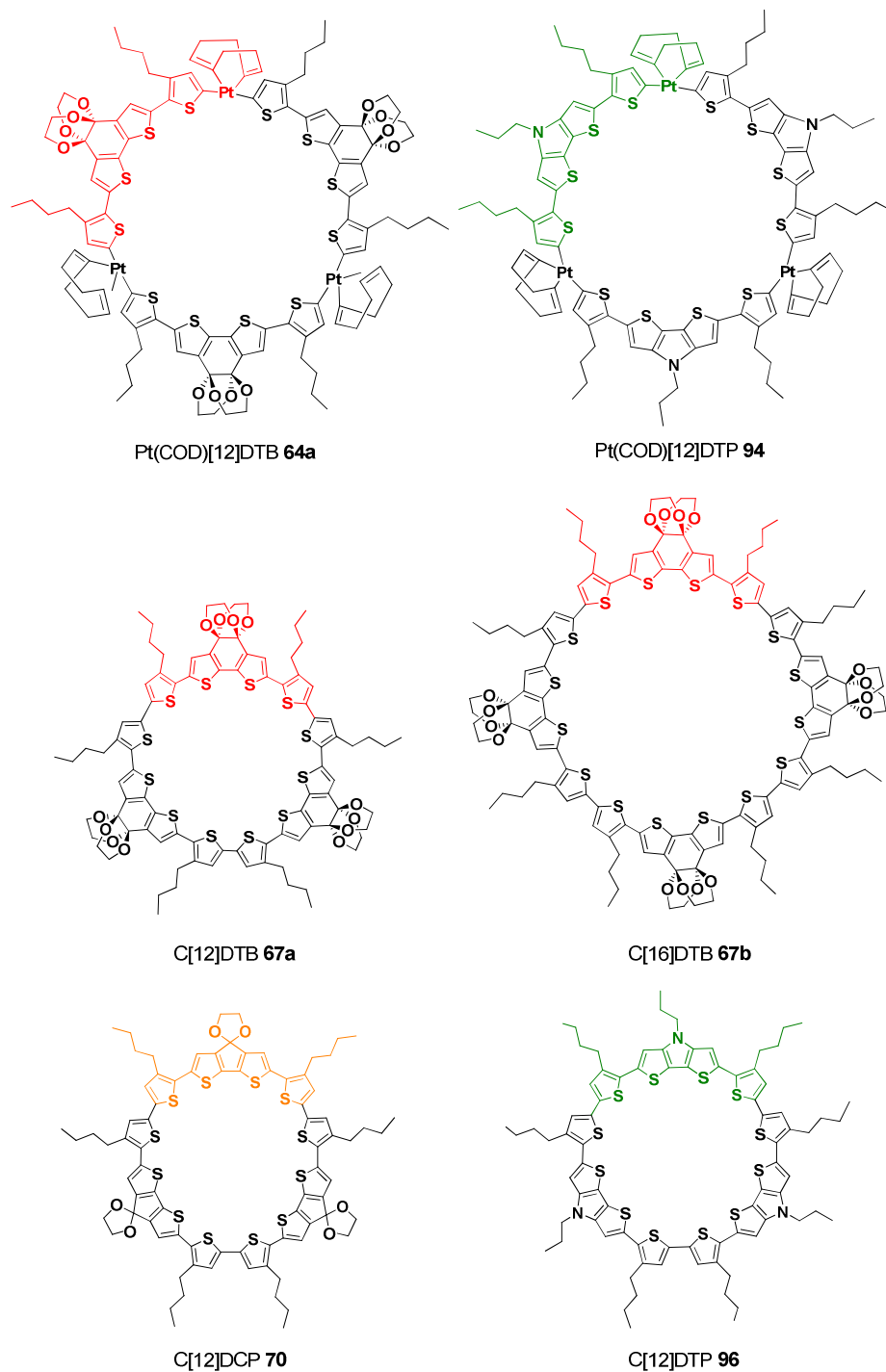


Abbildung 1: Strukturen der erfolgreich isolierten Makrocyclen **64a**, **94**, **67a**, **67b**, **70** und **96**.

Werden die Absorptionskurven der linearen Homologen **79a**, **79b** und **97** (Abbildung 2) mit den entsprechend substituerten Cyclen verglichen, so entspricht die Absorption des Rings in etwa der Absorption für lineare Oligomere mit der Hälfte der Anzahl an Thiophenmolekülen. Diese Tatsache

kann auf den entarteten Zustand des $S_0 \rightarrow S_2$ Übergangs zurückgeführt werden, genauso wie die enorm hohen Extinktionskoeffizienten.

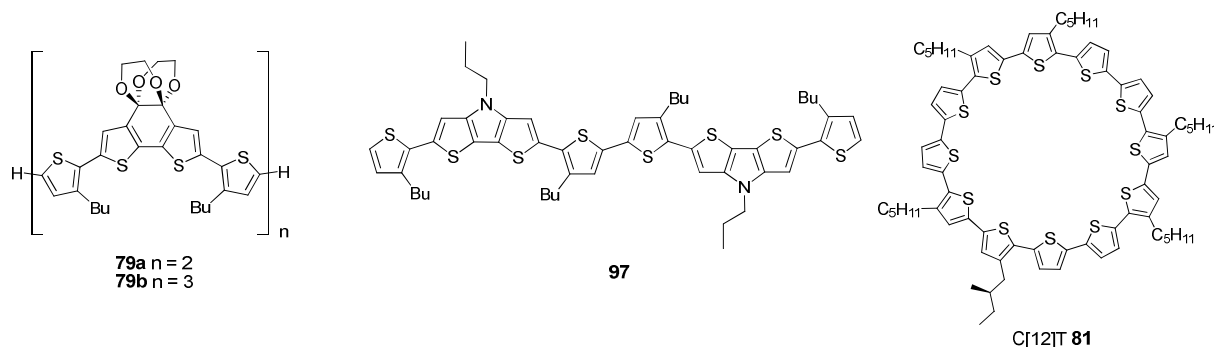


Abbildung 2. Strukturen der linearen Oligomeren **79a**, **79b** und **97** sowie des rein Thiophen-basierenden Makrocyclus **81**.

Im Fluoreszenzspektrum zeigen alle makrocyclischen Systeme eine schwingungsstrukturierte Bande, da die Ringe im angeregten Zustand eine eher quinoide, starre Struktur annehmen und daher auch vibronische Banden sichtbar werden. Die Emissionsspektren der Cyclen **67a** und **67b** unterscheiden sich stark in ihrer Form und der Lage der Maxima. Cyclus **67b** emittiert im Vergleich zu **67a** blauverschoben und gleicht eher der Emission linearer Oligomere. Es wird angenommen, dass die Emission hier aus einem angeregten S_1 -Zustand stattfindet und der gespannte trimere Cyclus **67a** aus einem energetisch tieferliegenden Niveau emittiert.

Bei den elektrochemischen Untersuchungen mittels Cyclovoltammetrie (CV) zeigen die untersuchten trimeren Cyclen C[12]DTB **67a** und C[12]DTP **96** mehrere reversible ein-Elektronen Redox-Wellen. Die Wellen zeigen ihrerseits teilweise Aufspaltungen, welche auf mehrere Oxidationsprozesse innerhalb eines ein-Elektronen-Übertragungsvorgangs schließen und auf die Entstehung π -dimerer Aggregate geladener makrocyclischer Spezies deuten, welche ebenfalls oxidiert werden. Dies wurde durch temperaturabhängige CV-Messungen am Cyclus **67a** bestätigt, wobei die Aufspaltungen bei höheren Temperaturen zurückgingen und die Wellen eine eher gausförmige Kurve annahmen und dadurch die Auflösung der Aggregate angenommen werden kann. Ein Vergleich der Makrocyclen untereinander zeigt ein sehr niedriges erstes Oxidationspotential für den DTP-Cyclus **96** auf Grund seiner hohen Elektronendichte. Bei dem DTB-Cyclus **67a** hingegen kann durch die verminderte Elektronendichte ein spätes erstes Oxidationspotential beobachtet werden. Bei der Oxidation der Makrocyclen entstehen stabile, geladene Zustände. Diese lassen sich über absorptionsspektroskopische Messungen im UV/vis/NIR-Bereich untersuchen. Dabei ist es möglich Aussagen über die elektronischen Zustände der geladenen Spezies zu treffen. Durch die schrittweise Zugabe eines chemischen Oxidationsmittels ($\text{TDBPA}^+\text{SbCl}_6^-$) zu Lösungen der Ringe **67a** und **96** konnten die oxidierten Zustände nach und nach erzeugt und deren optoelektronisches Verhalten untersucht werden. Die dabei erhaltenen Banden für die zweifach oxidierten Spezies mit zwei

Hauptabsorptionsbanden lassen auf die elektronische Konfiguration einer Polaronenpaar-ähnlichen Struktur mit zwei individuellen Polaronen und einer verzerrten Geometrie des konjugierten Rückgrats schließen. Die Vermutungen der Polaronenpaar-ähnlichen Konfiguration wurde über positive Signale während Elektronen-Spin-Resonanz (ESR)-Messungen bestätigt.

Die cyclische Struktur von Makrocyclus C[12]DTB **67a** wurde durch Röntgenstrukturanalyse eines Einkristalls bestätigt ($\text{CHCl}_3/n\text{-Hexan}$). Alle Thiophenmoleküle nehmen eine *syn*-Konformation ein, in der die Schwefelatome ins Innere des Hohlraums gerichtet sind. Die Cyclen zeigen eine fast planare, wenig gewölbte Struktur. In der Packung ordnen sie sich leicht versetzt übereinander zu Stapeln an und greifen in benachbarten Stapel über.

Im zweiten Modifizierungs-Konzept wurde die Anbringung organischer Funktionalitäten innerhalb der Peripherie der Makrocyclen behandelt. Die Synthese folgte gleicher "Metall-assistierten Templatierungsmethode" ausgehend einer bisstannylierten Monomereinheit und $\text{PtCl}_2(\text{COD})$ wie in Schema 1 beschrieben. Die Darstellung Aldehyd-funktionalisierter Makrocyclen resultierte in einem 1:1 Isomerengemisch der Cyclen **114** und **115** in einer Gesamtausbeute von 21% (Abbildung 3). Die Bildung des untrennbaren Gemischs wurde durch die Verwendung des asymmetrischen Ausgangsbausteins **108** ausgelöst. Durch seine stark gewinkelte Struktur mit sehr kleinem Innenwinkel gelang die definierte Synthese von nur einer Makrocyclengröße mit sechs Thiopheneinheiten. Das Gemisch wurde über ^1H -NMR-Spektroskopie und Massenspektrometrie charakterisiert und die optischen und elektrochemischen Eigenschaften untersucht.

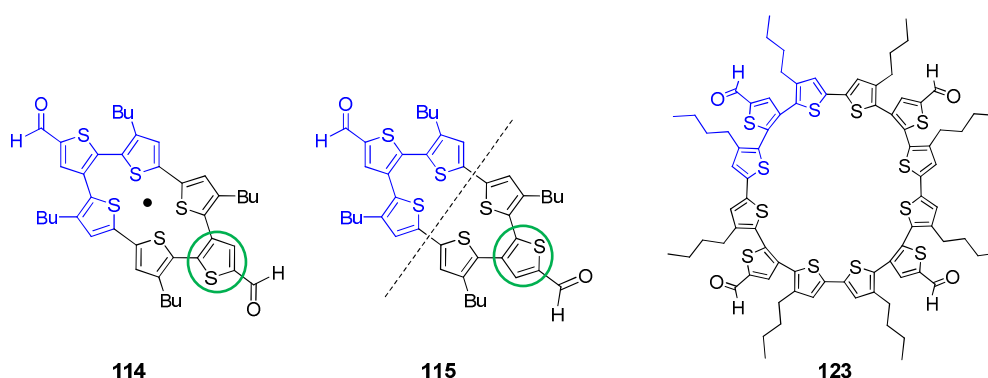


Abbildung 3: Strukturen des 1:1 Isomerengemisch **114:115** sowie des isomeren-freien Makrocyclus **123**.

Ein breites, unstrukturiertes Absorptionsband deutet auf die Unebenheit des gespannten Systems hin, was durch computertechnische Berechnungen bestätigt wurde. Die Drehung der einzelnen Thiophene aus der Ebene führt zu einer Überlagerung unterschiedlicher Absorptionsbanden nicht miteinander verbundenen π -konjugierten Untereinheiten.

Makrocyclus **123** wurde auf einem alternativ entwickelten Syntheseweg über Stille-Kreuzkupplungsreaktionen in einer Ausbeute von 12% als Zielverbindung eines isomerenfreien, peripher-funktionalisierten π -konjugierten Makrocyclus synthetisiert. Die Untersuchungen mittels Absorptionsspektroskopie deuten auch hier auf ein stark gewölbtes, gespanntes System hin, da die Absorptionsbande ebenfalls sehr breit und unstrukturiert ist und auf die Überlagerung mehrere Absorptionsbanden verschiedener konjugierter Untereinheiten hindeutet. Die Stille-Reaktion könnte als weitere Möglichkeit zur Bildung von formstabilen Makrocyclen angesehen werden.

Zusammenfassend ist zu sagen, dass die Platin-assistierte Methode nun den Zugang zu formstabilen, maßgeschneiderten makrocyclischen Verbindungen mit einstellbaren optoelektronischen Eigenschaften erlaubt. Durch die Auswahl der Funktionalität besteht somit die Möglichkeit einer bewusst geplanten elektronischen Veränderung der ringförmigen Komponenten, welche so in der elektronischen Nanotechnologie Anwendung finden könnten. Die Anbringung selbstorganisierender Gruppen, intermolekulare Wechselwirkungen oder chemische Reaktionen zwischen den Cyclen kann zur potentiellen Anordnung der Moleküle in perfekt geordneten zwei- oder dreidimensionalen Netzwerken auf Oberflächen oder in der Festphase führen. Diese Möglichkeit kann für eine verbesserten Leitfähigkeit sorgen und die Cyclen attraktiv für den Einsatz in der Halbleitertechnologie, wie in organischen Feldeffekttransistoren (OFETs), machen.

Zudem wurde ein weiterer Syntheseweg zur Darstellung eines vollständig π -konjugierten Makrocyclus über die Stille Kreuzkupplungsreaktion als entscheidender Cyclisierungsschritt erarbeitet. Diese Strategie kann nun als alternativer Weg zur Synthese formstabiler Cyclen angesehen werden.

CURRICULUM VITAE

Dipl.-Chem. Melanie Bader

24 October 1984 born in Ulm, Germany

Nationality: German

Education

Jan 2010 – March 2014	PhD in organic chemistry about „Synthesis and Characterization of Functionalized, Fully π -Conjugated Cyclo[n]thiophenes“ at the University of Ulm, Institute of Organic Chemistry II and Advanced Materials, supervised by Prof. Dr. P. Bäuerle
Sep 2009	Diploma in chemistry (final grade 1.2)
Feb 2009 – Sep 2009	Diploma thesis in organic chemistry about „ <i>Synthese von Nukleosid-Funktionalisierten Quaterthiophen-Konjugaten zur Ausbildung selbstorganisierender Überstrukturen und deren Untersuchung in Lösung</i> “ at the University of Ulm, supervised by Prof. Dr. P. Bäuerle
Oct 2004 – Sep 2009	Studies of chemistry at the University of Ulm
July 2004	A levels (final grade 2.0)
Sep 1995 – July 2004	Nikolaus-Kopernikus-Gymnasium in Weißenhorn

Experience

Jan 2013 – Feb 2013	Cooperation at the University of Melbourne with Prof. Dr. A. B. Holmes, VIC, Australia
Oct 2012 – Dec 2012	Assistant in the „Fortgeschrittenenpraktikum organische Chemie“, University of Ulm
Nov 2009 – Dec 2009	Academic research assistant at the University of Ulm, Institute of Organic Chemistry II and Advanced Materials with Prof. Dr. P. Bäuerle

Conferences & Presentations

ISNA 14, Eugene, USA, 24-29 July 2011

Poster Session „*Functionalized α -Conjugated Cyclo[n]thiophenes*“

Melanie Bader, Günther Götz, Matthias Weil, Peter Bäuerle*

Integrated Graduate School of SFB 569, July 5th 2011

Oral Presentation: *Functionalized α -Conjugated Cyco[n]thiophenes*

Integrated Graduate School of SFB 569, September 30th 2011

Oral Presentation: *Synthetic Strategies of Different Conjugated Macrocycles and their Properties*

M. Bader, G. Götz, M. Weil, P. Bäuerle, *Tuning the Physical Properties of Fully α -Conjugated Cyclo[n]thiophenes by Inserting Acceptor Functionalities*, manuscript in preparation.